Integrating Phosphoinositide Metabolism, Platelet Functional Data and Computational Modelling to Decipher GPVI-Signalling in Platelet Activation

By

Yam Fung Hilaire Cheung

A thesis submitted to the University of Birmingham and Maastricht University for the degree of DOCTOR OF PHILOSOPHY

January 2023

UNIVERSITY OF BIRMINGHAM

Institute of Cardiovascular Sciences

College of Medical and Dental Sciences

University of Birmingham

isas Leibniz-Institut für Analytische Wissenschaften

Maastricht University

Bioanalytics Department,

Leibniz-Institut für Analytische Wissenschaften-ISAS-e.V.

CARIM School for Cardiovascular Diseases

Faculty of Health, Medicine & Life Sciences

Maastricht University

Supervisors University of Birmingham
Prof S.P. Watson
Dr N.S. Poulter
Supervisors Maastricht University
Prof J.W.M. Heemskerk
Dr M.J. Kuijpers
Supervisors Leibniz-Institut für Analytische Wissenschaften-ISAS-e.V.
Prof Dr A. Sickmann
Examiners
Prof D.M. Owen (University of Birmingham, United Kingdom, Chair)
Dr S. Jabbari (University of Birmingham, United Kingdom, Internal examiner)
Prof P.T. Hawkins (The Babraham Institute, United Kingdom, External examiner)

The research in this thesis was supported by a joint PhD scholarship of the European Union's Horizon 2020 research and innovation program under the Marie Sklodowska-Curie grant agreement TAPAS No. 766118. This thesis is submitted as a result of the joint doctorate programme of Yam Fung Hilaire Cheung at the Leibniz Institute for Analytical Sciences, the University of Birmingham and the Maastricht University, for obtaining a double PhD degree. Admission to the joint doctorate programme has been confirmed in the Individual Joint PhD Learning Agreement between the two universities and the postgraduate researcher. The modelling work is a collaborative work supported by Dr J.L. Dunster at the University of Reading and Dr C. Wierling at Alacris Theranostics GmbH, two of the beneficiaries of the TAPAS program.

Abstract

Cardiovascular diseases are the leading cause of mortality worldwide, and platelets are critical in their pathophysiology. Current antiplatelet therapies come with a risk of bleeding, so treatments targeting new pathways that preserve haemostasis are needed. Two potential inter-related candidates being investigated in this thesis are collagen and fibrin(ogen) receptor GPVI, which has a major role in thrombosis but a minor one in haemostasis, and phosphoinositides and their associated kinase/phosphatases, which are involved in Ca^{2+} mobilisation and regulation of pleckstrin homology (PH) domains-containing proteins.

The key to efficient GPVI and phosphoinositides targeting is understanding the interconnections between the proteins and lipid intermediates. In this thesis, I have developed an ion chromatography-mass spectrometry (IC-MS) based method to differentiate the phosphoinositides' positional isomers, particularly PtdIns(3,4)P_2 and PtdIns(3,5)P_2. This is followed by the development of a mathematical model that can simulate phosphoinositides metabolism upon GPVI activation. Our model predicts the effect of phosphatidylinositol 4-kinase A (PI4KA) inhibitor GSK-A1 on inositol triphosphate ($InsP_3$) and Ca^{2+} mobilisation, demonstrating its role on PtdIns(4,5)P_2 resynthesis to sustain downstream signalling.

I further investigate the role of tyrosine kinase inhibitors, integrin αIIbβ3 and GPVI antagonists in GPVI activation and platelet aggregation. The results show that collagen-related peptide (CRP)-induced sustained tyrosine phosphorylation is reversed upon inhibition of GPVI signalling but not aggregation in light transmission aggregometry (LTA), and that platelet disaggregation depends on the choice of agonist and the presence of shear based on published data. I have developed a dimer and tetramer of the GPVI-blocking nanobody, nanobody 2 (Nb2). My results show that Nb2 dimer Nb2-2 is a more potent antagonist than Nb2 against GPVI, while Nb2 tetramer

Nb2-4 acts as a potent GPVI agonist at the nanomolar range making it the first agonist for GPVI in human platelets of known stoichiometry. We have further developed an ordinary differential equation (ODE) based model to illustrate the relation of ligand valency with GPVI clustering and activation. Overall, this suggests that dimerisation of GPVI alone does not induce activation of human platelets, and a tetravalent but not a divalent ligand induces measurable GPVI clustering and activation. The dimeric ligand Nb2-2 has the potential to be developed into a viable antithrombotic. The tetravalent nanobody is the first agonist of known stoichiometry for GPVI and could be used to enable the comparison of results between laboratories and a clinically defined test for the study of platelet function.

Publications arising from this thesis

Cheung, H. Y. F., Coman, C., Westhoff, P., Manke, M., Sickmann, A., Borst, O., Gawaz, M., Watson, S. P., Heemskerk, J. W., and Ahrends, R. 2021. 'Targeted phosphoinositides analysis using high-performance ion chromatography-coupled selected reaction monitoring mass spectrometry', J. Proteome Res., 20: 3114-23.

Cheung, H. Y. F., Moran, L. A., Sickmann, A., Heemskerk, J. W., Garcia, Á., and Watson, S. P. 2022. 'Inhibition of Src but not Syk causes weak reversal of GPVI-mediated platelet aggregation measured by light transmission aggregometry', Platelets, 33: 1293-300.

Cheung, H. Y. F., Zou, J., Tantiwong, C., Fernandez, D. I., Huang J., Ahrends R., Roest M., Cavill R., Gibbins J. and Heemskerk, J.W.M. 'High-throughput assessment identifying major platelet Ca^{2+} entry pathway via tyrosine kinase-linked and G protein-coupled receptors'. Submitted to Cell Calcium.

Clark, J. C., Damaskinaki, F.-N., **Cheung, Y. F. H.**, Slater, A., and Watson, S. P. 2021. 'Structure-function relationship of the platelet glycoprotein VI (GPVI) receptor: does it matter if it is a dimer or monomer?', Platelets, 32(6): 724-32.

Fernández, D. I., Provenzale, I., **Cheung, H. Y. F.**, van Groningen, J., Tullemans, B. M., Veninga, A., Dunster, J. L., Honarnejad, S., van den Hurk, H., and Kuijpers, M. J. 2022. 'Ultra-high-throughput Ca2+ assay in platelets to distinguish ITAM-linked and G-protein-coupled receptor activation', Iscience, 25: 103718.

Maqsood, Z., Clark, J. C., Martin, E. M., **Cheung, Y. F. H.**, Morán, L. A., Watson, S. E., Pike, J. A., Di, Y., Poulter, N. S., and Slater, A. 2022. 'Experimental validation of computerised models of clustering of platelet glycoprotein receptors that signal via tandem SH2 domain proteins', PLoS Comp. Biol., 18: e1010708.

Borgmeyer, M., Coman, C., Has, C., Schött, H.-F., Li, T., Westhoff, P., **Cheung, Y. F.**, Hoffmann, N., Yuanxiang, P., and Behnisch, T. 2021. 'Multiomics of synaptic junctions reveals altered lipid metabolism and signaling following environmental enrichment', Cell Rep., 37: 109797.

Zhi, Z., Jooss, N. J., Sun, Y., Colicchia, M., Slater, A., Moran, L. A., **Cheung, H. Y. F.**, Di, Y., Rayes, J., and Poulter, N. S. 2022. 'Galectin-9 activates platelet ITAM receptors glycoprotein VI and C-type lectin-like receptor-2', J. Thromb. Haemost., 20: 936-50.

D'alessandro E., Becker C., Bergmeier W., Bode C., Bourne J.H., Brown H., Buller H.R., Ten Cate-Hoek A., Ten Cate V., Van Cauteren Y.J., **Cheung Y.F.**, Cleuren A., Coenen D., Crijns H.J., De Simone I., Dolleman S.C., Klein C.E., Fernandez D.I., Granneman L., Van 'T Hof A., Henke P., Henskens Y.M., Huang J., Jennings L.K., Jooss N.J., Karel M., Van

Den Kerkhof D., Klok F.A., Kremers B., Lämmle B., Leader A., Lundstrom A., Mackman N., Mannucci P.M., Maqsood Z., Van Der Meijden P.E., Van Moorsel M., Moran L.A., Morser J., Van Mourik M., Navarro S., Neagoe R.A., Olie R.H., van Paridon P., Posma J., Provenzale I., Reitsma P.H., Scaf B., Schurgers L., Seelig J., Siegbahn A., Siegerink B., Soehnlein O., Soriano E.M., Sowa M.A., Spronk H.M., Storey R.F., Tantiwong C., Veninga A., Wang X., Watson S.P., Weitz J., Zeerleder S.S., Ten Cate, H. 2020. 'Thrombo-inflammation in cardiovascular disease: an expert consensus document from the third Maastricht consensus conference on thrombosis', Thromb. Haemost., 120: 538-64.

Acknowledgements

I would like to express my sincere gratitude to all the people who have supported me in my journey of completing my PhD over the past four years. These four years have been a period full of challenges, such as relocating to different countries and adapting to the various visa policies and the COVID pandemic.

I am deeply indebted to the TAPAS programme, which generously provided me with both financial and administrative support throughout my PhD journey. I am also immensely thankful to Professor Steve Watson, my primary supervisor, who guided me with his continuous support and review of my works, manuscripts, and thesis. His enthusiasm and commitment were instrumental in inspiring me to complete my PhD.

I started my PhD at ISAS in Dortmund, and I am immensely thankful to Professor Robert Ahrends for offering me the opportunity to pursue my research in mass spectrometry and lipidomics. I am also grateful to Professor Albert Sickmann for providing the necessary funds and resources to the institute. I am also very thankful to Cristina, Bing and Philipp, who trained me in LCMS and helped me with fixing the instrument when it malfunctioned. I am also thankful to Jingnan for helping me settle in Dortmund and search for rentals.

At the University of Birmingham, I would like to thank Luis for working and publishing several works with me and for being a joy to work and talk with. I am also deeply thankful to Alex for training and helping me in molecular biology and protein purification. I am also grateful to Zahra, Jo, Fay, and Harry for the collaborative works and papers we published together. I would like to express my gratitude to Caroline, who helped me with the administrative work and organising the TAPAS events. I am also thankful to Xueqing for helping me settle in

Birmingham, searching for rentals and supporting me during the lockdown.

At Maastricht University, I am thankful to my supervisor Professor Johan Heemskerk for his support and guidance in my research work. I am also thankful to Dr Marijke Kuipers for helping me integrate into the lab and for her support. I am also very grateful to Delia and Jinmi for the work and manuscripts we collaborated on. I am also thankful to Dr Joanne Dunster and Chukiat at the University of Reading for their help and support in the collaborative modelling work.

Finally, I need to express my immense gratitude to my family, who have been supportive of my work and research throughout these four years, despite not having the chance to meet them during this period due to my studies and the pandemic. I am forever thankful to all the people who have made this journey possible. Without their support and guidance, I would not have been able to complete my PhD.

Table of contents

Chapter 1 General introduction **1**

1.1 Platelets in thrombosis and haemostasis 1
1.1.1 Role of platelets in thrombotic disorders 1
1.1.2 Role of platelets in haemostasis 2
1.1.3 Platelet tethering and activation 2
1.1.4 Platelet spreading 3
1.1.5 Platelet degranulation and thromboxane formation 4
1.1.6 Integrin activation 4
1.1.7 The interplay between the coagulation cascade and platelets 4
1.1.8 Structure of the thrombus 5

1.2 Platelet receptors and signalling 6
1.2.1 GPVI 6
1.2.2 Role of GPVI in thrombosis and haemostasis 9
1.2.3 CLEC-2 10
1.2.4 G protein-coupled receptors 12
1.2.5 Integrin αIIbβ3 14

1.3 Phosphoinositides in platelets 15
1.3.1 History of studies on phosphoinositide 16
1.3.2 Phosphoinositides in platelets 17
1.3.3 Role and regulation of PI3K in platelets 19
1.3.3.1 Class I PI3Ks 19
1.3.3.2 Class II PI3K 21
1.3.3.3 Class III PI3K 22
1.3.4 PI3K as an antithrombotic target 22
1.3.5 PLC and Ca^{2+} haemostasis 24
1.3.5.1 Role and regulation of PLC 24
1.3.5.2 Ca^{2+} mobilisation and haemostasis 25
1.3.6 Measurement of phosphoinositides 26

1.4 Systems biology and mathematical modelling 28
1.4.1 Ordinary differential equation-based model 28

1.4.2 Kinetic modelling of biological networks 29
1.4.3 Mathematical models describing the biology of platelets 30

1.5 Aims of this thesis 32

Chapter 2 Materials and methods 34

2.1 Materials 35
2.1.1 Reagents 35
2.1.2 Antibodies 36

2.2 Methods 36
2.2.1 Preparation of human washed platelets and cell culture 36
2.2.2 OP9 Cell culture 37
2.2.3 P2 fraction preparation from rat hippocampal tissue 37
2.2.4 Expression and purification of nanobodies 38
2.2.4.1 Extraction of plasmid DNA from E. coli cells 38
2.2.4.2 Transformation of competent E. coli cells 38
2.2.4.3 Expression and purification of nanobodies 38
2.2.5 Phosphoinositides sample preparation, extraction and analysis 39
2.2.5.1 Platelet stimulation experiment 39
2.2.5.2 Phosphoinositides extraction 40
2.2.5.3 IC−MS/MS 40
2.2.6 $InsP_1$ and Ca^{2+} mobilisation measurement 41
2.2.6.1 Platelet Isolation and Loading with Fura-2 41
2.2.6.2 Cytosolic Ca^{2+} Measurements 42
2.2.6.3 Platelet stimulation and $InsP_1$ ELISA 42
2.2.7 Light transmission aggregometry 43
2.2.8 Platelet stimulation for tyrosine phosphorylation study 43
2.2.9 SDS-PAGE and Western blot 44
2.2.10 Flow cytometry 44
2.2.11 Surface plasmon resonance 45
2.2.12 Data and statistical analysis 45

Chapter 3 Targeted phosphoinositides analysis using high-performance ion

chromatography-coupled selected reaction monitoring mass spectrometry 47

3.1 Introduction 48

3.2 Aims 50

3.3 Results 51
3.3.1 Establishing profiling strategies for phosphoinositides. 51
3.3.1.1 Extraction strategies for phosphoinositides. 51
3.3.1.2 Optimisation of IC method for phosphoinositides analysis. 53
3.3.1.3 Quantification of phosphoinositides using targeted mass spectrometry. 55
3.3.2 Phosphoinositides profile in biological samples. 60
3.3.2.1 Phosphoinositides profile in resting and stimulated human platelets. 60
3.3.2.2 Phosphoinositides profile in OP9 pre-adipocytes and rat hippocampus. 63

3.4 Discussion 63

Chapter 4 Development of a mathematical model of platelet phosphoinositide metabolism 66

4.1 Introduction 67

4.2 Aims 69

4.3 Results 70
4.3.1 Development of mathematical model on phosphoinositides metabolism downstream of GPVI signalling 70
4.3.1.1 Details of the model network, reactions and parameters 70
4.3.2 Time course profiling of protein phosphorylation and Ca^{2+} mobilisation in CRP-stimulated platelets 77
4.3.3 Time course profiling of phosphoinositides in CRP-stimulated platelets 79
4.3.4 CRP-induced accumulation of $InsP_1$ in platelet 81
4.3.5 Model calibration and comparing model simulations with experimental profile 82

4.3.6 Model prediction of the effect of phosphoinositides kinase and phosphatase inhibitors 85
4.3.7 Effect of phosphoinositides kinase/phosphatase inhibitors on Ca^{2+} mobilisation 89
4.3.8 Validation of model using $InsP_1$ measurement and phosphoinositides kinase/phosphatase inhibitors 92

4.4 Discussion 95

Chapter 5 Inhibition of src causes weak reversal of gpvi-mediated platelet aggregation as measured by light transmission aggregometry 99

5.1 Introduction 100

5.2 Aims 103

5.3 Results 104
5.3.1 Tyrosine kinase inhibitors reverse GPVI-mediated tyrosine phosphorylation 104
5.3.2 GPVI-induced platelet aggregation is minimally reversed by the addition of inhibitors of Src but not Syk and Btk inhibitors 107
5.3.3 Platelet aggregation is sustained in the presence of tyrosine kinase inhibitors when combined with apyrase and indomethacin 109
5.3.4 Tyrosine kinase inhibitors partially reversed GPVI-mediated platelet aggregation together with integrin αIIbβ3 antagonist 111
5.3.5 Tyrosine kinase inhibitors reverse integrin αIIbβ3 activation 112

5.4 Discussion 113

Chapter 6 Experimental validation of computerised models of clustering of platelet glycoprotein receptors that signal via tandem sh2 domain proteins 115

6.1 Introduction 116

6.2 Aim 118

6.3 Results 119

6.3.1 Cloning, purification and characterisation of Nb2-2 and Nb2-4 119
6.3.2 Nb2 and Nb2-2 inhibit GPVI-mediated platelet aggregation 121
6.3.3 Nb2-4 induces GPVI-mediated platelet aggregation 123
6.3.4 Nb2-4 induced GPVI-mediated protein phosphorylation, which was delayed by Nb2 124
6.3.5 Using the ODE model to monitor ligand binding and clustering 127
6.3.5.1 ODE modelling of the interaction of monovalent ligands and receptors 127
6.3.5.2 ODE modelling of the interaction of divalent ligands and receptors 129
6.3.5.3 ODE modelling of the interaction of tetravalent ligands and receptors 131

6.4 Discussion 133

Chapter 7 General discussion 136

7.1 Summary of results 137

7.2 The platelet phosphoinositide metabolism as an antithrombotic target 138
7.2.1 A comprehensive method for quantifying platelet phosphoinositide isomers 138
7.2.2 Spatial-temporal model of conversions in phosphoinositide metabolism 140
7.2.3 Expanding the scope of the phosphoinositide conversion model 141
7.2.4 Targeting the platelet phosphoinositide metabolism beyond class I PI3K isoforms 143

7.3 Platelet receptor GPVI as an antithrombotic target 144
7.3.1 Method-dependent reversal of GPVI-induced platelet aggregation 144
7.3.2 Development of nanobody Nb2-2 as a GPVI-blocking agent 145
7.3.3 Development of Nb2-4 as a platelet GPVI agonist 147
7.3.4 Improved modelling of GPVI receptor clustering 148

7.4 Conclusions 150

Chapter 8 Appendix **151**

Chapter 9 References **154**

List of Figures

Figure 1.1 Schematic diagram of major platelet receptors involved in platelet activation. 3
Figure 1.2 Schematic diagram of spatial heterogeneity of thrombus. 6
Figure 1.3 Schematic diagram of the signalling cascade of platelet receptors GPVI and CLEC-2. 12
Figure 1.4 Structures of phosphoinositides isomers. 15
Figure 1.5 Schematic diagram of phosphoinositide signalling upon GPVI activation. 19
Figure 1.6 PI3K isoforms and their associated platelet receptors. 21
Figure 3.1 Flowchart for the analysis of targeted phosphoinositides analysis using an IC-MS system. 52
Figure 3.2 Extraction efficiency of the phosphoinositides extraction and derivatisation workflow. 52
Figure 3.3 Comparison of IC gradients. 54
Figure 3.4 Elution time stability of gradient C. 55
Figure 3.5 GroPInsPs fragment ion spectra. 57
Figure 3.6 Internal standard calibration curve for absolute quantification of GroPInsPs. 59
Figure 3.7 Limit of detection and limit of quantification of PtdIns(3,4,5)P_3. 59
Figure 3.8 Resting phosphoinositides amount in platelets, OP9 pre-adipocytes, and rat hippocampus heavy membrane fraction. 61
Figure 3.9 Effect of CRP and thrombin on human platelets phosphoinositides profile. 62
Figure 4.1 Network diagram of the phosphoinositides metabolism model. 72
Figure 4.2 CRP-induced sustained tyrosine phosphorylation and Ca^{2+} mobilisation and the determination of *stim* function. 78
Figure 4.3 CRP-induced changes in phosphoinositides profile in human platelet. 80
Figure 4.4 CRP induced sustained accumulation of $InsP_1$. 81
Figure 4.5 Assessing parameter fitting with cost function and range of parameters approximations. 83
Figure 4.6 Comparison of model simulation profile with experimental data. 84

Figure 4.7 Schematic diagram of the phosphoinositides metabolism in the model and the mode of action of GSK-A1 and YU142670. 86
Figure 4.8 Simulation of the effect of YU142670 on phosphoinositides metabolism. 87
Figure 4.9 Simulation of the effect of GSK-A1 on phosphoinositides metabolism. 88
Figure 4.10 Effect of GSK-A1 and YU142670 on Ca^{2+} mobilisation. 91
Figure 4.11 Comparison of experimental data and model predictions on the effect of GSK-A1 and YU142670 on $InsP_1$ accumulation. 94
Figure 5.1 Tyrosine phosphorylation is sustained in GPVI-mediated protein phosphorylation. 105
Figure 5.2 Kinase inhibitors reverse GPVI-mediated protein phosphorylation. 106
Figure 5.3 Src kinase inhibitor PP2 partially reversed GPVI-mediated platelet aggregation. 108
Figure 5.4 Kinase inhibitors together with secondary mediators partially reversed GPVI-mediated platelet aggregation. 110
Figure 5.5 Tyrosine kinase inhibitors partially reversed GPVI mediated platelet aggregation together with integrin αIIbβ3 antagonist..... 111
Figure 5.6 Tyrosine kinase inhibitors reverse integrin αIIbβ3 activation. 112
Figure 6.1 Domain structure and size comparison of human IgG, Fab fragment, camelid antibody and nanobody. 117
Figure 6.2 Cloning, purification and characterisation of Nb2-2 and Nb2-4. 120
Figure 6.3 Nb2 and Nb2-2 are potent GPVI antagonists. 122
Figure 6.4 Nb2-4 induces GPVI-mediated aggregation. 123
Figure 6.5 Nb2-4 induced GPVI-mediated protein phosphorylation. 125
Figure 6.6 Nb2 delays Nb2-4 induced protein phosphorylation. 126
Figure 6.7 Interaction of monovalent ligand with receptor. 128
Figure 6.8 Interaction of divalent ligand with receptor. 130
Figure 6.9 Interaction of tetravalent ligand with receptor. 132
Figure 6.10 Schematic diagram of Nb2 delaying Nb2-4 induced GPVI clustering. 134
Figure 7.1 Summary representation of GPVI-mediated platelet signalling cascades. 138

Figure 7.2 Proposed expansion of the phosphoinositides model. 143
Figure 8.1 Posterior parameter ranges for s_1 and θ_6. 153
Figure 8.2 Donor variability in the production of PtdIns(3,4,5)P_3. 153

List of Tables

Table 2.1 Details of the antibodies used, target, host species, dilution and source 36
Table 3.1 SRM transition list used for GroPInsPs analysis. 56
Table 4.1 Variables and initial conditions for the mathematical models 1 and 2. 75
Table 4.2 Model parameters and fitting constraint in the phosphoinositides metabolism model. 76
Table 7.1 Summary of phosphoinositides isomers fold change 140
Table 8.1 Results of parameter fitting Model 1 to experimental data. 151
Table 8.2 Results of parameter fitting Model 2 to experimental data. 152

Abbreviations

ACD	Acid-citrate-dextrose
ADP	Adenosine diphosphate
ANOVA	Analysis of variance
ATP	Adenosine triphosphate
BSA	Bovine serum albumin
cAMP	Cyclic adenosine monophosphate
CLEC-2	C-type lectin-like receptor 2
COX	Cyclooxygenase
CRP	Collagen-related peptides
Cyt	Cyosol
DAG	1,2-diacylglycerol
DAPT	Dual antiplatelet therapy
DMSO	Dimethyl sulfoxide
DNA	Deoxyribonucleic acid
DOAC	Direct oral anticoagulant
DTS	Dense tubular system
DTT	Dithiothreitol
EC50	Half maximal effective concentration
ECL	Enhanced chemiluminescence
ECM	Extracellular matrix
EDTA	Ethylenediaminetetraacetic acid
EGTA	Ethylene glycol bis (2-aminoethyl ether)-N,N,N′,N′-tetraacetic acid
ELISA	Enzyme-linked immunosorbent assay
ER	Endoplasmic reticulum
ESI	Electrospray ionisation
EU	European Union
FA	Formic acid
Fab	Fragment antigen-binding
FBS	Fetal bovine serum
FcRγ	Fc receptor γ-chain
FDA	The United States Food and Drug Administration
GDP	Guanosine diphosphate
GPCR	G protein-coupled receptor
GPO	Glycine-proline-hydroxyproline
GPVI	Glycoprotein VI
GroPIns	Glycerophosphoinositol
GroPIns3P	Glycerophosphoinositol 3-phosphate
GroPIns4P	Glycerophosphoinositol 4-phosphate
GroPIns5P	Glycerophosphoinositol 5-phosphate
GroPIns(3,4)P_2	Glycerophosphoinositol 3,4-bisphosphate
GroPIns(4,5)P_2	Glycerophosphoinositol 4,5-bisphosphate

GroPIns(3,5)P_2	Glycerophosphoinositol 3,5-bisphosphate
GroPIns(3,4,5)P_3	Glycerophosphoinositol 3,4,5-trisphosphate
GTP	Guanosine triphosphate
HEPES	4-(2-hydroxyethyl)-1-piperazineethanesulfonic acid
HRP	Horseradish peroxidase
IC50	Half maximal inhibitory concentration
IC	Ion chromatography
IP	Prostacyclin receptor
$InsP_1$	Inositol monophosphate
$InsP_3$	Inositol 1,4,5-trisphosphate
IPA	Isopropyl alcohol
IPTG	Isopropyl β-D-1-thiogalactopyranoside
ITAM	Immunoreceptor tyrosine-based activation motif
K_D	Dissociation constant
KO	Knock out
KOH	Potassium hydroxide
LAT	Linker of activated T cells
LB	Lysogeny broth
LC	Liquid chromatography
LOD	Limit of detection
LOQ	Limit of quantification
LTA	Light transmission aggregometry
MCS	Multiple cloning site
MFI	Mean fluorescence intensity
MS	Mass spectrometry
MS2	Tandem mass spectrometry
N_2	Nitrogen
OCRL	Inositol polyphosphate 5-phosphatase
OD	Optical density
ODE	Ordinary differential equations
ORAI1	Calcium release-activated calcium channel protein 1
P110	Phosphatidylinositol-4,5-bisphosphate 3-kinase, catalytic subunit
$P2X_1$	$P2X_1$ ATP receptor
$P2Y_1$	$P2Y_1$ ADP receptor
$P2Y_{12}$	$P2Y_{12}$ ADP receptor
PAGE	Polyacrylamide gel electrophoresis
PAR	Protease-activated receptor
PBS	Phosphate-buffered saline
PDK1	Phosphoinositide-dependent kinase-1
PF4	Platelet factor 4
PGI_2	Prostaglandin I_2
PH	Pleckstrin homology
PI	Phosphatidylinositol
PI3K	Phosphoinositide 3-kinase

PI3KC2	Phosphatidylinositol-4-phosphate 3-kinase C2 domain
PI4K	Phosphatidylinositol 4-kinase
PIP4K	Phosphatidylinositol 5-phosphate 4-kinase
PIP5K	Phosphatidylinositol-4-phosphate 5-kinases
PITP	Phosphatidylinositol transfer protein
PKC	Protein kinase C
PLCβ	Phospholipase C-β
PLCγ2	Phospholipase C-γ2
PM	Plasma membrane
PRP	Platelet rich plasma
PS	Phosphatidylserine
PtdIns	Phosphatidylinositol
PtdIns3P	Phosphatidylinositol 3-phosphate
PtdIns4P	Phosphatidylinositol 4-phosphate
PtdIns5P	Phosphatidylinositol 5-phosphate
$PtdIns(3,4)P_2$	Phosphatidylinositol 3,4-bisphosphate
$PtdIns(4,5)P_2$	Phosphatidylinositol 4,5-bisphosphate
$PtdIns(3,5)P_2$	Phosphatidylinositol 3,5-bisphosphate
$PtdIns(3,4,5)P_3$	Phosphatidylinositol 3,4,5-trisphosphate
PTEN	Phosphatase and tensin homolog
QTRAP	Quadrupole ion trap
R^2	Coefficient of determination
RNA	Ribonucleic acid
RPLC	Reversed-phase liquid chromatography
SD	Standard deviation
SDS	Sodium dodecyl sulphate
SERCA	Sarcoendoplasmic reticulum Ca^{2+}-ATPase
SFK	Src family kinase
SH2	Src homology 2
SH3	Src homology 3
SHIP1	SH2-domain containing inositol phosphatase-1
SHIP2	SH2-domain containing inositol phosphatase-2
SLP-76	Lymphocyte cytosolic protein 2
SPR	Surface plasmon resonance
SRM	Selected reaction monitoring
SSE	Sum of square errors
TB	Terrific broth
TBS	Tris-buffered saline
TES	Tris/EDTA/Sucrose buffer
TIC	Total ion chromatogram
TP	Thromboxane receptor
TRAP-6	Thrombin receptor-activating peptide 6 (Sequence: SFLLRN)
TxA_2	Thromboxane A_2

VWF	von Willebrand factor
WT	Wild type
XIC	Extracted ion chromatogram

Chapter 1

General introduction

1.1 Platelets in thrombosis and haemostasis

1.1.1 Role of platelets in thrombotic disorders

Thrombotic disorders, which include arterial thrombosis, venous thrombosis and thrombo-inflammation, contribute to the pathophysiology of significant health problems such as heart attack, stroke, cancer, and infection. They are believed to be responsible for 40% of cardiovascular fatalities in the EU and cost the EU economy more than €200 billion each year (Timmis *et al.* 2020).

Arterial thrombosis is caused by the rupture of atherosclerotic plaque followed by the formation of platelet-rich arterial thrombi that can block blood vessels (Koupenova *et al.* 2017). Currently, dual-antiplatelet therapy (DAPT) is initially used for preventing platelet activation in arterial thrombosis, with patients treated with aspirin plus a platelet $P2Y_{12}$ receptor inhibitor, such as clopidogrel, prasugrel, or ticagrelor, before moving to long-term treatment with aspirin. Integrin αIIbβ3 inhibitors such as eptifibatide, abciximab, and tirofiban are also used but only in acute situations in the clinic, due to the bleeding risk associated with their use (Hall *et al.* 2011). While these therapeutics are helpful in a high proportion of patients, a considerable number of patients experience further thrombotic events that result in mortality, and treated patients may experience clinically meaningful bleeding that may necessitate blood transfusion, which in some cases can be deadly (Hall *et al.* 2011). Thrombo-inflammation refers to thrombosis driven by the interaction of thrombotic and inflammatory pathways, which occurs in deep-vein thrombosis, ischaemic stroke, and sepsis (Rayes *et al.* 2019). Current antiplatelet therapies are mostly unsuccessful against thrombo-inflammatory disorders, which are treated with anticoagulants such as heparin and direct oral anticoagulants (DOACs).

With an ageing population, the EU's unmet clinical demand for viable treatment regimens is expanding (Næss *et al.* 2007). This huge social issue necessitates the

development of new and better antiplatelet agents that effectively target thrombosis while maintaining haemostasis.

1.1.2 Role of platelets in haemostasis

Haemostasis prevents excessive bleeding/haemorrhage and contributes to blood vessel integrity. This process includes vasoconstriction to reduce blood loss, platelet adhesion and aggregation on the damaged vessel wall to form a platelet thrombus that covers the injury, and the activation of the coagulation cascade to create thrombin and a covalently cross-linked fibrin network that stabilises the thrombus.

1.1.3 Platelet tethering and activation

Upon vascular injury, platelets come into contact with the extracellular matrix (ECM) which contains platelet-activating proteins like collagen, fibronectin and laminin (Watson 2009), via surface receptors such as glycoprotein (GP) VI and integrin α2β1. Von Willebrand factor (VWF) in plasma binds to collagen in the ECM and interacts with the platelet VWF receptor GPIb-IX-V complex, which captures platelets on the collagen surface; this is especially important under high blood flow (Sadler 1998). Through a complex network of signal transduction, the adhered platelets become activated and undergo various processes including platelet spreading, degranulation of intracellular vesicles, activation of integrin αIIbβ3, and exposure of phosphatidylserine (PS) to promote platelet thrombus formation (Versteeg *et al.* 2013) (Figure 1.1).

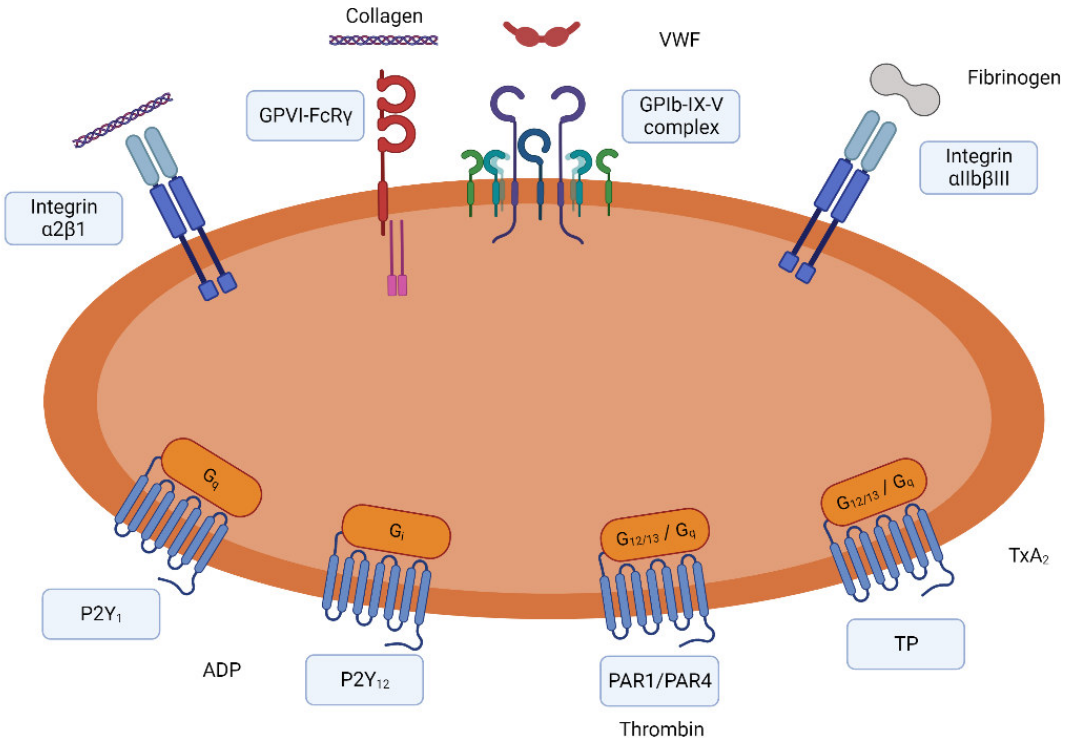

Figure 1.1 Schematic diagram of major platelet receptors involved in platelet activation. The tyrosine kinase-linked receptor GPVI and the G protein-coupled receptor (GPCR) for thromboxane A2 (TxA_2), thrombin, and ADP are the primary signalling receptors that mediate platelet activation. The VWF receptor GPIb-IX-V complex is required for platelet tethering, while integrins α2β1 and αIIbβ3 are required for stable adhesion and platelet aggregation. Figure created in biorender.com.

1.1.4 Platelet spreading

The capturing of platelets on the damaged surface leads to the reorganisation of the actin cytoskeleton, which results in platelet morphology change from the original biconcave shape to a distinctive ‘fried egg’ form, a process known as spreading (Hartwig 1992). During spreading, filopodia are grown from the platelets' perimeter, followed by the formation of lamellipodia and the movement of granules and organelles to the centre of the cell (Hartwig 1992). This increases the contact surface area of platelets with the damage site or with other platelets via adhesive proteins, promoting the adhesion of platelets on the surface and protecting the thrombus against the flow and shear stress of the blood vessels.

1.1.5 Platelet degranulation and thromboxane formation

Following platelet activation, platelets undergo degranulation of dense granules and α-granules which release soluble secondary mediators like ADP, Ca^{2+} and serotonin, and adhesive proteins like VWF and fibrinogen, respectively, and generate thromboxane A_2 (TxA_2) through cyclooxygenase (COX). ADP and TxA_2 are potent platelet agonists that enhance the activation of adhering platelets while also recruiting and activating other circulating platelets, promoting platelet aggregation and thrombus formation (Versteeg *et al.* 2013). Together with VWF and fibrinogen that crosslink and activate adjacent platelets, these secreted molecules act as positive feedback stimuli that support the formation of the thrombus.

1.1.6 Integrin activation

Platelet activation and aggregation are reinforced by integrin αIIbβ3 activation via inside-out signalling. Integrin αIIbβ3 is the most abundant surface protein on platelets. It undergoes a conformational change and converts into a high-affinity state, which increases its binding affinity with fibrin, fibrinogen, VWF and fibronectin to enhance its adhesion with the vasculature, and bridge platelets together, leading to aggregation (Huang *et al.* 2019). The binding of integrin αIIbβ3 with its ligands also activates platelets via outside-in signalling, further promoting platelet aggregation and supporting thrombus formation.

1.1.7 The interplay between the coagulation cascade and platelets

The blood coagulation system works in tandem with platelet activation in haemostasis (Heemskerk *et al.* 2002). Tissue factor is exposed to the circulation upon damage of blood vasculature (Yau *et al.* 2015). It activates the coagulation cascade and leads to the production of thrombin, a proteolytic enzyme that converts soluble fibrinogen into insoluble cross-linked strands of fibrin to stabilise the thrombus (Davie *et al.* 1991).

Thrombin and fibrinogen are important in haemostasis due to their essential role in both the coagulation cascade and platelet activation (Heemskerk *et al.* 2002). In addition to producing fibrin, thrombin is a potent platelet activator that activates platelet protease-activated receptors (PAR) 1 and 4 (De Candia 2012). Fibrinogen forms bridges between platelets via integrin αIIbβ3, which stabilises the thrombus at the site of injury, and activates platelets via integrin outside-in signalling, and other fibrinogen receptors, such as GPVI (Smyth *et al.* 2000).

The exposure of phosphatidylserine (PS) on the surface of activated platelets and damaged endothelial cells by PS translocase and scramblase also promotes the coagulation cascade (Reddy *et al.* 2020). PS exposure requires a consistently high level of cytosolic Ca^{2+} which occurs in platelets stimulated by the combination of strong agonists such as collagen and thrombin (Heemskerk *et al.* 2013). The anionic PS surface facilitates the assembly and activity of the tenase complex and prothrombinase complex and contributes to thrombin generation, which in turn promotes fibrin formation, platelet activation and thrombus growth (Heemskerk *et al.* 2013).

1.1.8 Structure of the thrombus

Thrombi contain an inner core of densely packed platelets and fibrin next to the damage site and an outer shell of loosely packed platelets bound together by fibrinogen (Ivanciu *et al.* 2015) (Figure 1.2). The platelets in the core are highly active, as evidenced by their drastic morphological change, and the region is weakly permeable to plasma solutes, limiting their accessibility to anti-platelet or thrombolytic drugs in plasma. They are strongly activated by thrombin, released by the coagulation cascade near the damaged site, secondary mediators ADP and TxA_2, produced by other activated platelets, and by fibrin and fibrinogen that activate integrin αIIbβ3 and GPVI. ADP and TxA_2 diffusing from the core make up the shell of a large number of

loosely packed platelets in their original biconcave form that are weakly activated. Because of the redundancy with thrombin, the creation of ADP and TxA_2 is important for the development of the shell but not the core in this model (Ivanciu *et al.* 2015). The core-shell heterogeneity has a profound implication on the action and design of anti-platelet and thrombolytic drugs.

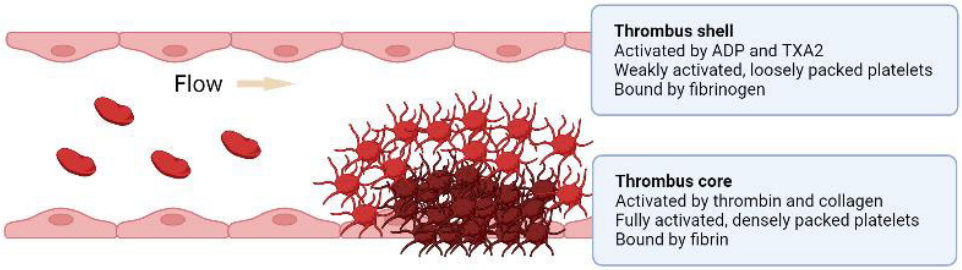

Figure 1.2 Schematic diagram of spatial heterogeneity of thrombus. Thrombi contain a core of densely packed platelets and fibrin and a shell of loosely packed platelets bound together by fibrinogen. Figure created in biorender.com.

1.2 Platelet receptors and signalling

Platelets interact with pro-aggregatory proteins and soluble secondary mediators as described above. Activation of these platelet receptors and their downstream signal transduction leads to Ca^{2+} mobilisation, vesicle degranulation, and shape change, all of which contribute to the platelet's role in thrombosis and haemostasis.

1.2.1 GPVI

Glycoprotein VI (GPVI) is a key signalling receptor involved in collagen-induced platelet activation, as well as a prospective antithrombotic target in diseases such as atherothrombosis, coronary artery thrombosis and ischaemic stroke. GPVI is only found on the membranes of megakaryocytes and platelets, at a level of around 3500 copies per human platelet (Nieswandt *et al.* 2003; Best *et al.* 2003). It is a member of the immunoglobulin receptor superfamily, with two external immunoglobulin domains,

D1 and D2, which are connected to the transmembrane domain by a glycosylated stem (Clark, Damaskinaki, *et al.* 2021). GPVI is constitutively associated with the Fc receptor γ-chain (FcRγ) which contains an immunoreceptor tyrosine-based activation motif (ITAM) in the cytoplasmic tail. An ITAM motif is formed by two YXXL/I sequences (where Y is tyrosine, L is leucine and I is isoleucine) separated by 6-12 amino acids. The FcRγ is a covalently linked homodimer, with one copy of ITAM in each chain. A salt bridge within the transmembrane regions of the two proteins is crucial for the interaction between GPVI and the FcRγ (Bori-Sanz *et al.* 2003). On platelets, the GPVI-FcRγ complex is expressed as a mixture of monomers and dimers (Clark, Neagoe, *et al.* 2021).

Collagen, an abundant subendothelial matrix protein, is the major endogenous ligand for GPVI and integrin α2β1 (Knight *et al.* 1999). GPVI binds to the collagen fibre at a distinct GPO (single amino acid code) sequence, where G is glycine, P is proline and O is hydroxyproline (Knight *et al.* 1999). To create a GPVI-specific ligand, Morton *et al.* synthesised collagen-related peptide (CRP) consisting of 10 repeats of GPO, cross-linked by cysteine or lysine, which caused integrin α2β1-independent platelet aggregation (Morton *et al.* 1995). Collagen and CRP are commonly used agonists for platelet studies.

GPVI can also be activated by a variety of multivalent endogenous ligands including; fibrinogen (Mangin *et al.* 2018), fibrin (Alshehri *et al.* 2015), laminin (Inoue *et al.* 2006), fibronectin (Bültmann *et al.* 2010), vitronectin (Schönberger *et al.* 2012), snake venom proteins such as convulxin (Horii *et al.* 2009), and the crosslinked anti-GPVI monoclonal antibodies (mAb) JAQ1 (Nieswandt *et al.* 2000) and 1G5 (Al-Tamimi *et al.* 2009). On the other hand, monovalent ligands such as fragment antigen-binding (Fab fragments) of anti-GPVI mAb glenzocimab (Lecut *et al.* 2003), 1G5 (Al-Tamimi *et*

al. 2009) and JAQ1 (Nieswandt *et al.* 2000), and the single-domain nanobody Nb2 (Slater *et al.* 2021) serve as GPVI antagonists.

Among these antagonists, glenzocimab has a dissociation constant (K_D) of 4.1 nM towards GPVI (Lebozec *et al.* 2017) and is currently in use in a phase 2 trial study in combination with a thrombolytic agent, in thrombotic stroke patients (Alenazy *et al.* 2021). The nanobody Nb2 has an even higher affinity towards GPVI with K_D = 0.6 nM, showing potential to be further developed as a therapeutic for treating cardiovascular diseases (Slater *et al.* 2021). One way to further improve the binding affinity is to multimerise the nanobody to enhance its affinity via avidity (Sadeghnezhad *et al.* 2019). On the other hand, multimeric ligands such as the octameric convulxin and crosslinked JAQ1 are known to activate GPVI. This warrants further studies to strike the balance between increasing binding affinity and preventing receptor activation.

Ligand binding leads to GPVI dimerisation and higher-order clustering. This leads to the phosphorylation of the ITAM motif of FcRγ by the constitutively active Src family kinases (SFKs) Fyn and Lyn, which bind to the proline-rich motif in the cytosolic domain on GPVI through their Src homology 3 (SH3) domain (Senis et al. 2014; Suzuki-Inoue et al. 2002; Watson et al. 2005). Afterwards, the spleen tyrosine kinase (Syk) is recruited and bound to the phosphorylated ITAM of FcRγ, via its tandem Src homology 2 (SH2) domain. Syk undergoes phosphorylation by Src kinases and autophosphorylation upon binding to the phosphorylated ITAM. (Spalton *et al.* 2009). This initiates the downstream signalling characterised by the formation of the linker for the activation of T-cells (LAT) signalosome complex, as well as recruitment and activation of the effector proteins Bruton's tyrosine kinase (Btk), phospholipase C gamma 2 (PLCγ2) and phosphoinositide 3-kinases (PI3K), resulting in platelet activation (Figure 1.3) (Zhang *et al.* 2000; Watson *et al.* 2005). The activation and

actions of PLCγ2 and PI3K are described in detail below.

1.2.2 Role of GPVI in thrombosis and haemostasis

Platelet collagen receptor GPVI plays a minor role in haemostasis, as GPVI deficiency has minimal effect on bleeding in humans or mice. In humans, a novel homozygous GPVI mutation that leads to GPVI deficiency has been reported to only cause a mild bleeding disorder despite a lack of platelet response to collagen or convulxin (Matus *et al.* 2013). A GPVI-blocking Fab fragment, glenzocimab, was reported to not affect bleeding times or platelet counts in healthy volunteers in a phase 1 trial (Voors-Pette *et al.* 2019). In mice, GPVI deficiency that is caused by GPVI knockout (Lockyer *et al.* 2006) or by immunodepletion by injection of anti-GPVI mAb JAQ1 (Nieswandt *et al.* 2001), does not increase tail bleeding time.

A possible explanation for these observations is that haemostasis is maintained by parallel platelet pathways. As mentioned above, upon vascular damage, platelets can be activated by thrombin and the secondary mediators ADP and TxA_2. The redundancy in GPVI and thrombin in platelet activation and haemostasis was shown using GPVI and PAR4 knockout mice (Bynagari-Settipalli *et al.* 2014). Platelets also contain numerous adhesive protein receptors which share roles with GPVI, such as the collagen receptor integrin α2β1 and VWF receptor GPIb-V-IX. In particular, VWF attaches to locations on exposed collagen in high-flow circumstances, exposing binding sites on the A1 domain for high-affinity binding with GPIb for platelet adhesion on the injured site (Clemetson 2012). The importance of VWF and GPIb-V-IX is demonstrated in Von Willebrand disease (VWD), a bleeding disorder that arises from VWF deficiency or function-disrupting mutations (Sadler 1998).

On the other hand, GPVI appears to be an important factor for thrombosis. GPVI deficiency caused by immunodepletion (Nieswandt *et al.* 2001) or knockout

(Lockyer *et al.* 2006) was reported to reduce mortality in mice that were challenged by lethal thrombin-induced acute pulmonary thromboembolism, with a reduction in platelet adhesion to collagen and thrombus growth. Similarly, GPVI immunodepletion or knockout protects mice from vessel occlusion in ferric chloride and mechanically-induced injury models, with delayed thrombus formation and reduced thrombus growth (Bender *et al.* 2011). The role of GPVI in thrombus growth and stability can be explained by its interaction with its agonists, fibrin and fibrinogen (Rayes *et al.* 2019).

Furthermore, GPVI drives thrombus development in atherosclerotic plaques. Type I collagen is a prominent component of atherosclerotic plaques, and its exposure during plaque erosion stimulates platelet activation and promotes clotting (Jiang *et al.* 2014). In a thrombosis model, in which blood was perfused at an arterial shear rate over homogenates of human atherosclerotic plaques, GPVI inhibition led to a huge reduction in thrombus development (Cosemans *et al.* 2005; Reininger *et al.* 2010).

In summary, GPVI plays a major role in thrombosis and a minor role in haemostasis. GPVI deficiency or inhibition delayed thrombus formation and reduced thrombus growth in various thrombosis models, making it an attractive anti-platelet target.

1.2.3 CLEC-2

The C-type lectin receptor 2 (CLEC-2) is a platelet-activating receptor that exists as a mixture of monomers and dimers on the platelet surface and is a single transmembrane protein containing a single YxxL, known as the hemITAM motif, in its cytosolic tail (Watson *et al.* 2010). Upon activation by the endogenous ligand podoplanin or snake venom protein rhodocytin, the hemITAM motif is phosphorylated by SFKs and Syk (Watson *et al.* 2010; Suzuki-Inoue *et al.* 2007; Séverin *et al.* 2011). This leads to Syk recruitment to the two phosphorylated hemITAMs in dimerised

CLEC-2 receptors (Hughes *et al.* 2010). The subsequent signalling events downstream of Syk are similar to that of GPVI, including the formation of the LAT signalosome and activation of a signalling cascade that culminates in the activation of PLCγ2 and PI3K (Figure 1.3) (Watson *et al.* 2010).

Similar to GPVI, CLEC-2 is activated by higher-order clustering of receptors by multivalent ligands. Rhodocytin is a heterotetramer of two α and β subunits and activates both mouse and human platelets (Hughes *et al.* 2010; Watson *et al.* 2008). Dimeric Fc-fusion podoplanin (Suzuki-Inoue *et al.* 2007) and the dimeric CLEC-2 mAb INU1 (May *et al.* 2009) promote aggregation of mouse platelets. However, monomeric INU1 Fab has no impact on mouse platelets. In human platelets, Fab fragments of the anti-CLEC-2 mAb AYP1 inhibit platelet activation triggered by rhodocytin, while crosslinking of the AYP1 Fab fragments with a secondary antibody induces platelet aggregation (Gitz *et al.* 2014). These observations suggest that the dimerisation of monomers or possibly pre-existing dimers is necessary to trigger CLEC-2 activation.

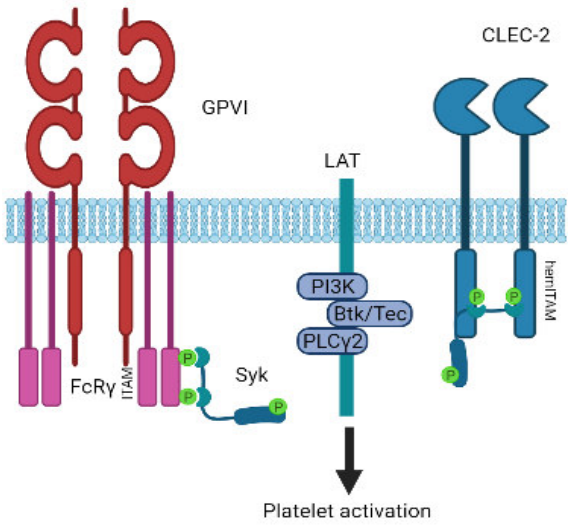

Figure 1.3 Schematic diagram of the signalling cascade of platelet receptors GPVI and CLEC-2. When GPVI is activated, the constitutively active SFKs Fyn and Lyn phosphorylate the tyrosine residues within the ITAM, permitting Syk recruitment and activation. For CLEC-2, the hemITAM motif is phosphorylated by SFKs and Syk, which then recruits and activates Syk. Subsequently, Syk phosphorylates and activates downstream proteins such as LAT. When LAT is phosphorylated, additional proteins including PI3K, Btk, and PLCγ2 are recruited and docked to create the LAT signalosome. These proteins are further phosphorylated which leads to platelet activation. Figure created in biorender.com.

1.2.4 G protein-coupled receptors

Another major class of platelet receptors are the G protein-coupled receptors (GPCRs). GPCRs are transmembrane proteins with seven transmembrane domains and are associated with heterotrimeric G proteins which are comprised of G_{α} and $G_{\beta\gamma}$ subunits. Upon ligand binding, a GPCR undergoes a conformational change and activates the associated G proteins by exchanging the G_{α}-bound guanosine diphosphate (GDP) with guanosine triphosphate (GTP), leading to its dissociation from the $G_{\beta\gamma}$ subunits. This exposes the GTP-bound G_{α} subunit to effector proteins that transduce downstream responses (Offermanns 2006; Smyth *et al.* 2009). In platelets, all four G protein families, G_s, G_i, G_q and $G_{12/13}$ can be found coupled with GPCRs, resulting in platelet-activating or inhibiting effects.

The major platelet-activating GPCRs are protease-activated receptor (PAR) 1 and PAR4, receptors for thrombin that are produced in the coagulation cascade (De Candia 2012). PARs are activated by a tethered ligand formed by thrombin cleavage of its N-terminal extracellular domain. PAR1 is the major thrombin receptor on human platelets, while PAR4 is a lower-affinity thrombin receptor and can form a heterodimer with the high-affinity PAR1 receptor (Arachiche *et al.* 2013). Another important set of platelet-activating GPCRs, $P2Y_1$ and $P2Y_{12}$, are receptors for ADP, a secondary mediator that is produced from dense granules during platelet activation and works with other agonists to facilitate platelet aggregation (Smyth 2010; Hardy *et al.* 2004). The TxA_2 receptor (TP) is yet another crucial platelet GPCR that is activated by TxA_2, a secondary mediator that is generated by COX (Smyth 2010; Hardy *et al.* 2004).

PAR1, PAR4 and TP are coupled to both $G_{12/13}$ and G_q (Offermanns 2006). The activation of G_q activates phospholipase C-β (PLCβ) which produces the secondary messengers inositol 1,4,5 trisphosphate ($InsP_3$) and 1,2-diacylglycerol (DAG), which are essential for Ca^{2+} mobilisation and PKC activation. $G_{12/13}$ on the other hand activates Rho and Rho kinase, which are associated with cytoskeletal rearrangements, platelet shape change and granule release (Offermanns 2006). $P2Y_1$ is only coupled to G_q which activates PLCβ, while $P2Y_{12}$ is coupled to $G_{iα}$ which activates the coupled PI3Kβ and PI3Kγ and its downstream kinase Akt upon ADP stimulation (van der Meijden *et al.* 2005).

Platelets also express inhibitory GPCRs, such as the prostacyclin I_2 (PGI_2) receptor IP and the adenosine A_{2A} receptor which keep platelets inactive in intact blood vessels (Nagy *et al.* 2018; Fuentes *et al.* 2014). They are coupled with G_s, which upon ligand stimulation activates adenylyl cyclase and produces cyclic adenosine monophosphate (cAMP). cAMP mediates its inhibitory effect by the activation of

protein kinase A (PKA), which inhibits PLC activation, Ca^{2+} mobilisation, and actin dynamics modulation (Nagy *et al.* 2018). These actions inhibit platelet adhesion, aggregation and granule release.

1.2.5 Integrin αIIbβ3

Integrin αIIbβ3 is a prominent integrin found on the surface of platelets (Smyth *et al.* 2000). It is the most abundant receptor on platelets and is critical in thrombus formation as the primary fibrin and fibrinogen binding receptor on platelets (Bennett 2005). Other endogenous ligands of integrin αIIbβ3 include VWF, fibronectin, thrombospondin and vitronectin (Huang *et al.* 2019; Cosemans *et al.* 2008).

Integrins are expressed on the cell surface in a low-affinity conformational state in resting platelets, leaving them unable to bind to their substrates (Huang *et al.* 2019). In response to activation and Ca^{2+} mobilisation, integrin αIIbβ3 undergoes inside-out activation and a conformational shift, allowing it to adopt a high-affinity conformation and undergo adhesion to fibrinogen and VWF, facilitating the formation of a thrombus (Shattil 1999). This inside-out activation of integrin αIIbβ3 is dependent on the activation of a variety of proteins, including small GTPase Rap1b, protein kinase C (PKC) and Ca^{2+} and DAG-regulated guanine nucleotide exchange factor I (CALDAG-GEFI), to stimulate the recruitment of proteins such as Talin-1 and Kindlin-3 to the integrin's intracellular tail (Nieswandt *et al.* 2009).

Ligand binding to integrin αIIbβ3 also leads to platelet activation via an outside-in signalling mechanism that relies on receptor clustering (Versteeg *et al.* 2013). This initiates a chain of events that includes the activation of the SFKs (Watson *et al.* 2005). This can result in direct but relatively weak stimulation of PI3K and PLCγ2 signalling, boosting intracellular Ca^{2+} levels and stimulating platelet activation (Cosemans *et al.* 2008).

1.3 Phosphoinositides in platelets

Phosphoinositides are a subcategory of glycerophospholipids with a wide range of functions. The eight known phosphoinositides positional isomers (Figure 1.4) are phosphatidylinositol (PtdIns), phosphatidylinositol 3-phosphate (PtdIns3P), phosphatidylinositol 4-phosphate (PtdIns4P), phosphatidylinositol 5-phosphate (PtdIns5P), phosphatidylinositol 4,5-bisphosphate (PtdIns(4,5)P_2), phosphatidylinositol 3,4-bisphosphate (PtdIns(3,4)P_2), phosphatidylinositol 3,5-bisphosphate (PtdIns(3,5)P_2), and phosphatidylinositol 3,4,5-trisphosphate (PtdIns(3,4,5)P_3). These unique lipids are produced by reversible phosphorylation of the *myo*-inositol headgroup of phosphatidylinositol, which is highly controlled by the interplay of phosphoinositides kinases, phosphatases, and phospholipases. The lipids are integral to the signal transduction system, and also serve as constitutive signals that aid in the identification of organelles and govern protein localisation and membrane integrity (Di Paolo *et al.* 2006; Balla 2013).

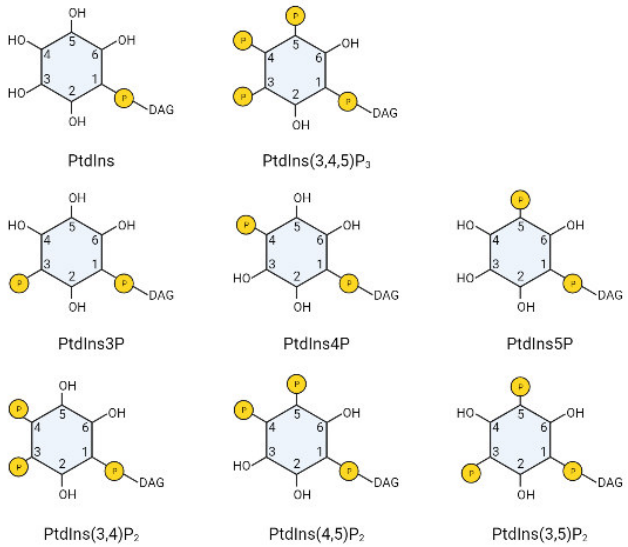

Figure 1.4 Structures of phosphoinositides isomers. Each phosphoinositide is a phospholipid with a *myo*-inositol headgroup that can undergo reversible phosphorylation. The yellow circle with P indicates a phosphate group, while DAG indicates the 1,2-diacylglycerol group.

1.3.1 History of studies on phosphoinositide

Phosphoinositides were first discovered by Folch in the 1940s, who found the lipid in the ethanol-insoluble phospholipid fraction of the bovine brain which contained phosphates and inositol in a molar ratio of 2:1. He termed this lipid diphosphoinositide or DPI (PtdIns4P) at the time (Folch 1942). DPI was also demonstrated to be rapidly labelled with [^{32}P]-phosphate in guinea pigs (Dawson 1954a, 1954b). The structures of mono-, di-, and tri-phosphoinositides (MPI, DPI, and TPI, equivalent to PtdIns, PtdIns4P and PtdIns(4,5)P_2) were subsequently identified as glycerophospholipids, with an inositol ring linked to a DAG backbone via the D1-OH group of *myo*-inositol, and containing a phosphate at the 4-position or both the 4- and 5-positions respectively (Figure 1.4) (Dittmer *et al.* 1961; Tomlinson *et al.* 1961).

These lipids gained increasing attention when their biological significance was unveiled. [^{32}P]-phosphate labelling in PtdIns4P and phosphatidic acid (PtdOH) was found to be dramatically elevated in brain slices and pancreas slices with an increased secretory response (Hokin *et al.* 1953; Hokin *et al.* 1955; Hokin 1968). Another study showed that lymphocytes stimulated with growth factor phytohemagglutinin had increased phosphoinositide turnover, represented by enhanced [^{32}P]-phosphate and [^{3}H]-inositol labelling of PtdIns4P and PtdOH (Fisher *et al.* 1971), linking phosphoinositide turnover to cellular functions.

With these observations, Michell and Lapetina suggested that the enhanced phosphoinositide turnover was due to the stimulation of cell surface receptors and that the hydrolysis products of phosphoinositides act as secondary messengers (Lapetina *et al.* 1973). This was later proven by a series of studies, with PtdIns(4,5)P_2 being first shown as the initial target of PLC-mediated hydrolysis, yielding InsP_3 and DAG as the primary hydrolytic product (Berridge *et al.* 1983; Berridge 1983; Creba *et al.* 1983). This was followed by the work of Streb *et al.* discovering the role of InsP_3 in Ca^{2+}

release from Ca^{2+} stores, linking PtdIns(4,5)P_2 hydrolysis and Ca^{2+} signalling (Streb *et al.* 1983). The other hydrolysis product of PLC and PtdIns(4,5)P_2, DAG, was also found to regulate the PKC family by Nishizuka (Nishizuka 1988, 1984). These studies established the PtdInsP_2-PLC-Ca^{2+}-PKC signalling cascade.

The discovery of the PI3K-Akt pathway began in the late 1980s and 1990s, with the identification of PtdIns kinase that phosphorylated the 3-postion of the inositol ring (Stephens *et al.* 1989; Whitman *et al.* 1988) and the subsequent discovery of PtdIns(3,4)P_2 and PtdIns(3,4,5)P_3 in cells stimulated with growth factor. This is followed by the discovery of Akt kinase as the downstream effector of PI3K (Burgering *et al.* 1995; Franke *et al.* 1995), and the Pleckstrin homology (PH) domains as PtdIns(3,4,5)P_3–binding domains in signalling proteins that allow their recruitment and activation (Kavran *et al.* 1998; Lemmon *et al.* 1995). The importance of the PI3K-Akt pathway in oncological signalling, cell growth and proliferation was also recognised during this period (Vivanco *et al.* 2002; Engelman *et al.* 2006).

1.3.2 Phosphoinositides in platelets

The study of phosphoinositides in platelets took place alongside the studies mentioned above. Numerous studies have observed that collagen (Narita *et al.* 1985; Gaudette *et al.* 1990), thrombin (Mauco *et al.* 1984) and the TP agonist U46619 (Gaudette *et al.* 1990) lead to a transient decrease in PtdIns4P and PtdIns(4,5)P_2 due to PLC hydrolysis, followed by a delayed rise during stimulation. Thrombin was also found to greatly increase PtdIns(3,4)P_2 and PtdIns(3,4,5)P_3 in [^{3}H]-inositol-labelled platelets (Gaudette *et al.* 1990; Yamamoto *et al.* 1990; Kucera *et al.* 1990; Nolan *et al.* 1991). The role of PtdIns(4,5)P_2 and PLC in collagen signalling was also demonstrated in studies showing that collagen induces rapid [^{3}H]-inositol bis- and trisphosphate formation by phosphodiester bond cleavage (Watson, Reep, *et al.* 1985).

Phosphoinositide metabolism is essential in platelet activation and regulation. PtdIns(4,5)P_2 and PtdIns(3,4,5)P_3 are important signalling molecules in signal transduction (Figure 1.5). Platelets contain several PLC isoforms, including PLCγ2 and PLCβ2, which are activated by the tyrosine kinase-linked receptors, GPVI and CLEC-2, and GPCRs, respectively. They hydrolyse the polar head group of PtdIns(4,5)P_2 to generate DAG, an activator of PKC, and InsP_3, which stimulate Ca^{2+} release from the endoplasmic reticulum (Brass *et al.* 1985; Min *et al.* 2013). Platelets contain class I PI3Ks, which convert PtdIns(4,5)P_2 to PtdIns(3,4,5)P_3 downstream of GPVI and GPCR signalling. PtdIns(3,4,5)P_3 binds to the PH domain of several platelets signalling proteins including Btk, Akt, and PDK1 to organise highly active signalling complexes (Guidetti *et al.* 2015; Saito *et al.* 2001; Hongu *et al.* 2014).

In addition to their role in signalling, phosphoinositides regulate membrane dynamics. PtdIns(4,5)P_2 can regulate ion channel permeability or cytoskeleton rearrangement (Kolay *et al.* 2016). PtdIns(3,4)P_2 may contribute to strengthening platelet aggregation by regulating actin cytoskeleton dynamics, including the actomyosin system and potentially podosome-like structures via its interaction with the adapter proteins Tks4 and Tks5 (Anquetil *et al.* 2018). PtdIns3P interacts with proteins through an FYVE or phox homology (PX) domain to control endosomal membrane dynamics via Early Endosome Antigen 1 (EEA1) and regulate vesicle transport between the trans-Golgi network, endosomes and plasma membrane, via sorting nexin 9 (SNX9) (Ribes *et al.* 2020; Schink *et al.* 2013). Depletion or inactivation of phosphatidylinositol 4-phosphate 3-kinase C2α (PI3KC2α) in platelets leads to a deficiency in thrombus formation (Valet *et al.* 2015), showing the importance of the housekeeping PtdIns3P pool in the regulation of membrane remodelling, and proper platelet synthesis and function.

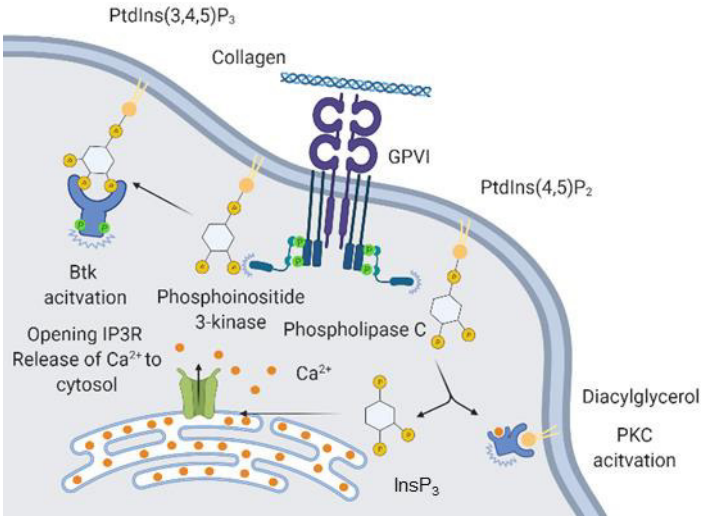

Figure 1.5 Schematic diagram of phosphoinositide signalling upon GPVI activation. GPVI activation culminates in the activation of PLCγ2 and PI3K. PLCγ2 hydrolyses the polar head group of PtdIns(4,5)P_2, to generate DAG, an activator of PKC, and $InsP_3$, which stimulate Ca^{2+} release from the endoplasmic reticulum. PI3K converts PtdIns(4,5)P_2 to PtdIns(3,4,5)P_3 which binds and activates platelet signalling proteins including Btk, Akt and PDK1 to organise highly active signalling complexes. Figure created in biorender.com.

1.3.3 Role and regulation of PI3K in platelets

1.3.3.1 Class I PI3Ks

The class I PI3Ks are essential in ITAM and GPCR-mediated signalling. They convert PtdIns(4,5)P_2 into the secondary messenger PtdIns(3,4,5)P_3, which recruits their major downstream effector, serine/threonine kinase Akt, via the PH domain. They are critical in the regulation of outside-in and inside-out signalling of integrin αIIbβ3 and platelet activation (Woulfe 2010). PI3K and Akt contribute to inside-out signalling of integrin via the small GTPase Rap1b, which leads to a conformational change of integrin αIIbβ3 that increases its affinity for fibrinogen, allowing platelet adhesion in the formation of thrombus (Guidetti *et al.* 2012; Stefanini *et al.* 2010).

Class I PI3Ks are heterodimers composed of a 110-kDa catalytic subunit associated with a regulatory subunit and are divided into two classes: IA and IB (Figure 1.6) (Balla 2013). Class IA PI3Ks include one of three catalytic subunits: P110α, -β

and -δ isoforms, which are associated with one of the regulatory subunits: P85α, P85β, P55α, P55γ and P50α. These regulatory subunits contain SH3 and SH2 domains that bind to phosphotyrosine downstream of GPVI signalling cascade, which allows the exposure and activation of the catalytic domain of P110 (Guidetti *et al.* 2015; Durrant *et al.* 2020). Class IB PI3Ks include the catalytic subunit P110γ, associated with p101 or p84/p87, which are typically activated downstream of GPCRs, such as PAR, TP, $P2Y_1$ and $P2Y_{12}$ (Guidetti *et al.* 2015; Durrant *et al.* 2020).

Human platelets express all Class I PI3K isoforms, and the expression level of these isoforms is in the order of P110β>P110γ>P110α>P110δ (Kim *et al.* 2014). These four isoforms play an overlapping but non-redundant role in platelet activation. Among these isoforms, P110β is essential for PtdIns(3,4,5)P3 production and Akt phosphorylation as demonstrated by P110β knockout mice and P110β specific inhibitor TGX221 (Canobbio *et al.* 2009; Jackson *et al.* 2005; Cosemans *et al.* 2006; Martin *et al.* 2010). It plays a central role in both GPVI and GPCR-mediated activation and is probably a co-incidence detector that is synergistically activated by phosphorylation of ITAM receptors and Gβγ subunits (Kurosu et al. 1997; Maier et al. 1999). Platelet PI3Kβ is demonstrated to be essential for preserving the generated thrombus integrity under elevated shear rates, raising the possibility of embolisation when using PI3Kβ inhibitors (Laurent et al. 2015). Studies using P110γ inactive or KO mice showed that P110γ is essential for ADP-induced platelet aggregation and Akt phosphorylation, but is less essential in GPVI or thrombin-mediated activation (Canobbio *et al.* 2009; Martin *et al.* 2010). P110α cooperates with P110β to contribute to GPVI and insulin-like growth factor-1 (IGF-1) mediated Akt phosphorylation (Gilio *et al.* 2009; Blair *et al.* 2014; Kim *et al.* 2007), while PI3Kδ only plays a minor role in platelet function (Senis *et al.* 2005).

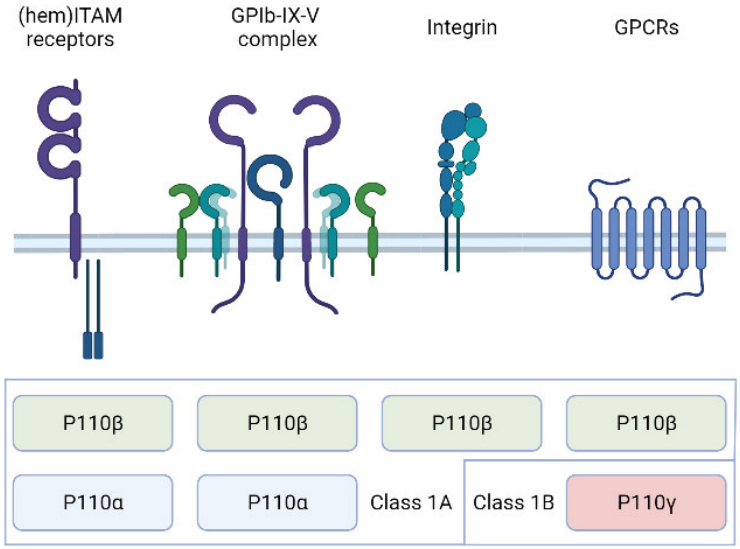

Figure 1.6 PI3K isoforms and their associated platelet receptors. The four major types of platelet receptors that lead to platelet activation are all associated with PI3K. (hem)ITAM receptors (such as GPVI and CLEC-2) and the VWF receptor GPIb-IX-V complex are associated with both P110β and P110α. Integrins (such as integrin α2β1 and αIIbβ3 are associated with P110β, and GPCRs are associated with both P110β and P110γ. Figure created in biorender.com.

1.3.3.2 Class II PI3K

The class II PI3K PI3KC2 has three isoforms: PI3KC2α, -β and –γ. They catalyse the conversion of PtdIns to PtdIns3P and PtdIns4P to PtdIns(3,4)P_2 and are involved in internal membrane modelling. Homozygous transgenic mice with a deactivating mutation in the kinase domain of PI3KC2α (PI3KC2α^{D1268A}) are embryonic lethal (embryonic day 10.5-11.5) due to abnormal angiogenesis and vascular barrier function, showing the importance of the PI3K and the phosphoinositide products in regulating membrane dynamics, cell signalling and vesicle trafficking (Bilanges *et al.* 2019; Di Paolo *et al.* 2006; Balla 2013).

Human platelets express PI3KC2α and –β isoforms. Viable heterozygous PI3KC2α$^{WT/D1268A}$ mouse platelets with a 50% reduction in PI3KC2α activity exhibit faulty thrombus formation, creating unstable thrombi under shear. In contrast, platelets

from PI3KC2β-deficient mice behave similarly to WT mice (Valet *et al.* 2015; Mountford *et al.* 2015). PI3KC2α$^{WT/D1268A}$ platelets and megakaryocytes showed a variety of structural and biophysical abnormalities in their membranes, such as defects in α-granules, reduced filopodia, and enhanced membrane tethering, caused by a defect in barbell-shaped proplatelet scission (Valet *et al.* 2015; Mountford *et al.* 2015). Interestingly, platelets from PI3KC2α-deficient, PI3KC2β-deficient and PI3KC2α and –β double deficient mice showed unaltered basal or agonist-stimulated levels of PtdIns3P, PtdIns(3,4)P_2 or PtdIns(3,4,5)P_3 compared to wild type (Valet *et al.* 2015; Mountford *et al.* 2015).

1.3.3.3 Class III PI3K

Class III PI3K VPS34 catalyses the conversion of PtdIns to PtdIns3P and regulates secretion and vesicle trafficking. VPS34 is a member of protein complex Complex I, which supports autophagosome formation and elongation, and Complex II, which supports the maturation of endosomes and their fusion with autophagosomes (Backer 2016). Studies using transgenic VPS34$^{-/-}$ mice generated using PF4-Cre techniques showed defective granule distribution, secretion, and reduced PtdIns3P production upon CRP and thrombin stimulation (Liu *et al.* 2017; Valet *et al.* 2017).

1.3.4 PI3K as an antithrombotic target

Class I PI3Ks have the potential to be strong antithrombotic target candidates due to their crucial role in integrin activation. Inhibiting PI3K in activated platelets with the pan PI3K inhibitors wortmannin or LY29002 was shown to decrease fibrinogen binding and platelet aggregation (Kovacsovics *et al.* 1995; Kauffenstein *et al.* 2001; Lagrue *et al.* 1999). These compounds, however, have had limited success in clinical use due to their high toxicity and off-target action against other kinases (Workman *et al.* 2010). Another pan-PI3K inhibitor, S14161, was found to extend the occlusion time of ferric chloride-induced carotid artery injury after intraperitoneal injection in mice,

without prolonging tail bleeding time (Yi *et al.* 2014).

PI3Kβ has been widely studied as an antithrombotic target due to its central role in signalling downstream of major platelet receptors. TGX-221, a first-generation PI3Kβ inhibitor, was found to increase tail and renal bleeding in mice at antithrombotic doses (Bird *et al.* 2011). AZD6482, another PI3Kβ inhibitor with potency in the nanomolar range, resulted in a full antithrombotic effect in the modified Folts' model when intravenously administrated to dogs, with no increase in bleeding time or blood loss (Nylander *et al.* 2012). Nevertheless, in human testing, AZD6482 was found to increase the bleeding time by 60% at the highest observed plasma concentration of 6.2 μM (2 hours after the start of infusion) in human volunteers, hampering its use as an antithrombotic agent (Nylander *et al.* 2012).

Overall, these studies demonstrate a long history of employing class I PI3K inhibitors as antithrombotics, as well as the role of PI3K in platelet function and thrombosis. In the long run, due to the prevalence and importance of PI3K in all cell types and the huge variety of PI3K isoforms, as well as the role of various PI3K isoforms in haemostasis and thrombus integrity, further studies using better efficacy and isoform-specific inhibitors are needed to justify the use of PI3K inhibitors as antithrombotics, while minimising any potential adverse effects like bleeding or off-target toxicity.

1.3.5 PLC and Ca^{2+} haemostasis

1.3.5.1 Role and regulation of PLC

PLC is essential to platelet function and signalling, it catalyses the hydrolysis of PtdIns(4,5)P_2 generating the second messengers InsP_3, which stimulate Ca^{2+} release from the endoplasmic reticulum, and DAG, an activator of PKC.

The predominant PLC isoforms in platelet are PLCβ2, PLCβ3 and PLCγ2 (Offermanns 2000; Nakamura *et al.* 2017). PLCβ2 and PLCβ3 are solely regulated by GPCRs through the α-subunit of Gq (Offermanns 2000), while PLCγ2 signals downstream of (hem)ITAM receptors (Watson *et al.* 2010), the GPIb-V-IX complex (Falati *et al.* 1999) and integrins α2β1 (Inoue *et al.* 2003) and αIIbβ3 (Goncalves *et al.* 2003). Studies using platelets from PLCγ2 deficient mice showed a reduced response to stimulation by CRP or convulxin, and a normal response towards ADP and thrombin, which signal through PLCβ isoforms (Suzuki-Inoue *et al.* 2003). Btk and SFKs phosphorylate PLCγ2 at residues Y759 and Y1217, which are important for the catalytic activity and interaction of PLCγ2 with its activator proteins (Kim *et al.* 2004; Özdener *et al.* 2002).

The LAT signalosome and its cytosolic adapters SLP-76, Grb2, and Gads are essential in regulating PLCγ (Zhang *et al.* 1998). In the absence of SLP-76, activation of PLCγ2 by GPVI is nearly eliminated, whereas it is severely or marginally hindered in the absence of LAT or Gads, respectively (Judd *et al.* 2002). For Grb2 deficiency, studies on $Grb2^{-/-}$ mice reported severely impaired GPVI-mediated platelet activation and phosphorylation of PLCγ2 (Dütting *et al.* 2014). The Vav family of GDP/GTP exchange factors (GEFs) also support the PLCγ cascade as an adapter protein (Kuhne *et al.* 2000). Studies in the mouse KO model revealed a functional redundancy between the Vav proteins, as platelets deficient in both Vav1 and Vav3 had reduced PLCγ2 phosphorylation and associated functional responses downstream of GPVI

(Pearce *et al.* 2004), while platelets from mice deficient only in Vav1, Vav2, Vav3, or in Vav1/Vav2, did not reveal such a defect (Pearce *et al.* 2002).

Tec family kinases Btk and Tec also regulate PLCγ downstream of GPVI. Platelets from X-linked agammaglobulinemia (XLA) patients who have a functional Btk deficiency show decreased aggregation and PLCγ2 phosphorylation in response to collagen and CRP (Quek *et al.* 1998). Functional redundancy between Btk and Tec was described in a mouse KO model, as activation of PLCγ2 by GPVI was marginally, moderately or completely abolished in platelet of mice deficient in Btk, Tec, or both, respectively (Atkinson *et al.* 2003).

1.3.5.2 Ca^{2+} mobilisation and haemostasis

Platelets have a tightly regulated resting cytosolic Ca^{2+} level that is controlled by Ca^{2+} pumps, such as the sarco-endoplasmic reticulum Ca^{2+}-ATPase (SERCA) and the plasma membrane Ca^{2+}-ATPase (PMCA). These Ca^{2+} pumps transfer cytosolic Ca^{2+} to the endoplasmic reticulum lumen and extracellular medium respectively (Gitz *et al.* 2014).

Elevated cytosolic Ca^{2+} leads to the activation of multiple signalling proteins and pathways, such as PKC, activation of integrins, and granule secretion (Varga-Szabo *et al.* 2009) and is critical for platelet procoagulant actions (Versteeg *et al.* 2013). Activation of PLC isoforms, via either the tyrosine kinase (PLCγ2) or the $G_{q\alpha}$ protein (PLCβ), is a common stimulus for initial cytosolic Ca^{2+} elevation (Banno *et al.* 1988). $InsP_3$ generated by PLC releases Ca^{2+} via $InsP_3$ receptors in the endoplasmic reticulum membrane (Varga-Szabo *et al.* 2009). Through the process of store-regulated Ca^{2+} entry (SOCE), stromal interaction molecule 1 (STIM1) is a reticular membrane protein that senses Ca^{2+} store depletion and activates the plasma membrane Ca^{2+} channel, ORAI1, which allows the influx of Ca^{2+} (Varga-Szabo *et al.*

2011). Mice deficient in functional ORAI1 had significantly diminished Ca^{2+} responses to particular platelet agonists, such as adenosine diphosphate (ADP), collagen, or thrombin (Bergmeier *et al.* 2009).

Platelets have several plasma membrane cation channels that can raise cytosolic Ca^{2+} in response to physiological agonists. Non-selective $P2X_1$ cation channels are a fast way to increase Ca^{2+} once ATP is released from injured cells and platelet-dense granules, but are swiftly deactivated (Mahaut-Smith *et al.* 2011). Isoforms of the transient receptor potential channels (TRPC), TRPC1 and TRPC6, both play a minor role in Ca^{2+} entry and platelet activation (Hassock *et al.* 2002; Varga-Szabo *et al.* 2008).

1.3.6 Measurement of phosphoinositides

The isolation, identification and quantification of phosphoinositides are challenging because of their low abundance, and their amphipathic nature, with two hydrophobic acyl chains and a negatively charged hydrophilic inositol phosphate headgroup. Initial research measuring phosphoinositides required the labelling of platelets with radioactive [^{32}P]-phosphate or [^{3}H]-inositol, lipid extraction, thin layer chromatography separation, high-performance liquid chromatography (HPLC) separation and detection using autoradiography (Serunian *et al.* 1991; Hama *et al.* 2000; Whitman *et al.* 1988). The method is highly sensitive, but it can only detect phosphoinositide turnover, which neglects quiescent phosphoinositide pools. Currently, phosphoinositides are measured using liquid chromatography-mass spectrometry (LC-MS) (Mujalli *et al.* 2018; Clark *et al.* 2011), confocal fluorescence microscopy with phosphoinositide-specific antibodies (Bura *et al.* 2021; Bertović *et al.* 2020), enzyme-linked immunosorbent assay (He *et al.* 2016), or mass assay (Chicanne *et al.* 2012).

In the LC-MS-based method, phosphoinositides are extracted by acidified

chloroform/methanol (Bui *et al.* 2018; Clark *et al.* 2011; Haag *et al.* 2012; Jeschke *et al.* 2017; Wang *et al.* 2016) or acidic n-butanol/chloroform extraction (Traynor-Kaplan *et al.* 2017). The acidification is needed to neutralise the negatively charged inositol phosphate headgroup to facilitate its partition in the non-polar phase. The extracted phosphoinositides are then derivatised with TMS-diazomethane to methylate the phosphate groups (Clark *et al.* 2011; Traynor-Kaplan *et al.* 2017; Wang *et al.* 2016), or deacylated with methylamine to remove the acyl chains and produce glycerophosphoinositol phosphates (GroPInsPs) (Jeschke *et al.* 2017). The methylated phosphoinositides are subsequently separated and detected using reverse-phase liquid chromatography (RPLC)-MS. This method provides high sensitivity (limit of detection for PtdIns(3,4,5)P_3 = 0.5 pmol (Clark *et al.* 2011)), information about the acyl chain compositions, high quantitative accuracy and high throughput. However, it is unable to provide spatial resolution or isomeric resolution, which are important in deciphering signalling activities in platelets (Mujalli *et al.* 2018; Clark *et al.* 2011). Deacylated GroPInsPs are also measured using RPLC-MS, with the need for the addition of an ion-pairing reagent to shield the polar phosphate group and facilitate isomer separation. This method has the advantage of separating the positional isomers (Jeschke *et al.* 2017), but it is unable to obtain the acyl chain information of the lipid, and the additional ion-pairing reagent may contaminate the MS, which causes ion suppression that reduces sensitivity, and affect the ionisation pattern of ions when it is used for other purposes (Gustavsson *et al.* 2001; Holčapek *et al.* 2004). Recently, Morioka et al. and Li et al. have reported a method for measuring methylated phosphoinositide isomers using chiral column chromatography with a cellulose tris(3,5-dimethylphenylcarbamate) chiral selector. This can separate isomers without losing the ability to measure acyl chain composition. However, the elution order

of the isomers and retention time shift due to acyl chain combinations differ between the two methods. This suggests that significant method development may be required to differentiate between eluted peaks and identify isomers accurately (Morioka et al. 2022; Li et al. 2021). This warrants further studies to improve the existing method, which can provide both acyl chain and positional isomer information while retaining sensitivity and minimising contamination.

1.4 Systems biology and mathematical modelling

Systems biology is an integrated method for examining how biological processes behave as a whole and comprehending the interactions and interdependence of the constituents (Breitling 2010). This is in contrast to the reductionist approach typically used in biology study, which can identify the role of individual pathways or components, but is less capable of understanding the whole biological process. Systems biology uses simplified models of cells and organisms, to simulate population dynamics (Iannelli *et al.* 2015), regulatory networks (Bolouri 2008), metabolic networks (Martínez-Gómez *et al.* 2012) or signalling networks (Purvis *et al.* 2008; Dunster *et al.* 2015). Mathematical modelling is commonly used by systems biologists for deciphering the operation of complex biological systems and providing predictions on potential outcomes. Platelets are an ideal subject for mathematical models due to their lack of a nucleus and gene regulatory networks, and the complexities associated with defining gene expressions such as binding protein transcription factors with DNA and DNA transcription can be avoided. This simplifies the construction of metabolic and signalling networks in platelets.

1.4.1 Ordinary differential equation-based model

An ordinary differential equation (ODE) based model is a collection of ODEs for

simulating concentration changes of multiple species over time. ODEs are one of the most widely used models for studying dynamic systems. Many biological processes in systems biology, such as signal transduction and gene regulation, can be modelled using reaction-rate equations that express the rate of production of one species (e.g. proteins, metabolites and mRNA) as a function of the concentration of another species in the system. This provides a general framework to model continuous, dynamic systems with time elements.

1.4.2 Kinetic modelling of biological networks

Different kinds of kinetic equations are utilised to construct a system of ordinary differential equations [90; 139]. Mass action kinetics, which was developed by Guldberg and Waage in the 19th century (Waage *et al.* 1864), stating that the rate of reaction is proportional to the concentrations and activities of the reactants, provides a straightforward description of the rate of a chemical reaction. The reaction rate v in mass action kinetics v equals:

$$v = k_i y_x,$$

where y_x is the concentration of the reactant, and k_i is the reaction rate constant that represents the activity of the reactant.

Michaelis-Menten kinetics which was developed by Michaelis and Menten in the 19th century (Michaelis *et al.* 1913) describes reactions catalysed by enzymes. The reaction rate v is determined by:

$$v = \frac{v_{max} \times y_x}{K_M + y_x},$$

where y_x is the concentration of the reactant, v_{max} is the maximum rate of the system, and K_M is the Michaelis constant, defined as the substrate concentration at half of the maximum velocity. Hill equations were developed by A. Hill in 1910 to explain the

equilibrium connection between oxygen tension and haemoglobin saturation (Hill 1910). For species that are involved in multiple reactions, the rate of consumption or formation of the species is the sum of all involved reactions.

In addition to the choice of kinetics, every species in a network starts with initial concentration values for the species. The initial concentration can be determined by experimental data or model calibration, a process of estimating parameter values from other experimental data (Ashyraliyev *et al.* 2009). Meanwhile, the reaction rate constants in biological systems are usually unknown and difficult to obtain experimentally compared to the initial concentration and are mostly derived from model calibration.

1.4.3 Mathematical models describing the biology of platelets

Mathematical models have been developed to study the functional response of platelets to agonists and the mechanics of signalling pathways. For example, Dunster *et al.* have developed a model for predicting Syk tyrosine phosphorylation in GPVI-stimulated signal transduction and suggested that the phosphatase TULA-2 (T-Cell Ubiquitin Ligand-2) is important in regulating GPVI-mediated phosphorylation (Dunster *et al.* 2015).

There are also several models of phosphoinositide metabolism in platelets. Purvis *et al.* developed a model that captures GPCR signalling and the PI cycle, which can predict the platelet dose-dependent response of Ca^{2+} flux and $InsP_3$ production (Purvis *et al.* 2008). Mazet *et al.* have described an ODE-based model on the phosphatidylinositol cycle and suggested that lipid- and protein-binding proteins help regulate $PtdIns(4,5)P_2$ and $InsP_3$ in GPCR signalling (Mazet *et al.* 2020). These studies have shown the potential of mathematical models in elucidating platelet signalling through the interplay of protein phosphorylation and phosphoinositide

metabolism and predicting platelet homeostasis and activation. However, these models did not account for other phosphoinositide isomers. For the model by Purvis *et al.*, the enzyme copy number and parameters used for model constructions were based on cells that are unrelated to platelets. The model simulations by Mazet *et al.* on time course phosphoinositide change are also not physiologically relevant.

Future challenges of developing a comprehensive ODE platelet-based phosphoinositide model will be to include more platelet-based parameters, utilise comprehensive time-course data covering protein phosphorylation and phosphoinositides, and expand these ODE models to further capture the interplay between platelet receptors and downstream effectors.

1.5 Aims of this thesis

Phosphoinositide metabolism is deeply integrated with platelet activation and function. Whilst the protein phosphorylation cascade and phosphoinositide metabolism involved in the GPVI signalling pathways are well established, these studies are based on qualitative data and focus on individual pathways, which fail to integrate multiple pathways or include kinetic analysis. In addition, existing LC-MS methods are not optimised to measure the phosphoinositide positional isomers in platelets, despite their significance in signalling. The existing computational models on phosphoinositides also possess several limitations.

Considering this, the primary aim of this thesis is to comprehensively study phosphoinositide signalling in platelets by integrating time-course phosphorylation and phosphoinositide data and mathematical modelling. Chapter 3 described the development of a novel LC-MS-based method for the measurement of phosphoinositide positional isomers. Chapter 4 profiled the time-course change in phosphoinositides and develops an ODE-based model that represents phosphoinositide metabolism downstream of GPVI signalling. The model is validated by comparing model predictions with experimental data on the effect of PI4KA inhibitor GSK-A1 and OCRL inhibitor YU142670.

On the other hand, GPVI plays a major role in thrombosis and a minor role in haemostasis through fibrinogen-GPVI and fibrinogen-integrin αIIbβ3 interactions, making it an attractive antithrombotic target. The recently established anti-GPVI Nb2 is a potent GPVI antagonist with the potential to be developed into a new antithrombotic drug. Multimerisation of Nb2 could enhance the ligand-binding affinity up to a point, but could also result in the activation of GPVI. Understanding the differential functional effects of multimeric nanobodies could also deepen our knowledge of the clustering and activation of GPVI.

Considering this, the secondary aim of the thesis was to investigate the role of tyrosine kinase inhibitors, integrin αIIbβ3 and GPVI blockers in GPVI activation and platelet aggregation. Chapter 5 investigated whether small molecule inhibitors of Src, Syk, and Btk disrupt signalling through GPVI and have better accessibility to the aggregate core to reverse tyrosine phosphorylation and aggregation, using phosphospecific antibody and Western blot, LTA and flow cytometry. Chapter 6 described the development and functional characterisation of recombinant dimeric and tetrameric Nb2, and the development of an ODE model that integrates the functional data to illustrate the relation of ligand valency with GPVI clustering and activation.

Chapter 2

Materials and methods

2.1 Materials

2.1.1 Reagents

Crosslinked collagen related-peptide (CRP) was purchased from Cambcol Laboratories (Cambridge, UK). Thrombin was purchased from Roche (Mannheim, Germany). Sodium citrate, PP2, GSK-A1 and YU142670 were obtained from Sigma-Aldrich, dasatinib was purchased from LC Laboratories (Woburn, MA, USA), PRT-060318 was purchased from ApexBio (Houston, TX, USA), ibrutinib (PCI-32765) was from Selleckchem (Munich, Germany), and eptifibatide was from GSK (Brentford, UK). Rhodocytin was supplied by Dr Johannes A. Elbe (University of Münster, Germany). Thrombin receptor-activating peptide 6 (TRAP-6, Sequence: SFLLRN) was purchased from Bachem (Bubendorf, Switzerland). Bicinchoninic acid (BCA) assay was purchased from Thermo Scientific (Schwerte, Germany). Nb2-2 and Nb2-4 plasmid constructs were purchased from VIB (Ghent, Belgium). Fura-2 acetoxymethyl ester and human fibrinogen were obtained from Invitrogen (Waltham, Ma). Pluronic F-127 from Molecular Probes (Eugene OR, USA).

For solvent used in mass spectreometry (MS) experiments, MS-grade methanol (MeOH) was obtained from Biosolve (Valkenswaard, The Netherlands); formic acid (FA), 37% hydrochloric acid (HCl), chloroform ($CHCl_3$) and methylamine in MeOH were from Sigma-Aldrich (Steinheim, Germany); sodium chloride (NaCl), 1-butanol and isopropanol (IPA) from Merck (Darmstadt, Germany); Tris(hydroxymethyl)-aminomethane (Tris) was purchased from Applichem (Darmstadt, Germany); For standards, 16:0/16:0 PtdIns4P and 16:0/16:0 PtdIns(4,5)P_2 α-fluorovinylphosphonate (PtdIns(4,5)P_2-FP) from Echelon Biosciences (Salt Lake City, UT); and 17:0/20:4 PtdIns3P, 18:1/18:1 PtdIns(3,4)P_2, 18:1/18:1 PtdIns(4,5)P_2, 18:1/18:1 PtdIns(3,5)P_2 and 17:0/20:4 PtdIns(3,4,5)P_3 from Avanti Polar Lipids

(Alabaster, AL).

2.1.2 Antibodies

Table 2.1 Details of the antibodies used, target, host species, dilution and source

Antibody	Host species	Usage	Source
Phosphotyrosine	Mouse	Western Blot (WB) 1:1000	Millipore (Watford, UK)
pLAT Tyr200	Rabbit	WB: 1:500	Abcam (Cambridge, UK)
pPLCγ2 Tyr1217	Rabbit	WB: 1:250	Cell Signalling Technology (Massachusetts, USA)
pSyk Tyr525/526	Rabbit	WB: 1:500	Cell Signalling Technology
pBtk Tyr223	Rabbit	WB: 1:500	Abcam
pBtk Tyr551	Rabbit	WB: 1:500	Abcam
α-Tubulin	Mouse	WB: 1:1000	Sigma-Aldrich
Fluorescein isothiocyanate-conjugated anti-PAC-1 antibody (PAC-1-FITC)	Mouse	Flow cytometry 1:25	Invitrogen
HRP-conjugated anti-mouse IgG	Sheep	WB: 1:1000	GE Healthcare (Little Chalfont, UK)
HRP-conjugated anti-rabbit IgG	Donkey	WB: 1:1000	GE Healthcare

2.2 Methods

2.2.1 Preparation of human washed platelets and cell culture

Healthy volunteers who gave their consent and had not taken anti-platelet medication in the previous ten days had their blood drawn into 4% sodium citrate (1 mL sodium citrate/10mL blood), followed by a 10:1 addition of acid-citrate-dextrose (ACD, 85 mM sodium citrate, 75 mM citric acid, and 111 mM glucose), and centrifugation at 200 g for 20 min. The supernatant that was platelet-rich plasma (PRP) was centrifuged at 1000 g for 10 minutes in the presence of 2.8 M prostacyclin. The platelet pellet was resuspended in Tyrodes-HEPES buffer (134 mM NaCl, 0.34 mM

Na_2HPO_4, 2.9 mM KCl, 12 mM $NaHCO_3$, 20 mM HEPES, 5 mM glucose, 1 mM $MgCl_2$, pH 7.3) in the presence of 2.8 M prostacyclin before a second centrifugation at 1000 g for 10 min. The platelet pellet was then resuspended in Tyrodes-HEPES buffer and allowed to rest for 30 min at room temperature.

2.2.2 OP9 Cell culture

OP9 cells were grown as described earlier (Park *et al.* 2012). Briefly, cells were grown in Eagle's minimal essential medium (MEM) supplemented with L-glutamine, 20% fetal bovine serum (FBS), and 100 U/mL penicillin/streptomycin. Cultures were maintained at 37°C in a humidified atmosphere with 5% CO_2, and the medium was renewed every 4 days. After reaching 80% confluence, the cells were trypsinised, washed with PBS (137 mM NaCl, 2.7 mM KCl, 10 mM NaH_2PO_4, 2 mM KH_2PO_4, pH 7.4) and collected from the culture dish. The cells were aliquoted to $1x10^7$ cells per sample, centrifuged at 400 g for 5 min, the supernatant was removed, and the cell pellets were shock-frozen in liquid nitrogen.

2.2.3 P2 fraction preparation from rat hippocampal tissue

Rat hippocampus tissue generation and preparation were done in Michael R. Kreutz's lab (University Medical Center Hamburg-Eppendorf, Germany). Subcellular fractionation of rat hippocampus was prepared following a previously published protocol (Dieterich *et al.* 2016). 3.5 g of rat hippocampal tissue was homogenised in 10 mL/g buffer A (0.32 M sucrose, 5 mM HEPES, pH 7.4, supplemented with protease and phosphatase inhibitor cocktail) and centrifuged at 1 000 g for 10 min. The resulting pellet 1 containing nuclei and cell debris was discarded and the supernatants were collected. The supernatants were centrifuged at 12 000 g for 20 min (Sorvall RC6, F13-14 x 50cy rotor). The resulting pellet 2 (P2) fraction was collected as the hippocampus heavy membrane fraction for further analysis.

2.2.4 Expression and purification of nanobodies

2.2.4.1 Extraction of plasmid DNA from E. coli cells

A single colony of E. coli containing the plasmid of interest was grown in 10 ml LB in a 50 mL tube supplemented with 100 µg/mL ampicillin overnight at 37°C with shaking at 250 rpm. The cells were spun down at 500 g for 15 min and the supernatant was discarded. To purify plasmids from the bacterial pellet, the miniprep kit (Sigma-Aldrich) was used, according to the manufacturer's instructions. The plasmid concentration was determined by Nanodrop (OD280) based on its absorbance at 260 nm.

2.2.4.2 Transformation of competent E. coli cells

100 ng plasmid DNA was added to a tube of competent cells and incubated on ice for 30 min. The cells were then heat-shocked in a 42°C warm water bath for 45 s and placed back on the ice for 5 min. Afterwards, 500 ml LB solution was added to the cells and the cells were incubated at 37°C for 1 hour under shaking at 250 rpm. 100 µL of the cell solution was then plated out onto LB-agar plates that were supplemented with ampicillin and incubated at 37°C overnight. On the second day, single colonies were picked from the LB-agar plate, the plasmid was purified, and the transformation was confirmed by the Sanger sequencing service from Eurofins (Ebersberg Germany).

2.2.4.3 Expression and purification of nanobodies

On day 1, E. coli cells transformed with the plasmid containing nanobody of interest were inoculated into 10 ml of LB in the presence of ampicillin (100 µg/mL), and the pre-culture incubated at 37°C overnight with shaking at 250 rpm.

On the next day, 1 mL of the pre-culture was added to 1 L of Terrific Broth (TB) media (2.3 g KH_2PO_4,16.4 g $K_2HPO_4.3H_2O$, 12 g tryptone, 24 g yeast extract, 4 mL glycerol) supplemented with 100 µg/mL ampicillin, and incubated at 37°C with shaking at 250 rpm until an optical density at 600 nm (OD_{600}) was reached. Afterwards, 1 mM

of Isopropyl β- d-1-thiogalactopyranoside (IPTG, Sigma-Aldrich) was added to the TB media to induce nanobody expression, and the media was incubated at 28°C overnight with shaking at 250 rpm.

On the third day, the pellet in the overnight culture was harvested by centrifuging for 15 min at 500 g. The supernatant was discarded, and the cell pellet was resuspended in 12 mL TES buffer (0.2 M Tris pH 8.0, 0.5 mM EDTA, 0.5 M sucrose), followed by 1 hour shaking in a 4°C cold room. After one hour, 18 mL of diluted TES buffer (TES diluted 4 times in water) was added to the cells and followed by another 1 hour of shaking in 4°C cold room. Afterwards, the cells were centrifuged for 30 min at 8000 rpm at 4°C. Then the supernatant containing proteins extracted from the bacterial periplasmic space was collected into fresh falcon tubes. Next, Ni-NTA resin (Thermo Scientific) was added to the supernatant and incubated for 30 min at room temperature with shaking to allow the nanobody to bind to the resin. After 30 min, the mixture was loaded onto a PD-10 gravity column (Cytvia) and washed with PBS to remove the unbound proteins. The nanobodies were eluted with 1 mL of 0.5 M imidazole in PBS three times. The eluent was dialysed overnight at 4°C against PBS to remove imidazole. Agarose gel electrophoresis and nanodrop were used to confirm the presence of the nanobody and purity, and the eluent was aliquoted and snap-frozen with liquid N2.

2.2.5 Phosphoinositides sample preparation, extraction and analysis

2.2.5.1 Platelet stimulation experiment

For Chapter 3, washed platelets at a concentration of $1x10^9$ platelets/mL were stimulated with 1 μg/mL CRP or 0.1 U/mL thrombin for 5 min. The pellets were then snap-frozen in liquid nitrogen and kept at -80°C after the platelets had been centrifuged for 5 min at 640 g at 25°C.

For the time point measurement in Chapter 4, washed platelets at a

concentration of $1x10^9$ platelets/mL were stimulated with 30 µg/mL CRP in the presence of apyrase (2.5 U/mL) and indomethacin (10 µM), before the addition of 10X volume of cold HCl to stop the reaction. The pellets were then shock frozen in liquid nitrogen and kept at -80°C after the platelets had been centrifuged for 5 min at 640 g at 25°C.

2.2.5.2 Phosphoinositides extraction

For platelet samples, after the addition of 242 µL $CHCl_3$, 484 µL MeOH, 23.6 µL 1M HCl, 170 µL water and internal standard (100 pmol of PtdIns(4,5)P_2-FP) to the cell pellets containing $1x10^8$ platelets, the mixture was allowed to stand at room temperature for 5 min with occasional vortexing. Next, 725 µL of $CHCl_3$ and 170 µL 2M HCl were added to induce phase separation and the samples were centrifuged at 1 500 g for 5 min at room temperature (Eppendorf, Hamburg, Germany). The lower organic layer was then transferred to another tube and dried under a continuous stream of nitrogen (1 L/min N_2 at 25°C).

The lipid extracts were then deacylated following the protocol of Jeschke *et al.*(Jeschke *et al.* 2017) The dried lipid extracts were resuspended in 50 µL methylamine in methanol/water/1-butanol (46:43:11) and incubated at 53°C for 50 min in a thermomixer at 1 000 rpm (Thermomixer Comfort; Eppendorf, Hamburg, Germany). Then 25 µL cold IPA was added to the mixture, and the mixture was dried under a continuous stream of nitrogen to obtain dried lipid extracts (1 L/min N_2 at 25°C). The dried and deacylated lipid extract was resuspended in 50 µL water and stored at -80°C before further analysis.

2.2.5.3 IC−MS/MS

IC-MS/MS was conducted using a Dionex ICS-5000 instrument (Thermo Fischer Scientific, Darmstadt, Germany) connected to a QTRAP 6500 instrument (AB

Sciex, Darmstadt, Germany) that was equipped with an electrospray ion source (Turbo V ion source). Chromatographic separation was accomplished with a Dionex IonPac AS11-HC column (250 mm × 2 mm, 4 µm; Thermo Fischer Scientific) fitted with a guard column (50 mm × 2 mm, 4 µm; Thermo Fischer Scientific). A segmented linear gradient was used for the separation of GroPInsP: Initial 15 mM potassium hydroxide (KOH), held at 15 mM KOH from 0.0 to 5.0 min, 15 to 25 mM KOH from 5.0 to 15.0 min, 50 to 65 mM KOH from 15.0 to 30.0 min, 100 mM KOH from 30.0 to 34.0 min, 10 mM KOH from 34.0 to 38.0 min, 100 mM KOH from 38.0 to 42.0 min, and 15 mM KOH from 42.0 to 45.0 min. The IC flow rate was 0.38 mL/min, supplemented postcolumn with 0.15 mL/min makeup flow of 0.01% FA in MeOH. The temperatures of the autosampler, column oven and ion suppressor were set at 10, 30 and 20 °C, respectively. The injector needle was automatically washed with water and 5 µL of each sample was loaded onto the column.

The following ESI source settings were used: curtain gas, 20 arbitrary units; temperature, 400°C; ion source gas I, 60 arbitrary units; ion source gas II, 40 arbitrary units; collision gas, medium; ion spray voltage, -4500 V; declustering potential, -150 V; entrance potential, -10 V; and exit potential, -10 V. For scheduled selected reaction monitoring (SRM), Q1 and Q3 were set to unit resolution. The collision energy was optimised for each GroPInsP by direct infusion of the corresponding deacylated standard. The scheduled SRM detection window was set to 3 min, and the cycle time was set to 1.5 s. Data were acquired with Analyst version 1.6.2 (AB Sciex).

2.2.6 $InsP_1$ and Ca^{2+} mobilisation measurement

2.2.6.1 Platelet Isolation and Loading with Fura-2

Washed platelets were resuspended in HEPES buffer (10 mM HEPES, 136 mM NaCl, 2.7 mM KCl, 2 mM $MgCl_2$, 5.5 mM glucose, and 0.1% bovine serum albumin,

pH 7.45) to a concentration of 2 x 10^8/mL, supplemented with 3 µM Fura-2 acetoxymethyl ester and 0.4 µg/mL pluronic and incubated for 40 min at room temperature. After the incubation, apyrase (2.5 U/mL) and 1:15 v/v ACD were added to the platelets, followed by another centrifugation at 2000 g for 2 min [48]. The platelet pellet was resuspended in HEPES buffer to a concentration of 2 x 10^8/mL.

2.2.6.2 Cytosolic Ca^{2+} Measurements

Platelet cytosolic Ca^{2+}were measured in 96-well plates using a FlexStation 3 (Molecular Devices, San Jose, CA, USA). In brief, 200 µL of Fura-2 loaded platelets were pretreated with the stated concentration of GSK-A1, YU142670, or DMSO as vehicle together with apyrase (2.5 U/mL) and indomethacin (10 µM) for 10 min or left untreated. After the addition of 1 mM $CaCl_2$ or 0.1 mM EGTA, the platelets were stimulated by automated pipetting with CRP (10 µg/mL). Changes in Fura-2 fluorescence were measured over time at 37°C by ratiometric fluorometry at dual excitation wavelengths of 340 and 380 nm and an emission wavelength of 510 nm. To determine background fluorescence, certain wells contained Fura-2-loaded platelets that were lysed with 0.1% Triton-X-100 in the presence of either 1 mM $CaCl_2$ or 0.1 mM EGTA (Feijge *et al.* 1998). After correction for background fluorescence, $[Ca^{2+}]_i$ (as nM) was calculated from the fluorescence intensity ratio of 340/380 nm (Grynkiewicz *et al.* 1985).

2.2.6.3 Platelet stimulation and $InsP_1$ ELISA

Washed platelets were resuspended in Tyrode's buffer at a concentration of 8x10^8 platelets/mL supplemented with 50 mM LiCl which prevents $InsP_1$ hydrolysis. Before stimulation, washed platelets were pre-treated with GSK-A1, YU142670, or DMSO as vehicle together with 2.5 U/mL apyrase, 10 uM indomethacin for 10 min (presence of 2.5 U/mL apyrase, 10 uM indomethacin). Afterwards, the washed

platelets were stimulated by 10 μg/mL CRP and lysed with 1% lysis buffer (IP-ONE ELISA kit, Cisbio, Bedford, MA). After cell lysis, the lysed platelets were snap-frozen in liquid nitrogen for future analysis. The $InsP_1$ ELISA was conducted according to IP-ONE ELISA kit manufacturer's instructions, and the final result was measured in 96-well plates using a FlexStation 3 (Molecular Devices, San Jose, CA, USA).

2.2.7 Light transmission aggregometry

Platelet aggregation was monitored using a Chrono-log optical aggregometer (Labmedics, Manchester, UK) at 37°C with constant stirring at 1200 rpm. Washed platelets at $2x10^8$/mL were used for all experiments. For inhibitors pre-treatment studies, platelets were pre-treated for 10 min with inhibitors at the stated concentration. The platelets were then stimulated with the stated concentration of agonists, including collagen, CRP, TRAP-6 and Nb2-4. The aggregation traces were then monitored for 5-60 min.

For platelet disaggregation studies, the inhibitors mentioned above were added at 150 sec after agonist stimulation, and the aggregation traces were monitored for 20 min. The degree of disaggregation (%) was calculated based on maximal aggregation minus the percentage of aggregation at 20 min after agonist stimulation.

2.2.8 Platelet stimulation for tyrosine phosphorylation study

In a Chronolog model 700 aggregometer, washed platelets at $4x10^8$/mL were treated in the same manner as the inhibitors pre-treatment studies and the platelet disaggregation studies mentioned above. At stated time points after the addition of agonists, 5x SDS reducing sample buffer (10% SDS, 0.5 M DTT, 50% glycerol, 0.125 M Tris, pH 6.8) was added to washed platelets to lyse the platelets. The platelet lysate was then boiled for 5 min before being stored at -20°C for future phosphorylation analysis using phosphotyrosine-specific antibodies in Western Blot.

2.2.9 SDS-PAGE and Western blot

Platelet lysates or purified protein samples in SDS-reducing sample buffer were boiled for 5 min and separated with SDS-PAGE at 80 V for 15 min, followed by 120 V for 40 min on a pre-cast, gradient gel (NuPAGE, 4 to 12%, Bis-Tris, Invitrogen). Alongside the samples, a pre-stained molecular weight marker ladder was loaded to help with the identification of proteins of interest.

After separation, the protein bands on the PAGE gels were transferred to a polyvinylidene difluoride (PVDF) membrane using the Trans-Blot Turbo Transfer System (Biorad). The blots were blocked with blocking buffer (5% BSA in TBST; 200 mM Tris, 1.37 M NaCl, 0.2% (v/v) Tween-20, pH 7.6) and were treated overnight with primary antibody (diluted 1/1000 in blocking buffer). On the next day, the blots were washed with 3X TBST and 10 min each, followed by 1-hour incubation with HRP-conjugated secondary antibody (diluted 1/10000 in TBST) at room temperature. After secondary antibody incubation, three 10 min washes with TBST were applied to the blots before being incubated with ECL chemiluminescence agents (Thermo, Paisley, UK) for 1 min. Membranes were analysed using either ECL autoradiographic film (GE Healthcare) used to generate representative western blots or the LiCor Odyssey-FC imaging system (LiCor, Cambridge, UK) to quantify the protein bands.

2.2.10 Flow cytometry

Washed platelets ($2x10^7$/mL) platelets were incubated with PAC-1-FITC for 20 min and then stimulated with 10 µg/mL CRP at 37°C. PP2 (20 µM), PRT-060318 (1 µM) or DMSO were added 150 sec after stimulation and incubated for 20 min at 37°C. Platelets were identified and gated in an Accuri BD Flow Cytometer (BD Biosciences) according to the forward and side scatter signals. A total of 10,000 platelet events were acquired per sample, and the mean of the fluorescence intensity (MFI) was analysed.

2.2.11 Surface plasmon resonance

Surface plasmon resonance experiments were conducted by Dr Eleyna Martin at the University of Birmingham Biacore. T200 (GE Healthcare) was used for surface plasmon resonance. Amine-coupling was used to immobilise GPVI directly onto the CM5 chip. To block reference surfaces, 1 M of pH 8 ethanolamine was used. At least two duplicate injections each cycle were made, along with experimental replicates of n = 3. All sensorgrams displayed are double reference removed. Flow rates of 30 L/min were used for the experiments in the HBS-EP running buffer (10 mM HEPES, pH 7.4, 0.15 M NaCl, 3 mM EDTA, and 0.005% v/v surfactant P20) at 25°C. The following procedure was used for each concentration of Nb2-2 and Nb2-4: 120-sec injection, 900-sec dissociation. The Biacore T200 Evaluation software was used to conduct kinetic analysis utilising a global fitting to a 1:1 binding model.

2.2.12 Data and statistical analysis

GraphPad Prism 7 (GraphPad Software Inc. La Jolla, USA) or Microsoft Office 2016 was used for all statistical analyses. Unless otherwise stated, data are provided as mean ± standard deviation (SD) of the mean, with statistical significance set at $p < 0.05$. Welch's t-test, one-way ANOVA multiple comparisons and Tukey's test were used for statistical analysis, as stated in the figure. The dose-response fit in Origin (version 8.6, OriginLab, Northampton, MA) was used to fit dose-response curves.

Chromatographic resolution (*R*) in Chapter 3 is calculated by:

$$R = 1.18 \times \left(\frac{RT_{P2} - RT_{P1}}{FWHM_{P2} + FWHM_{P1}}\right)$$

where *RT* stands for peak retention time, *FWHM* for full width at half maximum of the peak, and *P2* and *P1* are the two peaks being compared.

For MS data, Skyline (64-bit, 3.5.0.9319) was used to visualise results, integrate signals over time, and quantify all lipids that were detected by MS (Peng *et al.* 2015).

For all phosphoinositides, the calibration curves are created in Microsoft Excel by plotting the analyte: internal standard area ratio against the concentration of analyte. The amount of phosphoinositides was calculated from the calibration curve. For PtdIns, the amount in each sample is calculated by analyte:internal standard area ratio times amount of internal standard added (Clark *et al.* 2011). The conversion of units in Chapters 3 and 4 between molecules/platelet used in the model and pmol/mg protein used in the phosphoinositides experiment, and nM in $InsP_1$ and Ca^{2+} assay are based on the assumptions that platelets contain 1.5 mg protein/10^9 platelets (Burkhart *et al.* 2012) and that Avogadro's number = $6.023x10^{23}$,

Chapter 3

Targeted phosphoinositides analysis using high-performance ion chromatography-coupled selected reaction monitoring mass spectrometry

The work conducted and the results produced in this Chapter have been published (Cheung *et al.*, 2021).

3.1 Introduction

Phosphoinositides are crucial in signal transduction and platelet activation (Clapham 2007; Balla 2013; Osaki *et al.* 2004). The quantification and identification of phosphoinositides are challenging, because of their high polarity and low abundance (Balla 2013). Multiple reversed-phase liquid chromatography-mass spectrometry (RPLC-MS)-based methods have been developed to quantify phosphoinositides, as described in Chapter 1. The methods that analyse methylated phosphoinositides were able to achieve high sensitivity, and obtain information about the acyl chain compositions, but they were unable to provide isomeric resolution, a key for understanding phosphoinositides metabolism and signalling (Clark *et al.* 2011; Traynor-Kaplan *et al.* 2017; Wang *et al.* 2016). The methods that analyse the glycerolphosphoinositol phosphate (GroPInsPs) resulting from phosphoinositides deacylation could provide spatial resolution or isomeric resolution (Jeschke *et al.* 2017; Jeschke *et al.* 2015), but they required the addition of an ion-pairing reagent to shield the polar phosphate group, which could cause ion suppression that reduces sensitivity and affects the ionisation pattern of ions (Gustavsson *et al.* 2001; Holčapek *et al.* 2004).

To overcome the unwanted effects of adding an ion-pairing reagent, ion chromatography (IC) could be an alternative over RPLC for the separation of GroPInsPs. In contrast to RPLC which separates molecules based on their hydrophobicity, IC is well-established for the analysis of hydrophilic or polar metabolites. However, the presence of salt in the IC eluent can severely reduce molecule ionisation efficiency, making it unsuitable for use with MS (Metwally *et al.* 2015). The recent development of eluent suppression technology that desalts the eluent in IC allowed the coupling of IC with MS for targeted metabolites detection (such

as carbohydrates, organic acids, and sugar phosphates) or untargeted metabolomics profiling (Burgess *et al.* 2011; Hu *et al.* 2015; Wang *et al.* 2014). However, its application to phosphoinositides analysis has not yet been explored.

3.2 Aims

This chapter aims to develop an IC-MS-based method for the identification and quantification of the phosphoinositide's positional isomers. The method validity is assessed by extraction efficiency, peak resolution, retention time stability, MS and MS/MS profile, sensitivity and calibration curve range and linearity. The developed method was subsequently validated in biological matrices including stimulated platelets, OP9 cells and rat brain tissues.

3.3 Results

3.3.1 Establishing profiling strategies for phosphoinositides.

The quantitative IC-MS/MS approach for phosphoinositides analysis developed in this chapter comprises an optimised extraction and deacylation workflow, the inclusion of internal standards for absolute quantification, and a specific IC-MS acquisition method, to yield a comprehensive quantitative workflow, as shown in the schematic Figure 3.1.

3.3.1.1 Extraction strategies for phosphoinositides.

The workflow employed in this chapter combined the acidified chloroform/methanol method established by Clark *et al.* (Clark *et al.* 2011), with the deacylation protocol adopted from Jeschke *et al* (Jeschke *et al.* 2017). In this workflow, the samples were first spiked with a constant amount of synthetic internal standards PtdIns(4,5)P_2-FP for normalisation, followed by lipid extraction. PtdIns(4,5)P_2-FP is a metabolically stabilised counterpart of PtdIns(4,5)P_2 with an α-fluoro vinyl-phosphonate group rather than a phosphodiester link (Figure 3.2B). The extracted phosphoinositides are deacylated with methylamine to remove the fatty acid chain and generate GroPInsPs. The GroPInsPs were dried with a nitrogen stream and reconstituted in water before IC-MS/MS analysis.

The extraction efficiency of the workflow is next confirmed by injecting unstimulated human platelets with phosphoinositides standards before or after extraction (Figure 3.2A). The recoveries for PtdIns4P, PtdIns(4,5)P_2, and PtdIns(3,4,5)P_3 were determined to be 103 ± 12%, 109 ± 11% and 134 ± 13%, respectively, indicating that the phosphoinositides were extracted with good recoveries and low variations. The higher recovery could be due to interference with the matrix.

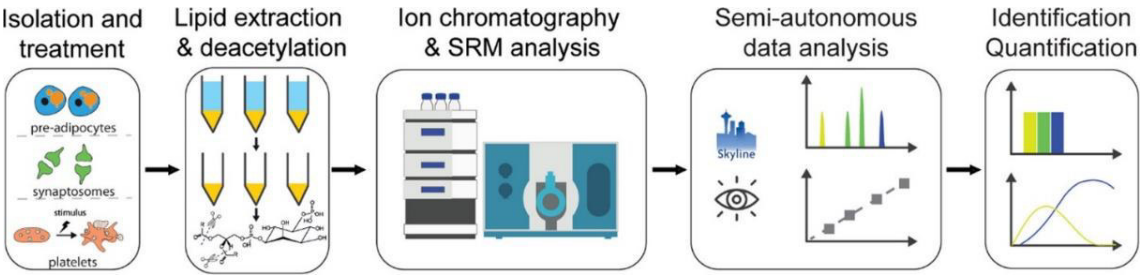

Figure 3.1 Flowchart for the analysis of targeted phosphoinositides analysis using an IC-MS system. Phosphoinositides were isolated from platelets, OP9 cells, and rat hippocampus brain tissue using acidified chloroform/methanol and subsequently deacylated with methylamine. The phosphoinositides were then separated by a KOH gradient on an anion-exchange column and evaluated using selected reaction monitoring (SRM). Skyline was used to analyse the data, and the absolute amounts of each positional isomer were calculated.

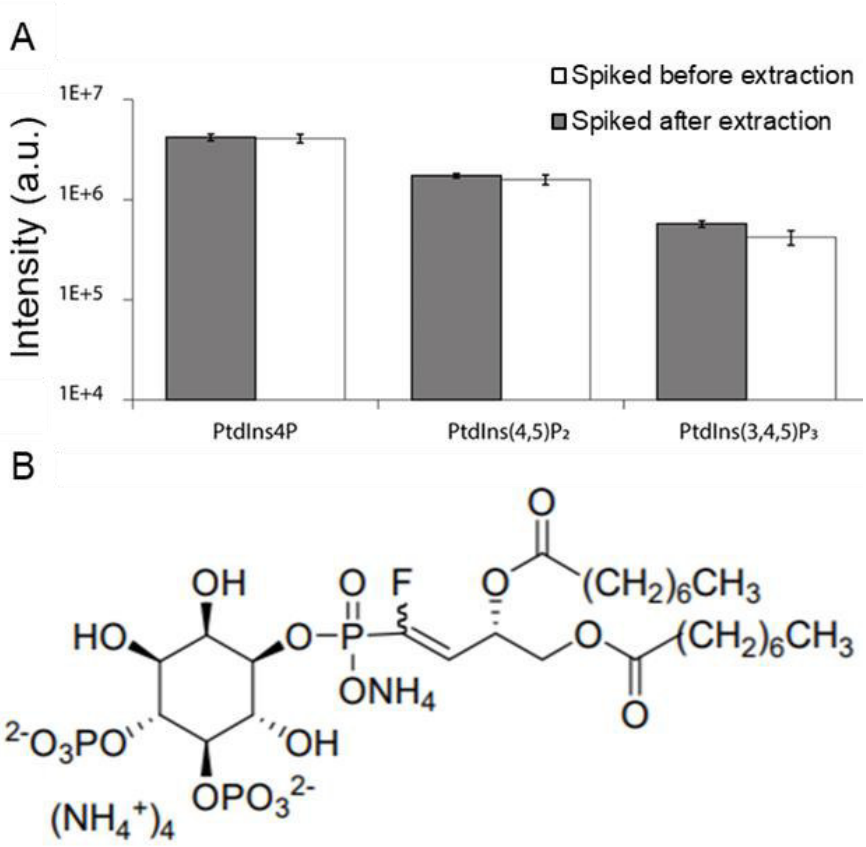

Figure 3.2 Extraction efficiency of the phosphoinositides extraction and derivatisation workflow. (A) Bar chart showing the peak area of the phosphoinositides with endogenous and internal standards spiked into unstimulated human platelets before (grey) or after (white) extraction. Results are presented in mean ± SD. n = 3 (B) Structure of internal standard 16:0/16:0 PtdIns(4,5)P_2 α-fluorovinyl-phosphonate (PtdIns(4,5)P_2-FP).

3.3.1.2 Optimisation of IC method for phosphoinositides analysis.

Following extraction and deacylation, the GroPInsPs in the samples were separated in ion chromatography by an anion exchange column and eluted using a KOH gradient based on the negative charges on the analyte molecules. Following the removal of hydroxide ions in the eluent by the ion suppressor, the output flow was mixed with a make-up flow of 0.01% FA in MeOH and analysed in the MS.

The IC gradient for resolving GroPInsPs was subsequently optimised to improve GroPInsPs positional isomers resolution. The performance of the gradient used in this chapter (Gradient C) was compared with other IC gradients that were previously reported for metabolomics analysis (Gradient A and B) (Burgess *et al.* 2011z; Wang *et al.* 2014). In Figure 3.3A, the gradient was represented by the black dotted line and the total ion chromatogram of the three GroPInsPs classes in coloured solid lines. All three gradients can separate GroPInsP, GroPInsP$_2$ and GroPInsP$_3$. For the three GroPInsP positional isomers (Figure 3.3B), all investigated gradients were unable to distinguish GroPIns3P from GroPIns5P because of their structural similarities. For GroPIns4P and GroPIns3P + GroPIns5P, gradient B [chromatographic resolution (R), 100%] and C (R, 100%) yielded better separation than gradient A (R, 70.2%). For the three GroPInsP$_2$ positional isomers, gradient C and A outperforms gradient B, with better resolutions between GroPIns(3,4)P$_2$ and GroPIns(4,5)P$_2$ (A: 104%, B: 75% and C: 100%) and between GroPIns(4,5)P$_2$ and GroPIns(3,5)P$_2$ (A: 96%, B: 70% and C: 100%). These results show that the optimised gradient C utilised in this study is the best option for separating the GroPInsP and GroPInsP$_2$ classes.

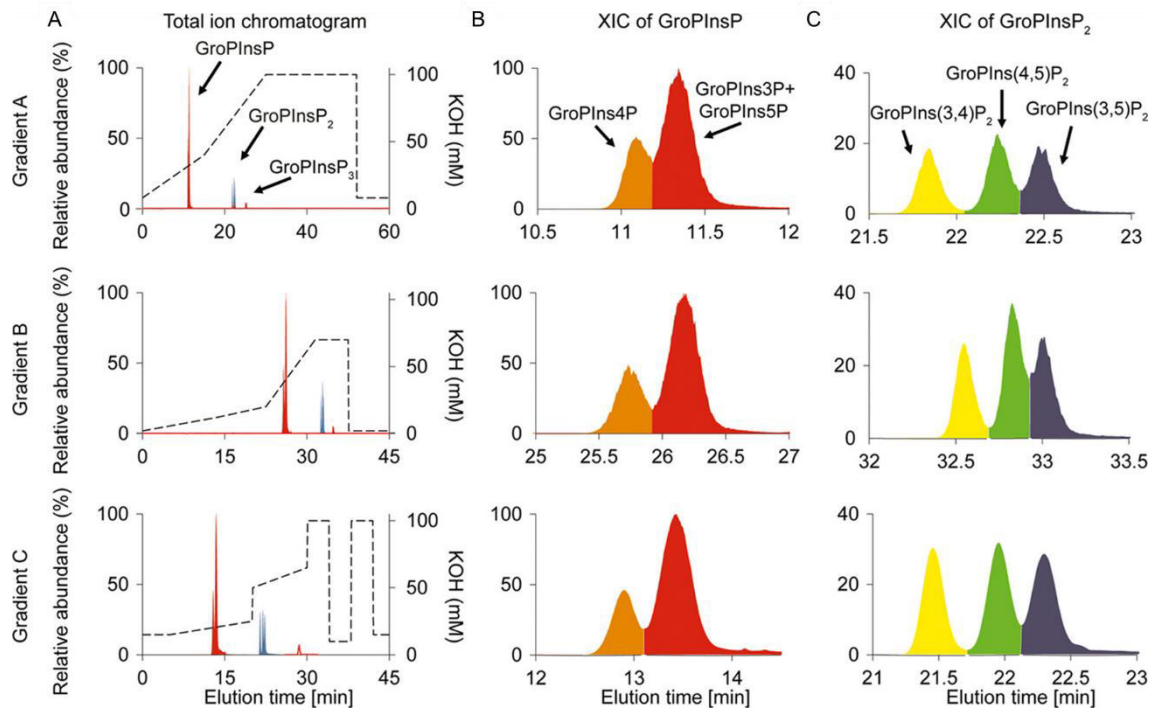

Figure 3.3 Comparison of IC gradients. (A) Total ion chromatogram (TIC) of the GroPInsP standard mix spiked into unstimulated platelet extracts and the IC gradient of gradients A, B, and C. The left axis shows the relative abundance of the ions in the TIC, and the right axis shows the concentration of KOH used in each gradient. (B) Extracted ion chromatogram (XIC) of the GroPInsP, gradients C and B yielded better separation gradient A. All three gradients failed to resolve GroPIns3P from GroPIns5P. (C) XIC of $GroPInsP_2$, gradients C and A yielded better separation than gradient B. The IC gradients of gradients A, B, and C are derived from references 11 and 13 and this study, respectively.

The elution time stability of gradient C was also examined across 110 injections of standards and phosphoinositides-containing samples derived from human platelets, OP9 cells, and hippocampal P2 fraction (Figure 3.4). The retention times for GroPIns4P, GroPIns(4,5)P_2, GroPIns(3,4,5)P_3, and GroPIns(4,5)P_2-FP were 13.18 ± 0.11 min, 22.13 ± 0.08 min, 28.87 ± 0.24 min, and 22.03 ± 0.09 min, respectively, showing that the IC technique for GroPInsP separation is highly reproducible.

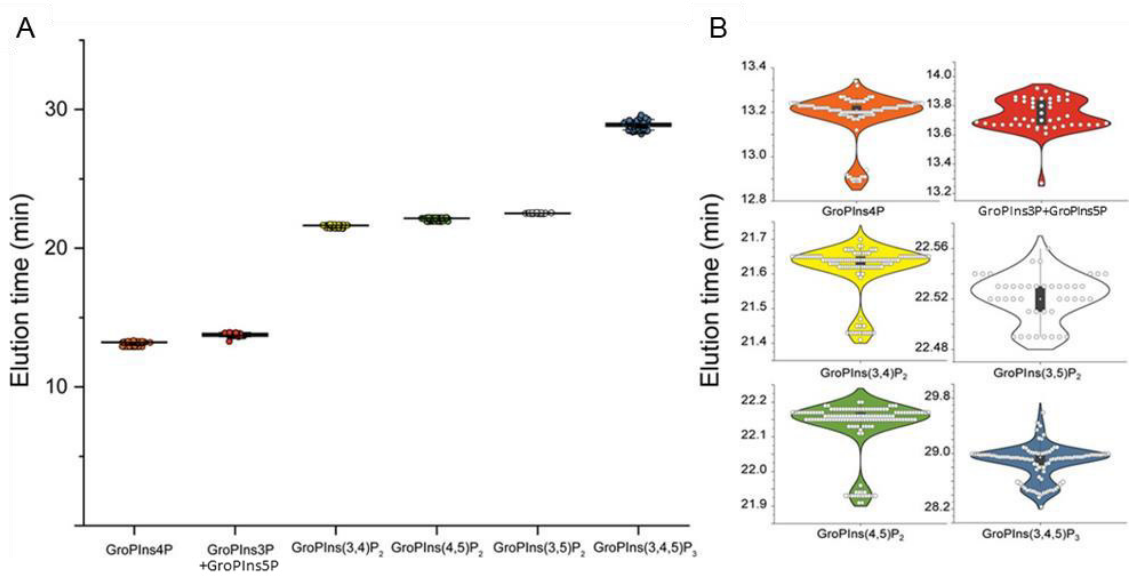

Figure 3.4 Elution time stability of gradient C. The elution times of the GroPInsP standards and phosphoinositide-containing materials taken from human platelets, OP9 cells, and rat hippocampus brain tissue in a large number of injections (n = 40) are shown in (A) dot plot and (B) violin plot.

3.3.1.3 Quantification of phosphoinositides using targeted mass spectrometry.

The selection reaction monitoring mode was used in the MS for phosphoinositides measurement. Because of deacylation, all GroPInsPs with the same number of phosphates has the same mass which simplified the mass spectra. The fragment-ion spectra of GroPInsP, GroPInsP$_2$, and GroPInsP$_3$ classes are shown in Figure 3.5A. The collision energy for GroPIns(3,4,5)P_3 was selected to be -32 eV and -27 eV for the other precursor molecules (Table 3.1). Collision-induced

dissociation of these headgroups led to the formation of fragments that lost $-C_3H_7O_5P$, $-H_2O$, or $-O_3P$ molecules. However, it was observed that GroPInsPs with the same number of phosphate also share identical MS2 fragmentation patterns (Figure 3.5B). As a result, an optimal LC gradient was required to separate and identify the GroPInsP and $GroPInsP_2$ isomers (gradient C in Figure 3.3).

Table 3.1 SRM transition list used for GroPInsPs analysis. A summary of the monitored quadrupole 1 (Q1) mass, quadrupole 3 (Q3) mass, collision energy and monitoring window for each GroPInsP species. m/z = mass-to-charge ratio, eV = electronvolt.

Species	Q1 Mass (m/z)	Q3 Mass (m/z)	Collision energy (eV)	Monitoring window (min)
Glycerophosphoinositol phosphate (GroPInsP)	413	241	-27	11 - 17
Glycerophosphoinositol bisphosphate ($GroPInsP_2$)	493	395	-27	21 - 25
Glycerophosphoinositol triphosphate ($GroPInsP_3$)	573	321	-32	26 - 32
Glycerophosphoinositol (4,5)-bisphosphate α-fluorovinyl-phosphonate ($GroPIns(4,5)P_2$-FP)	509	411	-27	21 - 25

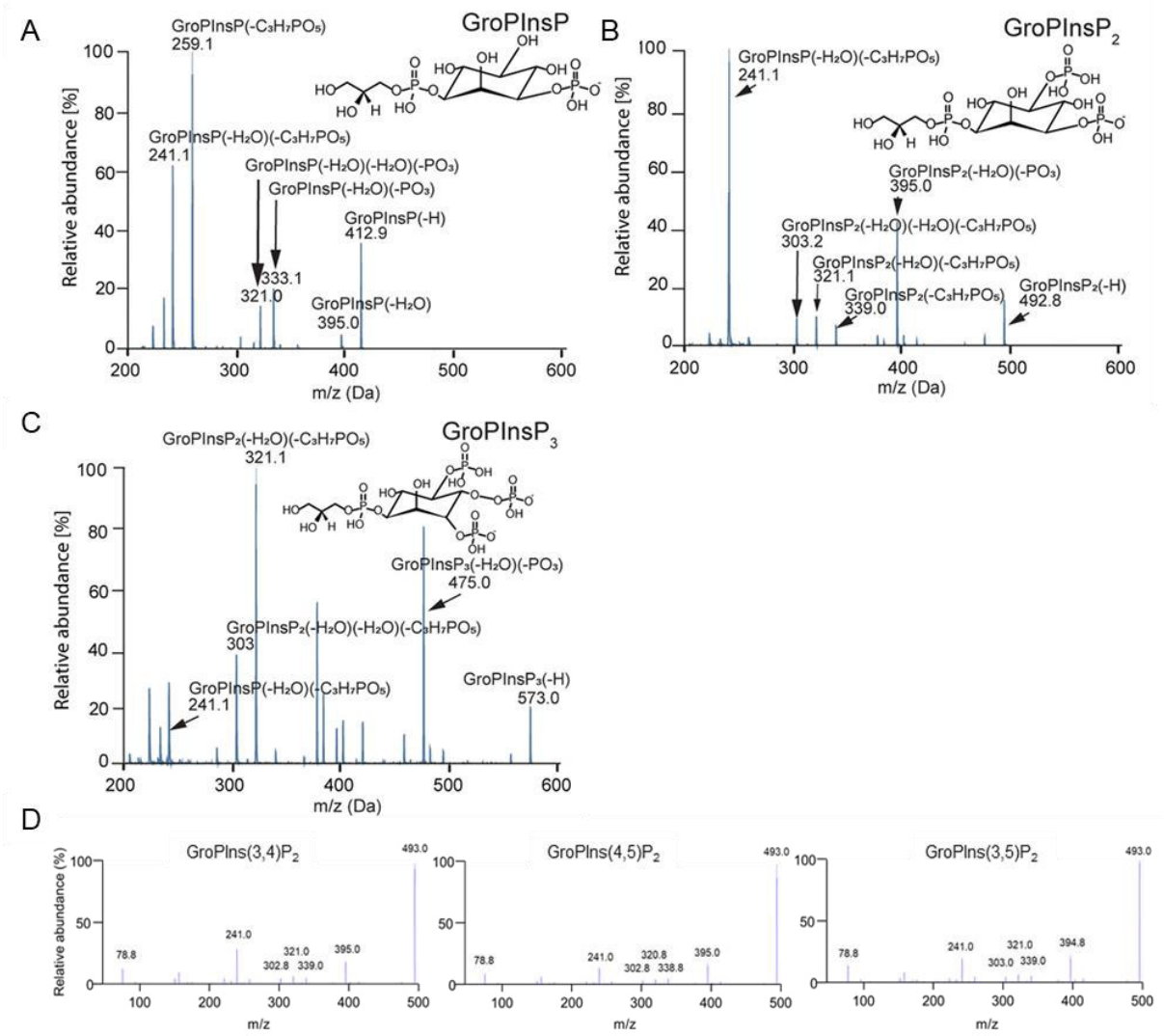

Figure 3.5 GroPInsPs fragment ion spectra. Standard phosphoinositides were isolated, deacylated into GroPInsPs and injected into IC-MS/MS for analysis. Fragment-ion spectra of (A) GroPInsP, (B) GroPInsP$_2$, and (C) GroPInsP$_3$. Collision-induced dissociation led to the formation of fragments that lost $-C_3H_7O_5P$, $-H_2O$, or $-O_3P$ molecules. (D) The three GroPInsP$_2$ isomers had similar MS2 fragmentation patterns and fragment ion ratios at a collision energy of -27 eV.

To increase accuracy in quantifying phosphoinositides, the internal calibration curve technique was adopted. Unstimulated human platelets were spiked with known levels of phosphoinositides and 100 pmol internal standard PtdIns(4,5)P_2-FP. The area ratio was computed by dividing the greatest intensity fragment at -27 eV for GroPInsP, GroPInsP$_2$, and GroPInsP$_3$ by the internal standard at -27 eV. The obtained calibration curves had a good degree of linearity ($R^2 \approx 0.99$) and ranged from 312.5 fmol to 10 pmol (Figure 3.6). These findings suggest that using a synthetic internal standard, PtdIns(4,5)P_2-FP, to adjust for recovery during extraction, deacylation, and the IC-SRM test is a sensitive and robust approach for quantifying phosphoinositides.

The method's limit of detection (LOD) and limit of quantification (LOQ) were defined as the analyte concentration necessary to generate a signal intensity three or ten times greater than the noise signal, respectively. Using these criteria, the LOD and LOQ of GroPIns(3,4,5)P_3 were 312.5 fmol (S/N >3) and 625 fmol (S/N > 10), respectively (Figure 3.7).

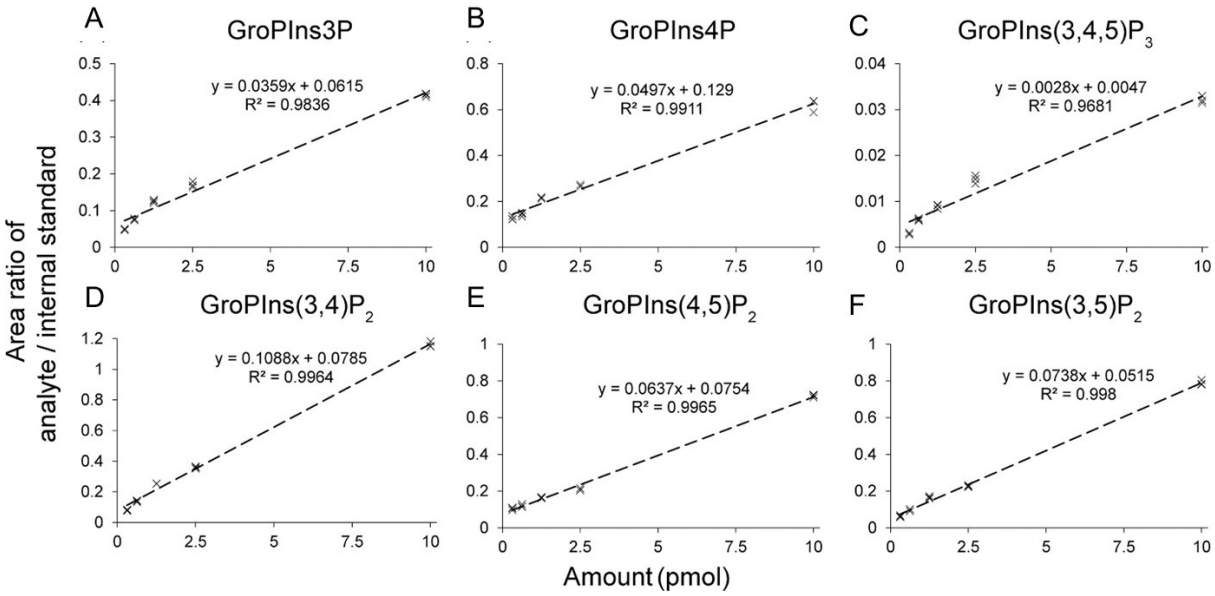

Figure 3.6 Internal standard calibration curve for absolute quantification of GroPInsPs. The phosphoinositides were extracted and deacylated after serially diluted phosphoinositides standards and 100 pmol of the internal standard PtdIns(4,5)P_2-FP were spiked into unstimulated human platelet extracts. The areas underneath the XIC peaks of (A) GroPIns3P, (B) GroPIns4P, (C) GroPIns(3,4,5)P_3, (D) GroPIns(3,4)P_2, (E) GroPIns(4,5)P_2, and (F) GroPIns(3,5)P_2 were divided by the internal standard, and the area ratio was plotted against the quantity of the species spiked. The calibration curve, data points, and R^2 value (n = 3 replicates) are displayed.

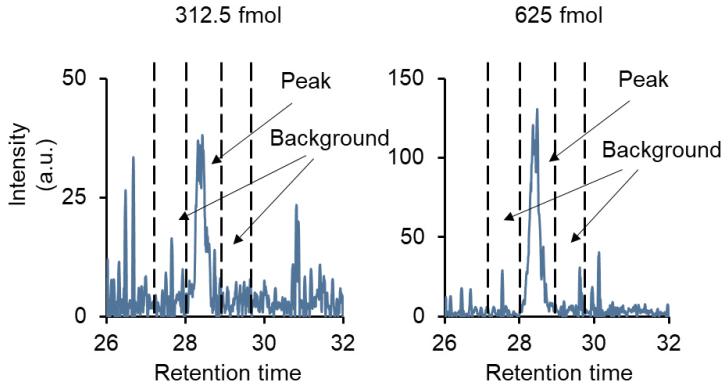

Figure 3.7 Limit of detection and limit of quantification of PtdIns(3,4,5)P_3. The XIC of fragment ion of GroPIns(3,4,5)P_3 at 321 m/z where 3.125 pmol and 6.25 pmol PtdIns(3,4,5)P_3 standard were spiked into unstimulated human platelets extract, with 1/10 of the sample injected into the IC. Signal-to-noise ratio = 3.9 for 312.5 fmol and 12.5 for 625 fmol.

3.3.2 Phosphoinositides profile in biological samples.

The method was applied to pre-adipocyte OP9 cells, rat brain tissue and human platelets to illustrate its effectiveness in biological matrices. It was also able to quantify the phosphoinositides' positional isomers and the rapid phosphoinositides profile changes in human platelets upon CRP and thrombin stimulation.

3.3.2.1 Phosphoinositides profile in resting and stimulated human platelets.

The levels of PtdIns4P, PtdIns(3,4)P_2, and PtdIns(4,5)P_2 in resting platelets were found to be 94.7 ± 11.1, 3.1 ± 0.2 and 59.2 ± 12.4 pmol/1x10^8 platelets, respectively (Figure 3.8A). Previous research found that the levels of PtdIns4P and PtdIns(4,5)P_2 in platelets were 150-245 and 55-139 pmol/1x10^8 platelets respectively (Perret *et al.* 1983; Tysnes 1992; Mauco *et al.* 1984), using radioactive labelling-based measurement. We were unable to detect PtdIns3P or PtdIns5P in the platelet samples, likely due to their lower abundance compared to PtdIns4P. As a result, the peak of PtdIns4P may have overshadowed those of PtdIns3P and PtdIns5P during analysis. The phosphoinositide levels obtained in the current investigation are consistent with prior findings, demonstrating the reliability of the workflow (Figure 3.8B).

To demonstrate that the workflow can detect transitory changes in phosphoinositides signalling, the influence of CRP and thrombin on phosphoinositides metabolism in stimulated human platelets was investigated (Figure 3.9). After 5 min of CRP treatment, the level of PtdIns4P and PtdIns(4,5)P_2 were increased by 2 fold, from 1043.6 ± 237.1 to 2079.6 ± 393.7 pmol/mg protein ($P<0.01$) and 1.5 fold, from 672.2 ± 116.6 to 1008.2 ± 174.9 pmol/mg protein ($P<0.05$) respectively, due to the increased activity of phosphatidylinositol cycle, including phosphoinositides kinase PIP4K and PIP5K as previously reported (Perret *et al.* 1983; Wilson *et al.* 1985). Furthermore, PtdIns(3,4)P_2 was increased by 4.3 fold, from 34.0 ± 6.6 to 146.0 ± 29.5 pmol/mg protein ($P<0.001$) after 5 min of stimulation, probably resulting from the

dephosphorylation of PtdIns(3,4,5)P_3 by phosphoinositides phosphatases SHIP that is present in platelets (Kavanaugh *et al.* 1996; Kisseleva *et al.* 2000). The use of a threshold concentration (0.1 U/mL) of thrombin as a stimulus, on the other hand, did not result in a significant change in PtdIns4P or PtdIns(4,5)P_2 profiles, but it did result in a 2-fold rise in PtdIns(3,4)P_2, from 34.0 ± 6.6 to 22.2 ± 70.2 pmol/mg protein ($P<0.01$). For PtdIns(3,4,5)P_3, it was originally undetectable in unstimulated platelets and became detectable after simulation with CRP (4.0 ± 16.7 pmol/mg protein) or thrombin (41.5 ± 46.9 pmol/mg protein).

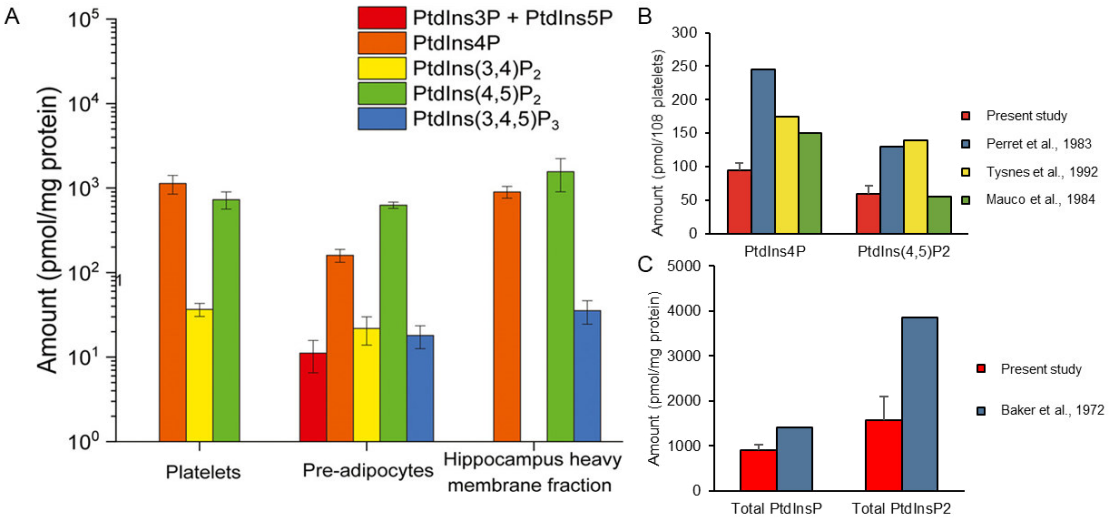

Figure 3.8 Resting phosphoinositides amount in platelets, OP9 pre-adipocytes, and rat hippocampus heavy membrane fraction. (A) Bar chart showing phosphoinositides profile in different biological samples, including human platelets, OP9 pre-adipocytes cell culture, and rat hippocampus heavy membrane fraction. Results are presented in mean ± SD. n = 3. The phosphoinositides quantified in (B) unstimulated human platelets and (C) hippocampus heavy membrane fraction were compared with previous reports.

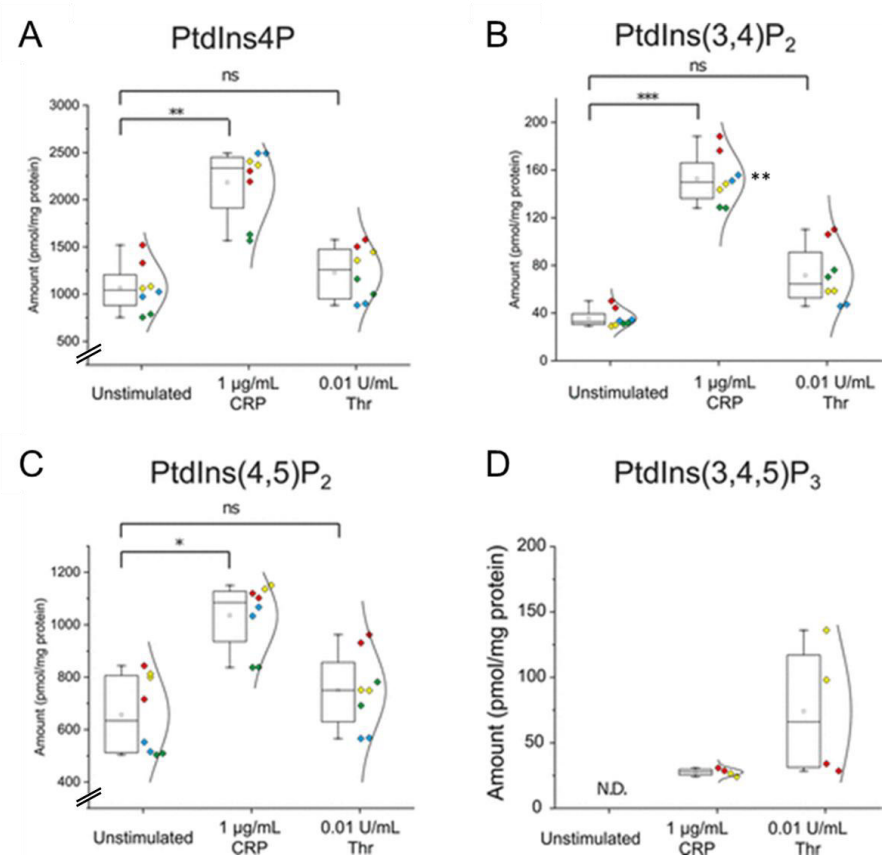

Figure 3.9 Effect of CRP and thrombin on human platelets phosphoinositides profile. Box plot showing changes in the phosphoinositides species, including (A) PtdIns4P, (B) PtdIns(3,4)P_2, (C) PtdIns(4,5)P_2, and (D) PtdIns(3,4,5)P_3 in human platelets after thrombin and CRP stimulation, quantified by internal calibration curve, with a half-violin plot showing the distribution of phosphoinositides of each donor. Each colour represents one of four different donors as biological duplicates, and each dot represents one of the technological duplicates. Results are presented in mean ± SD. *P < 0.05, **P < 0.01, and ***P < 0.001 calculated by Welch's t-test indicate statistically significance. ns, not significant. N.D., not detectable (n = 4 donors).

3.3.2.2 Phosphoinositides profile in OP9 pre-adipocytes and rat hippocampus.

OP9 cells are pre-adipocytes that can differentiate into mature adipocytes (Wolins *et al.* 2006). Most phosphoinositide species were detected in OP9 cells extract (Figure 3.8A), and the concentration of PtdIns3P + PtdIns5P, PtdIns4P, PtdIns(3,4)P_2, PtdIns(4,5)P_2, and PtdIns(3,4,5)P_3 were 11.1 ± 4.6, 160 ± 4, 21.8 ± 8.0, 630 ± 53, and 18.0 ± 5.4 pmol/mg protein, respectively.

In the P2 membrane fraction enriched from rat hippocampus, three phosphoinositides species were identified, including PtdIns4P, PtdIns(4,5)P_2 and PtdIns(3,4,5)P_3, and their concentrations were 901 ± 116, 1560 ± 540 and 6.8 ± 2.0 pmol/mg protein, respectively (Figure 3.8A). In comparison to earlier research that estimated the levels of PtdIns4P and PtdIns(4,5)P_2 to be 1400 and 3860 pmol/mg protein (Baker *et al.* 1972) (assuming 114 mg/g protein in the rat hippocampus (Banay-Schwartz *et al.* 1992)), the phosphoinositides levels reported in this study were consistent with prior studies and was also capable of detecting PtdIns(3,4,5)P_3 (Figure 3.8B), confirming the increased sensitivity of the selected technique.

3.4 Discussion

The use of IC rather than RPLC to separate GroPInsP retained the ability to separate the positional isomers while avoiding the requirement for ion-pairing reagents such as dimethylhexylamine (DMHA) in the eluent, which is added to shield the polar inositol phosphate headgroup and facilitate isomers separation using RPLC. This is a significant advantage of the current method over the RPLC method as ion-pairing agents are known to contaminate the MS equipment, cause ion suppression which lowers the MS detection sensitivity, and affects the ionisation pattern of ions, hindering the use of the same MS instrument for analysis of other analytes (Gustavsson *et al.* 2001; Holčapek *et al.* 2004).

Wang *et al.* have reported an RPLC-based method for analysing methylated phosphoinositides, with the ability to separate the positional isomers with no ion-pairing agents (Wang *et al.* 2016). However, high concentrations of lithium ions (10 mM Li^+) have to be added to the sample to form lithiated adduct ions, which affects the ionisation pattern of ions, hindering the use of the same MS instrument for analysis of other analytes. In addition, the positional isomers ratios were determined based on the ratio of phosphoinositides-lithiated adduct ions, which could easily be changed if a different sample matrix is used, reducing the robustness and accuracy of the method.

Morioka et al. and Li et al. have recently described a technique for measuring methylated phosphoinositide isomers using chiral column chromatography and a cellulose tris(3,5-dimethylphenylcarbamate) chiral selector. The method allows for the separation of isomers while maintaining the ability to measure acyl chain composition. However, there are differences in the elution order of isomers and retention time shifts between the two methods, and it is unclear if the elution order will be affected by the acyl chain combination as both methods only reported the elution order of phosphoinositides with the same fatty acyl chains 17:0/20:4 (Morioka et al. 2022; Li et al. 2021).

The IC-MS workflow reported in this chapter is able to detect GroPIns(3,4,5)P_3 with a LOD of 312.5 fmol. This is comparable with the most sensitive method reported so far by Clark *et al.* which reported a limit of detection of 250 pg (equivalent to 250 fmol) C18:0/C20:4-PtdIns(3,4,5)P_3, with added positional isomers resolution (Clark *et al.* 2011).

The study from Mujalli *et al.* has reported that a 10 min CRP treatment in human platelets raised the level of PtdIns4P and PtdIns(4,5)P_2 by 1.5 and 1.25 times, respectively, similar to the current report (Mujalli *et al.* 2018). However, their study was

unable to differentiate PtdIns(3,4)P_2 from PtdIns(4,5)P_2. Knowing and differentiating the level of PtdIns(4,5)P_2 and PtdIns(3,4)P_2 would provide information about the formation and flux change of PtdIns(3,4,5)P_3, because PtdIns(3,4)P_2 is a product of SHIP1 and SHIP2, two PtdIns(3,4,5)P_3 5-phosphatases that are known to regulate the level of PtdIns(3,4,5)P_3 in platelets (Kisseleva *et al.* 2000).

The presence of insulin-like growth factor 1 (IGF1) in FBS in culture media, which activated the IGF1 receptor on the cell surface and resulted in the creation of PtdIns(3,4,5)P_3 and derived species, might explain the increased variety and detection of PtdIns(3,4,5)P_3 in OP9 cells (Kurtz *et al.* 1985; Ridderstråle *et al.* 1995). Previous studies have also reported the production of PtdIns(3,4,5)P_3 in other pre-adipocyte cell lines such as 3T3-L1 upon IGF1 stimulation, which induced pre-adipocyte growth and survival (Gagnon *et al.* 2001; Sorisky *et al.* 1996).

In conclusion, this chapter reported an IC-MS-based workflow that greatly improves isomer resolution in phosphoinositide analysis which can be used to investigate the phosphoinositide composition in platelets, pre-adipocytes, and rat hippocampus membrane fraction. Except for GroPIns3P and GroPIns5P, this approach was able to isolate the physiologically important GroPInsPs isomers and reach a LOD and LOQ for phosphoinositides of 312.5 fmol and 625 fmol, respectively. The approach enhances sample preparation and analysis, resulting in increased confidence in phosphoinositide separation and quantification. The workflow's adaptability and capacity to uncover unique functions performed by each of the phosphoinositides are demonstrated by its application to diverse cell types and tissues.

Chapter 4

Development of a mathematical model of platelet phosphoinositide metabolism

4.1 Introduction

Phosphoinositides metabolism is deeply integrated with major signalling pathways such as G protein-coupled receptors (GPCRs) or tyrosine kinase receptors in all cell types, including the glycoprotein VI (GPVI) signalling cascade and Ca^{2+} mobilisation, as discussed in Chapter 1. Given the importance of phosphoinositides to subcellular signalling, many mathematical models incorporate these lipids, though often in a reduced form. Several mathematical models capture the interaction of lamellipodium and cell polarisation, which included PtdIns(4,5)P_2, PtdIns(3,4,5)P_3, phosphoinositide 3-kinase (PI3K) and phosphatase and tensin homolog (PTEN), and explored their role in shape changes and chemotaxis (Marée *et al.* 2012; Dawes *et al.* 2007). Olivença *et al.* developed a detailed mathematical model that captures the complete phosphoinositide pathway that accounts for all species of phosphoinositides and their interconverting enzymes (Olivença *et al.* 2018). The authors validated the model by predicting the effect of small interfering ribonucleic acid (siRNA) knockdown of phosphoinositides kinase and phosphatase on steady-state PtdIns(4,5)P_2 level in human alveolar epithelial cells. The time-dependent model comprising a system of 10 ordinary differential equations (ODEs) and 19 kinetic parameters were calibrated to steady-state data, neglecting the transient nature of the pathway.

Other recent studies attempt to describe mathematical elements of phosphoinositide metabolism in platelets. Diamond *et al.* developed a homogeneous mathematical model that captures GPCR signalling and the phosphatidylinositol cycle (PI cycle), which can predict the platelet dose-dependent response of Ca^{2+} mobilisation and inositol trisphosphate ($InsP_3$) production (Purvis *et al.* 2008). However, the author utilised 11 enzyme copy numbers and parameter values for model simulations that were taken from data from cells and tissues that are unrelated to platelets, such as rat liver, human cerebrospinal fluid, plant cells and yeast cells. These

approximations cover enzymes participating in phosphoinositides metabolism, including phosphatidylinositol-4-phosphate kinase, inositol monophosphate, inositol-1,4-bisphosphate 1-phosphatase, diacylglycerol kinase and cytidine diphosphate-diacylglycerol synthase. In addition, the model incorporates a reduced representation of the phosphoinositide pathway but neglects other phosphoinositide species such as PtdIns(3,4,5)P_3 and PtdIns(3,4)P_2.

Mazet *et al.* developed an ODE-based mathematical model that captured the PI cycle in platelets (Mazet *et al.* 2020). The author took parameter values from the literature and adjusted them so that simulations match experimental data and suggested that lipid- and protein-binding proteins help regulate PtdIns(4,5)P_2 and $InsP_3$ in GPCR signalling. Nevertheless, the model predicted changes of 10^8 molecules of inositol or PtdIns in less than 10 sec which we believe is too drastic to be physiologically relevant, as the majority of enzymes have turnover rates between 1 and 10,000. (Smejkal *et al.* 2019; Eremin *et al.* 2008).

4.2 Aims

The protein phosphorylation cascade and phosphoinositide metabolism downstream of GPVI signalling is well understood, as outlined in Chapter 1. Many of these studies, however, focus on single routes and do not combine several pathways or involve kinetic analyses. This chapter aims to develop a new dynamic mathematical description of phosphoinositide metabolism in platelets that is inferred from and validated against experimentally consistent high-density data. The model is calibrated against experimental data describing the time course of 5 phosphoinositides species (PtdIns, PtdIns4P, PtdIns(4,5)P_2, PtdIns(3,4)P_2 and PtdIns(3,4,5)P_3) and tyrosine phosphorylation of Linker for activation of T cells (LAT) at Y200 and phospholipase C (PLCγ2) at Y1217, which represent the CRP stimulus on phosphoinositides metabolism. The model is subsequently used to predict the effect of phosphatidylinositol 4-Kinase A (PI4KA) inhibitor GSK-A1 and inositol polyphosphate-5-phosphatase (OCRL) phosphatase inhibitor YU142670 on phosphoinositides metabolism and platelet activation, and cross-validated with inositol monophosphate ($InsP_1$) and Ca^{2+} measurements.

4.3 Results

4.3.1 Development of mathematical model on phosphoinositides metabolism downstream of GPVI signalling

4.3.1.1 Details of the model network, reactions and parameters

The mathematical model describing phosphoinositides metabolism downstream of GPVI signalling was developed together with Dr Joanne Dunster at the University of Reading. The model is developed using ODEs and as such is based on two assumptions: (i) all species that are located in the same compartment are evenly distributed, and (ii) all reactions in the model follow the law of mass action which states the rate of reaction is proportional to the concentration of the reactant and the rate constant. In the model, the reactions that comprise the phosphoinositide pathway are determined based on the copy number of the relevant enzyme in platelets, as shown in Figure 4.1 (Balla 2013; Burkhart *et al.* 2012). This is a simplified interpretation of the phosphoinositide pathway that neglects regulation via kinases and phosphatases and any diffusion or trafficking happening in the cytosol and the inner membranes, and represents the ER-PM membrane contact site (MCS) that is emerged in response to agonist stimulation and facilitates lipid-transfer proteins to shuttle phosphatidic acid and PtdIns back and forth across membranes.

In Model 1, we integrated phosphoinositides metabolism with collagen-related peptide (CRP)-induced activities of PI3K and phospholipase C-γ2 (PLCγ2), which convert PtdIns(4,5)P_2 into PtdIns(3,4,5)P_3 and hydrolyse PtdIns(4,5)P_2 into InsP_3 in the plasma membrane compartment (PM). We assumed all phosphoinositide species are in the PM. This is supported by a staining study showing that PtdIns4P and PtdIns(4,5)P_2 are localised in the PM of resting and activated platelets (Bura *et al.* 2021). We also incorporated the PI cycle to recycle the hydrolysed PtdIns(4,5)P_2 with no dead-end species. To increase the ability of the model to be inferred from the data,

the rest of the PI cycle is reduced to three components $InsP_3$, $InsP_1$ and Ipool, which comprises inositol and other inositol phosphates, residing in the cytosol (Cyt) compartment. Similarly, the variable Ppool localises at the PM compartment and comprises PtdIns3P, PtdIns5P, and PtdIns(3,5)P_2, which are unable to be measured by the IC-MS method due to their low abundance and overlap with the more prominent species PtdIns4P and PtdIns(4,5)P_2. We have also excluded diacylglycerol (DAG), phosphatidic acid, and cytidine diphosphate diacylglycerol (CDP-DAG) which are part of the PI cycle from the model, primarily because of a lack of data on their time-course changes or initial amount. We have instead incorporated these species into Ipool, which reduces the number of variables and parameters in the model, and prevent potential overfitting.

This model was modified (named Model 2) to consider the transportation of phosphatidylinositol from Cyt to PM compartment by phosphatidylinositol transfer protein type α (PITPα), which was shown to contribute to thrombin-induced $InsP_3$ production in platelets (Zhao *et al.* 2017). The goal of this adjustment is to slow down the flux of PtdIns conversion to PtdIns4P in an effort to improve the simulations.

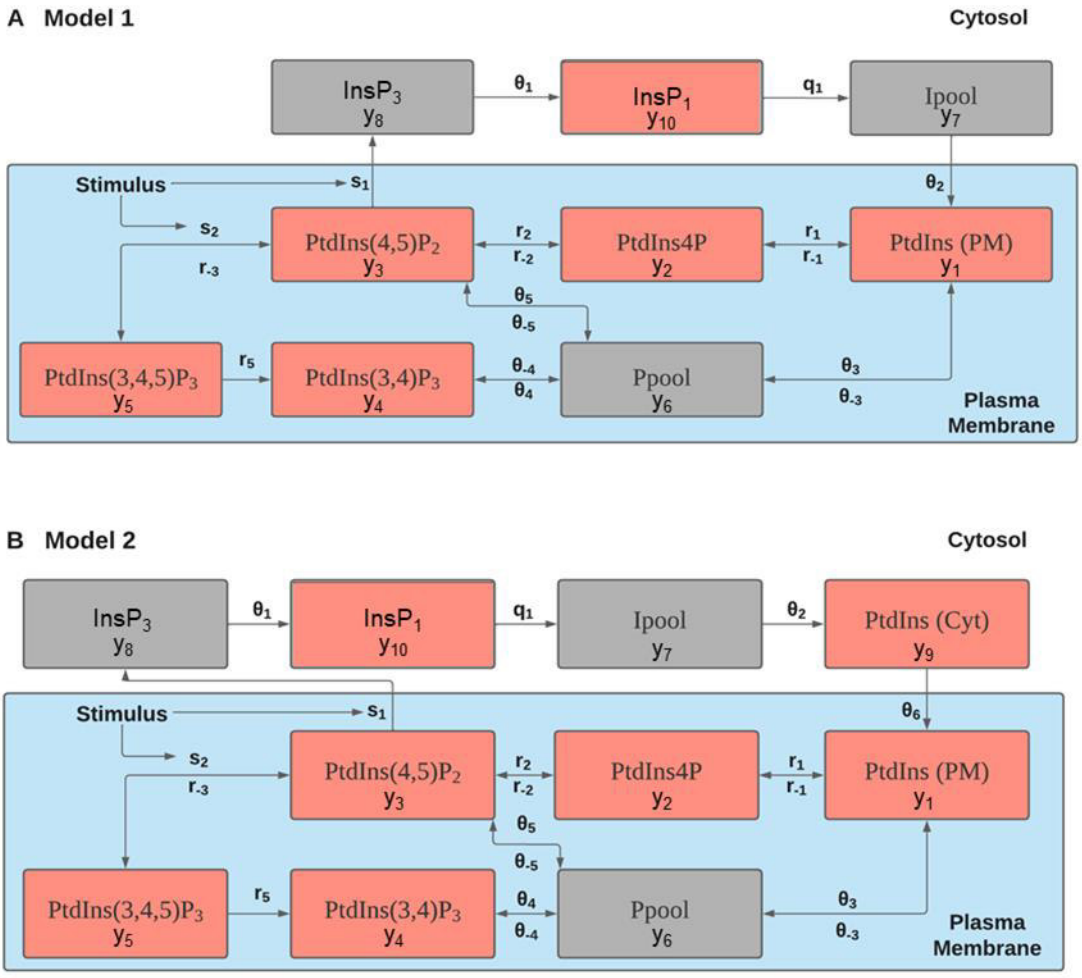

Figure 4.1 Network diagram of the phosphoinositides metabolism model. Network diagram of (A) Model 1 and (B) Model 2. Variables are represented by square boxes and the parameter associated with each process is placed next to the relevant arrow. See Tables 4.1 and 4.2 for a description of the variables and parameters. In Model 2, an additional species PtdIns (Cyt) and 1 new parameter θ_6 are added to incorporate the transportation of phosphatidylinositol from Cyt to PM compartment.

Utilising mass-action kinetics, the network diagram in Figure 4.1A is translated into the following system of nine ODEs for Model 1:

$$\frac{dy_1}{dt} = \theta_2 y_7 - r_1 y_1 + r_{-1} y_2 - \theta_3 y_1 + \theta_{-3} y_6, \quad (1.1)$$

$$\frac{dy_2}{dt} = r_1 y_1 - r_{-1} y_2 - r_2 y_2 + r_{-2} y_3, \quad (1.2)$$

$$\frac{dy_3}{dt} = r_2 y_2 - r_{-2} y_3 - s_1 stimy_3 - s_2 stimy_3 + r_{-3} y_5 - \theta_5 y_3 + \theta_{-5} y_6, \quad (1.3)$$

$$\frac{dy_4}{dt} = r_5 y_5 - \theta_4 y_4 + \theta_{-4} y_6, \quad (1.4)$$

$$\frac{dy_5}{dt} = s_2 stimy_3 - r_{-3} y_5 - r_5 y_5, \quad (1.5)$$

$$\frac{dy_6}{dt} = \theta_3 y_1 - \theta_{-3} y_6 + \theta_5 y_3 - \theta_{-5} y_6 + \theta_4 y_4 - \theta_{-4} y_6, \quad (1.6)$$

$$\frac{dy_7}{dt} = q_1 y_{10} - \theta_2 y_7, \quad (1.7)$$

$$\frac{dy_8}{dt} = s_1 stimy_3 - \theta_1 y_8, \quad (1.8)$$

$$\frac{dy_{10}}{dt} = \theta_1 y_8 - q_1 y_{10}\,. \quad (1.9)$$

The function *stim(t)* that appears in Equations 1.3, 1.4 and 1.8 captures the effect of CRP stimulus on phosphoinositides metabolism i.e. activation of PI3K and PLCγ2. This assumes that any changes in phosphoinositides metabolism do not affect tyrosine phosphorylation.

Similarly, the network diagram in Figure 4.1B can be translated into the following system of ten ODEs for Model 2:

$$\frac{dy_1}{dt} = \theta_6 y_9 - r_1 y_1 + r_{-1} y_2 - \theta_3 y_1 + \theta_{-3} y_6, \tag{2.1}$$

$$\frac{dy_2}{dt} = r_1 y_1 - r_{-1} y_2 - r_2 y_2 + r_{-2} y_3, \tag{2.2}$$

$$\frac{dy_3}{dt} = r_2 y_2 - r_{-2} y_3 - s_1 stimy_3 - s_2 stimy_3 + r_{-3} y_5 - \theta_5 y_3 + \theta_{-5} y_6, \tag{2.3}$$

$$\frac{dy_4}{dt} = r_5 y_5 - \theta_4 y_4 + \theta_{-4} y_6, \tag{2.4}$$

$$\frac{dy_5}{dt} = s_2 stimy_3 - r_{-3} y_5 - r_5 y_5, \tag{2.5}$$

$$\frac{dy_6}{dt} = \theta_3 y_1 - \theta_{-3} y_6 + \theta_5 y_3 - \theta_{-5} y_6 + \theta_4 y_4 - \theta_{-4} y_6, \tag{2.6}$$

$$\frac{dy_7}{dt} = q_1 y_{10} - \theta_2 y_7, \tag{2.7}$$

$$\frac{dy_8}{dt} = s_1 stimy_3 - \theta_1 y_8, \tag{2.8}$$

$$\frac{dy_9}{dt} = \theta_2 y_7 - \theta_6 y_9, \tag{2.9}$$

$$\frac{dy_{10}}{dt} = \theta_1 y_8 - q_1 y_{10}. \tag{2.10}$$

The model's variables, their units of measure, and initial conditions are summarised in Table 4.2. The model's parameters and their units are summarised in Table 4.3.

Variable	Description	Initial amount	Reference
y_1	PtdIns (PM)	1,350,000	This study, (Lagarde *et al.* 1982)
y_2	PtdIns4P	640,000	This study
y_3	PtdIns(4,5)P_2	310,000	This study
y_4	PtdIns(3,4)P_2	5,200	This study
y_5	PtdIns(3,4,5)P_3	1,900	This study
y_6	Ppool	25000	(Morris *et al.* 2000; Chicanne *et al.* 2012)
y_7	Ipool	100,000,000	(Binder *et al.* 1985)
y_8	InsP_3	0	This study
y_9	PtdIns (Cyt)	1,350,000	This study, (Lagarde *et al.* 1982)
y_{10}	InsP_1	2500	This study

Table 4.1 Variables and initial conditions for the mathematical models 1 and 2. Variable y_9, PtdIns(Cyt) only presents in Model 2. All species are measured in (and have units of measure in the model as) molecules per platelet.

Parameter	Description	Units	Model 1	Model 2	Fitting constraint
r_1	Rate of conversion of PtdIns to PtdIns4P	s^{-1}	✓	✓	10^{-4} - 10^{2}
r_{-1}	Rate of conversion of PtdIns4P to PtdIns	s^{-1}	✓	✓	10^{-4} - 10^{2}
r_2	Rate of conversion of PtdIns4P to PtdIns(4,5)P_2	s^{-1}	✓	✓	10^{-4} - 10^{2}
r_{-2}	Rate of conversion of PtdIns(4,5)P_2 to PtdIns4P	s^{-1}	✓	✓	10^{-4} - 10^{2}
r_{-3}	Rate of conversion of PtdIns(3,4,5)P_3 to PtdIns(4,5)P_2	s^{-1}	✓	✓	10^{-4} - 10^{2}
r_5	Rate of conversion of PtdIns(3,4,5)P_3 to PtdIns(3,4)P_2	s^{-1}	✓	✓	10^{-4} - 10^{2}
θ_1	Rate of conversion of InsP_3 to InsP_1	s^{-1}	✓	✓	10^{-2} – 10^{-1}
θ_2	Rate of conversion of Ipool to PtdIns (PM)	s^{-1}	✓	N/A	10^{-4} - 10^{2}
θ_2	Rate of conversion of Ipool to PtdIns (Cyt)	s^{-1}	N/A	✓	10^{-4} - 10^{2}
θ_3	Rate of conversion of PtdIns to Ppool	s^{-1}	✓	✓	10^{-4} - 10^{2}
θ_{-3}	Rate of conversion of Ppool to PtdIns	s^{-1}	✓	✓	10^{-4} - 10^{2}
θ_4	Rate of conversion of PtdIns(3,4)P_2 to Ppool	s^{-1}	✓	✓	10^{-4} - 10^{2}
θ_{-4}	Rate of conversion of Ppool to PtdIns(3,4)P_2	s^{-1}	✓	✓	10^{-4} - 10^{2}
θ_5	Rate of conversion of PtdIns(4,5)P_2 to Ppool	s^{-1}	✓	✓	10^{-4} - 10^{2}
θ_{-5}	Rate of conversion of Ppool to PtdIns(4,5)P_2	s^{-1}	✓	✓	10^{-4} - 10^{2}
θ_6	Rate of conversion of PtdIns (Cyt) to PtdIns (PM)	s^{-1}	N/A	✓	10^{-8} - 10^{2}
s_1	Rate of hydrolysis of PtdIns(4,5)P_2 into InsP_3	s^{-1}	✓	✓	10^{-6} – 10^{-2}
s_2	Rate of conversion of PtdIns(4,5)P_2 into PtdIns(3,4,5)P_3	s^{-1}	✓	✓	10^{-4} - 10^{2}
q_1	Rate of conversion of InsP_1 to Ipool	s^{-1}	✓	✓	10^{-4} – 10^{-3}

Table 4.2 Model parameters and fitting constraint in the phosphoinositides metabolism model. N/A indicates that the parameter is not applicable in the specified model. The parameter values of the 10 best fits of the model can be found in the Appendix

4.3.2 Time course profiling of protein phosphorylation and Ca^{2+} mobilisation in CRP-stimulated platelets

Experiments were conducted to determine the time-course phosphorylation of linker of activating of T cells (LAT) at Y200 and PLCγ2 at Y1217 downstream of GPVI activation for the determination of the function *stim*, that represents stimulus of phosphoinositide metabolism in response to platelet activation with CRP. The phosphorylation of LAT was chosen as a proxy for PI3K as it recruits and activates PI3K (Ragab *et al.* 2007). Washed platelets at 4 x10^8 cells were simulated with 10 µg/mL CRP in the presence of 9 µM eptifibatide and were lysed with 5x reducing lysis buffer at the stated time after the addition of CRP. The cell lysates were probed against phospho-specific antibodies to determine tyrosine phosphorylation. The addition of eptifibatide prevents the interference of integrin αIIbβ3 outside-in signalling which signals through Src and Syk (Watson *et al.* 2005) and prevents aggregation in stirring conditions, which hinders complete cell lysis by lysis buffer.

As shown in Figure 4.2B, CRP induced a rapid increase in phosphorylation for LAT at Y200, and PLCγ2 at Y1217, both plateaued at 45 sec and were sustained for up to 50 min. The *stim* function was then determined by fitting to the phosphorylation data:

$$stim = \left(0.001te^{-0.0002t^2}\right) + tanh(0.02t),$$

with *t* representing the time following CRP stimulation. The resulting *stim* function (dotted line) closely matches the LAT Y200 and PLCγ2 Y1217 phosphorylation profile.

Experiments were also conducted to measure Ca^{2+} mobilisation in CRP-stimulated platelets. Fura-2 loaded washed platelets at 2x10^8 cells/mL were pre-treated for 10 min with ADP scavenger apyrase (2.5 U/mL) and cyclooxygenase-1 (COX-1) inhibitor indomethacin (20 µM) to prevent the interference of secondary mediators signalling. The platelets were stimulated with 10 µg/mL CRP in the presence of 1 mM $CaCl_2$, to provide extracellular Ca^{2+} at physiological conditions which allow Ca^{2+} extracellular influx. As shown in Figure 4.2C, similar to phosphorylation of LAT at Y200 and PLCγ2 at Y1217, Ca^{2+} mobilisation plateaued at 120 sec (from 35 ± 13 to 233 ± 68 nM) and slightly decreased to 283 ± 70 nM over 10 min.

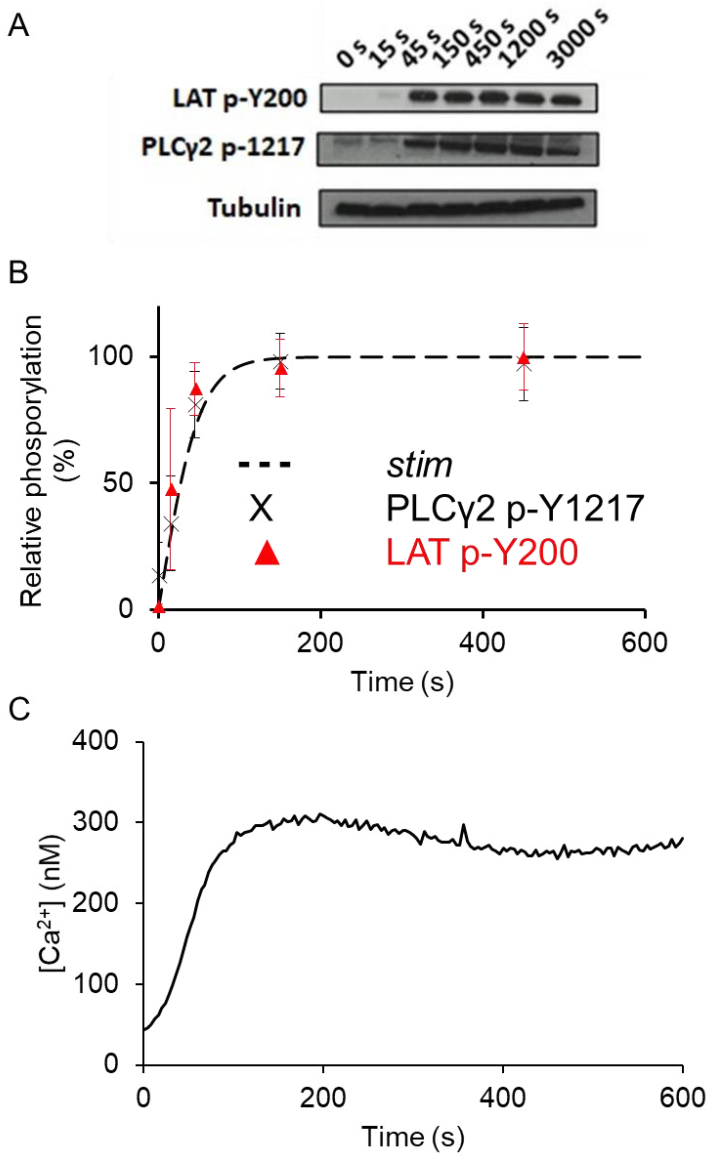

Figure 4.2 CRP-induced sustained tyrosine phosphorylation and Ca^{2+} mobilisation and the determination of *stim* function. (A) Washed platelets were stimulated with 10 µg/mL CRP in the presence of 9 µM eptifibatide. Platelets were lysed with 5x reducing lysis buffer at the stated time after the addition of CRP. Representative phosphorylation blots of whole-cell lysates after being probed using the stated antibodies. (B) Plot of mean ± SD % of relative phosphorylation for LAT at Y200, PLCγ2 at Y1217 and the extrapolated *stim* function. (C) Fura 2-loaded washed platelets at $2x10^8$ cells/mL were pre-treated for 10 min with apyrase (2.5 U/mL) and indomethacin (20 µM). The platelets were then stimulated with 10 µg/mL CRP in the presence of 1 µM $CaCl_2$. Representative traces of changes in $[Ca^{2+}]$ over the 600 sec were recorded. n = 3.

4.3.3 Time course profiling of phosphoinositides in CRP-stimulated platelets

Experiments were conducted to profile the time-course phosphoinositides changes downstream of GPVI activation. Washed platelets at 1.2 x109 cells were pre-treated for 10 min with apyrase (2.5 U/mL) and indomethacin (20 μM). Platelets were simulated with 30 μg/mL CRP, and the stimulation was stopped at the stated time with cold 1M HCl (Kielkowska et al. 2014). A greater platelet concentration compared to other platelet assays was used to improve detection sensitivity because of the low abundance of phosphoinositides, especially PtdIns(3,4,5)P3.

As shown in Figure 4.3, PtdIns show a slight initial increase (rising from 2.3 ± 0.5 to 2.9 ± 0.6 x 10^5 molecules/platelet over the first 60 sec) before declining to below base level (1.5 ± 0.2 x 10^5 molecules/platelet). In contrast, the amount of PtdIns(4,5)P2 gradually increased 1.6-fold over the first 120 sec (from 2.9 ± 0.6 to 4.8 ± 0.4 x 106 molecules/platelet), and remained elevated over basal for up to 30 min. PtdIns(3,4)P2 increased by 6-fold (from 0.5 ± 0.2 to 3.0 ± 0.8 x 10^4 molecules/platelet) over the first 180 sec and this elevated level was sustained for 10 min before dropping to 1.7 ± 0.1 x 10^4 molecules/platelet after 30 min. For PtdIns(3,4,5)P3, a 2.6-fold increase was observed over the first 180s, from 2.2 ± 0.8 to 5.8 ± 2.8 x 10^4 molecules/platelet. The large error bar is largely due to donor variability in the speed of signalling and PI3K activation upon agonist stimulation (Figure 8.2). Another explanation is the low abundance of PtdIns(3,4,5)P3 which increases the impact of background noise and lowers the accuracy of measurement. No significant change was observed for PtdIns4P, and its level remained near the basal level for 30 min. The fold change observed in Figure 4.3 is different from that reported in Figure 3.9, which can be attributed to the different experimental methods to stop the simulation reaction and platelet treatment as outlined in section 2.2.3.1.

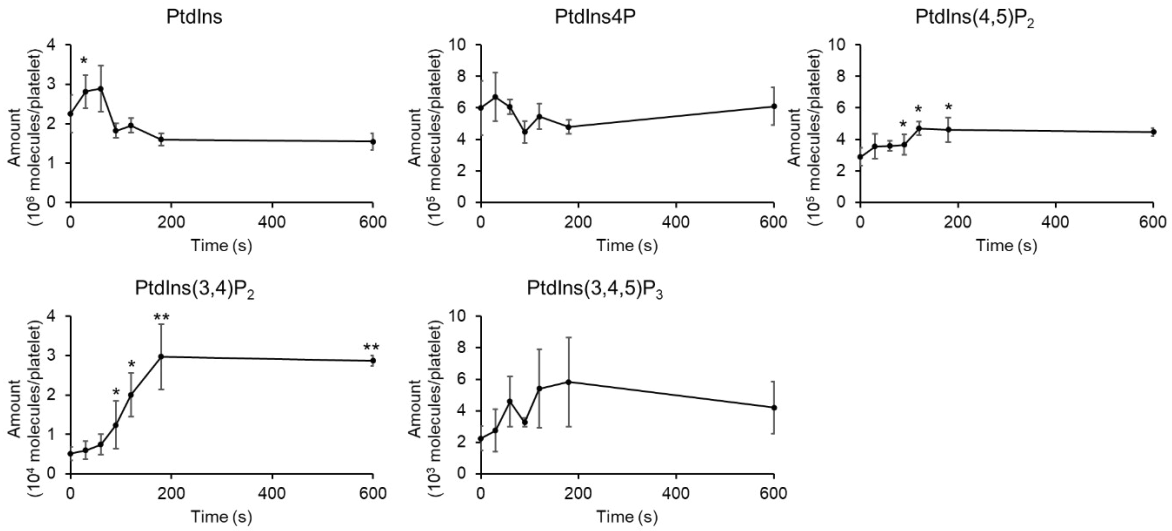

Figure 4.3 CRP-induced changes in phosphoinositides profile in human platelet. Washed platelets at 1.2x10^9 cells were stimulated with 30 µg/mL CRP in the presence of apyrase and indomethacin. The stimulation was stopped at the stated time with cold 1M HCl. The phosphoinositides in the samples were analysed and quantified using IC-MS. Results are expressed in molecules/platelet and are mean ± SD from 3 experiments. *($P < 0.05$) and **($P < 0.01$) calculated by one-way ANOVA followed by Tukey's test indicate statistically significant differences compared to t = 0 s.

4.3.4 CRP-induced accumulation of $InsP_1$ in platelet

CRP-induced accumulation of $InsP_1$ due to $InsP_3$ production and rapid hydrolysis was also investigated. Washed platelets at $8x10^8$ cells/mL were pre-treated for 10 min with DMSO vehicle in the presence of apyrase (2.5 U/mL), indomethacin (20 µM) and 50 mM LiCl. The presence of Li^+ inhibits inositol-phosphate phosphatase and prevents $InsP_1$ hydrolysis to inositol (Leech *et al.* 1993). The concentration of platelet, inhibitors and LiCl used is based on similar studies and manufacturer's instructions (Gilio *et al.* 2009; Bura *et al.* 2021).

As shown in Figure 4.4, in the DMSO vehicle, $InsP_1$ accumulation increased linearly, from 30 ± 12 to 284 ± 112 nM over 10 min. This is consistent with previous reports by Chen *et al.* who reported a CRP-induced accumulation of $InsP_1$ of 200 nM in 2 min and 600 nM over 15 min using washed platelets at $8x10^8$ cells/mL (Chen *et al.* 2014).

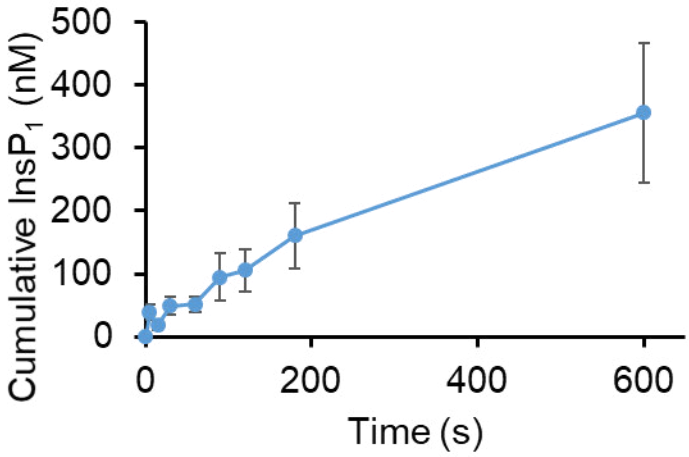

Figure 4.4 CRP induced sustained accumulation of $InsP_1$. Washed platelets at $8x10^8$ cells/mL were pre-treated for 10 min with DMSO vehicle in the presence of apyrase (2.5 U/mL), indomethacin (20 µM), and 50 mM LiCl to prevent $InsP_1$ hydrolysis. Afterwards, the platelets were stimulated with 10 µg/mL CRP, and the stimulation was stopped at the stated time with lysis buffer. Cumulative $InsP_1$ production was quantified using ELISA according to the manufacturer's instructions. n = 3 separate donors.

4.3.5 Model calibration and comparing model simulations with experimental profile

The 2 models were calibrated to the experimental data (Figure 4.2-4) utilising a Bayesian approach. We sampled parameter values via a Latin Hypercube from log-normal fitting constraints between 10^{-4} and 10^{2} for 20,000 times, as summarised in Table 4.2. The constraints for s_1, θ_1, θ_6 and q_1 are different from the listed range and adjusted according to literature which shows the hydrolysis rate of inositol phosphates (Watson, and Lapetina 1985; Watson, Reep, *et al.* 1985), or by the examination of posteriors distribution after the initial fitting. Based on the constraint, a gradient-based method (fmincon, MATLAB) was used to find the local minimum, minimising the distance between the mathematical model's simulations and the experimental data through the cost function:

$$SSE = \left(y_{i,x}(a) - Data_{i,x}\right)^2,$$

where SSE denotes sum squared error, $y_{i,x}(a)$ is model simulations for species x at time points i and $Data_{i,x}$ represents the experimental profile of species x at time points i. The 'best' parameter values are those that allow the mathematical model to produce simulations with the lowest SSE and are closest to the experimental data.

Figure 4.5A shows that both models are able to fit the data equally well, with similar minimum (both at 0.01) and median SSE/n (0.014 for Model 1 and 0.012 for Model 2). In Figure 4.5B, the posterior distributions of the parameter values show that this dataset cannot constrain the parameter values and that the approximated parameters in Model 2 are more widespread compared to Model 1. The ten 'best' simulations (utilising parameter values with the lowest SSE) are compared to the experimental data as shown in Figure 4.6. In both models, we observed that the top 10 simulations (black lines) fit well with the experimental profile (red lines). In addition, most best-fit lines had similar trajectories and were able to converge to their steady state over 600 sec except Ipool and Ppool.

In Model 1, the best-fitting simulations predicted a rapid depletion of Ipool from 10^8 molecules to 10^4 molecules in the first 200 sec. These molecules are subsequently converted to Ppool, which rapidly increases from $2\text{x}10^4$ molecules to 10^8 molecules in the first 200 sec through PtdIns as an intermediate. In contrast, Model 2 predicted a much less drastic change in Ipool and Ppool. The number of molecules in Ipool stayed constant over 600 sec of simulations, while the amount of Ppool slightly increases to around 10^5 molecules. The observed variations in the model simulations are due to

the lack of experimental data available for calibration. Nevertheless, the simulations of Model 1 seem too drastic to be physiologically possible within 200 sec, while the predictions of Model 2 fit better to our understanding of phosphoinositide metabolism in platelets. Model 2's prediction on Ppool increase is also comparable to a study by Valet *et al.* that showed a 3-fold increase in PtdIns3P after 3 min of CRP stimulation (Valet *et al.* 2015), assuming that PtdIns5P and PtdIns(3,5)P_2 remain unchanged.

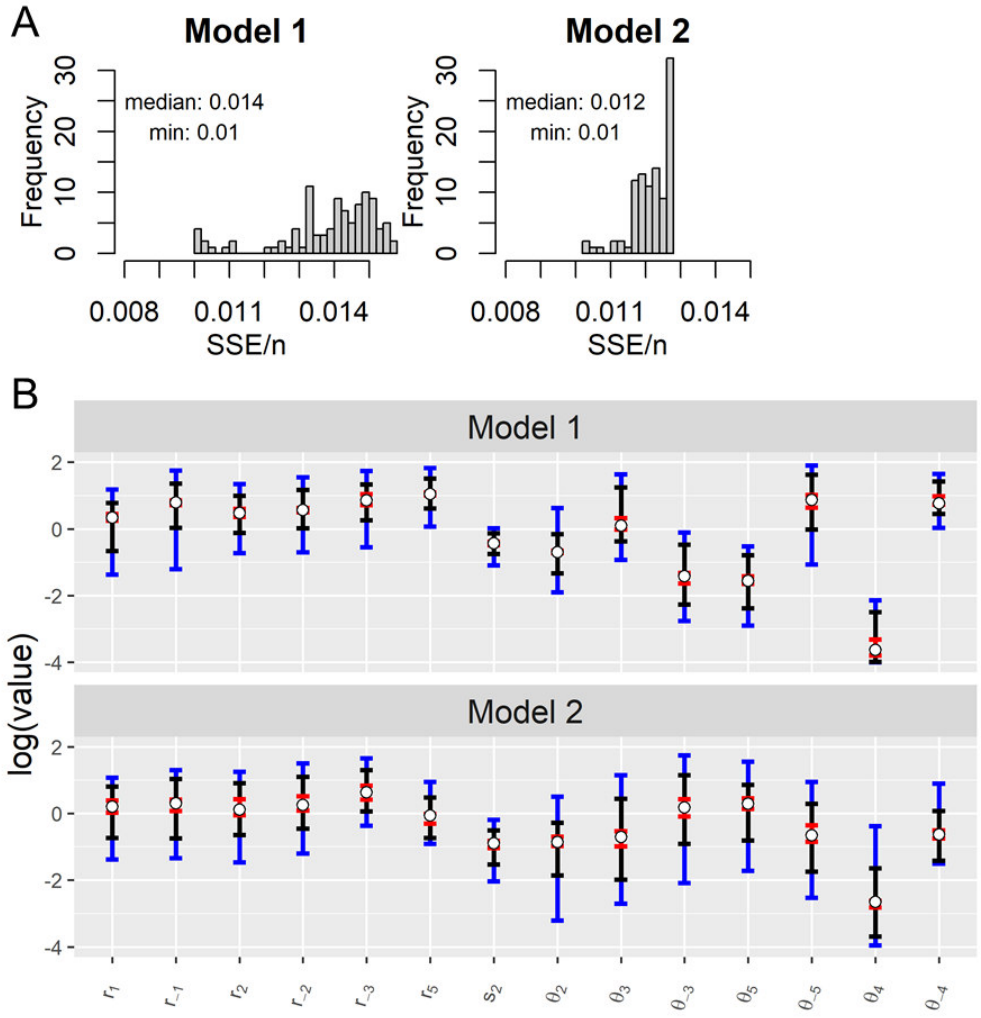

Figure 4.5 Assessing parameter fitting with cost function and range of parameters approximations. (A) Histograms showing the frequency of cost function SSE/n for the best 100 simulations for Models 1 (Left) and 2 (Right). The median and minimum SSE/n are also listed. (B) Posterior parameter ranges are shown for Models 1 (Top) and 2 (Bottom). The blue, black, and red lines and hollow circles show the full range, interquartile range, the inner 10% range and median of each estimated parameter. Posteriors for s_1, θ_1, θ_6 and q_1 are constrained to values from the literature and are shown in the Appendix.

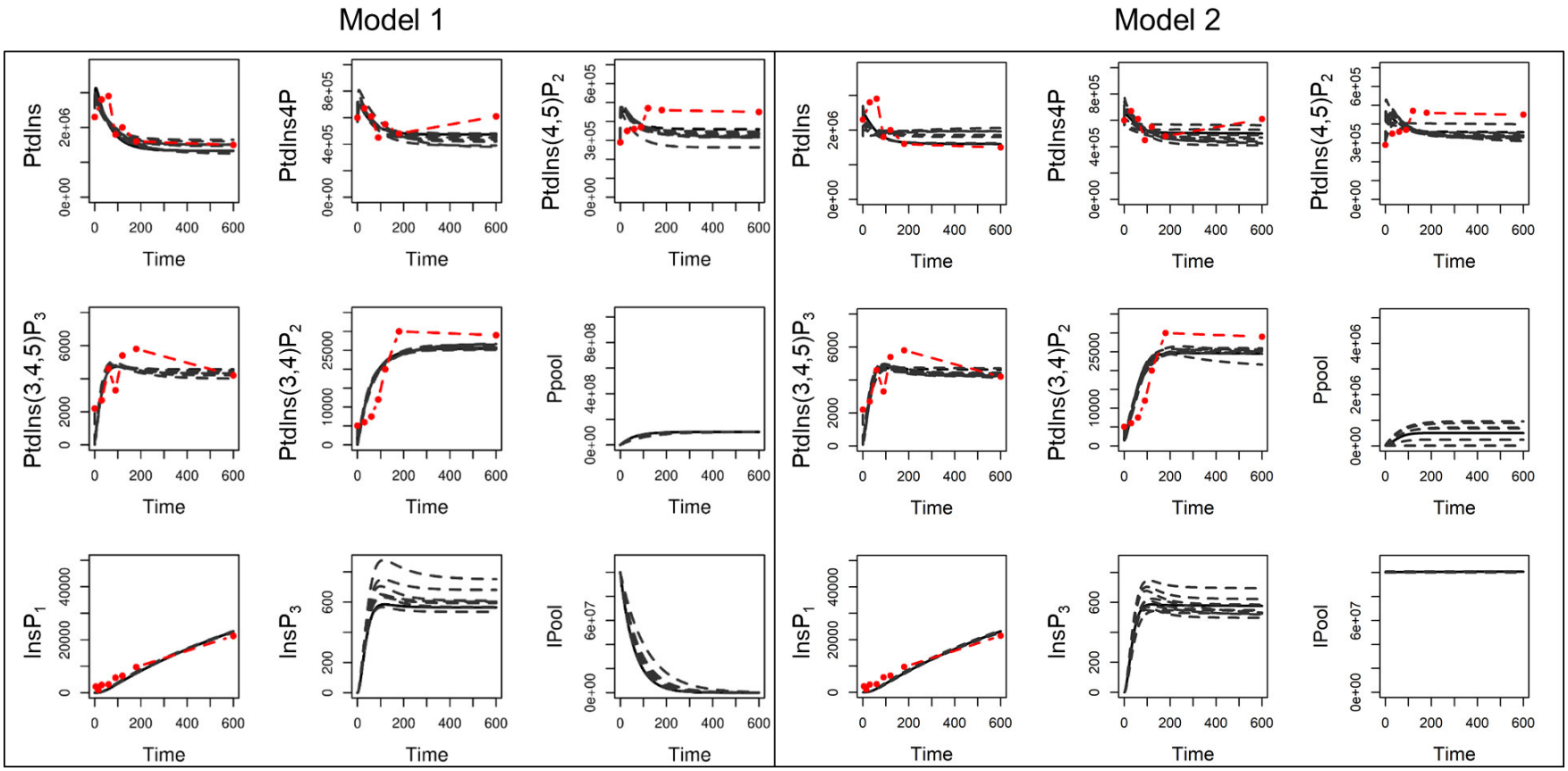

Figure 4.6 Comparison of model simulation profile with experimental data. The best-fitting model profiles of Model 1 (Left) and Model 2 (Right). The 10 best simulations (black dotted lines) and the average trajectory (black solid line) were compared to experimental observations in Figure 4.3 (red dotted lines).

4.3.6 Model prediction of the effect of phosphoinositides kinase and phosphatase inhibitors

The mathematical models capture the relationship between phosphoinositides in agonist-stimulated platelets. To test the models under alternative conditions, functional studies were undertaken using PI4KA inhibitor GSK-A1 (Bojjireddy *et al.* 2014) and OCRL inhibitor YU142670 (Pirruccello *et al.* 2014) on platelet activation and compared with the model's predictions. The use of these inhibitors is based on the hypothesis that these inhibitors would inhibit the resynthesis of PtdIns(4,5)P_2 level or dephosphorylation of PtdIns(4,5)P_2, respectively, thereby affecting CRP-induced InsP_3 production and Ca^{2+} mobilisation (Figure 4.7). To predict the effects of the phosphatase inhibitor YU122670, the model was simulated using the original parameters listed in Table 8.2 in the Appendix except for lowering the rate of conversion of PtdIns to PtdIns4P r_1 to 10% of the original value for GSK-A1 and lowering the rate of conversion of PtdIns(4,5)P_2 to PtdIns4P r_{-2} to 10% of the original value. We arbitrarily set it to 10% to simulate a 90% inhibition of the enzyme.

For the simulation of YU142670 treatment (Figure 4.8), both Models 1 and 2 have similar profile trends and predicted a lower steady-state level of PtdIns4P than the original model because of the inhibition of PtdIns(4,5)P_2 phosphatase which reduces the amount of PtdIns4P formed by PtdIns(4,5)P_2 dephosphorylation. At the same time, the predicted levels of PtdIns(4,5)P_2, PtdIns(3,4)P_2 and PtdIns(3,4,5)P_3, InsP_3 and InsP_1 are higher compared to the original model, due to the lack of removal of PtdIns(4,5)P_2 through dephosphorylation, and those fluxes are instead transferred to other species that are produced from PtdIns(4,5)P_2. The effect of r_{-2} on Ipool and Ppool is minimal and similar to that observed in Figure 4.6. The simulation is consistent with Bura *et al.* who reported an increase of intracellular PtdIns(4,5)P_2 in activated platelet compared to the unstimulated (Bura *et al.* 2021), visualised by anti-PtdIns4P, anti-PtdIns(4,5)P_2 antibodies labelled platelets.

For the simulation of treatment with the PI4KA inhibitor GSK-A1 (Figure 4.9), both models predicted the steady-state level of PtdIns to be higher than the original model due to the inhibition of PI4K which reduces PtdIns removal through phosphorylation in both models. Consequently, the resynthesis of PtdIns(4,5)P_2 is reduced, and the predicted steady-state levels of PtdIns(4,5)P_2 PtdIns(3,4)P_2 PtdIns(3,4,5)P_3 are 50% lower than the original model. Model 1 predicted a rapid drop in PtdIns4P and PtdIns(4,5)P_2 within 10 sec of agonist stimulation followed by slow

resynthesis of these species. This indicates the huge metabolic flux of r_1 (conversion of PtdIns to PtdIns4P) and r_2 (conversion of PtdIns4P to PtdIns(4,5)P_2) in Model 1, and with inhibition of r_1 these two species are rapidly depleted with slow replenishment.

Model 2 predicted that the level of PtdIns(4,5)P_2 PtdIns(3,4)P_2 PtdIns(3,4,5)P_3 and $InsP_3$ match the profile for the first 100 s, showing that inhibition of PI4K mostly has a less pronounced effect immediately affect agonist stimulation. Model 2 also predicted that GSK-A1 led to an increase in Ppool, possibly because of increased production of PtdIns3P and PtdIns5P due to more PtdIns being present. This increase is not observed in Model 1. The simulation is consistent with Bura *et al.* who reported a decrease of both PtdIns(4,5)P_2 and PtdIns4P levels in activated platelets compared to the control (Bura *et al.* 2021).

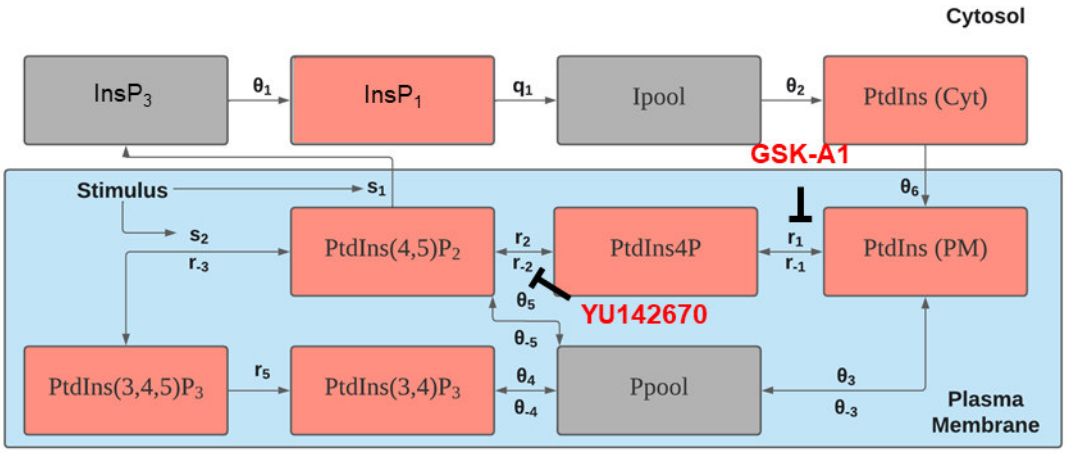

Figure 4.7 Schematic diagram of the phosphoinositides metabolism in the model and the mode of action of GSK-A1 and YU142670.

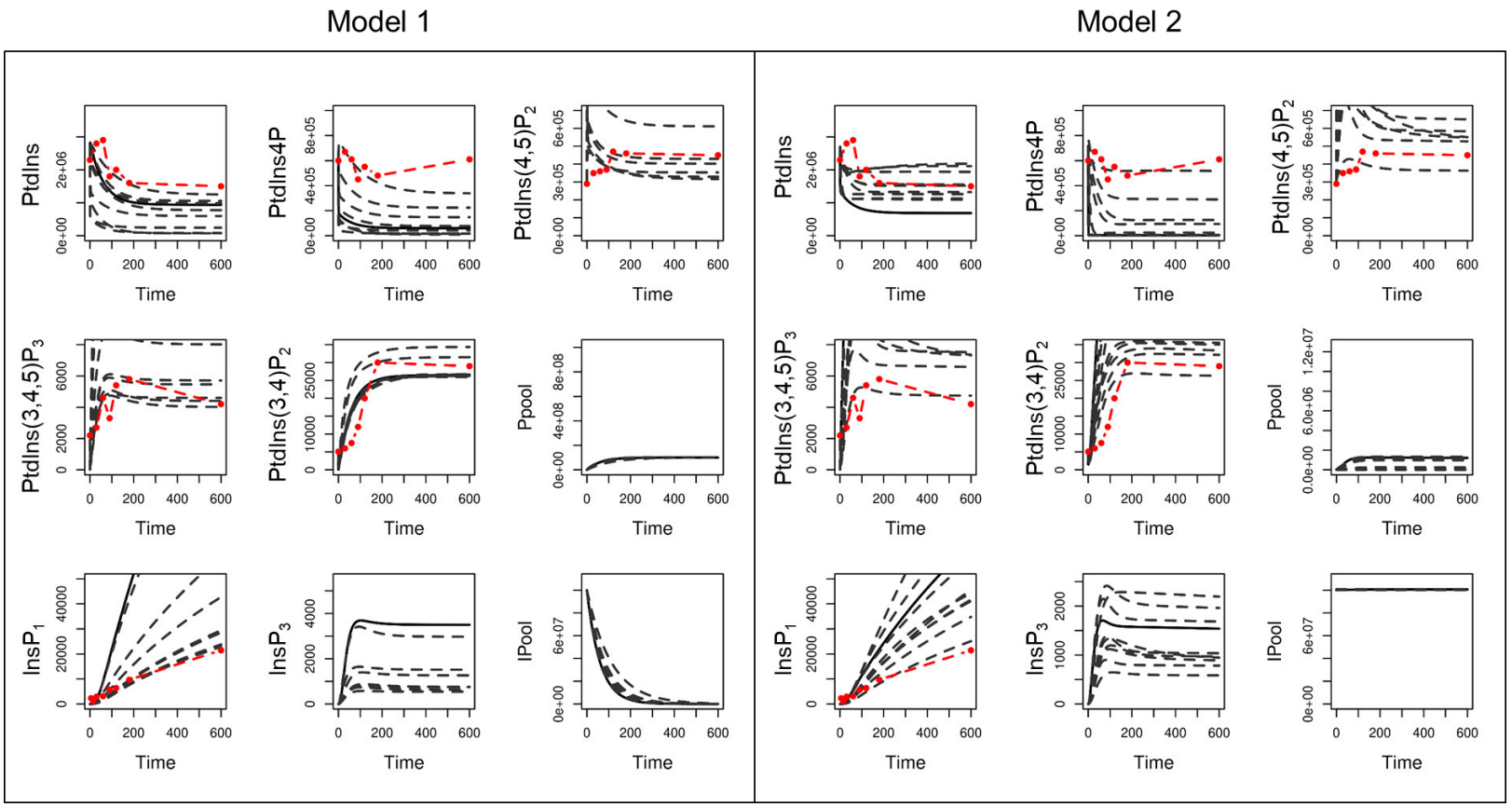

Figure 4.8 Simulation of the effect of YU142670 on phosphoinositides metabolism. The model is simulated by adjusting r_{-2} to 10% of its original value, while keeping all other parameters the same as in previous simulations. The ten best-fitting model profiles (black dotted lines) and the average trajectory (black solid line) were compared to the original experimental data (red dotted lines).

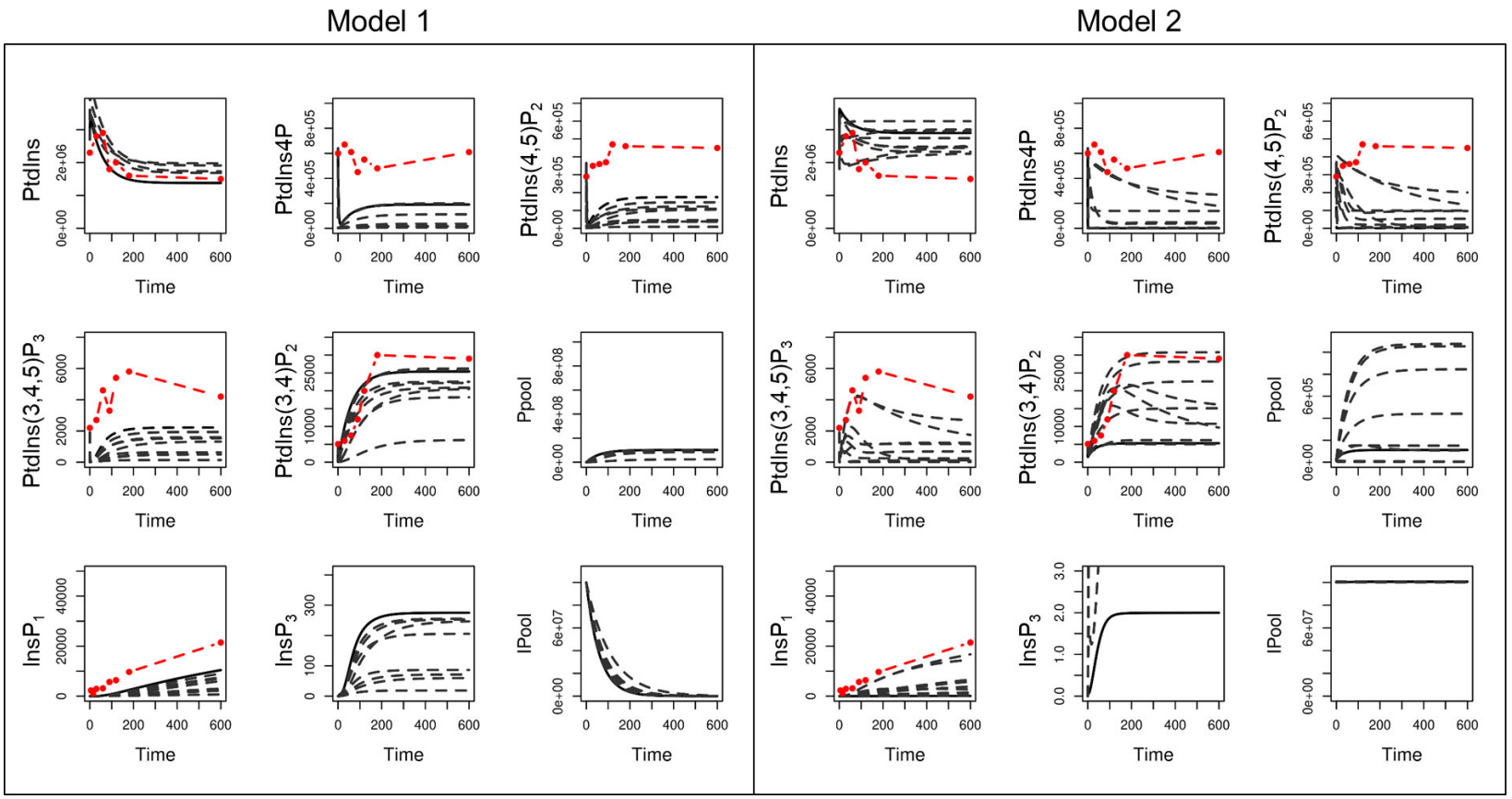

Figure 4.9 Simulation of the effect of GSK-A1 on phosphoinositides metabolism. The model is simulated by adjusting r_1 to 10% of its original value, while keeping all other parameters the same as in previous simulations. The ten best-fitting model profiles (black dotted lines) and the average trajectory (black solid line) were compared to the original experimental data (red dotted lines).

4.3.7 Effect of phosphoinositides kinase/phosphatase inhibitors on Ca^{2+} mobilisation

To validate the predictions of the models, functional experiments were conducted to investigate the effect of GSK-A1 and YU142770 on Ca^{2+} mobilisation. The dose-dependent response of these inhibitors was investigated to choose the optimal concentration for subsequent Ca^{2+} and $InsP_1$ assay. Fura-2 loaded washed platelets at $2x10^8$ cells/mL were pre-treated for 10 min with DMSO vehicle, GSK-A1 or YU142670 at the listed concentration in the presence of apyrase (2.5 U/mL) and indomethacin (20 μM). The platelets were then stimulated with 10 μg/mL CRP in the presence of 1 mM $CaCl_2$.

As shown in Figure 4.10A-B, for DMSO treatment, after CRP stimulation, Ca^{2+} mobilisation plateaued within the first 3 min increased from 23 to 330 nM, and remained above 300 nM over 10 min. 0.3 μM YU142670 treatment does not affect Ca^{2+} mobilisation, while treatment at 1, 3, 10 and 30 μM lead to a slight reduction in Ca^{2+} mobilisation, reaching 250 nM over the first 5 min and sustained over 10 min. Therefore, 1 μM YU142670 was chosen as the lowest concentration to affect the Ca^{2+} mobilisation. For GSK-A1, 3 and 10 μM treatment almost eliminates any Ca^{2+} mobilisation, with cytosolic Ca^{2+} level remaining within 100 nM over 10 min. Meanwhile, for 0.1, 0.3 and 1 μM GSK-A1 treatment, the Ca^{2+} also increased to 250 nM over the first 2 min, which returned to around 30 nM at basal at 10 min. Therefore, 1 μM GSK-A1 is chosen as it did not affect the initial Ca^{2+} mobilisation while inhibiting prolonged Ca^{2+} response.

The above experiments were repeated in three separate donors at 1 μM YU142670 and 1 μM GSK-A1 for both Ca^{2+} and $InsP_1$ assay (Figure 4.10 C-E). YU142670 has no effect on Ca^{2+} mobilisation in platelet. YU142670-treated platelets behaved similarly to that of the vehicle, with cytosolic Ca^{2+} increased rapidly for the

first two min, from the basal level at 35 ± 13 to 233 ± 68 (DMSO) and 262 ± 108 nM (YU142670). Afterwards, the Ca^{2+} level remained sustained and slightly decreased to 183 ± 70 (DMSO) and 190 ± 88 nM (YU142670) over 10 min. Meanwhile, for GSK-A1 treated platelets, the Ca^{2+} also increased rapidly for the first two min to 233 ± 82 nM, but it steadily decreased back to basal level for the next 8 min and reached 44 ± 9 nM, significantly lower than the vehicle ($P<0.01$).

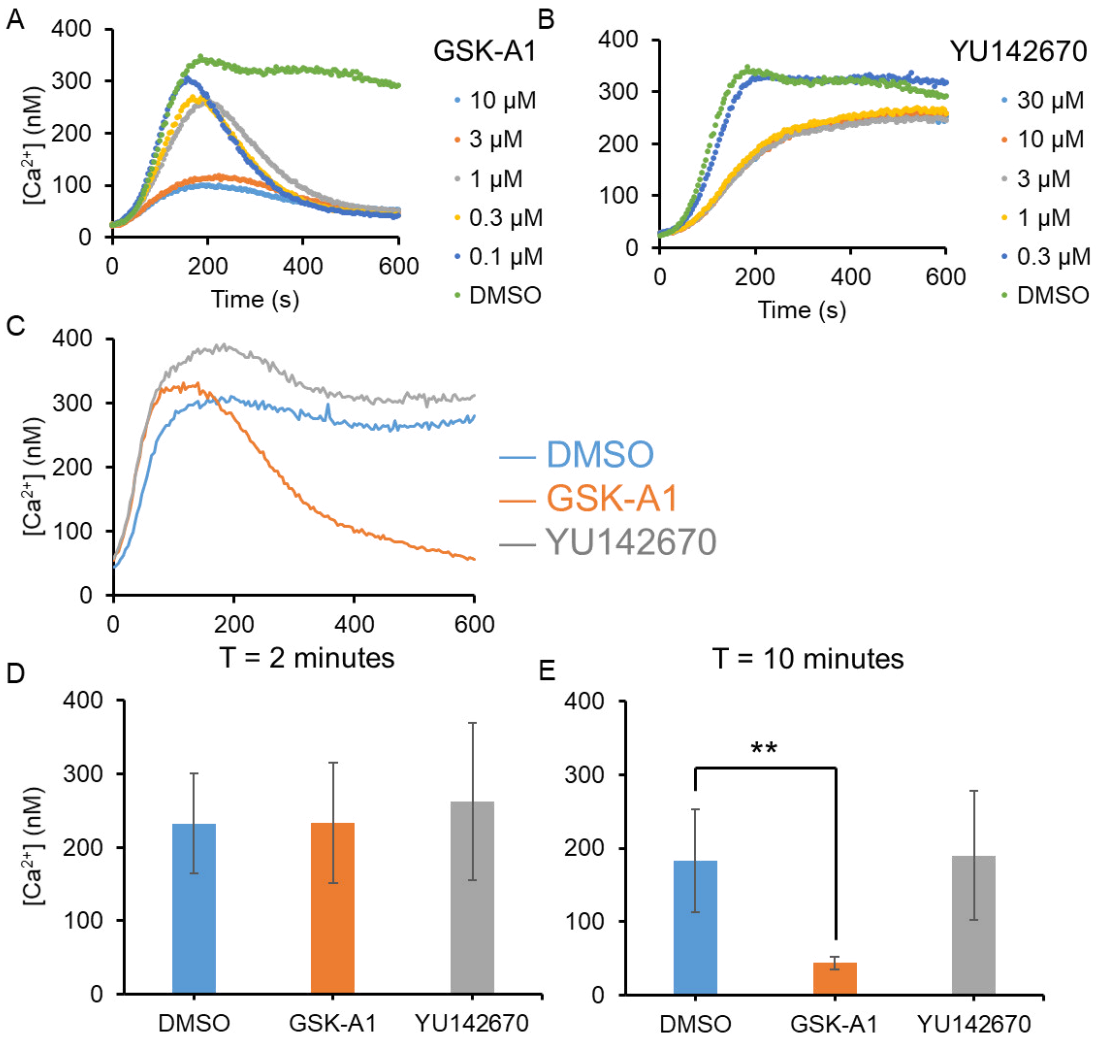

Figure 4.10 Effect of GSK-A1 and YU142670 on Ca^{2+} mobilisation. Fura 2-loaded washed platelets at $2x10^8$ cells/mL were pre-treated for 10 min with DMSO vehicle, or at the stated concentration of GSK-A1 or YU142670 in the presence of apyrase (2.5 U/mL) and indomethacin (20 µM). The platelets were then stimulated with 10 µg/mL CRP in the presence of 1 µM $CaCl_2$. (A-B) Dose-response curve of the effect of GSK-A1 and YU142670 on Ca^{2+} mobilisation. (n = 1) (C) Representative traces of changes in $[Ca^{2+}]$ of 1 µM GSK-A1 and YU142670-treated platelets over 600 sec were recorded. n = 3. Quantification of increases in $[Ca^{2+}]$ for (D) 2 min (E) 10 min after CRP stimulation, reported in mean ± SD **($P < 0.01$) calculated using Welch's t-test indicates statistically significant differences.

4.3.8 Validation of model using $InsP_1$ measurement and phosphoinositides kinase/phosphatase inhibitors

Experiments were also conducted to determine the effect of GSK-A1 and YU142670 on the accumulation of $InsP_1$. Washed platelets at $8x10^8$ cells/mL were pre-treated for 10 min with DMSO vehicle, 1 μM GSK-A1 or 1 μM YU142670 in the presence of apyrase (2.5 U/mL), indomethacin (20 μM) and 50 mM LiCl. The concentration of platelet, inhibitors and LiCl used is based on similar studies and manufacturer's instructions (Gilio *et al.* 2009; Bura *et al.* 2021).

As shown in Figure 4.11A, similar to vehicle (from 30 ± 12 to 284 ± 112 nM), YU142670 pre-treatment led to the accumulation of $InsP_1$ to 334 ± 41 nM after 10 min of CRP stimulation, which was not significantly different from DMSO treatment. On the contrary, 10 min pre-treatment of GSK-A1 was able to eliminate CRP-induced $InsP_1$ production, and remain at the basal level of 21 ± 3 nM after 10 min ($P < 0.05$ compared to vehicle). The results show that GSK-A1 inhibit $PtdIns(4,5)P_2$ resynthesis that prolonged the Ca^{2+} response, and that GSK-A1 treatment did not affect the initial Ca^{2+} mobilisation despite the lack of $InsP_1$ accumulation. This may suggest that the initial Ca^{2+} mobilisation is induced by $InsP_3$ is produced from the starting $PtdIns(4,5)P_2$.

The model's predictions were compared with the experimental data in Figure 4.11B. The predictions were produced by simulating the model with the same parameters as the original model except for 10% θ_1 (the rate of conversion of $InsP_1$ to Ipool) only for DMSO, or together with 10% r_1 for GSK-A1 or 10% r_{-2} for YU142670. Both models predicted the inhibition of $InsP_1$ accumulation for GSK-A1, with most of the best-fitting model profiles (black dotted lines) matching the experimental data (orange line in Figure 4.11A), accumulating to 1,000 to 10,000 molecules after 10 min (equivalent to around 13 to 130 nM for $8x10^8$ platelets/mL). For YU142670, the model predicted an enhancement in $InsP_1$ accumulation which was not observed in the

experiment. Comparing both models, in general simulation profiles of model 1 deviates more from the red lines, compared to Model 2. In addition, the best-fitting model profiles failed to converge or reach steady states, and the predicted $InsP_1$ level after 10 min ranges from 20,000 to 50,000 molecules (equivalent to 260 to 650 nM for $8x10^8$ platelets/mL).

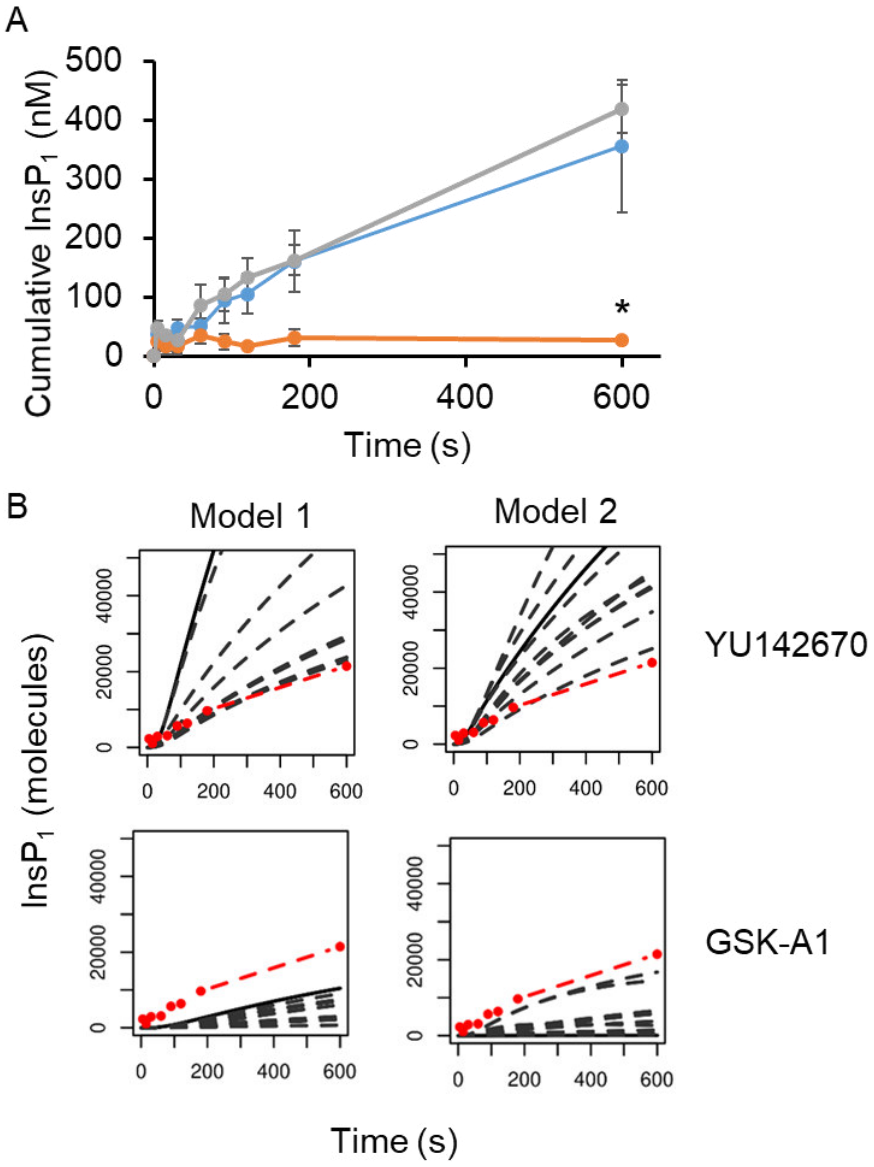

Figure 4.11 Comparison of experimental data and model predictions on the effect of GSK-A1 and YU142670 on $InsP_1$ accumulation. (A) Washed platelets at $8x10^8$ cells/mL were pre-treated for 10 min with DMSO vehicle, 1 μM GSK-A1 or 1 μM YU142670 in the presence of apyrase (2.5 U/mL), indomethacin (20 μM), and 50 mM LiCl to prevent $InsP_1$ hydrolysis. Afterwards, the platelets were stimulated with 10 μg/mL CRP, and the stimulation was stopped at the stated time with lysis buffer. Cumulative $InsP_1$ production was quantified using ELISA according to the manufacturer's instructions. *($P < 0.05$) calculated using Welch's t-test indicates statistically significant differences. n = 3 separate donors. (B) Models 1 (Left) and 2 (Right) were simulated at 10% r_{-2} to represent the effect of YU142670 (Top) or 10% r_1 to represent the effect of GSK-A1 (Bottom). The 6 best-fitting model profiles (black dotted lines) were compared to the observation in (A) (red dotted lines).

4.4 Discussion

In this chapter, we created a biological model of the phosphoinositides metabolism that uses kinetic rate characteristics determined in platelets downstream of GPVI, allowing a more accurate representation of platelets.

It has long been known that PtdIns(4,5)P_2 has a high turnover rate, which has been linked to "futile cycles" of dephosphorylation and rephosphorylation that are thought to occur on the PM (Hawkins *et al.* 1984). This is shown by the rapid labelling kinetics of PtdIns(4,5)P_2 and PtdIns4P compared to the much slower labelling kinetics of PtdIns and other phospholipids (Downes *et al.* 1982). In our model, we are able to simulate the high turnover mathematically between PtdIns(4,5)P_2, PtdIns4P and PtdIns which provided the kinetic basis for the futile cycle and demonstrated the system can reach a steady state in the simulated platelets system.

Controlling the amount of PtdIns(4,5)P_2 in the PM is crucial for regulating signalling and membrane dynamics. Cells must replenish this pool since PtdIns(4,5)P_2 only make up a tiny portion of all cellular PtdIns, particularly during prolonged PLC and PI3K activity. Early research in rat hepatocytes had shown that even a 10 min stimulation causes huge turnover in PtdIns(4,5)P_2 pool (Creba *et al.* 1983). This can be explained by the sequential phosphorylation by PI4K and PIP5K (Balla 2013), and the ER-PM membrane contact site (MCS) that is emerged in response to agonist stimulation and facilitate lipid-transfer proteins to shuttle phosphatidic acid and PtdIns back and forth across membranes, to sustain PtdIns(4,5)P_2 level(Posor *et al.* 2022). In the model, we integrated this concept by reducing the platelet environment into PM and Cyt compartments, with Cyt representing the cytosol and the inner membrane at the opposite side of MCS. This makes it possible for PtdIns to be transferred from the Cyt to the PM compartment by PITP in MCS in activated platelets without the need for vesicle transport, which would impede the replenishment of PtdIns and is unable to

support continuous secondary mediators generation. And as a result, the model is constructed based on an activated platelet and is unable to simulate the resting condition in an unstimulated platelet.

The Ca^{2+} assay shows that GSK-A1 treatment did not affect the initial Ca^{2+} mobilisation despite the lack of $InsP_1$ accumulation, but it inhibited prolonged Ca^{2+} response. The discrepancy is probably because platelet Ca^{2+} response is regulated by $InsP_3$ receptor activity, extracellular Ca^{2+} entry and Ca^{2+} back-pumping. In the first two minutes, $InsP_3$ is mainly produced by the initial pool of $PtdIns(4,5)P_2$ that is present in the PM, causing the opening of $InsP_3$ receptor and Ca^{2+} release from DTS. The Ca^{2+} spiking is caused by the co-stimulatory effect of $InsP_3$ and released Ca^{2+} (Clapham 2007). However, in the presence of GSK-A1 and inhibition of PI4KA, $PtdIns(4,5)P_2$ gradually depletes without replenishment from PtdIns. Together with the continuous hydrolysis of $InsP_3$ and its dissociation from $InsP_3$ receptors, the ion channels are eventually closed, and the cytosolic Ca^{2+} is pumped back to DTS by SERCA until returning to the basal level.

Model 1 predicted a rapid depletion of Ipool from 10^8 molecules to 10^4 molecules in the first 200 sec, which is converted to Ppool, increasing from $2x10^4$ molecules to 10^8 molecules in the first 200 sec through PtdIns as an intermediate. These predictions are too drastic to be physiologically possible within 200 sec. While for the predictions in Model 2, which predicted a stable pool of Ipool and a tiny increase in Ppool, are more physiologically feasible. The reason Model 1 produces such a simulation is that all 10^8 molecules of Ipool can participate in the reaction to synthesise PtdIns. By the law of mass action, with such a huge amount of reactant, the conversion rate of Ipool to PtdIns is huge, and these molecules are subsequently converted to Ppool instead of PtdIns4P, as its level is constrained by experimental data. Model 2

prevents such a large flux by having half of the PtdIns and its synthesis located in a separate intracellular compartment. Therefore PtdIns (PM) can only be converted from PtdIns(Cyt), which is 2 orders of magnitude lower than Ipool, resulting in a much lower conversion rate compared to Model 1. This highlights the importance of spatial regulation, trafficking on maintaining the futile cycle and equilibrium of interconversion of phosphoinositides.

The model predicted a slight enhancement in $InsP_1$ accumulation for YU142670 which was not observed in the experiment. In addition, YU142670 produced a similar Ca^{2+} mobilisation trace as vehicle. The lack of effect of YU142670 can be because OCRL is localised in the trans-Golgi network instead of the PM compartment (Faucherre *et al.* 2003). On the contrary, GSK-A1 inhibits PI4KA which localises in PM (MJ *et al.* 2022). Therefore, inhibition of OCRL may assert minimal short-term effect on the pool of high turnover phosphoinositides that localise in PM in activated platelets. Another possible explanation is that PLC, PI3K and the enzymes involved in PtdIns(4,5)P_2 resynthesis are saturated, and that the addition of YU142670 cannot increase the rate of $InsP_1$ accumulation past the saturated rate limit.

There are several limitations of the model. First, the model does not account for spatial effects, combining cytosol and the inner membranes into the same Cyt compartment. This is not the full representation of the platelet system, ignoring the cytosol-inner membrane interface which would, for example, limit the amount of inositol available to be incorporated into PtdIns, and prevent the huge flux from happening in Model 1. Second, the posterior parameter approximations generated in this study (Figure 4.6B) span two orders of magnitude, showing that there are insufficient experimental data to constrain the parameter values. Acquiring extra data under different experimental conditions, such as the use of different levels of agonist

and other phosphoinositides kinase/phosphatase inhibitors would help in constraining the range of approximated parameters. In addition, the model combined PtdIns3P, PtdIns5P, and PtdIns(3,5)P_2 into a single variable Ppool, because I was unable to quantitate their abundance by the developed IC-MS method due to their peak overlap.

In conclusion, this chapter develops an experimentally calibrated dynamic mathematical model of phosphoinositide metabolism in platelets. Despite advances in mass spectrometry-based profiling or imaging techniques, our quantitative knowledge of these transient and unstable phosphoinositides is still limited. This is because of the lack of tools available to real-time measure the absolute concentrations and subcellular resolution of lipids in living cells at the same time. The mathematical model developed in this chapter can circumvent these problems and shed light on the interconnectedness of phosphoinositide metabolism. The model is also able to predict the effect of GSK-A1 on phosphoinositides metabolism and platelet activation, proving the hypothesis it would inhibit the resynthesis of PtdIns(4,5)P_2 level thereby reducing CRP-induced $InsP_3$ production and sustained Ca^{2+} mobilisation.

Chapter 5

Inhibition of Src causes weak reversal of GPVI-mediated platelet aggregation as measured by light transmission aggregometry

The work conducted and the results produced in this Chapter have been published (Cheung *et al.*, 2022). This Chapter contains the work I have contributed to which is relevant to this thesis.

5.1 Introduction

Thrombi contain an inner core of densely packed platelets next to the damaged site and an outer shell of loosely packed platelets bound together by fibrinogen. Dissolution of the thrombus aggregates is an attractive strategy for preventing arterial blockage and ischaemic diseases.

Ahmed *et al.* have recently studied the disaggregation effect of targeting glycoprotein VI (GPVI), which can interact with fibrinogen in the thrombus shell to support its growth and stability as described in Chapter 1 (Ahmed *et al.* 2020). They demonstrated that inhibitors of tyrosine kinases Src, Syk and GPVI, PP2, PRT-060318 and glenzocimab, enhanced disaggregation of platelets on a collagen surface at arterial shear (Ahmed *et al.* 2020), and suggested that thrombus stabilisation is supported by the interaction of GPVI and fibrinogen (Ahmed *et al.* 2020). However, Ahmed *et al.* have also reported that glenzocimab was unable to reverse aggregation as measured by light transmission aggregometry (LTA), and proposed that platelet disaggregation occurring required the presence of shear forces which is absent in LTA (Ahmed *et al.* 2020). Similarly, Perrella *et al.* have reported that PRT-060318 and Src inhibitor dasatinib promoted thrombus disaggregation at arterial shear. They also reported that an anti-GPVI nanobody Nb21 caused a minor thrombus disaggregation

on a collagen surface, and attributed the effect to the inability to block fibrinogen-dependent activation of GPVI (Perrella *et al.* 2022).

In addition to these studies, Andre *et al.* have shown that Syk inhibitor PRT-060318 reduced thrombus stability and enhanced thrombus disaggregation on a collagen surface at arterial shear (Andre *et al.* 2011). In addition, Auger *et al.* have demonstrated the role of Src family kinases in maintaining aggregates stability on collagen surfaces at arteriolar flow rates (Auger *et al.* 2008). Another study by Perrella *et al.* has also shown the role of Src and Syk kinases in the signalling of fibrinogen-GPVI interaction in aggregate growth and stability under shear (Perrella *et al.* 2021). These studies highlighted the importance of sustained GPVI signalling and fibrinogen-GPVI interaction on thrombus stability.

In addition to fibrinogen-GPVI interaction, fibrinogen-integrin αIIbβ3 plays a major role in thrombus stability. Several other studies have demonstrated that integrin αIIbβ3 antagonists can reverse adenosine diphosphate (ADP)-induced aggregation in LTA in the absence of shear force (Moser *et al.* 2003; Frojmovic *et al.* 2005; Speich *et al.* 2009). Both Moser *et al.* and Speich *et al.* reported an almost complete disaggregation of ADP-induced aggregates after the addition of small molecule integrin αIIbβ3 antagonist eptifibatide (Moser *et al.* 2003; Speich *et al.* 2009). Another small molecule integrin αIIbβ3 antagonist lamifiban was also reported to completely

reverse ADP-induced aggregation (Frojmovic *et al.* 2005). Nevertheless, anti-integrin αIIbβ3 Fab abciximab has minor to no effect on ADP-induced aggregation, probably because of its larger size and poorer aggregate penetration (Moser *et al.* 2003; Frojmovic *et al.* 2005; Speich *et al.* 2009). In addition, eptifibatide has been reported to elicit a ~20% reversal of collagen-induced aggregation in LTA, when used at a 100-fold larger concentration than that is needed in pre-treatment to inhibit aggregation (Speich *et al.* 2013).

5.2 Aims

Evidence of the role of sustained GPVI signalling, fibrinogen-GPVI and fibrinogen-integrin αIIbβ3 interactions in thrombi and aggregates stabilisation has been demonstrated in disaggregation experiments in flow experiments and LTA using GPVI blocker, Src and Syk inhibitors and integrin αIIbβ3 antagonists. However, the difference in magnitude of reversal observed in these experiments shows that whereas aggregation may be reversed, it is affected by the choice of agonist and experimental design.

Therefore, in this chapter, I investigated the role of GPVI activation in sustained signalling and disaggregation. I used small molecule inhibitors of Src, Syk, and Btk to disrupt signalling through GPVI and to reverse tyrosine phosphorylation and aggregation, as examined by phosphospecific antibody and Western blot, LTA and flow cytometry.

5.3 Results

5.3.1 **Tyrosine kinase inhibitors reverse GPVI-mediated tyrosine phosphorylation**

Experiments were conducted to profile the time-course tyrosine phosphorylation downstream of GPVI activation (Figure 5.1). Washed platelets at $4x10^8$/mL were stimulated with 10 μg/mL CRP in the presence of 9 μM eptifibatide. Starting from 15-150 sec after stimulation by 10 μg/ml CRP, tyrosine phosphorylation of Syk at Y525/526, LAT at Y200, and Btk at Y551 was raised over 20-fold and sustained for up to 50 min. For PLCγ2 at Y1217 and Btk at Y223, which lie further downstream, their tyrosine phosphorylation increased at a slower rate, increasing up to 5-fold from 45-150 sec, and being sustained for 50 min (Figure 5.1).

Next, the effect of tyrosine kinase inhibitors on CRP-induced tyrosine phosphorylation was investigated. When the Src kinase inhibitors PP2 and dasatinib were given at 150 sec after the phosphorylation induced by CRP had plateaued, they caused dephosphorylation of Syk Y525/526, LAT Y200, Btk Y551, Btk Y223, and PLCγ2 Y1217, with phosphorylation falling to baseline within 20 min (Figure 5.2). The Syk inhibitor PRT-060318 inhibited tyrosine phosphorylation of proteins downstream of Syk, including LAT Y200, Btk Y551, and PLCγ2 Y1217, but has no significant effect on Syk Y525/526, which is phosphorylated by Src kinases and Syk itself (Figure 5.2). Similarly, the Btk inhibitor ibrutinib decreased tyrosine phosphorylation of proteins downstream of Btk, specifically Btk Y223, and PLCγ2 Y1217, but not Syk Y525/526, LAT Y200, or Btk Y551 (Figure 5.2).

These findings reveal that CRP induces prolonged tyrosine phosphorylation, which is inhibited in the presence of kinase inhibitors. This suggests that the inability of kinase inhibitors to completely reverse aggregation is not caused by the lack of tyrosine phosphorylation inhibition.

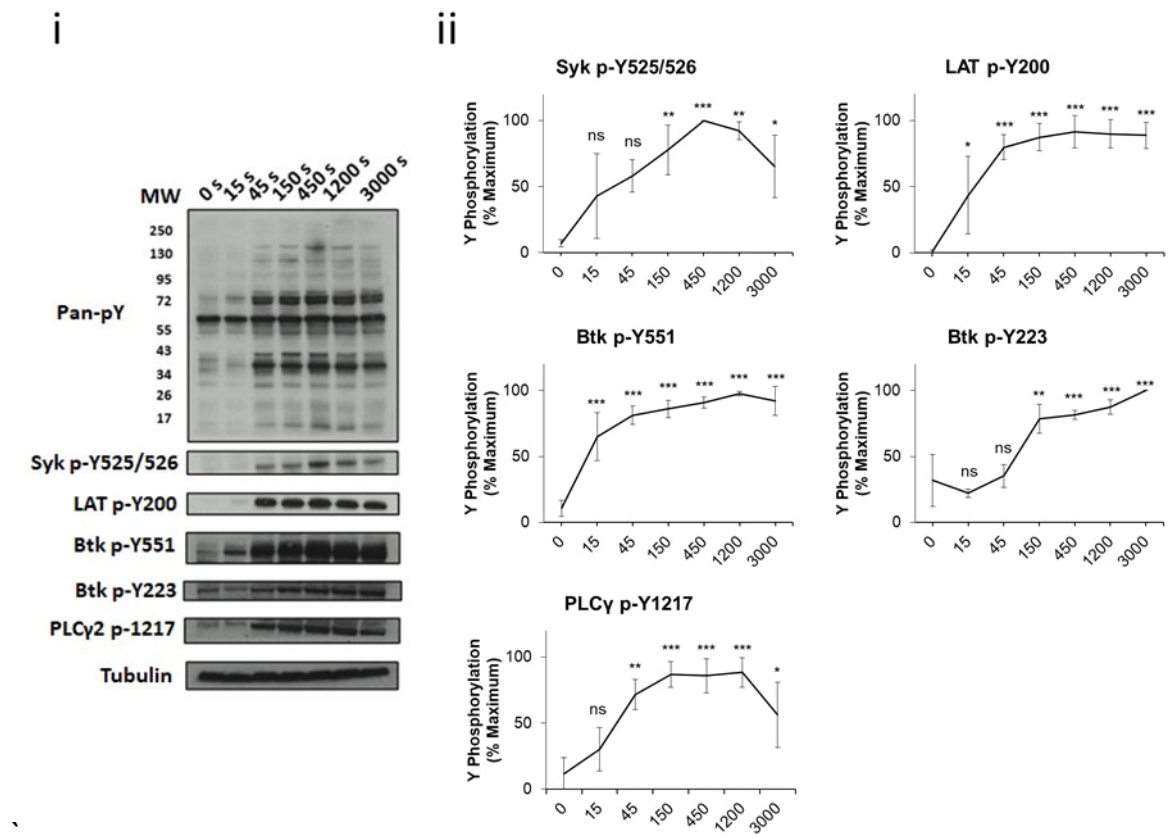

Figure 5.1 Tyrosine phosphorylation is sustained in GPVI-mediated protein phosphorylation. Washed platelets were stimulated with 10 µg/mL CRP in the presence of 9 µM eptifibatide. Platelets were lysed with 5x reducing sample buffer at the stated time after the addition of CRP. Whole-cell lysates were probed for phosphorylation. (i) Representative blot and (ii) mean ± SD % of tyrosine phosphorylation. ns, not significant, *($P < 0.05$), **($P < 0.01$) and ***($P < 0.001$) assessed by one-way ANOVA analysis and Tukey's test indicate statistically significant differences. N = 3.

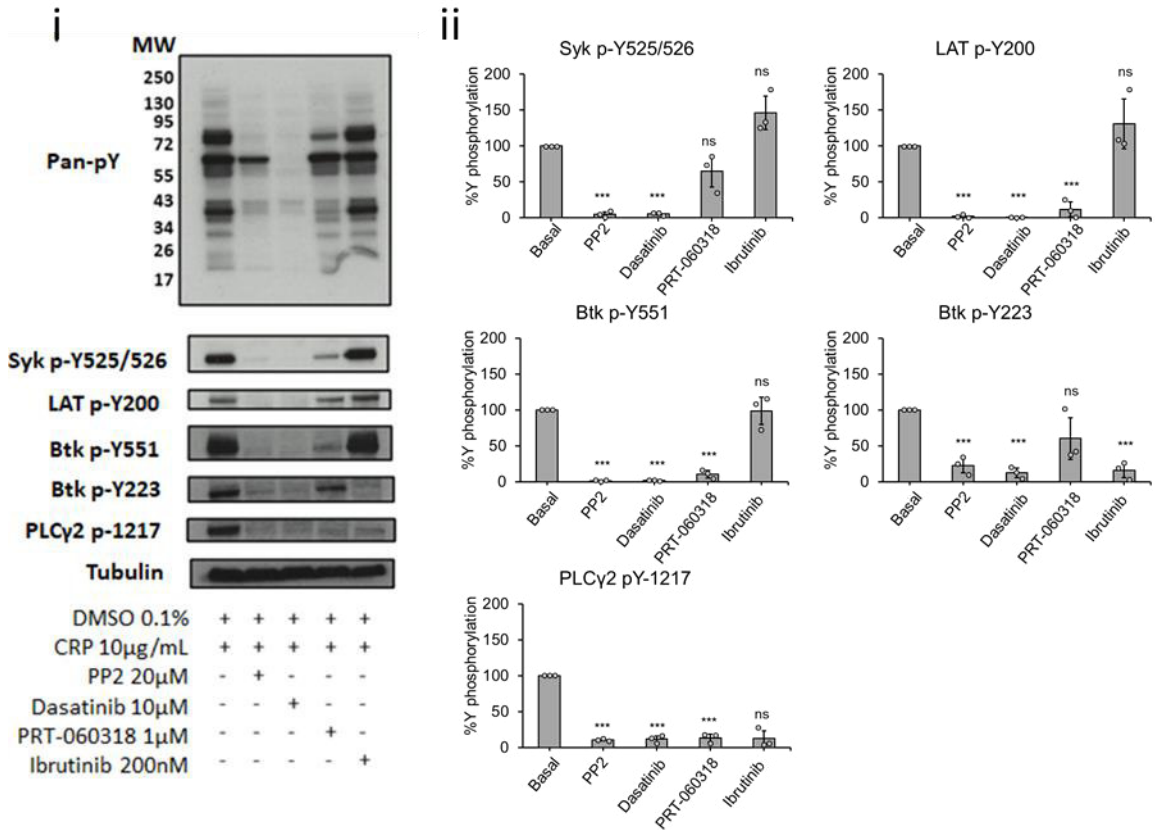

Figure 5.2 Kinase inhibitors reverse GPVI-mediated protein phosphorylation. Washed platelets were stimulated with 10 µg/mL CRP in the presence of 9 µM eptifibatide. Platelets were incubated with PP2 (20 µM), dasatinib (10 µM), PRT-060318 (1 µM), ibrutinib (200 nM) or vehicle after 150 sec of agonist stimulation. Platelets were then lysed with 5X reducing sample buffer 20 min after the addition of the agonist and probed for phosphorylation with the stated antibodies. (i) Representative blot and (ii) mean ± SD % of tyrosine phosphorylation. ns, not significant, *($P < 0.05$), **($P < 0.01$) and ***($P < 0.001$) calculated using Welch's t-test compared with basal. N = 3.

5.3.2 GPVI-induced platelet aggregation is minimally reversed by the addition of inhibitors of Src but not Syk and Btk inhibitors

I then looked into whether Src, Syk and Btk kinases can reverse GPVI-induced platelet aggregation in LTA. Aggregation to a maximally effective concentration of the GPVI ligand, CRP (10 µg/mL), peaked within the first 150 sec and was maintained for up to 50 min (Figure 5.3A). When aggregation had reached a plateau, kinase inhibitors were administered at maximum effective concentrations and light transmission was observed for 20 min. No significant reversal in light transmission at the end of 20 min was observed in the presence of Syk inhibitor PRT-060318 (3.0 ± 3.4%) and Btk inhibitor ibrutinib (0.4 ± 0.5%) compared to vehicle (1.5 ± 2.8%, Figure 5.3B). In contrast, the Src inhibitor PP2 induced a minor decrease in light transmission, with a reversal of 11.4 ± 4.0% ($P < 0.05$) over 20 min (Figure 5.3B). There was also a minor reversal of aggregation in the presence of dasatinib but the result was not significant (7.4 ± 7.2%) (Figure 5.3B)

The experiment was extended to protease-activated receptor 1 (PAR1) agonist TRAP-6. Similar to CRP, Src inhibitor PP2 (9.9 ± 3.1%) caused a small but significant reverse in light transmission relative to vehicle (1.0 ± 0.1%); in contrast, however, there was no significant reversal of aggregation in the presence of dasatinib (6.0 ± 5.0%) and PRT-060318 (2.1 ± 0.9%) (Figure 5.3C).

The findings reveal that CRP and TRAP-6-induced aggregation is sustained for up to 20 min in the presence of Syk and Btk inhibitors, but is partially reversed in the presence of Src kinase inhibitor PP2 but not dasatinib. This suggests that the inability of kinase inhibitors to completely reverse aggregation is not caused by the lack of tyrosine phosphorylation inhibition.

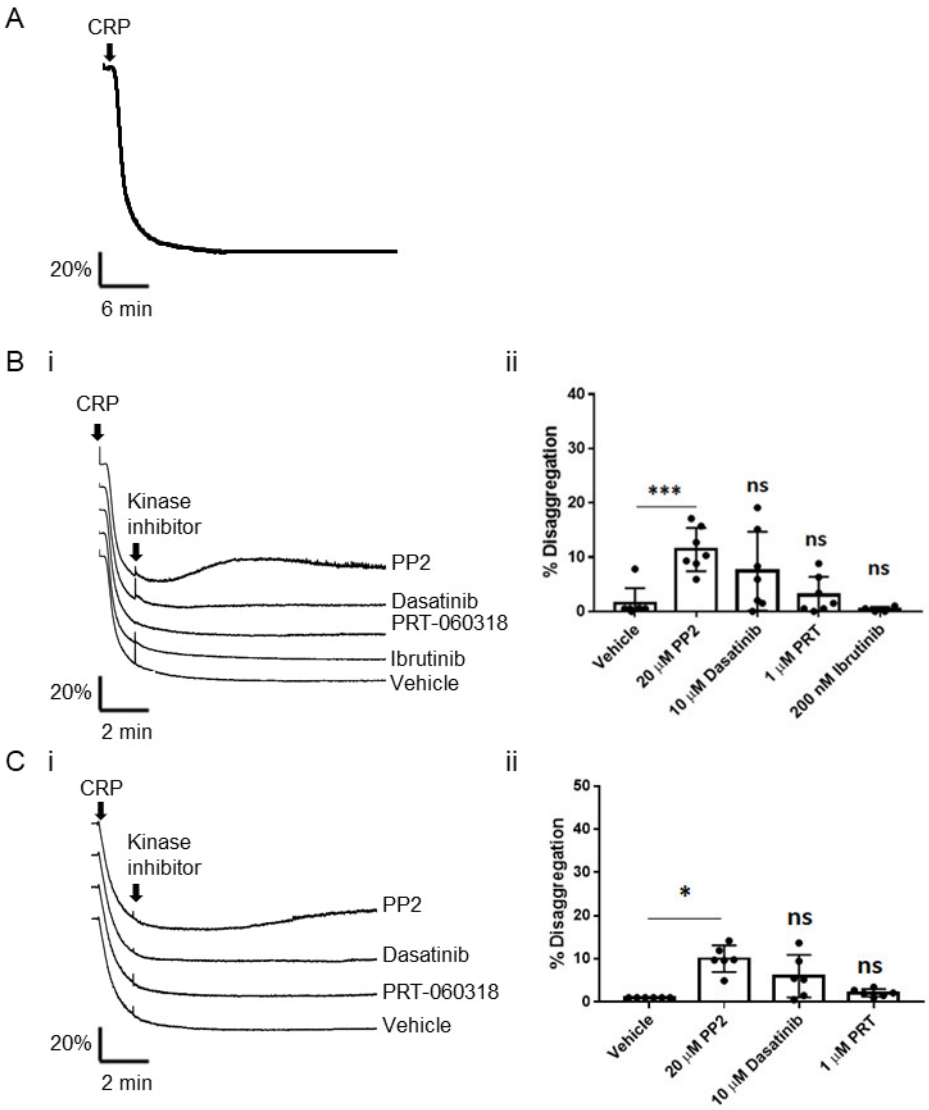

Figure 5.3 Src kinase inhibitor PP2 partially reversed GPVI-mediated platelet aggregation. (A) Washed platelets at $2x10^8$/ml were stimulated with 10 µg/mL CRP, and aggregation was monitored for 50 min. (B-C) Washed platelets were stimulated with (B) 10 µg/mL CRP or (C) 15 µM TRAP-6 and incubated with PP2 (20 µM), dasatinib (10 µM), PRT-060318 (1 µM), ibrutinib (200 nM) or vehicle, after 150 sec of agonist stimulation. LTA was monitored for 20 min. (i) Representative traces and (ii) Mean ± SD % disaggregation after 20 min of agonist stimulation. ns, not significant, *($P < 0.05$) and ***($P < 0.001$) calculated using Welch's t-test indicate statistically significant differences. N = 6.

5.3.3 Platelet aggregation is sustained in the presence of tyrosine kinase inhibitors when combined with apyrase and indomethacin

The observation that aggregation is maintained in the presence of inhibitors of Src, Syk and Btk indicates that aggregation is independent of GPVI signalling. One hypothesis is that the role of GPVI is overshadowed by the release of secondary mediators ADP and TxA_2. To study the role of secondary mediators in maintaining aggregation, I treated platelets with tyrosine kinases inhibitors in the presence of cyclooxygenase (COX) inhibitor indomethacin and ADP scavenger apyrase. As shown in Figure 5.4, when platelets were treated with apyrase and indomethacin alone or in combination with the kinase inhibitors after CRP-induced aggregation plateaued, no significant reversal was observed over 20 min for the vehicle (1.6 ± 3.0%), dasatinib (3.9 ± 1.4%), PRT-060318 (1.5 ± 1.2%) or ibrutinib (0.6 ± 0.3%) (Figure 5.4). Only PP2 caused a significant reversal compared to vehicle (7.2 ± 3.4%, $P < 0.05$). These results are similar to the observations without secondary mediators inhibitors and suggest that signalling through ADP and TxA_2 are not required for sustained platelet aggregation as measured by LTA.

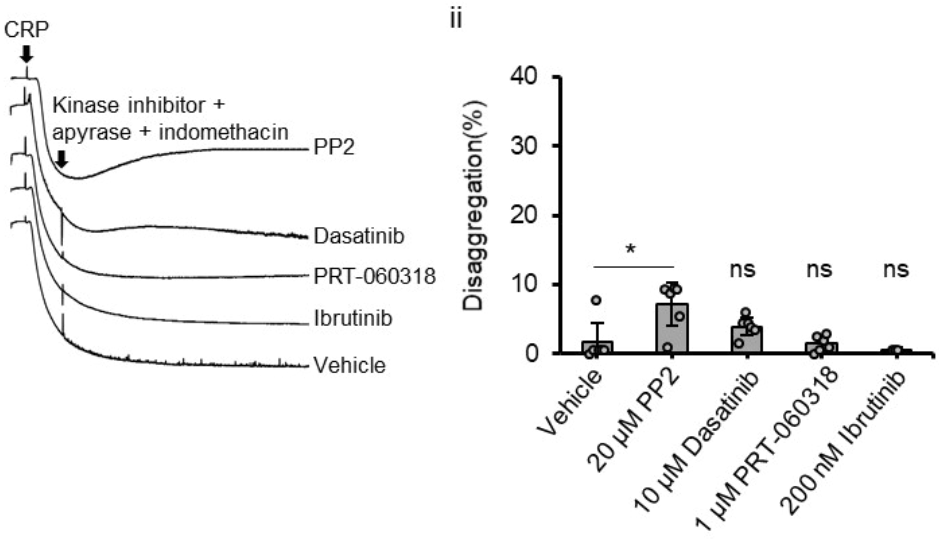

Figure 5.4 Kinase inhibitors together with secondary mediators partially reversed GPVI-mediated platelet aggregation. Washed platelets were stimulated with 10 µg/mL and incubated with PP2 (20 µM), dasatinib (10 µM), PRT-060318 (1 µM), ibrutinib (200 nM) or vehicle together with 10 µM indomethacin and 2.5 U/mL apyrase, after 150 sec of agonist stimulation and monitored by LTA for 20 min. (i) Representative traces and (ii) Mean ± SD % disaggregation after 20 min of agonist stimulation. *($P < 0.05$) and ns, not significant, calculated using Welch's t-test indicate statistically significant differences. N = 6 separate donors.

5.3.4 Tyrosine kinase inhibitors partially reversed GPVI-mediated platelet aggregation together with integrin αIIbβ3 antagonist

To study the involvement of integrin αIIbβ3 in GPVI-mediated aggregation, the above experiments were performed in the presence of the eptifibatide. The maximal reversal in the presence of eptifibatide alone was 4.5 ± 2.9%, which was further enhanced in combination with PP2 and PRT-060318 to 13.4 ± 11.6 and 13.7 ± 7.4%, respectively (Figure 5.5). These reversals were all significant compared to vehicle (0.7 ± 0.6%).

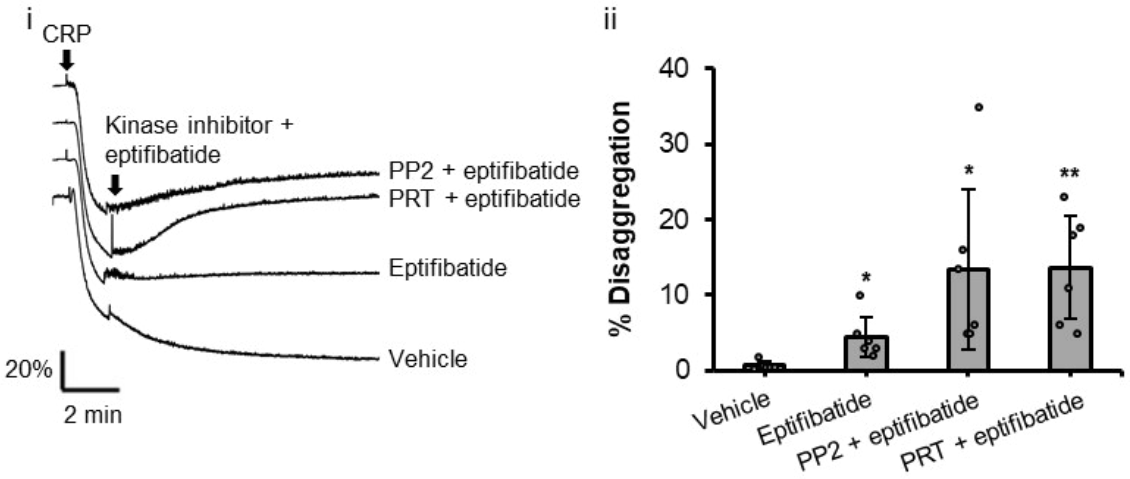

Figure 5.5 Tyrosine kinase inhibitors partially reversed GPVI mediated platelet aggregation together with integrin αIIbβ3 antagonist. Washed platelets ($2x10^8$/mL) were stimulated with CRP (10 µg/mL). After 150 sec of stimulation, they were incubated with eptifibatide 9µM alone or together with PP2 (20 µM) or PRT-060318 (1 µM) and monitored by LTA for 20 min. (i) Representative traces and (ii) Mean ± SD % of disaggregation. *($P < 0.05$) and **($P < 0.01$) calculated using Welch's t-test. N = 6.

5.3.5 Tyrosine kinase inhibitors reverse integrin αIIbβ3 activation

I further investigated whether the activation of integrin αIIbβ3 is reversible in the absence of outside-in signalling. To study this, activation of integrin αIIbβ3 was measured using PAC-1-FITC by flow cytometry in a dilute suspension of platelets which prevents aggregation, done by Luis Moran at the University of Birmingham. Upon CRP stimulation, the addition of vehicle without kinase inhibitors led to sustained integrin αIIbβ3 activation, with the mean fluorescence intensity (MFI) increased by 12.8 ± 10.5 fold compared to that of unstimulated platelets (Figure 5.6). On the contrary, the addition of PP2 and PRT-060318 reversed integrin αIIbβ3 activation over 20 min, with comparable MFI (1.1 ± 0.3 and 1.1 ± 0.5 fold) to those of unstimulated platelets (Figure 5.6). This demonstrates that GPVI-induced integrin αIIbβ3 activation is a reversible process in the absence of aggregation.

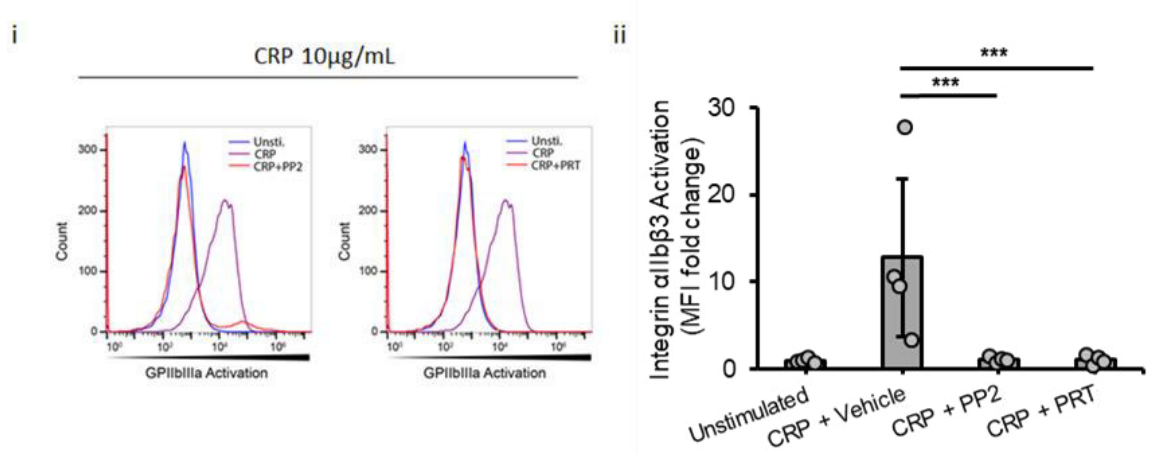

Figure 5.6 Tyrosine kinase inhibitors reverse integrin αIIbβ3 activation. Washed platelets ($2x10^7$/ml) were incubated with PAC-1-FITC and stimulated with 10 µg/mL CRP. After 150 sec of stimulation, vehicle, PP2 (20 µM) or PRT-060318 (1 µM) were added, and flow cytometry analyses were conducted after 20 min. (i) Flow cytometry histograms depicting the extent of integrin αIIbβ3 activation in platelets that were unstimulated (blue), stimulated by CRP followed by incubation with vehicle (purple), PP2 (red, left) or PRT-060318 (red, right). (ii) MFI fold change ± SD. ***($P < 0.001$) calculated using Welch's t-test indicates statistically significant differences. N = 4.

5.4 Discussion

The findings reveal that GPVI signalling and the secondary mediators ADP and TxA_2 are not necessary for prolonged aggregation in washed platelets as evaluated by LTA. However, in the presence of Src kinase inhibitor PP2 but not Syk and Btk inhibitors, a partial reversal in CRP and TRAP-6-induced aggregation are observed. This shows that the effect is independent of GPVI or GPCR-mediated signalling, and can be attributed to the loss of aggregate stabilising integrin αIIbβ3 outside-in signalling which is dependent on Src but not Syk or Btk (Watson *et al.* 2005). This is supported by the study by Auger *et al.* which demonstrated the dynamic process of maintaining stable aggregates in a compact form at high shear is regulated by Src kinases (Auger *et al.* 2008).

In the LTA, I have shown that dasatinib also has a tendency to reverse aggregation but failed to produce a significant result in both CRP and TRAP-6-induced aggregation. This is probably due to donor variability and the modest extent of the reversal, which caused a reversal in some but not all experiments and a large error bar. In addition, dasatinib was able to cause a minor and significant aggregation reversal for rhodocytin-induced aggregation, which was conducted in tandem with this work and has been published (Cheung *et al.* 2022).

I observed that Src and Syk inhibitors rapidly induce the reversal of activation of integrin αIIbβ3, indicating that inside-out activation of integrin αIIbβ3 is a reversible process and requires sustained GPVI signalling. This is in contrast with the condition used in LTA with a 10 times lower platelet concentration thereby preventing aggregation and outside-in signalling.

Inhibitors of Src, Syk and GPVI, PP2, PRT-060318 and glenzocimab were shown to enhance disaggregation of platelets on a collagen surface at arterial shear, in contrast to the current findings (Ahmed *et al.* 2020). Perrella *et al.* have

demonstrated Src and Syk kinases are also important in aggregation formation on fibrinogen which is mediated by binding to integrin αIIbβ3 and GPVI (Perrella *et al.* 2021). This might be because in these settings collagen was only present at the surface, in contrast to the current study where CRP is evenly distributed in washed platelets solution. As a result, the aggregates' outermost regions in the flow experiments were formed by the release of secondary mediators like ADP. The lower concentration of these mediators compared to the shell, and the temporary and weaker nature of secondary mediators-induced aggregation, may all contribute to the outer region's enhanced susceptibility to disaggregation when subjected to strong shear.

One limitation of this study is that in LTA, the platelets aggregates are subjected to low shear stress and are strongly activated by CRP at the surface. This is in contrast to flow experiments or physiological conditions, in which collagen is present only at the surface with strong shear, making the aggregates shells more susceptible to disaggregation compared to LTA studies. Therefore, the difference in aggregation observed in LTA and flow studies shows that whereas aggregation may be reversed, it is affected by the choice of agonist and experimental design.

In conclusion, the current work suggests that GPVI-induced aggregation in LTA is irreversible, despite inhibition of both GPVI or secondary mediators signalling pathways, or blocking of integrin αIIbβ3. This is in contrast to results reported on a collagen surface under arterial flow. The slight decrease in aggregation in LTA in the presence of Src kinase inhibitor could be attributed to the inhibition of integrin αIIbβ3 outside-in signalling.

Chapter 6

Experimental validation of computerised models of clustering of platelet glycoprotein receptors that signal via tandem SH2 domain proteins

The work conducted and the results produced in this Chapter have been published (Maqsood *et al.*, 2022). This Chapter contains part of Maqsood *et al.* that I have contributed to that is relevant to this thesis.

6.1 Introduction

Glycoprotein VI (GPVI) is activated by multivalent ligands such as collagen, collagen-related peptide (CRP), fibrinogen and convulxin, which causes receptor dimerisation and higher-order clustering. On the other hand, monovalent Fab fragments derived from the monoclonal antibodies (mAb) 1G5 (Al-Tamimi *et al.* 2009), JAQ1 (Nieswandt *et al.* 2000) and glenzocimab (Lecut *et al.* 2003) are unable to induce activation as they are unable to induce clustering and act as antagonists.

A promising GPVI-blocking candidate is the anti-GPVI nanobody 2 (Nb2) (Slater *et al.* 2021). Nanobodies are composed of a single variable domain derived from camelid antibodies. They vary from human antibodies in that they lack a light chain component and consist of two disulphide-linked heavy chains (Rahbarizadeh *et al.* 2011) (Figure 6.1). They have a similar antigen selectivity and binding affinity as full-length antibodies but are one-tenth the size of full antibodies (15 vs 150 kDa) and 30% the size of Fab fragments making them suitable for imaging studies and potential therapeutic agents. Nb2 has a K_D = 0.6 nM against GPVI compared with that of glenzocimab which has a K_D = 4.1 nM (Lebozec *et al.* 2017). The Nb2-binding site on GPVI has been mapped using X-ray crystallography to the D1 domain, adjacent to the binding site of CRP (Lebozec *et al.* 2017).

Cooper and Qian utilised an ordinary differential equation (ODE) model based on the law of mass action to explain how Src family kinases (SFK)-linked receptors signal via clustering (Cooper *et al.* 2008). Their model mathematically demonstrated how receptor clustering can produce a critical density of receptor tyrosines for phosphorylation and binding of SFK. This boosts SFK transphosphorylation and

receptor phosphorylation over the constant dephosphorylation pressure from phosphatases, resulting in a net SFK phosphorylation and activation. They also showed that the SFK phosphorylation does not require a net change in kinase activity, receptor shape, or migration to a specialised site in the membrane-like a lipid raft to achieve activation.

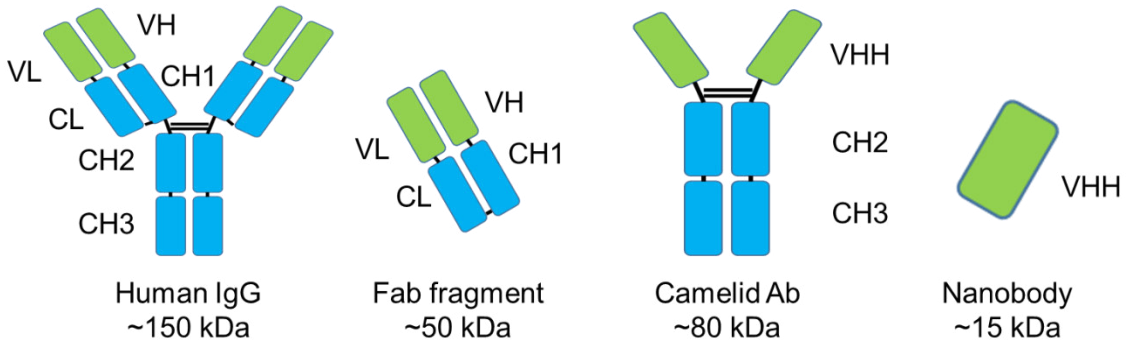

Figure 6.1 Domain structure and size comparison of human IgG, Fab fragment, camelid antibody and nanobody. The domain abbreviations are as follows: VH (light chain variable domain); VL (light chain variable domain); CL (light chain constant domain); CH1, CH2, CH3 (heavy chain constant domains); and VHH (single heavy chain variable domain).

6.2 Aim

Multimerisation of Nb2 can enhance its GPVI-binding affinity and potentially make it a more effective GPVI inhibitor that could be further developed into an antithrombotic. However, this also has the potential to activate GPVI like other multivalent ligands. In this Chapter, I aimed to generate Nb2 in divalent and tetravalent forms, termed Nb2-2 and Nb2-4, respectively and investigate their functional effects on platelet activation using surface plasmon resonance (SPR), light transmission aggregometry (LTA) and protein phosphorylation measurements. In addition, I have presented an ODE-based model developed by Zahra Maqsood and Sean Watson at the University of Birmingham that is capable of modelling the reversible binding of monovalent, divalent and multivalent ligands. The ODE model simulations were subsequently compared with the functional studies of monovalent, divalent and tetravalent ligands based on Nb2, Nb2-2 and Nb2-4, respectively.

6.3 Results

6.3.1 Cloning, purification and characterisation of Nb2-2 and Nb2-4

The domain structure of Nb2, Nb2-2 and Nb2-4 are shown in Figure 6.2A. The nanobody sequences contain an N-terminal PelB signal peptide sequence that allows for the secretion of nanobody into the periplasmic space. They also contain C-terminal His_6-tags for purification using nickel affinity chromatography and hemagglutinin (HA)-Tag for cleavage of the His_6-tag. The $(G_4S)_3$ linker is widely used in recombinant proteins that act as a soluble loop structure that separates each Nb2 domain (Trinh *et al.* 2004). The purified Nb2-2 and Nb2-4 were characterised by SDS-PAGE (Figure 6.2B), where the single band indicate the purity and molecular size of the purified nanobodies.

The binding affinity of these nanobodies to immobilised GPVI was determined by SPR by Dr Eleyna Martin at the University of Birmingham. The binding K_D of Nb2-2 and Nb2-4 to GPVI are 0.100 ± 0.003 and 0.20 ± 0.01 nM, respectively (Figure 6.2C). Their binding affinity is approximately 7 and 3.5 fold higher than Nb2 (Slater *et al.* 2021). In addition, comparing the 50 nM curves in the sensorgram, Nb2-2 (23 response unit/RU) has a better association with the immobilised GPVI than Nb2-4 (17RU), probably due to a less bulky size and orientation that may affect binding. Nevertheless, GPVI-Nb2-4 complexes (-6%) has a lower dissociation rate over the next 900 sec than that of Nb2-2 (-17%), which can be attributed to the fact that in Nb2-4 all 4 Nb2 domain has to be dissociated from GPVI before it can be flushed off the surface.

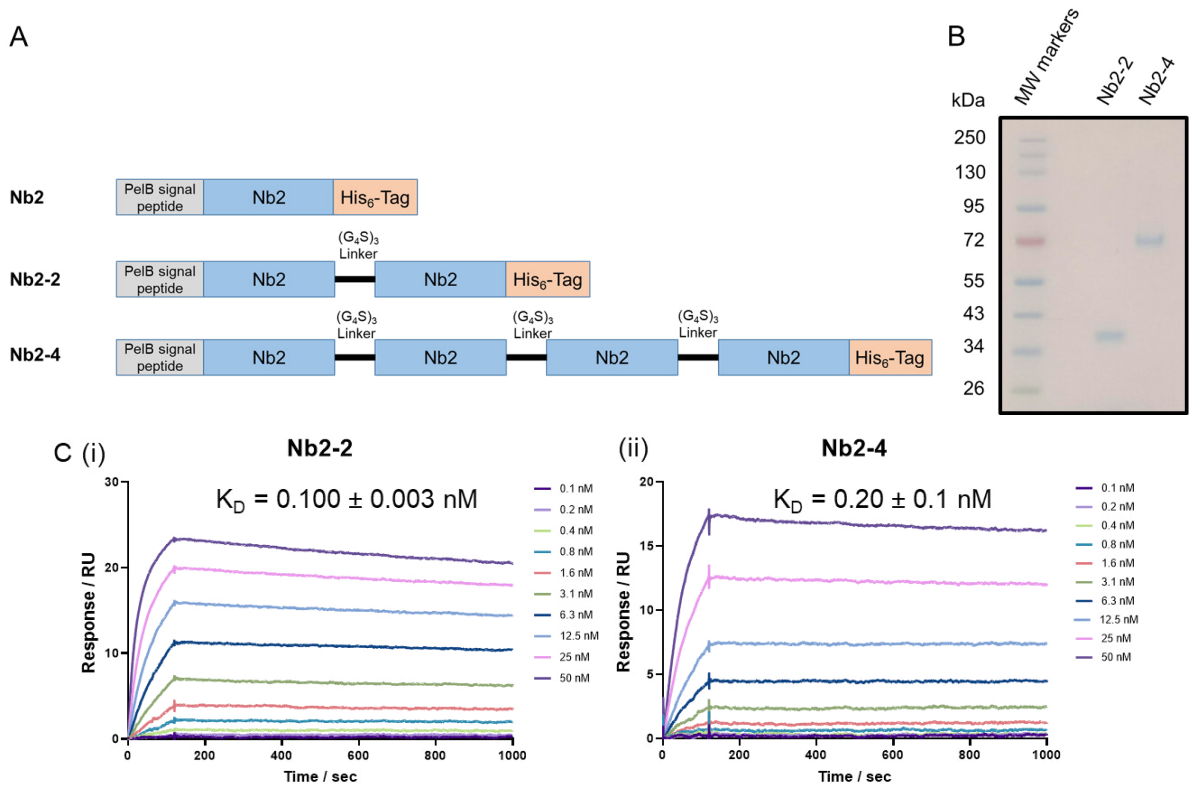

Figure 6.2 Cloning, purification and characterisation of Nb2-2 and Nb2-4. (A) The DNA construct structure of Nb2, Nb2-2 and Nb2-4. (B) SDS-PAGE of purified Nb2-2 and Nb2-4 protein. (C) Representative SPR sensorgrams of (i) Nb2-2 and (ii) Nb2-4 by Dr Eleyna Martin. GPVI was immobilised on the SPR chip and the nanobodies were flowed across the chip surface. n = 3.

6.3.2 Nb2 and Nb2-2 inhibit GPVI-mediated platelet aggregation

The functional effects of purified Nb2 and Nb2-2 on platelets were determined by LTA. Nb2-2 at 150 nM did not induce platelet aggregation when incubated with washed platelets for up to 60 min (Figure 6.3A). On the contrary, pre-treatment with Nb2 and Nb2-2 blocks collagen and CRP-induced platelet aggregation. Nb2 was able to block collagen (3 μg/mL) induced aggregation with a half-maximal inhibitory concentration (IC50) of 30.7 ± 1.9 nM, while Nb2-2 blocked collagen-induced aggregation with an IC50 of 4.68 ± 0.48 nM, 6 times more potent than monovalent Nb2 (Figure 6.3B). Similar observations were seen with CRP (3 μg/mL), where Nb2-2 blocked CRP-induced aggregation with an IC50 of 2.1 ± 0.2 nM, 2 times more potent than monovalent Nb2 which had an IC50 of 4.2 ± 0.5 nM (Figure 6.3C)

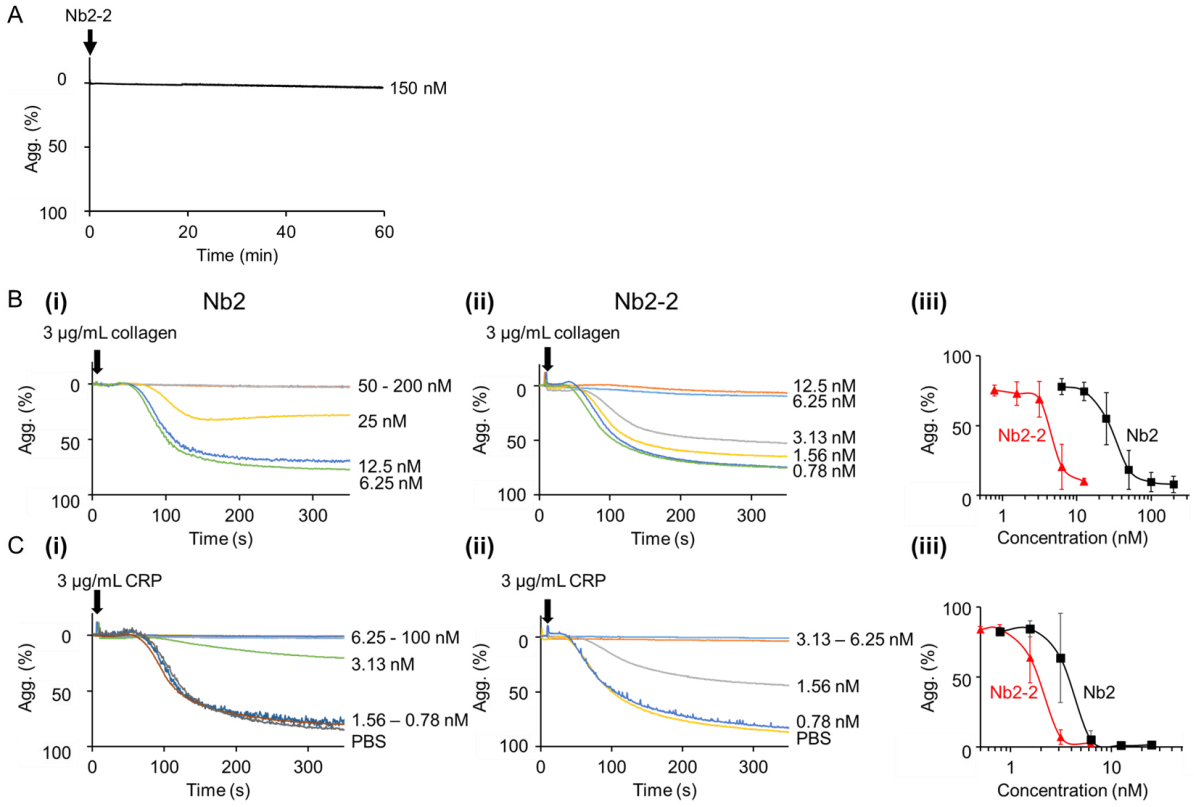

Figure 6.3 Nb2 and Nb2-2 are potent GPVI antagonists. Washed platelets at $2x10^8$/ml isolated from healthy donors were (A) incubated with 150 nM Nb2-2, or (B-C) pre-treated with the stated concentration of (i) Nb2 or (ii) Nb2-2 for 10 min before stimulation with (B) collagen (3 µg/mL) or (C) CRP (3 µg/mL). (i-ii) Representative traces of three experiments. (iii) Mean ± SD (%) aggregation (Agg.) after 5 min of agonist stimulation. N = 3 donors.

6.3.3 Nb2-4 induces GPVI-mediated platelet aggregation

Nb2-4 stimulated rapid aggregation of platelets as measured by LTA. To further validate this, a concentration-response curve to Nb2-4 (0.5-16 nM) was determined (Figure 6.4A). Nb2-4 induced platelet aggregation with a half-maximal effective concentration (EC50) of 1.8 ± 0.07 nM. Aggregation to Nb2-4 (16 nM) was blocked by pre-treatment with Nb2 (100 nM) and by the JAQ1 Fab (200 nM), confirming that it was mediated through GPVI (Figure 6.4B). Nb2-4-induced aggregation was also blocked by inhibitors of Src and Syk tyrosine kinases (Figure 6.4B).

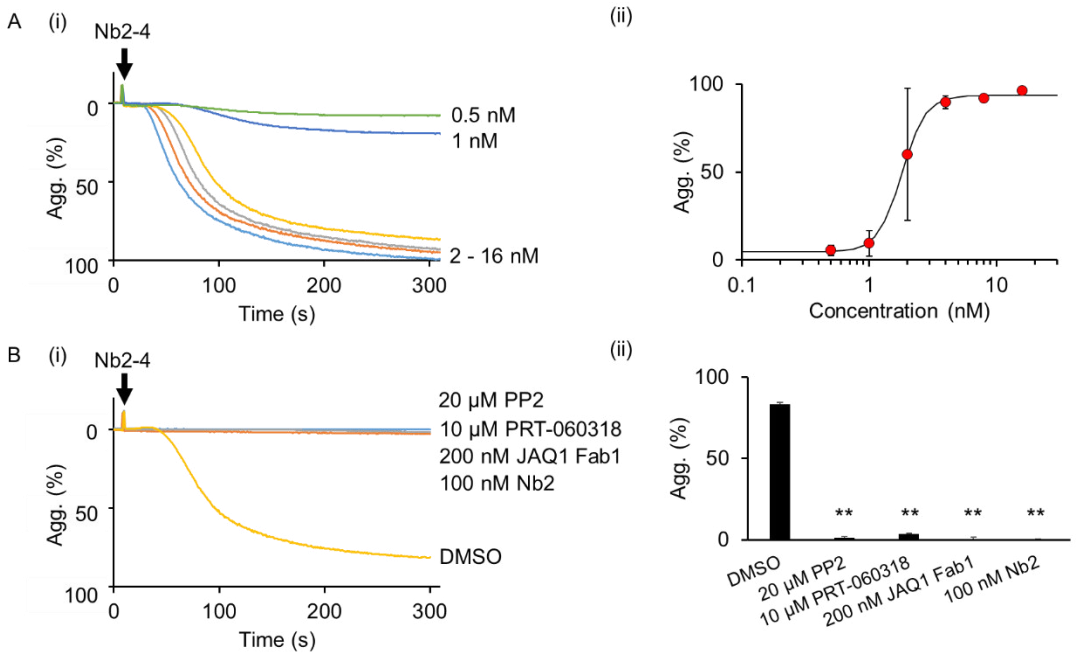

Figure 6.4 Nb2-4 induces GPVI-mediated aggregation. (A) Washed platelets at $2x10^8$/ml isolated from healthy donors were stimulated with the stated concentration of Nb2-4. (B) Washed platelets at $2x10^8$/ml were incubated with vehicle, PP2 (20 µM), PRT-060318 (10 µM), JAQ1 Fab1 (200 nM) or Nb2 (100 nM) for 10 min, before stimulation with 16 nM Nb2-4. LTA was monitored for 5 min. i) Representative traces of three experiments. ii) Mean Agg. ± SD (%) after 5 min of agonist stimulation. **($P < 0.01$) calculated using Welch's t-test indicates statistically significant differences. N = 3.

6.3.4 Nb2-4 induced GPVI-mediated protein phosphorylation, which was delayed by Nb2

The effect of Nb2-4 on protein phosphorylation was determined. Nb2-4 stimulated dose-dependent phosphorylation of Syk Y525/526 and LAT Y200, with an EC50 of 2.7 ± 0.3 nM (R^2 = 0.989) and 1.9 ± 0.4 nM (R^2 = 0.98), respectively (Figure 6.5A). These EC50 values were comparable to those obtained via aggregation experiments. Pre-treating washed platelets with PP2 (20 μM) or PRT-060318 (10 μM) reduced phosphorylation of Syk Y525/526 and LAT Y200 to 10.5 ± 3.7 and 9.8 ± 7.9%, respectively, which was significantly different from vehicle (Figure 6.5B). On the contrary, GPVI blocking Fab JAQ1 Fab1 (200 nM) and Nb2 (100 nM) were not able to completely block the phosphorylation. For Syk Y525/526, JAQ1 Fab1 (200 nM) and Nb2 (100 nM) reduced the phosphorylation level to 39.9 ± 25.8 and 32.2 ± 12.3% that of vehicle for JAQ1 Fab1 and Nb2, respectively, and the results were not significant. For LAT Y200, JAQ1 Fab1 and Nb2 did not significantly affect the phosphorylation level, at 85.5 ± 23.4 and 140 ± 37.1% compared to vehicle, respectively.

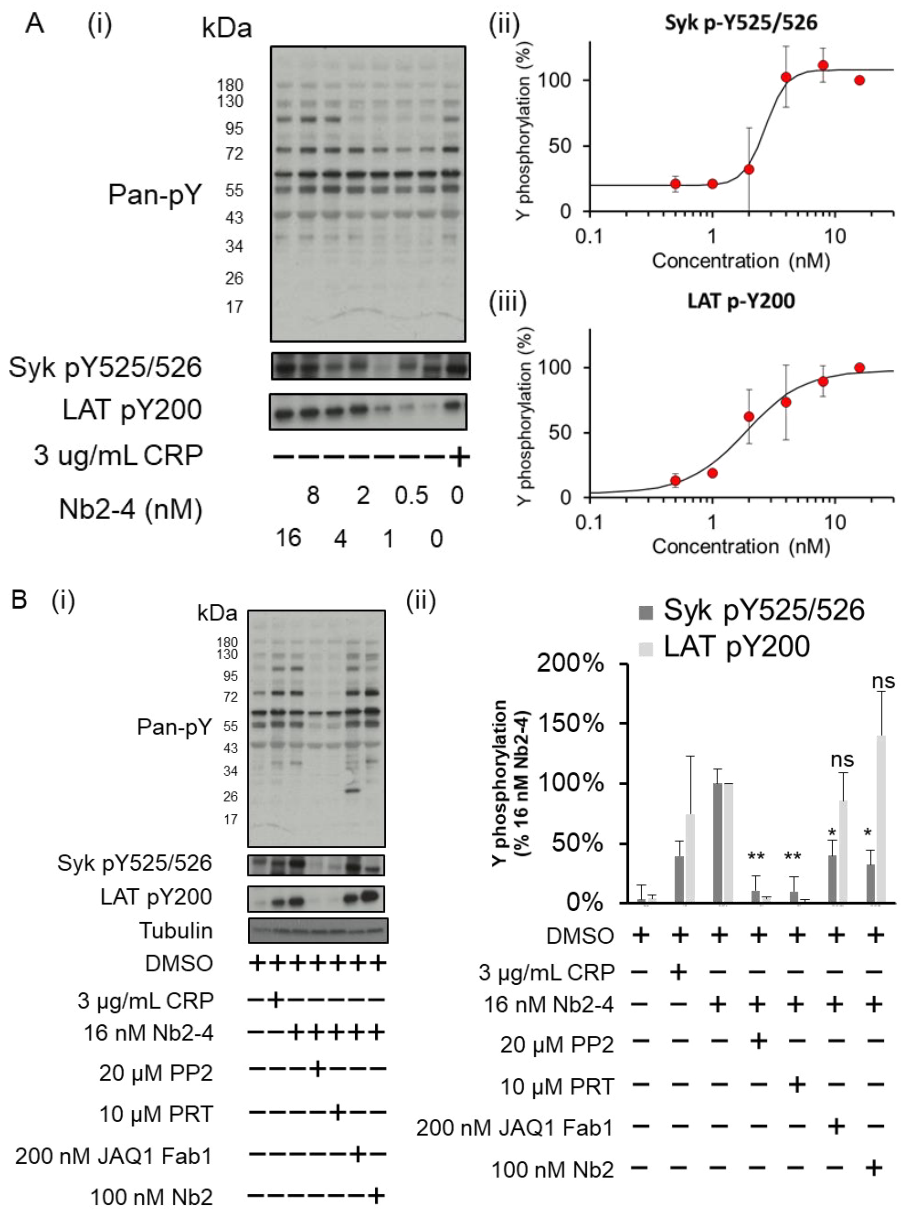

Figure 6.5 Nb2-4 induced GPVI-mediated protein phosphorylation. (A) Washed platelets at 4x10^8/mL were stimulated with the stated concentration of Nb2-4. (B) Washed platelets at 4x10^8/mL were pre-incubated with PP2 (20 µM), PRT-060318 (10 µM), JAQ1 Fab1 (200 nM), Nb2 (100 nM) or vehicle for 10 min before stimulated with Nb2-4 (16 nM). Unstimulated and CRP (3 µg/mL) stimulated platelets were included as negative and positive controls. Platelets were then lysed with 5X reducing sample buffer 5 min after the addition of the agonist. Whole-cell lysates were probed with the stated antibodies. (i) Representative blot and mean ± SD % of tyrosine phosphorylation of (ii) Syk p-Y525/526 and (iii) LAT p-Y200. ns (not significant), *(P<0.05), **(P < 0.01) calculated using Welch's t-test indicates statistically significant differences. N = 3.

The observation that JAQ1 Fab and Nb2 inhibit aggregation induced by Nb2-4 but not phosphorylation was unexpected. One potential explanation may be related to the time course of phosphorylation. As shown in Figure 6.6, without Nb2 pre-treatment, Nb2-4 was able to induce phosphorylation of Syk Y525/526 as early as 20 sec, which plateaued at 90 sec and was maintained for 5 min. It also led to phosphorylation of LAT Y200 at 45 sec which gradually increased over the 5 min. In contrast, in the presence of Nb2 (100 nM), phosphorylation of Syk Y525/526 remained low for the first 90 sec, and the maximum phosphorylation at 5 min was weaker than that without Nb2 pre-treatment. For LAT Y200, the phosphorylation level remained similar to basal for the first 45 sec and became observable at 90 sec and 5 min after Nb2-4 stimulations. These results suggest that Nb2 delays Nb2-4-induced protein phosphorylation and that this delay leads to the inhibition of platelet aggregation.

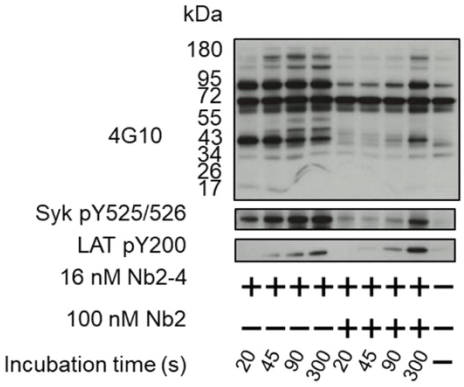

Figure 6.6 Nb2 delays Nb2-4 induced protein phosphorylation. Washed platelets at $4x10^8$/mL were pre-incubated with Nb2 (100 nM) or vehicle for 10 min before being stimulated with Nb2-4 (16 nM). Platelets were then lysed with 5X reducing sample buffer at the stated time after the addition of the agonist. Whole-cell lysates were probed with the stated antibodies and the representative blot is shown. n = 1.

6.3.5 Using the ODE model to monitor ligand binding and clustering

In the following part, a model of the ligand-receptor interactions of receptors with monovalent, divalent and tetravalent ligands based on the law of mass action published by Maqsood et al. (Maqsood *et al.*, 2022) is presented and compared with the experimental data. It is based on the following assumptions: (i) all reactions are reversible; (ii) the receptors exist as a monomer; (iii) there are no conformation changes or compartmentalisation of the receptor when interacting with the ligands; and (iv) the ligand concentration is constant. More details about the ODE model, its derivation and its analytical solutions can be found at

https://github.com/zeemaqsood/TAPAS_ESR9_Modelling_Project.

6.3.5.1 ODE modelling of the interaction of monovalent ligands and receptors

The interaction of a monovalent ligand with a monovalent receptor is shown in Figure 6.7A. The law of mass action defined the amount of ligand-receptor (LR) complex to the concentration of free ligand (L), receptor (R), and the association (k_1) and dissociation (k_{-1}) rate constants (Figure 6.7B). The relationship between ligand concentration [L] and equilibrium receptor occupancy $[LR]/[R]_{tot}$ is a sigmoidal curve as illustrated in Figure 6.7C, with $[R]_{tot}$ referring to the total receptor concentration. The time course of ligand binding to the receptor was also simulated (Figure 6.7D), showing that the time to equilibrium decreases with increasing ligand concentration, while the equilibrium receptor occupancy increases with increasing ligand concentration.

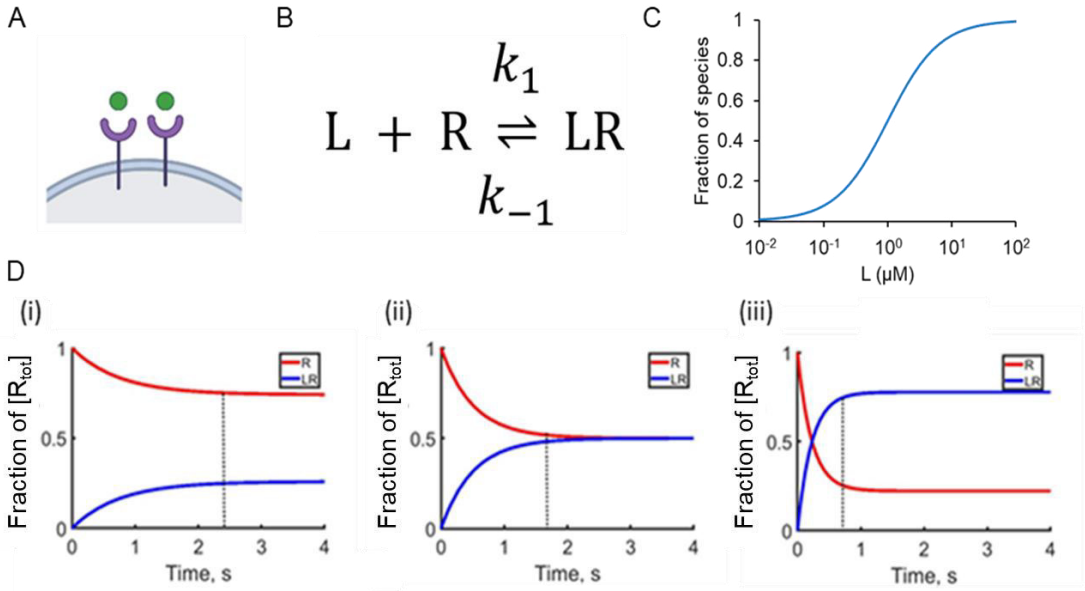

Figure 6.7 Interaction of monovalent ligand with receptor. (A) Schematic diagram of monovalent ligand-receptor interaction. (B) An equation describing the equilibrium of monovalent ligand (L), receptor (R), ligand-receptor (LR) complex, association rate (k_1) and dissociation rate (k_{-1}). (C) The effect of ligand concentration on equilibrium receptor occupancy. (D) The time-course effect of ligand concentration on receptor occupancy. The ligand concentrations were chosen to achieve (i) 25, (ii) 50 and (iii) 75% receptor occupancy *[LR]/[R_{tot}]* at equilibrium, with 95% equilibrium reached at 2.25, 1.50 and 0.75 sec, respectively. The following parameters were used for simulations in (C) and (D): R =1 μM, k_1 = 1 $\mu M^{-1}s^{-1}$, k_{-1} = 1 s^{-1}. The simulations were conducted in MATLAB by Zahra Maqsood and Sean Watson and the code can be found at https://github.com/zeemaqsood/TAPAS_ESR9_Modelling_Project.

6.3.5.2 ODE modelling of the interaction of divalent ligands and receptors

The above model was extended to a divalent ligand-receptor interaction (Figure 6.8A). In this extension, three new species are introduced, including the divalent ligand L^2 to reflect its two receptor-binding epitopes, and two ligand-receptor complexes, L^2R and L^2RR. It also included two new rate constants, the second association (k_2) and dissociation (k_{-2}) rate constant, and introduced two equilibrium dissociation constants, K_{D1} and K_{D2}. This generated two equilibria as shown in Figure 6.8B.

The concentration-response relationship for the formation of L^2R and L^2RR is shown in Figure 6.8C. Equilibrium receptor occupancy of the two complexes L^2R and L^2RR and varied $[L^2]$ at three different k_2 was plotted while keeping the other parameters constant. The plots showed a bell-shaped relationship between $[L^2RR]/[R]_{tot}$ and $[L^2]$ which peaks when $L^2 = K_{D1}$, independent of K_{D2}. The peak value of $[L^2RR]/[R]_{tot}$ increased in proportion to the second association rate constant k_2. On the other hand, a sigmoidal curve was observed for the plot of $[L^2R]/[R]_{tot}$ against $[L^2]$, similar to the monovalent ligand (Figure 6.8C).

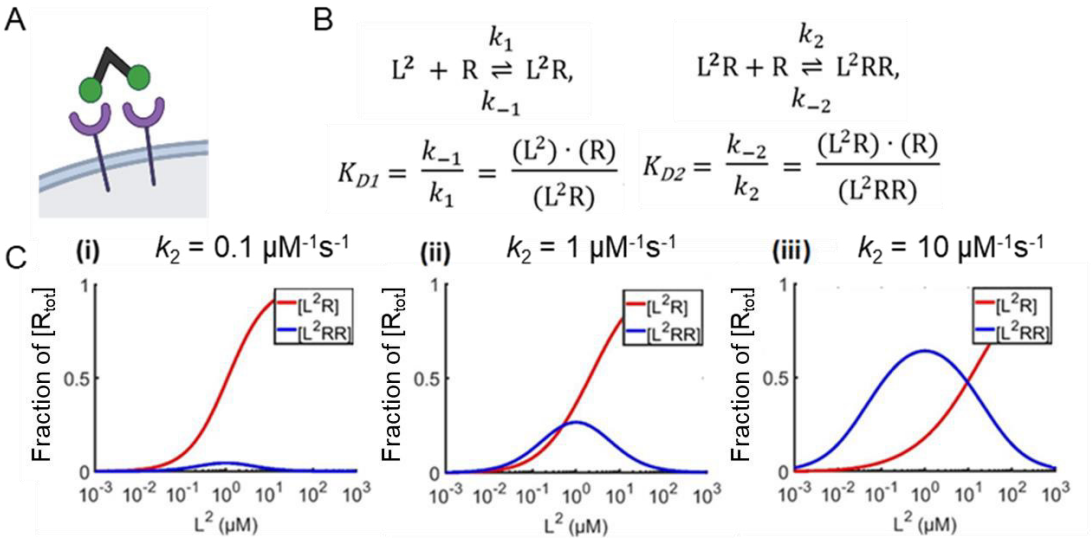

Figure 6.8 Interaction of divalent ligand with receptor. (A) Schematic diagram of divalent ligand-receptor interaction. (B) Equations describing the equilibrium of divalent ligand (L^2), receptor (R), ligand-receptor (L^2R, L^2RR) complex with the corresponding association (k_1, k_2), dissociation (k_{-1}, k_{-2}) rate, and equilibrium constant K_{D1} and K_{D2}. (C) The effect of k_{-2} on the equilibrium receptor occupancy of L^2R and L^2RR. (i) k_2 = 0.1 μM^{-1}s^{-1} (ii) k_2 = 1 μM^{-1}s^{-1} (iii) k_2 = 10 μM^{-1}s^{-1}. The following parameters were used: k_1 = 1 μM^{-1}s^{-1}, k_{-1} and k_{-2} = 1 s^{-1}. The simulations were conducted in MATLAB by Zahra Maqsood and Sean Watson and the code can be found at https://github.com/zeemaqsood/TAPAS_ESR9_Modelling_Project.

6.3.5.3 ODE modelling of the interaction of tetravalent ligands and receptors

We have further extended the model to include the interaction between receptor and tetravalent ligands (Figure 6.9A). The model included tetravalent ligand L^4 to reflect its four receptor-binding epitopes, with four possible ligand-receptor complexes with L^4 binding one to four receptor molecules (L^4R, L^4RR, L^4RRR and L^4RRRR), as well as their corresponding rate constant and equilibrium constant, as shown in Figure 6.9B.

Figure 6.9C shows the effect of varying $[L^4]$ and $[R]$ on ligand-receptor complexes at equilibrium. Similar to divalent ligand, the plots showed a sigmoidal curve representing the relationship between $[L^4R]/[R]_{tot}$ and $[L^4]$, and bell-shaped curves between $[L^4RR]/[R]_{tot}$, $[L^4RRR]/[R]_{tot}$, $[L^4RRRR]/[R]_{tot}$ and $[L^4]$ (Figure 6.9Ci). $[L^4RR]/[R]_{tot}$ peaks when $L^4 = K_{D1}$, while $[L^4RRR]/[R]_{tot}$, $[L^4RRRR]/[R]_{tot}$ peaks when $[L^4] < K_{D1}$. L^4R predominates at higher ligand concentrations, while L^4RRRR predominate at high receptor concentrations (Figure 6.9Cii). In summary, the simulations show that ligand valency, ligand concentration and receptor concentration all play roles in determining the stoichiometry and relative proportion of the ligand-receptor complexes.

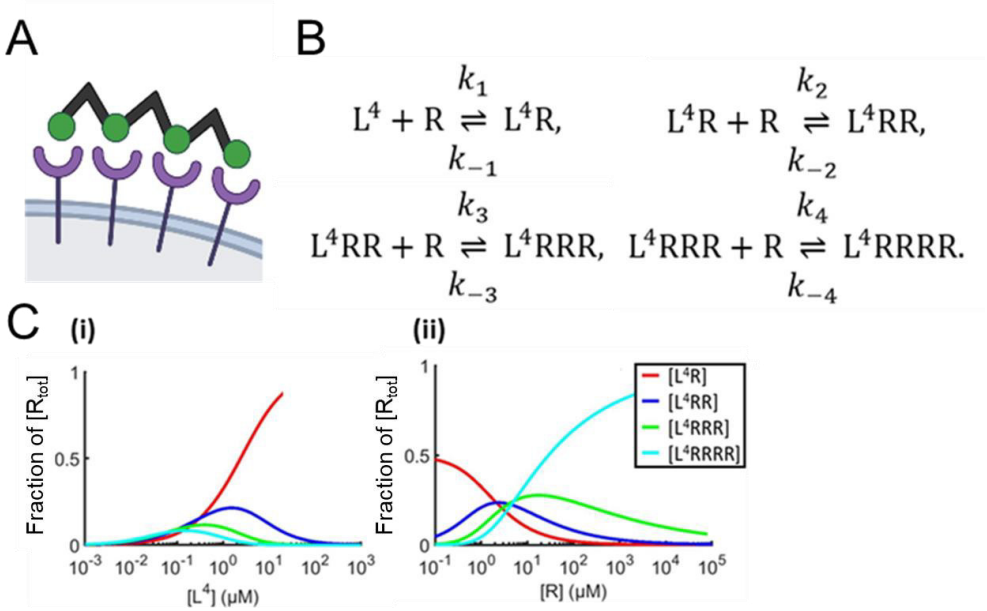

Figure 6.9 Interaction of tetravalent ligand with receptor. (A) Schematic diagram of tetravalent ligand-receptor interaction. (B) Equations describing the equilibrium receptor occupancy of tetravalent ligand L^4, ligand-receptor complexes binding one to four receptor molecules (L^4R, L^4RR, L^4RRR and L^4RRRR), with the association (k_1, k_2, k_3, k_4), dissociation (k_{-1}, k_{-2}, k_{-3}, k_{-4}) rate. (C) The concentration-occupancy relationship at equilibrium for varying the concentration of (i) tetravalent ligand $[L^4]$ and (ii) receptor $[R]$. For both simulations $[L^4]$ = 1 μM. The four association constants k_n = 1 $\mu M^{-1}s^{-1}$ and dissociation constants k_{-n} = 1 s^{-1}. The simulations were conducted in MATLAB by Zahra Maqsood and Sean Watson and the code can be found at https://github.com/zeemaqsood/TAPAS_ESR9_Modelling_Project.

6.4 Discussion

In this chapter, divalent Nb2-2 and tetravalent Nb2-4 were developed and characterised using a variety of assays. The SPR data showed that Nb2-2 and Nb2-4 have lower K_D towards GPVI compared to the parent nanobody Nb2, showing that multimerisation increases the binding affinity as a result of avidity. An ODE and computer model was also developed to simulate the ligand-receptor interactions between single monomeric receptors with monovalent, divalent and tetravalent ligands based on the law of mass action.

In aggregation assays, it was shown that Nb2-2 acts as a more potent GPVI blocker compared to Nb2 and blocks CRP and collagen-induced aggregation with lower IC50. This is consistent with another divalent GPVI ligand JAQ1 Fab2 which also acts as a GPVI blocker (Nieswandt *et al.* 2000). At the same time, the lower IC50 values observed for CRP compared to collagen may be due to collagen binding and activation through integrin α2β1, another collagen receptor on platelets.

On the other hand, Nb2-4 acts as a GPVI agonist and induces platelet aggregation and tyrosine phosphorylation. Similarly, other ligands with four or more GPVI-binding epitopes such as crosslinked anti-GPVI monoclonal antibodies (JAQ1 (Nieswandt *et al.* 2000) and 1G5 (Al-Tamimi *et al.* 2009)) can stimulate GPVI activation. This shows that for adequate clustering of GPVI to promote activation, a ligand must have at least three and potentially four epitopes. Other factors that may play a role include the distance between binding epitopes and the relative position of each epitope.

In the phosphorylation studies, Nb2 was shown to delay Nb2-4-induced phosphorylation at LAT pY200 and Syk pY525/526. One possible explanation for this is that Nb2 pre-treatment occupied the GPVI-binding site, and the slow dissociation rate prevents the binding with Nb2-4. Upon further incubation, due to avidity, Nb2-4 gradually displaces Nb2 through tetravalent interaction and the proximity of other Nb2

domains to GPVI, which subsequently clusters GPVI and causes downstream protein phosphorylation, as shown in Figure 6.7 (Oostindie *et al.* 2022).

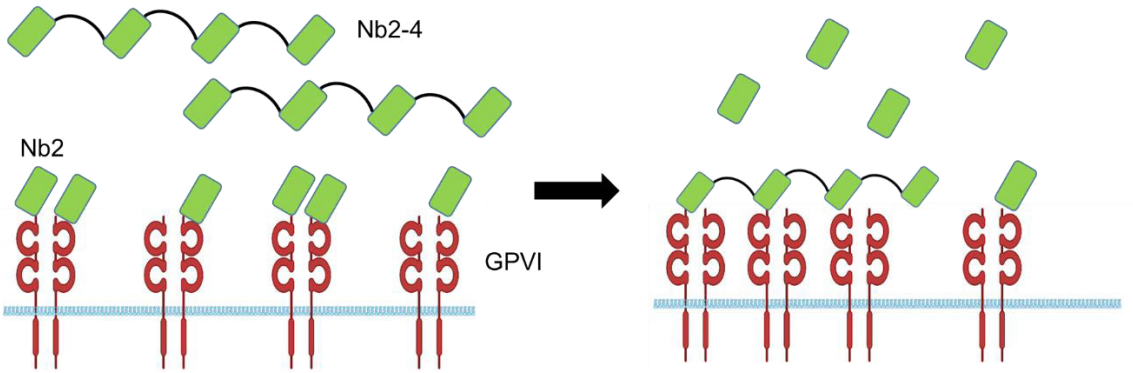

Figure 6.10 Schematic diagram of Nb2 delaying Nb2-4 induced GPVI clustering. Nb2-4 displaces Nb2 because of the proximity of other Nb2 domains to GPVI, which clusters and activates GPVI, causing downstream protein phosphorylation.

For the binding of divalent and tetravalent ligands, the ODE models indicate a bell-shaped concentration-response relationship. However, functional studies with divalent Nb2-2 and tetravalent Nb2-4 reveal no indications of a bell-shaped concentration-response relationship. This can be attributed to the stochastic character of the ligand-receptor interaction and the fact that GPVI is a combination of monomers and dimers (Clark, Neagoe, *et al.* 2021), allowing each Nb2-4 to bind to more GPVI. Furthermore, complete receptor occupancy (e.g. L^4RRRR) is not necessary for maximal aggregation, since collagen induces full aggregation of human platelets with 50% GPVI (Nagy *et al.* 2020) and mouse platelets with 20% GPVI (Snell *et al.* 2002). In addition, as GPVI exists as a mixture of monomer and dimer, each R in the L^4RRRR complex may represent a GPVI monomer or dimer (Clark, Neagoe, *et al.* 2021), favouring the formation of receptor complexes with more than 4 GPVI.

Another possible explanation for the discrepancy between the data and the simulation may be attributed to the choice of simulation parameters. The simulations

conducted in this study employed association constants (k_n) of 1 $\mu M^{-1}s^{-1}$ and dissociation constants (k_{-n}) of 1 s^{-1}. However, this does not reflect the conditions present on platelet surfaces due to avidity, which increases the association constant per binding of each Nb2 domain. As a result, the shape of the bell-shaped curve may be altered, requiring a higher concentration of ligands to achieve the other side of the bell-shaped curve. This increased concentration may exceed physiologically achievable levels, making it impossible to reach, meaning that the formation of multi-ligand-receptor complexes (clusters) is favoured at all physiologically possible concentrations.

An alternative option to ODE models would be agent-based modelling (ABM), a type of computer model for simulating the interactions and motions of autonomous agents. ABM is particularly adapted to the study of emergent phenomena such as receptor clustering, in which macroscale patterns emerge from local interactions (Lamerton *et al.* 2021; An 2009). It is possible to take into account additional parameters, such as receptor dimerisation, spatial considerations, and avidity, leading to a more accurate description of multivalent ligand-receptor interaction.

In conclusion, this chapter has developed multivalent novel anti-GPVI nanobodies which are GPVI antagonists in monovalent or divalent form but GPVI agonists when in a tetravalent form. Nb2-2, which has a greater affinity than Nb2, might be a viable antithrombotic by targeting GPVI. This chapter has also developed an ODE-based model to simulate the reversible binding of multivalent ligands (Nb2, Nb2-2 and Nb2-4) to GPVI receptors. The model shows that ligand valency, ligand concentration and receptor concentration all play roles in determining the stoichiometry and relative proportion of the ligand-receptor complexes.

Chapter 7

General discussion

7.1 Summary of results

This thesis investigates the changes in phosphoinositides and proteins in platelets stimulated via the key collagen receptor, glycoprotein VI (GPVI). To study phosphoinositide-related signalling, I have integrated the time-course data of phosphoinositides turnover in platelets by a mathematical modelling approach. The work described in Chapters 3-4 provides a novel method based on ion chromatography-mass spectrometry (IC-MS) that is capable of phosphoinositides positional isomers profiling. Using a mathematical model, a system-wide understanding of platelet phosphoinositide metabolism is obtained. The model predicts the effect of phosphatidylinositol 4-kinase A (PI4KA) inhibitor GSK-A1 on inositol triphosphate ($InsP_3$) and Ca^{2+} mobilisation, demonstrating its role in the synthesis of phosphatidylinositol 4,5-bisphosphate ($PtdIns(4,5)P_2$) to sustain downstream signalling.

In the second part of this thesis, I report on the effects of protein tyrosine kinase inhibitors and the multimeric GPVI ligands, Nb2-2 and Nb2-4, on GPVI-induced platelet activation and aggregation. Chapter 5 shows that i) the CRP-induced tyrosine kinase phosphorylation is reversible, but not the ensuing platelet aggregation when measured by light transmission aggregometry (LTA) in contrast to the reversible aggregation observed on collagen at arterial shear upon addition of a GPVI-blocking antigen-binding fragment (Fab) (Ahmed et al., 2020) or addition of an inhibitor of Syk (Perrella et al., 2022). Chapter 6 shows that i) dimerisation of GPVI alone does not induce activation of human platelets, ii) a tetravalent but not a divalent ligand induces measurable GPVI clustering and activation, and iii) presented a mathematical model which could be further expanded to demonstrate the dynamic of ligand-receptor complex formation with monovalent, divalent and tetravalent (nanobody) ligands. The key thesis findings are graphically summarised in Figure 7.1.

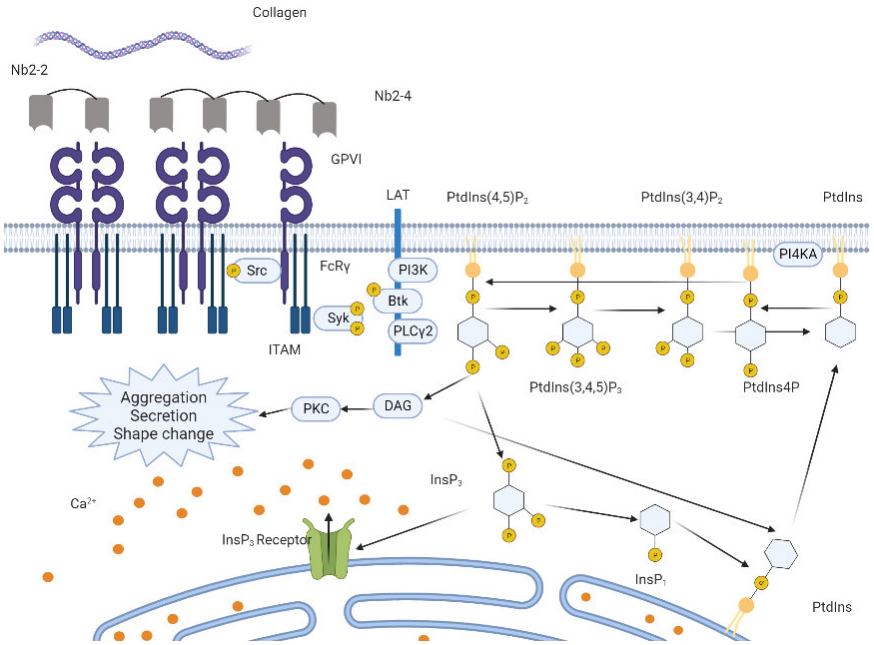

Figure 7.1 Summary representation of GPVI-mediated platelet signalling cascades. The binding of multimeric ligands such as CRP, collagen and Nb2-4 to GPVI leads to clustering and activation of the GPVI signalling cascade. The dimeric immune tyrosine activation motif (ITAM)-containing Fc receptor γ-chain (FcRγ) chain activates tyrosine kinases Src and Syk, and leads to the assembly of a linker for activation of T cells (LAT) signalosome to recruit and activate key proteins including Bruton's tyrosine kinase (Btk), phospholipase C-γ2 (PLCγ2) and phosphoinositide 3-kinase (PI3K). PI3K and PLCγ2 activation catalyse the generation of secondary messengers phosphatidylinositol 3,4,5-trisphosphate ($PtdInsP_3$), diacylglycerol (DAG) and $InsP_3$ from $PtdIns(4,5)P_2$). $InsP_3$ open the $InsP_3$ receptor that leads to Ca^{2+} mobilisation from the intracellular store. $PtdIns(4,5)P_2$ is synthesised from phosphatidylinositol 4-phosphate (PtdIns4P) and phosphatidylinositol (PtdIns) to sustain secondary messengers generation. The generation of $PtdInsP_3$, activation of protein kinase C (PKC) and rising intracellular Ca^{2+} level ultimately lead to platelet aggregation, secretion and shape change. Figure created in biorender.com.

7.2 The platelet phosphoinositide metabolism as an antithrombotic target

7.2.1 A comprehensive method for quantifying platelet phosphoinositide isomers

In platelets, quantitative understanding of the occurrence and turnover of the phosphoinositide isomers, particularly phosphatidylinositol 3,4-bisphosphate ($PtdIns(3,4)P_2$) and phosphatidylinositol 3,5-bisphosphate ($PtdIns(3,5)P_2$), has

remained limited. This is because of the lack of methods to measure absolute concentrations of these polar phospholipids in living cells and the uncertainty of their subcellular presence. However, using thin-layer chromatography or [^{3}H] and [^{32}P] labelling followed by high-performance liquid chromatography (HPLC), recent studies using other cells have been able to measure these phosphoinositide species (Sbrissa *et al.* 2012; Lees *et al.* 2020; Mücksch *et al.* 2019).

The novel label-free MS-based method developed in Chapter 3 provides an accurate way to quantify these and other phosphoinositides isomers. The maximum fold-change observed in Chapters 3 and 4 and the paper of Mujali *et al.* (Mujalli *et al.* 2018) are summarised in Table 7.1. The fold changes of these isomers by all studies are consistent, despite the differences in agonist concentration used to stimulate the platelets, showing that a saturating concentration of CRP has been used. Mujali *et al.* (Mujalli *et al.* 2018) were unable to differentiate between the PtdInsP_2 positional isomers. Therefore the change in PtdIns(3,4)P_2 is overshadowed by that of PtdIns(4,5)P_2, which has a higher copy number. However, we find a discrepancy in the PtdIns4P level, which concerns rises by 99% and 50%, respectively, in Chapter 3 and the paper from Mujali, but falls by 20% in Chapter 4. This mismatch can be attributed to the use of different platelet preparation protocols, and the presence of autocrine inhibitors apyrase and indomethacin, as outlined in Chapter 2.2.3.1.

In addition, some limitations of the developed method have to be taken into account. First, the method uses deacylated lipids for the separation and quantification of phosphoinositide isomers. However, the acyl chains may also contain important information regarding signalling. For example, Peng *et al.* revealed the role of arachidonate-containing 18:0-20:4 diacylglycerols in phosphoinositides as major precursors for the production of thromboxane and prostaglandin mediators of platelets

(Peng *et al.* 2018). Second, the method cannot resolve the PtdIns3P and PtdIns5P isomers. Although these isomers can be separated by a method developed by Jeschke *et al.*, the latter has a lower sensitivity because of the use of ion-pairing agents, as is discussed in Chapter 3 (Jeschke *et al.* 2017; Jeschke *et al.* 2015). For the future, I recommend the development of an IC-MS method that can separate phosphoinositide positional isomers without deacylation. Such a method could reveal the differential lipid composition in the inositol phospholipid isomers, and thereby identify the preference of regulating enzymes for specific arachidonate-containing molecular species of phosphoinositide forms.

Table 7.1 Summary of phosphoinositides isomers fold change. The fold changes of phosphoinositides from Chapters 3 and 4 and Mujali *et al.* are compared. N/A indicates not applicable; * indicates that total PtdInsP and $PtdInsP_2$ were quantified instead of respective positional isomers; ** indicates that $PtdIns(3,4,5)P_3$ is not detected in unstimulated platelets and therefore the fold change cannot be determined.

Source	Chapter 3	Chapter 4	Mujali *et al.*
Platelet treatment	5 µg/mL CRP	30 µg/mL CRP, apyrase (2.5 U/mL) and indomethacin (20 µM)	10 µg/mL CRP
PtdIns	N/A	-35%	-40%
PtdIns4P	+99%	-20%	+50%*
$PtdIns(4,5)P_2$	+50%	+66%	+25%*
$PtdIns(3,4)P_2$	+328%	+500%	N/A
$PtdIns(3,4,5)P_3$	Detected**	+164%	+200%

7.2.2 Spatial-temporal model of conversions in phosphoinositide metabolism

The model developed in Chapter 4 is able to predict turnover effects of the PI4KA inhibitor GSK-A1, but not of the inositol polyphosphate-5-phosphatase (OCRL) inhibitor YU142670, on $InsP_1$ accumulation and Ca^{2+} mobilisation. This difference in sensitivity may be attributed to a different localisation of OCRL and PI4KA in platelets (Faucherre *et al.* 2003; MJ *et al.* 2022), implying that not every phospholipid is

accessible to the converting enzymes. In other words, the absence of spatial-temporal information limits the scope of the phosphoinositide conversion model. One way to improve the model then is to include spatial distribution data of the abundance of phosphoinositide isomers.

The missing information can be obtained by subcellular fractionation of stimulated platelets, followed by lipid extraction and analysis. Such experiments are time-consuming and may result in less accuracy of quantitative measurements. Spatial-temporal data may also be acquired by sensors based on specific lipid-binding domains, such as the Fyve domain for PtdIns3P, or the pleckstrin homology domain for PtdIns(4,5)P_2 (Behnia *et al.* 2005). However, a drawback of the sensors is that the different subcellular pools of the lipids are labelled with different effectiveness. Distinct sensors are required to detect the PtdIns4P in Golgi, endo/lysosome and plasma membrane, which reduces the accuracy of quantitative measurements (Posor *et al.* 2022). Furthermore, as platelets are anucleated, they cannot be transfected with plasmids expressing these sensors.

7.2.3 Expanding the scope of the phosphoinositide conversion model

Chapter 4 shows that GSK-A1 treatment of platelets did not affect the initial Ca^{2+} mobilisation, despite an inhibition of $InsP_1$ accumulation, and an inhibited PtdIns(4,5)P_2 resynthesis that would sustain the Ca^{2+} response. We ascribed the discrepancy to the fact that Ca^{2+} mobilisation is regulated by the interplay of multiple factors, such as $InsP_3$ receptor activity, extracellular Ca^{2+} entry and Ca^{2+} back-pumping by Ca^{2+}-ATPases in the endoplasmic reticulum and the plasma membrane (see Chapter 1). In contrast, the generation of $InsP_3$ (being degraded to $InsP_1$) is only regulated by PLCγ2. To improve the prediction power of the existing model, it is possible to integrate it with a Ca^{2+} mobilisation module, similar to the model developed by Purvis *et al.* (Purvis *et al.* 2008).

Given the right prediction of GSK-A1 effects on phosphoinositide metabolism and platelet activation, the model developed in Chapter 4 can be extended to explore other hypotheses comparing the fitness of model simulation profiles. For example, in platelets, the cytosolic enzyme phospholipase A_2 ($cPLA_2$) cleaves arachidonic acid from phosphoinositides (Kramer *et al.* 1997), which is the precursor fatty acid of thromboxane A_2. The other $cPLA_2$ product lyso-phosphatidylinositol can be recycled back to phosphatidic acid and appear in other phosphoinositides (Peng *et al.* 2018). The $cPLA_2$ reaction can be considered and tested as an alternative pathway to slow down the flux of conversion from PtdIns to PtdIns4P. Another idea to integrate is the possible interference of PtdIns(4,5)P_2 sequestering proteins, which may concentrate the PtdIns(4,5)P_2 in unstimulated cells and release it in response to local increases in cytosolic Ca^{2+} concentration (McLaughlin *et al.* 2005). One such protein is myristoylated alanine-rich C kinase substrate (MARCKS), which is expressed in platelets (Burkhart *et al.* 2012), and has been proposed to contribute to the replenishing of PtdIns(4,5)P_2 for sustained production of $InsP_3$ and PtdIns(3,4,5)P_3 (Jahan *et al.* 2020). These potential changes are summarised in Figure 7.2.

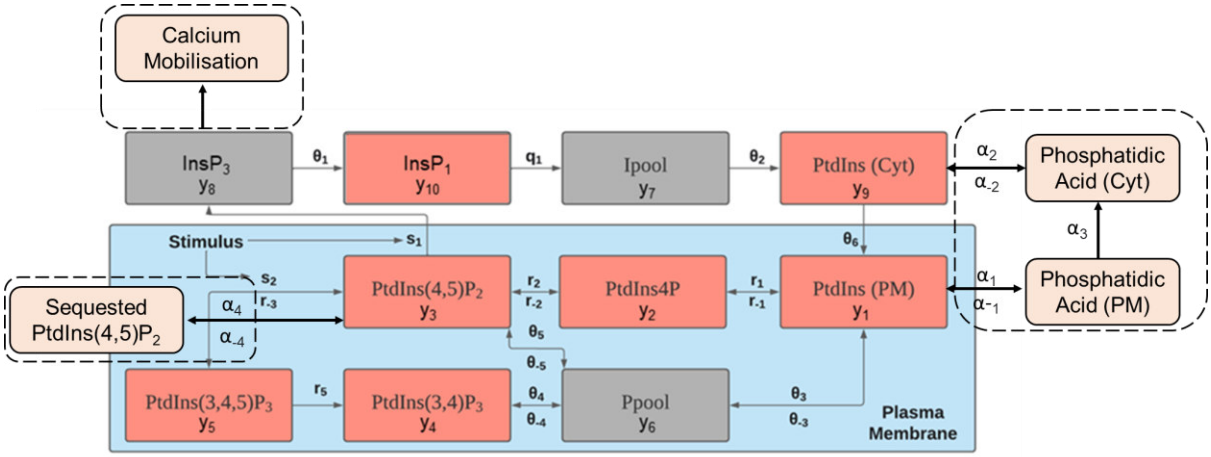

Figure 7.2 Proposed expansion of the phosphoinositides model. The proposed changes are circled by dashed lines, with newly introduced parameters and species in yellow boxes. The changes included the incorporation of a calcium mobilisation module, the inclusion of phosphatidic acid to account for cPLA$_2$ and the coupled PtdIns/phosphatidic acid transport and the sequestration of PtdIns(4,5)P$_2$ by its binding protein.

7.2.4 Targeting the platelet phosphoinositide metabolism beyond class I PI3K isoforms

The promising use of class I PI3K inhibitors as antithrombotics is discussed in Chapter 1. In addition, also class II and class III PI3K inhibitors are gaining interest in this respect. The PI3KC2α inhibitor MIPS-21335 was recently shown to reduce thrombus formation in an *ex vivo* microfluidic flow assay and an *in vivo* electrolytic injury-induced thrombosis model in mice, while it did not affect the tail bleeding time (Selvadurai *et al.* 2020). For the class III PI3K isoform VPS34, it was shown that *ex vivo* treatment of mouse or human platelets with the inhibitor SAR-405 reduced thrombus growth at arterial shear rates (Valet *et al.* 2017). In the context of thrombosis, the therapeutic potential of other phosphoinositide kinases, *i.e.* isoforms of PI4P5K, PI5P4K, PI4K and PIKfyve, has not been investigated. However, inhibitors for these proteins have already been explored for the treatment of cancer, viral infections or neurological illnesses (Burke *et al.* 2022). Our result of GSK-A1 on inhibiting InsP$_1$ accumulation and cytosolic Ca^{2+} mobilisation in Chapter 4 could serve as a basis for

further exploration of specific phosphoinositide-modulating enzymes as targets for a novel antithrombotic.

On the other hand, a drawback of using phosphoinositide-directed inhibitors as antithrombotics is their likely off-target effects. These phosphoinositide kinases are abundantly expressed, are constitutively active, and perform housekeeping work to maintain membrane integrity and intracellular vesicle transport. This is in contrast to the class I PI3K isoforms that in various cell systems are only activated by stimulation of the cells. Loss-of-function mutations of several of these enzymes have been linked to hereditary disorders (Chow *et al.* 2007; Tiosano *et al.* 2019), but so far not to a bleeding diathesis. The further development of class I PI3K inhibitors may also encounter such problems, given their abundant expression levels.

7.3 Platelet receptor GPVI as an antithrombotic target

7.3.1 Method-dependent reversal of GPVI-induced platelet aggregation

Microfluidic studies using whole-blood flowed over collagen surfaces have provided evidence for a sustained role of GPVI signalling, and fibrinogen-integrin αIIbβ3 interactions in the formation and stabilisation of thrombi. Accordingly, the inhibition of GPVI or the protein tyrosine kinases downstream of GPVI was found to promote thrombus disaggregation on collagen. Ahmed *et al.* showed that inhibition of GPVI signalling using GPVI antagonist glenzocimab or by inhibiting the kinases Src or Syk enhanced the disaggregation of platelet thrombi on collagen or human atherosclerotic plaque material (Ahmed *et al.* 2020). Similarly, André *et al.* pointed out that the Syk inhibitor PRT-060318 reduced thrombus stability and enhanced thrombus disaggregation on a collagen surface (Andre *et al.* 2011). Perrella *et al.* reported similar results for PRT-060318 and the Src inhibitor dasatinib, while the anti-GPVI nanobody Nb21 caused only minor thrombus disaggregation (Perrella *et al.* 2022).

In light transmission aggregometry (LTA) of rapidly stirred platelets without

arterial shear, ADP-induced platelet aggregation can be reversed by integrin αIIbβ3 antagonists like eptifibatide (Moser *et al.* 2003; Frojmovic *et al.* 2005; Speich *et al.* 2009). In contrast, platelet aggregation induced by GPVI agonists collagen or CRP appears to be irreversible (Ahmed *et al.* 2020; Zou *et al.* 2021). My results in Chapter 5 confirm this by showing an irreversible platelet aggregation when induced by GPVI signalling in the presence of the secondary mediators TxA_2 and ADP. Interestingly, this irreversible aggregation contrasts with the rapid reversal of tyrosine kinase phosphorylation in response to the same agonists. On the other hand, we observe a partial aggregation reversal in the presence of an Src kinase inhibitor or a blocker of integrin αIIbβ3. This can be attributed to the loss of αIIbβ3 outside-in signalling, which is dependent on Src but not Syk or Btk (Watson *et al.* 2005). This is further backed up by the findings of Auger *et al.* (Auger *et al.* 2008) which showed that Src family kinases and the actin cytoskeleton, but not secondary mediators, stabilised compact platelet aggregates on collagen at arterial shear.

The difference between a substantial reversibility of GPVI-induced thrombus formation under flow and a low reversibility of GPVI-induced platelet aggregation (measured as light transmission aggregometry) shows that measurement of the transiency of platelet responses is a matter of the experimental design and method. In light transmission aggregometry, the formed platelet aggregates are subjected to low shear stress with all platelets in the suspension being activated by CRP. This is in contrast to whole-blood flow experiments, in which the most potent GPVI agonist (collagen) is only present at the microfluidic surface, and the platelets adhere and aggregate at high shear rates. Therefore, whole-blood flow experiments appear to be preferable to LTA for studying platelet disaggregation.

7.3.2 Development of nanobody Nb2-2 as a GPVI-blocking agent

In Chapter 6, I study the effects of anti-GPVI nanobodies produced in dimeric

(Nb2-2) or tetrameric form (Nb2-4) on platelets. Binding studies by SPR show that both Nb2-2 and Nb2-4 have higher GPVI-binding affinity than monomeric Nb2. Using protein phosphorylation assessment and LTA, we further demonstrate that Nb2-2 acts as a GPVI blocker, as opposed to Nb2-4 which acts as a GPVI agonist.

In general, the natural monomeric cameloid nanobodies have a short plasma half-life *in vivo* of approximately 0.5 hours in mice, and 2 hours in cynomolgus monkeys. This is explained by the nanobodies' small size (around 15 kDa), making them susceptible to glomerular clearance (Roovers *et al.* 2007; Hoefman *et al.* 2015). Protein modification of a nanobody is thus needed to increase its plasma half-life, as most therapeutic agents need to be present for a prolonged time at an effective concentration. Nanobody multimerisation or fusion with an albumin-binding domain can increase the plasma half-life.

The first FDA-approved nanobody, Caplacizumab, for the treatment of acquired thrombotic thrombocytopenic purpura, is a 28 kDa dimeric protein, with the two VHH domains linked by a tri-alanine linker (Morrison 2019). Caplacizumab has a plasma half-life of 13-40 hours after intravenous injection of a single dose (0.5–12 mg) (Sargentini-Maier *et al.* 2019). It appears that its circulation time is extended by forming a complex with von Willebrand factor in plasma. Another therapeutically promising antibody, Vobarilizumab (ALX-0061), is a 26 kDa bispecific construct with a half-life of 6.6 days (a single dosage of 10 mg/kg) in cynomolgus monkeys (Van Roy *et al.* 2015). This drug is designed as the fusion construct of an anti-IL6 receptor nanobody with an albumin-binding nanobody, thereby giving it a similar half-life as albumin in plasma (Steiner *et al.* 2017). Based on these examples, it is expected that Nb2 dimerisation or linkage with an albumin-binding domain will improve circulation time and thereby their *in vivo* activity. In the future, the half-life enhanced Nb2-2 has the potential to be

developed into a viable antithrombotic like glenzocimab.

Nevertheless, it might not be advantageous for Nb2-2 to have an extended half-life. The presence of divalent ligands that bind GPVI at a different site as Nb2, such as Fab2 of glenzocimab (Billiald *et al.* 2022), may cause clustering and activation of GPVI. Antiplatelet medications are frequently taken alongside other antiplatelet medications, such as aspirin which is widely used for cardiovascular disease prevention (Ittaman *et al.* 2014). Another example is glenzocimab which is currently being investigated in a phase 2/3 study in combination with tissue plasminogen activator following acute ischemic stroke (Mazighi *et al.* 2019). Therefore, having a prolonged half-life and improved efficacy through multimerisation may risk supporting thrombosis in synergy with other endogenous ligands or co-administered drugs.

7.3.3 Development of Nb2-4 as a platelet GPVI agonist

In Chapter 6, the tetrameric nanobody Nb2-4 is shown to stimulate platelets via GPVI. Based on these results, it may be further developed to serve as an alternative GPVI receptor agonist, which then complements the selective ligands CRP and convulxin. When used in the crosslinked form, CRP is a potent GPVI-specific agonist and an accepted gold standard in various platelet function assays. Despite a low intra-batch variation and high stability, appreciable batch-to-batch variability due to crosslinking effects has been observed, necessitating the calibration of a fresh batch before assay usage (Lombardi *et al.* 2012; Garner *et al.* 2017; Sang *et al.* 2019). Convulxin, another gold standard GPVI agonist, is an octamer with a defined protein structure and sequence, of which the interaction with GPVI is well-characterised. However, the glycoprotein is purified from the venom of the South American rattlesnake *Crotalus durissus terrificus*, which is expensive to breed and purify (Prado-Franceschi *et al.* 1981). In addition, snake specimens can produce different amounts of platelet-activating convulxin.

In contrast, the amino acid sequence of Nb2-4 is well-defined, with no heterogeneity due to peptide modification such as crosslinking or glycosylation. The Nb2-4 can be purified from normal expression systems in *Escherichia coli* or HEK-293 cells, which makes it more cost-effective to produce in larger quantities.

At the moment, the production of Nb2, Nb2-2 and Nb2-4 has not been optimised for high yield and purity. Further development studies are needed such as clonal selection to obtain the highest yield clone, optimisation of the inoculation and fermentation conditions to maximise cell growth, purification improvement, and batch-to-batch variation studies before the nanobodies can be widely used as GPVI blocking or activating substances for platelet studies.

In addition to GPVI, this approach can be applied to C-type lectin-like receptor 2 (CLEC-2) and Platelet Endothelial Aggregation Receptor 1 (PEAR1), two platelets receptors that contain tyrosine-based signalling motifs in their cytosolic tails and activate through clustering (Chapter 1.2.3, (Kauskot *et al.* 2012)). Similar to Nb2 and Nb2-4, the development of dimeric and tetrameric nanobodies against CLEC-2 and PEAR1 can potentially produce receptor-specific blocking and activating ligands.

7.3.4 Improved modelling of GPVI receptor clustering

The ordinary differential equation (ODE) model developed for GPVI activity in Chapter 6 predicts that divalent and tetravalent (nanobody) ligands complex with more than one receptor molecule. A bell-shaped relationship is observed between the equilibrium receptor occupancy and ligand concentration, which suggests that a high ligand concentration would inhibit receptor clustering and activation. This prediction does not fit with the experimental data. The reasons for this likely are the stochastic character of ligand-receptor interactions and the fact that GPVI is present on the membrane as a combination of monomers and dimers (Clark, Neagoe, *et al.* 2021). Accordingly, each Nb2-4 molecule is able to bind to more than one GPVI receptor.

When GPVI exists as a mixture of monomers and dimers, each ligand-receptor complex can consist of a GPVI monomer or dimer (Clark, Neagoe, *et al.* 2021), leading to the formation of GPVI-enriched receptor complexes. The ODE model furthermore assumes the presence of a single ligand for each receptor, but it is known that next to collagen, also fibrinogen and fibrin can (competitively) bind to GPVI.

An alternative option to ODE models is the so-called agent-based modelling (ABM). This comprises a computer model for simulating the interactions and motions of autonomous agents. The ABM can easily be adapted to mimic self-organisation phenomena such as receptor clustering (Lamerton *et al.* 2021; An 2009). The use of ABM allows spatial consideration, GPVI receptor dimerisation and membrane heterogeneity to be considered in the model (Maqsood *et al.* 2022). In the ODE model, we assume that all receptors exist as a monomer to simplify the model, which is not the case on platelet surface as GPVI exist as a mixture of monomer or dimer (Clark, Neagoe, *et al.* 2021). While the presence of dimers or monomer/dimer mixture can be modelled using ODE, this complicates the model with more potential species. Also, in the ODE model, as the spatial considerations are not taken into account, the forced proximity due to avidity is not accounted for, although the concept can be incorporated through the use of cooperativity (White *et al.* 2019). On the other hand, spatial consideration can be readily modelled by ABM, as well as other factors such as the presence of receptors dimers or monomer/dimer and other cytosolic protein/crosslinkers that influence receptor clustering (Maqsood *et al.* 2022).

Nevertheless, ABM currently necessitates more technical knowledge, programming effort, and computational power compared to equation-based models, even though some modelling platforms like Netlogo attempt to improve the user interface to minimise programming efforts (Tisue *et al.* 1999). To conduct parameter

estimation or sensitivity analysis, ABM relies on grouping model outputs and empirical data into collections of arbitrary summary statistics, which results in a large portion of the data's spatial and temporal information being lost (Thiele *et al.* 2014).

7.4 Conclusions

Platelet activation is a multistep process that involves the activation of various receptors with downstream signalling proteins, the production of phosphoinositide isomers, and a culminating Ca^{2+} response, which leads to platelet functional responses. My work has resulted in a comprehensive understanding of the phosphoinositide turnover in platelets and provides better insight into the action mechanisms of tyrosine kinase inhibitors and GPVI, integrin αIIbβ3 blockers in the context of GPVI-induced activation and aggregation. The findings include: *i)* an IC-MS method capable of positional phosphoinositide isomers profiling; *ii)* an ODE-based phosphoinositide conversion model that predicts effects of kinase inhibition; *iii)* insight that the CRP-induced tyrosine kinase phosphorylation is reversible, but not the ensuing platelet aggregation; and *iv)* the discovery that monovalent, divalent, and tetravalent anti-GPVI nanobodies differentially cause GPVI inhibition or activation.

This thesis demonstrates how integrating functional data and mathematical modelling assists with hypothesis generation and validation. Due to the lack of spatial-temporal data encompassing several species generated under the same conditions as well as donor variability in protein copy number and platelet size, the models' applicability is currently limited. With the development of new sample preparation and analytical methods to acquire a more comprehensive dataset, I believe that the mathematical models created in this thesis can be combined and expanded to include the element of protein phosphorylation, calcium mobilisation, and interaction with other platelet agonists This would give the scientific community a valuable tool for testing hypotheses and developing new anti-platelet drugs.

Chapter 8 Appendix

Parameters of the 10 best-fitting profiles for phosphoinositides Models 1 and 2.

Set	r_1	r_{-1}	r_2	r_{-2}	r_{-3}	r_5	θ_2	θ_3	θ_{-3}	θ_5	θ_{-5}	θ_4	θ_{-4}	s_1	s_2
1	1.4E-01	5.8E-01	1.7E+00	2.5E+00	2.4E+01	1.6E+00	1.7E-02	4.9E-01	5.5E-03	1.3E-03	7.9E-02	7.3E-03	2.9E+01	1.5E-04	3.3E-01
2	2.0E-01	3.0E-01	1.4E+01	1.9E+01	9.7E-01	7.5E+00	1.4E-02	3.1E-01	5.3E-03	2.0E-03	8.5E-01	2.6E-02	1.0E+02	1.6E-04	1.1E-01
3	2.0E-01	3.0E-01	1.4E+01	1.9E+01	9.7E-01	7.5E+00	1.4E-02	3.1E-01	5.3E-03	2.0E-03	8.5E-01	2.6E-02	1.0E+02	1.6E-04	1.1E-01
4	2.7E+00	9.2E+00	1.2E+01	1.5E+01	3.9E+01	2.9E+00	1.6E-02	1.9E-03	1.1E-03	1.0E-02	3.3E+00	2.3E-02	9.1E+01	1.5E-04	5.5E-01
5	3.4E-01	1.0E+00	2.4E+00	3.2E+00	2.7E+01	4.2E+00	1.2E-02	3.1E-01	4.2E-03	1.8E-03	5.6E-01	4.5E-04	2.5E+00	1.6E-04	4.1E-01
6	5.4E+00	1.8E+01	3.7E+00	3.3E+00	6.2E+01	8.4E-01	1.2E-02	2.7E-02	5.5E-03	2.0E-03	2.3E+00	1.7E-04	8.2E-01	1.6E-04	8.4E-01
7	1.3E+01	4.4E+01	1.3E+01	1.9E+01	2.3E+01	5.4E+00	1.6E-02	1.2E-01	2.3E-03	8.0E-03	2.5E+00	3.2E-03	1.4E+01	1.6E-04	3.9E-01
8	1.2E+00	4.7E+00	7.8E-01	9.8E-01	7.6E-01	1.2E+01	1.3E-02	3.8E-01	5.4E-03	1.3E-03	2.1E-01	2.0E-03	9.9E+00	1.6E-04	1.8E-01
9	7.1E+00	2.6E+01	1.5E+01	2.6E+01	3.0E+01	9.0E-01	1.5E-02	4.3E-01	7.0E-03	1.4E-03	5.3E-01	1.3E-02	5.2E+01	2.0E-04	5.1E-01
10	2.8E-01	1.8E-02	1.0E+00	1.3E-01	1.5E-02	1.0E+00	9.0E-03	4.4E-02	3.9E-03	1.8E-03	1.6E+00	1.1E-04	5.7E-01	1.6E-04	1.3E-02

Table 8.1 Results of parameter fitting Model 1 to experimental data. Parameter sets of the ten best results from a sample of N = 20000 fits.

Set	r_1	r_{-1}	r_2	r_{-2}	r_{-3}	r_5	θ_2	θ_3	θ_{-3}	θ_5	θ_{-5}	θ_4	θ_{-4}	s_1	s_2
1	7.0E+00	1.3E+01	7.0E+00	9.8E+00	1.7E+00	2.7E+00	1.1E-04	1.4E-03	7.3E-03	2.2E-02	2.1E-03	1.1E+00	2.3E+01	1.5E-04	5.7E-02
2	1.1E-03	2.0E-03	3.4E-01	4.6E-01	1.0E+01	1.7E-01	6.3E-04	1.2E-03	6.2E-01	1.8E-01	3.0E-03	4.0E-03	3.3E-02	1.6E-04	1.4E-01
3	2.2E+01	4.8E+01	8.1E-03	1.1E-03	1.5E-03	8.5E-01	2.2E-02	1.0E-03	2.1E-02	1.0E-03	1.0E-03	4.8E-01	4.7E+00	1.6E-04	1.1E-02
4	4.3E-02	4.7E-02	7.1E-02	8.6E-02	4.6E-01	3.7E-02	2.3E-04	5.0E-03	6.0E-03	3.3E-03	1.8E-02	1.4E+00	5.2E+01	1.6E-04	6.4E-03
5	1.8E+00	3.0E+00	3.4E-01	4.8E-01	1.0E+01	9.6E-01	9.8E-01	3.0E-03	6.1E-03	7.2E-03	8.8E-03	1.2E-01	3.6E+00	1.6E-04	1.5E-01
6	6.9E+00	1.1E+01	3.5E-02	3.0E-02	5.2E+01	2.3E+00	2.5E-01	1.0E-03	1.1E-02	8.3E-03	6.5E-03	1.3E-01	4.0E+00	1.5E-04	6.8E-01
7	1.0E+00	1.4E+00	7.4E+00	1.0E+01	1.3E+01	1.3E-01	4.8E-01	8.2E-03	4.5E-03	4.9E-03	8.8E-03	2.2E-01	7.5E+00	1.6E-04	1.7E-01
8	3.6E-02	4.9E-02	3.7E-02	4.3E-02	2.2E-01	2.5E-01	2.8E-02	7.7E-03	5.9E-03	3.4E-03	1.0E-02	6.1E-02	2.3E+00	1.4E-04	6.1E-03
9	1.0E-03	2.7E-03	3.2E+00	4.3E+00	7.5E+01	9.9E-02	4.5E-02	1.0E-03	1.8E-01	3.6E+01	1.2E+00	1.9E-03	1.8E-02	1.6E-04	1.0E+00
10	7.0E+00	1.3E+01	7.0E+00	9.8E+00	1.7E+00	2.7E+00	1.1E-04	1.4E-03	7.3E-03	2.2E-02	2.1E-03	1.1E+00	2.3E+01	1.5E-04	5.7E-02

Table 8.2 Results of parameter fitting Model 2 to experimental data. Parameter sets of the ten best results from a sample of N = 20000 fits.

Parameters of the 10 best-fitting profile for phosphoinositides Models 1 and 2.

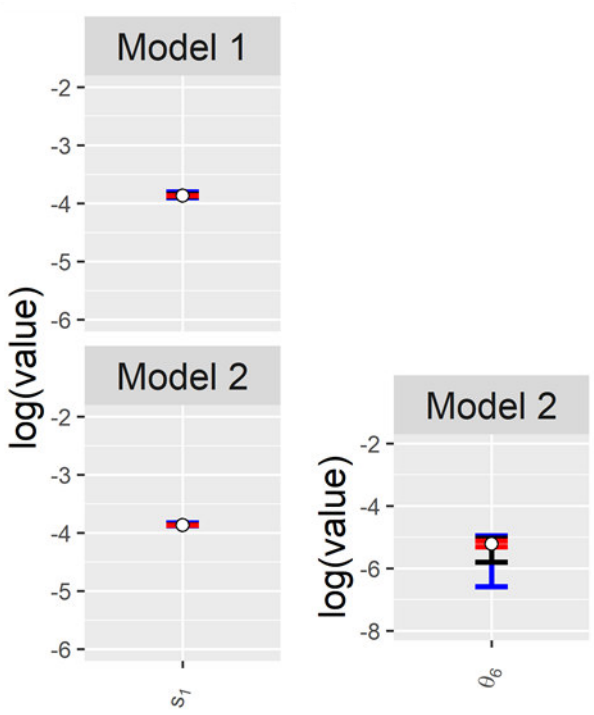

Figure 8.1 Posterior parameter ranges for s_1 and θ_6. Posterior parameter ranges are shown for Models 1 (Top) and 2 (Bottom). The blue, black, and red lines and hollow circles show the full range, interquartile range, the inner 10% range and median of each estimated parameter.

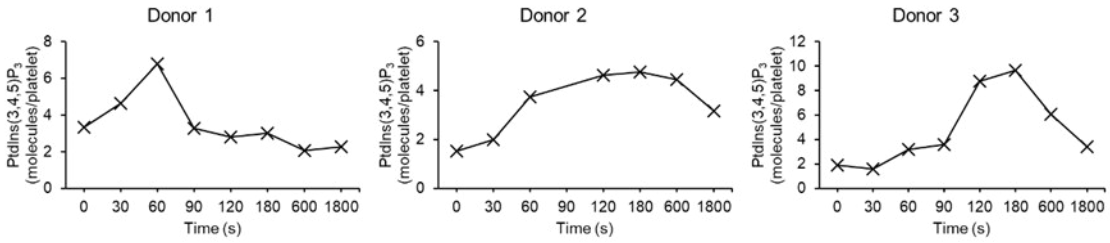

Figure 8.2 Donor variability in the production of PtdIns(3,4,5)P_3. Washed platelets at 1.2x109 cells were stimulated with 30 µg/mL CRP and the stimulation was stopped at the stated time with cold 1M HCl. The phosphoinositides in the samples were extracted, derivatised and analysed in IC-MS as described in Chapter 3. The peak areas of each species were normalised using internal standards and the amount of protein determined by BCA.

Chapter 9 References

Ahmed, M. U., Kaneva, V., Loyau, S., Nechipurenko, D., Receveur, N., Le Bris, M., Janus-Bell, E., Didelot, M., Rauch, A., and Susen, S. 2020. 'Pharmacological blockade of glycoprotein VI promotes thrombus disaggregation in the absence of thrombin', *Arterioscler. Thromb. Vasc. Biol.*, 40: 2127-42.

Al-Tamimi, M., Mu, F.-T., Arthur, J. F., Shen, Y., Moroi, M., Berndt, M. C., Andrews, R. K., and Gardiner, E. E. 2009. 'Anti-glycoprotein VI monoclonal antibodies directly aggregate platelets independently of Fc γ RIIa and induce GPVI ectodomain shedding', *Platelets*, 20: 75-82.

Alenazy, F., Harbi, M., Kavanagh, D., Price, J., Brady, P., Hargreaves, O., Harrison, P., Slater, A., Connolly, D., and Kirchhof, P. 2021. 'GPVI inhibition by glenzocimab synergistically inhibits atherosclerotic plaque-induced platelet activation when combined with conventional dual antiplatelet therapy', *Eur. Heart J.*, 42: ehab724. 1425.

Alshehri, O. M., Hughes, C. E., Montague, S., Watson, S. K., Frampton, J., Bender, M., and Watson, S. P. 2015. 'Fibrin activates GPVI in human and mouse platelets', *Blood*, 126: 1601-08.

An, G. 2009. 'A model of TLR4 signaling and tolerance using a qualitative, particle–event-based method: Introduction of spatially configured stochastic reaction chambers (SCSRC)', *Math. Biosci.*, 217: 43-52.

Andre, P., Morooka, T., Sim, D., Abe, K., Lowell, C., Nanda, N., Delaney, S., Siu, G., Yan, Y., and Hollenbach, S. 2011. 'Critical role for Syk in responses to vascular injury', *Blood*, 118: 5000-10.

Anquetil, T., Payrastre, B., Gratacap, M.-P., and Viaud, J. 2018. 'The lipid products of phosphoinositide 3-kinase isoforms in cancer and thrombosis', *Cancer Metastasis Rev.*, 37: 477-89.

Arachiche, A., Mumaw, M. M., de la Fuente, M., and Nieman, M. T. 2013. 'Protease-activated receptor 1 (PAR1) and PAR4 heterodimers are required for PAR1-enhanced cleavage of PAR4 by α-thrombin', *J. Biol. Chem.*, 288: 32553-62.

Ashyraliyev, M., Fomekong-Nanfack, Y., Kaandorp, J. A., and Blom, J. G. 2009. 'Systems biology: parameter estimation for biochemical models', *FEBS J.*, 276: 886-902.

Atkinson, B. T., Ellmeier, W., and Watson, S. P. 2003. 'Tec regulates platelet activation by GPVI in the absence of Btk', *Blood*, 102: 3592-99.

Auger, J. M., and Watson, S. P. 2008. 'Dynamic tyrosine kinase-regulated signaling and actin polymerisation mediate aggregate stability under shear', *Arterioscler. Thromb. Vasc. Biol.*, 28: 1499-504.

Backer, J. M. 2016. 'The intricate regulation and complex functions of the Class III phosphoinositide 3-kinase Vps34', *Biochem. J.*, 473: 2251-71.

Baker, R., and Thompson, W. 1972. 'Positional distribution and turnover of fatty acids in phosphatidic acid, phosphoinositides, phosphatidylcholine and phosphatidylethanolamine in rat brain in vivo', *Biochim. Biophys. Acta*, 270: 489-503.

Balla, T. 2013. 'Phosphoinositides: tiny lipids with giant impact on cell regulation', *Physiol. Rev.*, 93: 1019-137.

Banay-Schwartz, M., Kenessey, A., DeGuzman, T., Lajtha, A., and Palkovits, M. 1992. 'Protein content

of various regions of rat brain and adult and aging human brain', *Age*, 15: 51-54.

Banno, Y., Yada, Y., and Nozawa, Y. 1988. 'Purification and characterization of membrane-bound phospholipase C specific for phosphoinositides from human platelets', *J. Biol. Chem.*, 263: 11459-65.

Behnia, R., and Munro, S. 2005. 'Organelle identity and the signposts for membrane traffic', *Nature*, 438: 597-604.

Bender, M., Hagedorn, I., and Nieswandt, B. 2011. 'Genetic and antibody-induced glycoprotein VI deficiency equally protects mice from mechanically and FeCl3-induced thrombosis', *J. Thromb. Haemost.*, 9: 1423-26.

Bennett, J. S. 2005. 'Structure and function of the platelet integrin α IIb β 3', *J. Clin. Invest.*, 115: 3363-69.

Bergmeier, W., Oh-Hora, M., McCarl, C.-A., Roden, R. C., Bray, P. F., and Feske, S. 2009. 'R93W mutation in Orai1 causes impaired calcium influx in platelets', *Blood*, 113: 675-78.

Berridge, M. J. 1983. 'Rapid accumulation of inositol trisphosphate reveals that agonists hydrolyse polyphosphoinositides instead of phosphatidylinositol', *Biochem. J.*, 212: 849-58.

Berridge, M. J., Dawson, R., Downes, C., Heslop, J., and Irvine, R. 1983. 'Changes in the levels of inositol phosphates after agonist-dependent hydrolysis of membrane phosphoinositides', *Biochem. J.*, 212: 473-82.

Bertović, I., Kurelić, R., Milošević, I., Bender, M., Krauss, M., Haucke, V., and Jurak Begonja, A. 2020. 'Vps34 derived phosphatidylinositol 3-monophosphate modulates megakaryocyte maturation and proplatelet production through late endosomes/lysosomes', *J. Thromb. Haemost.*, 18: 1756-72.

Best, D., Senis, Y. A., Jarvis, G. E., Eagleton, H. J., Roberts, D. J., Saito, T., Jung, S. M., Moroi, M., Harrison, P., and Green, F. R. 2003. 'GPVI levels in platelets: relationship to platelet function at high shear', *Blood*, 102: 2811-18.

Bilanges, B., Posor, Y., and Vanhaesebroeck, B. 2019. 'PI3K isoforms in cell signalling and vesicle trafficking', *Nat. Rev. Mol. Cell Biol*, 20: 515-34.

Billiald, P., Slater, A., Welin, M., Clark, J. C., Loyau, S., Pugnière, M., Jiacomini, I. G., Rose, N., Lebozec, K., and Toledano, E. 2022. 'Targeting platelet GPVI with glenzocimab: a novel mechanism for inhibition', *Blood Adv.* Advance online publication, DOI: 10.1182/bloodadvances.2022007863

Binder, H., Weber, P. C., and Siess, W. 1985. 'Separation of inositol phosphates and glycerophosphoinositol phosphates by high-performance liquid chromatography', *Anal. Biochem.*, 148: 220-27.

Bird, J. E., Smith, P. L., Bostwick, J. S., Shipkova, P., and Schumacher, W. A. 2011. 'Bleeding response induced by anti-thrombotic doses of a phosphoinositide 3-kinase (PI3K)-β inhibitor in mice', *Thromb. Res.*, 127: 560-64.

Blair, T. A., Moore, S. F., Williams, C. M., Poole, A. W., Vanhaesebroeck, B., and Hers, I. 2014. 'Phosphoinositide 3-kinases p110α and p110β have differential roles in insulin-like growth factor-1–mediated Akt phosphorylation and platelet priming', *Arterioscler. Thromb. Vasc. Biol.*, 34: 1681-88.

Bojjireddy, N., Botyanszki, J., Hammond, G., Creech, D., Peterson, R., Kemp, D. C., Snead, M., Brown,

R., Morrison, A., and Wilson, S. 2014. 'Pharmacological and genetic targeting of the PI4KA enzyme reveals its important role in maintaining plasma membrane phosphatidylinositol 4-phosphate and phosphatidylinositol 4, 5-bisphosphate levels', *J. Biol. Chem.*, 289: 6120-32.

Bolouri, H. 2008. *Computational modeling of gene regulatory networks-a primer* (World Scientific Publishing Company).

Bori-Sanz, T., Inoue, K. S., Berndt, M. C., Watson, S. P., and Tulasne, D. 2003. 'Delineation of the region in the glycoprotein VI tail required for association with the Fc receptor γ-chain', *J. Biol. Chem.*, 278: 35914-22.

Brass, L. F., and Joseph, S. 1985. 'A role for inositol triphosphate in intracellular Ca2+ mobilization and granule secretion in platelets', *J. Biol. Chem.*, 260: 15172-79.

Breitling, R. 2010. 'What is systems biology?', *Front. physiol.*, 1:159.

Bui, H. H., Sanders, P. E., Bodenmiller, D., Kuo, M. S., Donoho, G. P., and Fischl, A. S. 2018. 'Direct analysis of PI (3, 4, 5) P3 using liquid chromatography electrospray ionization tandem mass spectrometry', *Anal. Biochem.*, 547: 66-76.

Bültmann, A., Li, Z., Wagner, S., Peluso, M., Schönberger, T., Weis, C., Konrad, I., Stellos, K., Massberg, S., and Nieswandt, B. 2010. 'Impact of glycoprotein VI and platelet adhesion on atherosclerosis—a possible role of fibronectin', *J. Mol. Cell. Cardiol.*, 49: 532-42.

Bura, A., and Jurak Begonja, A. 2021. 'Imaging of Intracellular and Plasma Membrane Pools of PI (4, 5) P2 and PI4P in Human Platelets', *Life*, 11: 1331.

Burgering, B. M. T., and Coffer, P. J. 1995. 'Protein kinase B (c-Akt) in phosphatidylinositol-3-OH kinase signal transduction', *Nature*, 376: 599-602.

Burgess, K., Creek, D., Dewsbury, P., Cook, K., and Barrett, M. P. 2011. 'Semi-targeted analysis of metabolites using capillary-flow ion chromatography coupled to high-resolution mass spectrometry', *Rapid Commun. Mass Spectrom.*, 25: 3447-52.

Burke, J. E., Triscott, J., Emerling, B. M., and Hammond, G. R. 2022. 'Beyond PI3Ks: targeting phosphoinositide kinases in disease', *Nat. Rev. Drug Discov.*, 14: 1-30.

Burkhart, J. M., Vaudel, M., Gambaryan, S., Radau, S., Walter, U., Martens, L., Geiger, J., Sickmann, A., and Zahedi, R. P. 2012. 'The first comprehensive and quantitative analysis of human platelet protein composition allows the comparative analysis of structural and functional pathways', *Blood*, 120: e73-e82.

Bynagari-Settipalli, Y. S., Cornelissen, I., Palmer, D., Duong, D., Concengco, C., Ware, J., and Coughlin, S. R. 2014. 'Redundancy and interaction of thrombin-and collagen-mediated platelet activation in tail bleeding and carotid thrombosis in mice', *Arterioscler. Thromb. Vasc. Biol.*, 34: 2563-69.

Canobbio, I., Stefanini, L., Cipolla, L., Ciraolo, E., Gruppi, C., Balduini, C., Hirsch, E., and Torti, M. 2009. 'Genetic evidence for a predominant role of PI3Kβ catalytic activity in ITAM-and integrin-mediated signaling in platelets', *Blood*, 114: 2193-96.

Chen, W., Thielmann, I., Gupta, S., Subramanian, H., Stegner, D., Van Kruchten, R., Dietrich, A., Gambaryan, S., Heemskerk, J., and Hermanns, H. 2014. 'Orai1-induced store-operated Ca2+ entry

enhances phospholipase activity and modulates canonical transient receptor potential channel 6 function in murine platelets', *J. Thromb. Haemost.*, 12: 528-39.

Cheung, H. Y. F., Moran, L. A., Sickmann, A., Heemskerk, J. W., Garcia, Á., and Watson, S. P. 2022. 'Inhibition of Src but not Syk causes weak reversal of GPVI-mediated platelet aggregation measured by light transmission aggregometry', *Platelets*, 33: 1293-300.

Chicanne, G., Severin, S., Boscheron, C., Terrisse, A.-D., Gratacap, M.-P., Gaits-Iacovoni, F., Tronchère, H., and Payrastre, B. 2012. 'A novel mass assay to quantify the bioactive lipid PtdIns3 P in various biological samples', *Biochem. J.*, 447: 17-23.

Chow, C. Y., Zhang, Y., Dowling, J. J., Jin, N., Adamska, M., Shiga, K., Szigeti, K., Shy, M. E., Li, J., and Zhang, X. 2007. 'Mutation of FIG4 causes neurodegeneration in the pale tremor mouse and patients with CMT4J', *Nature*, 448: 68-72.

Clapham, D. E. 2007. 'Calcium signaling', *Cell*, 131: 1047-58.

Clark, J., Anderson, K. E., Juvin, V., Smith, T. S., Karpe, F., Wakelam, M. J., Stephens, L. R., and Hawkins, P. T. 2011. 'Quantification of PtdInsP 3 molecular species in cells and tissues by mass spectrometry', *Nat. Methods*, 8: 267.

Clark, J., Neagoe, R., Zuidscherwoude, M., Kavanagh, D., Slater, A., Martin, E., Soave, M., Stegner, D., Nieswandt, B., and Poulter, N. 2021. 'Evidence that GPVI is Expressed as a Mixture of Monomers and Dimers, and that the D2 Domain is not Essential for GPVI Activation', *Thromb. Haemost.*, 121(11): 1435-47.

Clark, J. C., Damaskinaki, F.-N., Cheung, Y. F. H., Slater, A., and Watson, S. P. 2021. 'Structure-function relationship of the platelet glycoprotein VI (GPVI) receptor: does it matter if it is a dimer or monomer?', *Platelets*: 32(6):724-732.

Clemetson, K. J. 2012. 'Platelets and primary haemostasis', *Thromb. Res.*, 129: 220-24.

Cooper, J. A., and Qian, H. 2008. 'A mechanism for SRC kinase-dependent signaling by noncatalytic receptors', *Biochemistry*, 47: 5681-88.

Cosemans, J. M., Iserbyt, B. F., Deckmyn, H., and Heemskerk, J. W. 2008. 'Multiple ways to switch platelet integrins on and off', *J. Thromb. Haemost.*, 6: 1253-61.

Cosemans, J. M., Kuijpers, M. J., Lecut, C., Loubele, S. T., Heeneman, S., Jandrot-Perrus, M., and Heemskerk, J. W. 2005. 'Contribution of platelet glycoprotein VI to the thrombogenic effect of collagens in fibrous atherosclerotic lesions', *Atherosclerosis*, 181: 19-27.

Cosemans, J. M., Munnix, I. C., Wetzker, R., Heller, R., Jackson, S. P., and Heemskerk, J. W. 2006. 'Continuous signaling via PI3K isoforms β and γ is required for platelet ADP receptor function in dynamic thrombus stabilization', *Blood*, 108: 3045-52.

Creba, J., Downes, C. P., Hawkins, P. T., Brewster, G., Michell, R. H., and Kirk, C. J. 1983. 'Rapid breakdown of phosphatidylinositol 4-phosphate and phosphatidylinositol 4, 5-bisphosphate in rat hepatocytes stimulated by vasopressin and other Ca2+-mobilizing hormones', *Biochem. J.*, 212: 733-47.

Davie, E. W., Fujikawa, K., and Kisiel, W. 1991. 'The coagulation cascade: initiation, maintenance, and

regulation', *Biochemistry*, 30: 10363-70.

Dawes, A. T., and Edelstein-Keshet, L. 2007. 'Phosphoinositides and Rho proteins spatially regulate actin polymerization to initiate and maintain directed movement in a one-dimensional model of a motile cell', *Biophys. J.*, 92: 744-68.

Dawson, R. 1954a. 'The measurement of 32P labelling of individual kephalins and lecithin in a small sample of tissue', *Biochim. Biophys. Acta*, 14: 374-79.

Dawson, R. 1954b. 'Studies on the labelling of brain phospholipids with radioactive phosphorus', *Biochem. J.*, 57: 237.

De Candia, E. 2012. 'Mechanisms of platelet activation by thrombin: a short history', *Thromb. Res.*, 129: 250-56.

Di Paolo, G., and De Camilli, P. 2006. 'Phosphoinositides in cell regulation and membrane dynamics', *Nature*, 443: 651.

Dieterich, D. C., and Kreutz, M. R. 2016. 'Proteomics of the synapse–a quantitative approach to neuronal plasticity', *Mol. Cell. Proteomics*, 15: 368-81.

Dittmer, J., and Dawson, R. 1961. 'The isolation of a new lipid, triphosphoinositide, and monophosphoinositide from ox brain', *Biochem. J.*, 81: 535.

Downes, P., and Michell, R. H. 1982. 'Phosphatidylinositol 4-phosphate and phosphatidylinositol 4, 5-bisphosphate: lipids in search of a function', *Cell Calcium*, 3: 467-502.

Dunster, J. L., Mazet, F., Fry, M. J., Gibbins, J. M., and Tindall, M. J. 2015. 'Regulation of early steps of GPVI signal transduction by phosphatases: a systems biology approach', *PLoS Comp. Biol.*, 11: e1004589.

Durrant, T. N., and Hers, I. 2020. 'PI3K inhibitors in thrombosis and cardiovascular disease', *Clin. Transl. Med.*, 9: 1-21.

Dütting, S., Vögtle, T., Morowski, M., Schiessl, S., Schäfer, C. M., Watson, S. K., Hughes, C. E., Ackermann, J. A., Radtke, D., and Hermanns, H. M. 2014. 'Growth Factor Receptor–Bound Protein 2 Contributes to (Hem) Immunoreceptor Tyrosine-Based Activation Motif–Mediated Signaling in Platelets', *Circul. Res.*, 114: 444-53.

Engelman, J. A., Luo, J., and Cantley, L. C. 2006. 'The evolution of phosphatidylinositol 3-kinases as regulators of growth and metabolism', *Nat. Rev. Genet*, 7: 606-19.

Eremin, A., Moroz, I., and Mikhailova, R. 2008. 'Use of cadmium hydroxide gel for isolation of extracellular catalases from Penicillium piceum and characterization of purified enzymes', *Appl. Biochem. Microbiol.*, 44: 590-99.

Falati, S., Edmead, C. E., and Poole, A. W. 1999. 'Glycoprotein Ib-V-IX, a receptor for von Willebrand factor, couples physically and functionally to the Fc receptor γ-chain, Fyn, and Lyn to activate human platelets', *Blood*, 94: 1648-56.

Faucherre, A., Desbois, P., Satre, V., Lunardi, J., Dorseuil, O., and Gacon, G. 2003. 'Lowe syndrome protein OCRL1 interacts with Rac GTPase in the trans-Golgi network', *Hum. Mol. Genet.*, 12: 2449-56.

Feijge, M. A., Van Pampus, E. C., Lacabaratz-Porret, C., HamulyÀk, K., Lévy-Toledano, S., Enouf, J.,

and Heemskerk, J. W. 1998. 'Inter-individual variability in Ca2+ signalling in platelets from healthy volunteers: effects of aspirin and relationship with expression of endomembrane Ca2+-ATPases', *Br. J. Haematol.*, 102: 850-59.

Fisher, D. B., and Mueller, G. C. 1971. 'Studies on the mechanism by which phytohemagglutinin rapidly stimulates phospholipid metabolism of human lymphocytes', *Biochim. Biophys. Acta*, 248: 434-48.

Folch, J. 1942. 'Inositol, a consti-tuent of a brain phosphatide', *J. Biol. Chem.*, 142: 963-64.

Franke, T. F., Yang, S.-I., Chan, T. O., Datta, K., Kazlauskas, A., Morrison, D. K., Kaplan, D. R., and Tsichlis, P. N. 1995. 'The protein kinase encoded by the Akt proto-oncogene is a target of the PDGF-activated phosphatidylinositol 3-kinase', *Cell*, 81: 727-36.

Frojmovic, M., Labarthe, B., and Legrand, C. 2005. 'Inhibition and reversal of platelet aggregation by αIIbβ3 antagonists depends on the anticoagulant and flow conditions: differential effects of Abciximab and Lamifiban', *Br. J. Haematol.*, 131: 348-55.

Fuentes, E., Badimon, L., Caballero, J., Padró, T., Vilahur, G., Alarcón, M., Pérez, P., and Palomo, I. 2014. 'Protective mechanisms of adenosine 5′-monophosphate in platelet activation and thrombus formation', *Thromb. Haemost.*, 112: 491-507.

Gagnon, A., Dods, P., Roustan-Delatour, N., Chen, C.-S., and Sorisky, A. 2001. 'Phosphatidylinositol-3, 4, 5-trisphosphate is required for insulin-like growth factor 1-mediated survival of 3T3-L1 preadipocytes', *Endocrinology*, 142: 205-12.

Garner, S., Furnell, A., Kahan, B., Jones, C. I., Attwood, A., Harrison, P., Kelly, A., Goodall, A. H., Cardigan, R., and Ouwehand, W. 2017. 'Platelet responses to agonists in a cohort of highly characterised platelet donors are consistent over time', *Vox Sang.*, 112: 18-24.

Gaudette, D., and Holub, B. 1990. 'Effect of albumin-bound DHA on phosphoinositide phosphorylation in collagen stimulated human platelets', *Thromb. Res.*, 58: 435-44.

Gilio, K., Munnix, I. C., Mangin, P., Cosemans, J. M., Feijge, M. A., Van der Meijden, P. E., Olieslagers, S., Chrzanowska-Wodnicka, M. B., Lillian, R., and Schoenwaelder, S. 2009. 'Non-redundant roles of phosphoinositide 3-kinase isoforms α and β in glycoprotein VI-induced platelet signaling and thrombus formation', *J. Biol. Chem.*, 284: 33750-62.

Gitz, E., Pollitt, A. Y., Gitz-Francois, J. J., Alshehri, O., Mori, J., Montague, S., Nash, G. B., Douglas, M. R., Gardiner, E. E., and Andrews, R. K. 2014. 'CLEC-2 expression is maintained on activated platelets and on platelet microparticles', *Blood*, 124: 2262-70.

Goncalves, I., Hughan, S. C., Schoenwaelder, S. M., Yap, C. L., Yuan, Y., and Jackson, S. P. 2003. 'Integrin αIIbβ3-dependent calcium signals regulate platelet-fibrinogen interactions under flow: Involvement of phospholipase Cγ2', *J. Biol. Chem.*, 278: 34812-22.

Grynkiewicz, G., Poenie, M., and Tsien, R. Y. 1985. 'A new generation of Ca2+ indicators with greatly improved fluorescence properties', *J. Biol. Chem.*, 260: 3440-50.

Guidetti, G. F., Canobbio, I., and Torti, M. 2015. 'PI3K/Akt in platelet integrin signaling and implications in thrombosis', *Adv. Biol. Regul.*, 59: 36-52.

Guidetti, G. F., and Torti, M. 2012. 'The small GTPase Rap1b: a bidirectional regulator of platelet

adhesion receptors', *J. Signal Transduct.*, 2012.

Gustavsson, S. Å., Samskog, J., Markides, K. E., and Långström, B. 2001. 'Studies of signal suppression in liquid chromatography–electrospray ionization mass spectrometry using volatile ion-pairing reagents', *J. Chromatogr. A*, 937: 41-47.

Haag, M., Schmidt, A., Sachsenheimer, T., and Brügger, B. 2012. 'Quantification of signaling lipids by nano-electrospray ionization tandem mass spectrometry (Nano-ESI MS/MS)', *Metabolites*, 2: 57-76.

Hall, R., and Mazer, C. D. 2011. 'Antiplatelet drugs: a review of their pharmacology and management in the perioperative period', *Anesth. Analg.*, 112: 292-318.

Hama, H., Takemoto, J. Y., and DeWald, D. B. 2000. 'Analysis of phosphoinositides in protein trafficking', *Methods*, 20: 465-73.

Hardy, A. R., Jones, M. L., Mundell, S. J., and Poole, A. W. 2004. 'Reciprocal cross-talk between P2Y1 and P2Y12 receptors at the level of calcium signaling in human platelets', *Blood*, 104: 1745-52.

Hartwig, J. H. 1992. 'Mechanisms of actin rearrangements mediating platelet activation', *J. Cell Biol.*, 118: 1421-42.

Hassock, S. R., Zhu, M. X., Trost, C., Flockerzi, V., and Authi, K. S. 2002. 'Expression and role of TRPC proteins in human platelets: evidence that TRPC6 forms the store-independent calcium entry channel', *Blood*, 100: 2801-11.

Hawkins, P. T., Michell, R. H., and Kirk, C. 1984. 'Analysis of the metabolic turnover of the individual phosphate groups of phosphatidylinositol 4-phosphate and phosphatidylinositol 4, 5-bisphosphate. Validation of novel analytical techniques by using 32P-labelled lipids from erythrocytes', *Biochem. J.*, 218: 785-93.

He, F., Agosto, M. A., Anastassov, I. A., Tse, D. Y., Wu, S. M., and Wensel, T. G. 2016. 'Phosphatidylinositol-3-phosphate is light-regulated and essential for survival in retinal rods', *Sci. Rep.*, 6: 1-12.

Heemskerk, J., Mattheij, N., and Cosemans, J. 2013. 'Platelet-based coagulation: different populations, different functions', *J. Thromb. Haemost.*, 11: 2-16.

Heemskerk, J. W., Bevers, E. M., and Lindhout, T. 2002. 'Platelet activation and blood coagulation', *Thromb. Haemost.*, 88: 186-93.

Hill, A. V. 1910. 'The possible effects of the aggregation of the molecules of haemoglobin on its dissociation curves', *J. Physiol.*, 40: 4-7.

Hoefman, S., Ottevaere, I., Baumeister, J., and Sargentini-Maier, M. L. 2015. 'Pre-clinical intravenous serum pharmacokinetics of albumin binding and non-half-life extended Nanobodies®', *Antibodies*, 4: 141-56.

Hokin, L. E., and Hokin, M. R. 1955. 'Effects of acetylcholine on the turnover of phosphoryl units in individual phospholipids of pancreas slices and brain cortex slices', *Biochim. Biophys. Acta*, 18: 102-10.

Hokin, M. R. 1968. 'Studies on chemical mechanisms of the action of neurotransmitters and hormones: I. Relationship between hormone-stimulated 32P incorporation into phosphatidic acid and into phosphatidylinositol in pigeon pancreas slices', *Arch. Biochem. Biophys.*, 124: 271-79.

Hokin, M. R., and Hokin, L. E. 1953. 'Enzyme secretion and the incorporation of P32 into phospholipides of pancreas slices', *J. Biol. Chem.*, 203: 967-77.

Holčapek, M., Volná, K., Jandera, P., Kolářová, L., Lemr, K., Exner, M., and Cirkva, A. 2004. 'Effects of ion-pairing reagents on the electrospray signal suppression of sulphonated dyes and intermediates', *J. Mass Spectrom.*, 39: 43-50.

Hongu, T., and Kanaho, Y. 2014. 'Activation machinery of the small GTPase Arf6', *Adv. Biol. Regul.*, 54: 59-66.

Horii, K., Brooks, M. T., and Herr, A. B. 2009. 'Convulxin forms a dimer in solution and can bind eight copies of glycoprotein VI: implications for platelet activation', *Biochemistry*, 48: 2907-14.

Hu, S., Wang, J., Ji, E. H., Christison, T., Lopez, L., and Huang, Y. 2015. 'Targeted metabolomic analysis of head and neck cancer cells using high performance ion chromatography coupled with a Q Exactive HF mass spectrometer', *Anal. Chem.*, 87: 6371-79.

Huang, J., Li, X., Shi, X., Zhu, M., Wang, J., Huang, S., Huang, X., Wang, H., Li, L., and Deng, H. 2019. 'Platelet integrin αIIbβ3: signal transduction, regulation, and its therapeutic targeting', *J. Hematol. Oncol.*, 12: 1-22.

Hughes, C. E., Pollitt, A. Y., Mori, J., Eble, J. A., Tomlinson, M. G., Hartwig, J. H., O'Callaghan, C. A., Fütterer, K., and Watson, S. P. 2010. 'CLEC-2 activates Syk through dimerization', *Blood*, 115: 2947-55.

Iannelli, M., and Pugliese, A. 2015. *An introduction to mathematical population dynamics: along the trail of volterra and lotka* (Springer).

Inoue, O., Suzuki-Inoue, K., Dean, W. L., Frampton, J., and Watson, S. P. 2003. 'Integrin α2β1 mediates outside-in regulation of platelet spreading on collagen through activation of Src kinases and PLCγ2', *J. Cell Biol.*, 160: 769-80.

Inoue, O., Suzuki-Inoue, K., McCarty, O. J., Moroi, M., Ruggeri, Z. M., Kunicki, T. J., Ozaki, Y., and Watson, S. P. 2006. 'Laminin stimulates spreading of platelets through integrin α6β1–dependent activation of GPVI', *Blood*, 107: 1405-12.

Ittaman, S. V., VanWormer, J. J., and Rezkalla, S. H. 2014. 'The role of aspirin in the prevention of cardiovascular disease', *Clin. Med. Res.*, 12: 147-54.

Ivanciu, L., and Stalker, T. 2015. 'Spatiotemporal regulation of coagulation and platelet activation during the hemostatic response in vivo', *J. Thromb. Haemost.*, 13: 1949-59.

Jackson, S. P., Schoenwaelder, S. M., Goncalves, I., Nesbitt, W. S., Yap, C. L., Wright, C. E., Kenche, V., Anderson, K. E., Dopheide, S. M., and Yuan, Y. 2005. 'PI 3-kinase p110β: a new target for antithrombotic therapy', *Nat. Med.*, 11: 507-14.

Jahan, K. S., Shi, J., Greenberg, H. Z., Khavandi, S., Baudel, M. M.-A., Barrese, V., Greenwood, I. A., and Albert, A. P. 2020. 'MARCKS mediates vascular contractility through regulating interactions between voltage-gated Ca2+ channels and PIP2', *Vasc. Pharmacol.*, 132: 106776.

Jeschke, A., Zehethofer, N., Lindner, B., Krupp, J., Schwudke, D., Haneburger, I., Jovic, M., Backer, J. M., Balla, T., and Hilbi, H. 2015. 'Phosphatidylinositol 4-phosphate and phosphatidylinositol 3-phosphate regulate phagolysosome biogenesis', *Proc. Natl. Acad. Sci.*, 112: 4636-41.

Jeschke, A., Zehethofer, N., Schwudke, D., and Haas, A. 2017. 'Quantification of Phosphatidylinositol Phosphate Species in Purified Membranes.' in, *Methods Enzymol.* (Elsevier).

Jiang, P., and Jandrot-Perrus, M. 2014. 'New advances in treating thrombotic diseases: GPVI as a platelet drug target', *Drug Discov. Today*, 19: 1471-75.

Judd, B. A., Myung, P. S., Obergfell, A., Myers, E. E., Cheng, A. M., Watson, S. P., Pear, W. S., Allman, D., Shattil, S. J., and Koretzky, G. A. 2002. 'Differential requirement for LAT and SLP-76 in GPVI versus T cell receptor signaling', *J. Exp. Med.*, 195: 705-17.

Kauffenstein, G., Bergmeier, W., Eckly, A., Ohlmann, P., Leon, C., Cazenave, J., Nieswandt, B., and Gachet, C. 2001. 'The P2Y12 receptor induces platelet aggregation through weak activation of the αIIbβ3 integrin–a phosphoinositide 3-kinase-dependent mechanism', *FEBS Lett.*, 505: 281-90.

Kauskot, A., Di Michele, M., Loyen, S., Freson, K., Verhamme, P., and Hoylaerts, M. F. 2012. 'A novel mechanism of sustained platelet αIIbβ3 activation via PEAR1', *Blood*, 119: 4056-65.

Kavanaugh, W., Pot, D., Chin, S., Deuter-Reinhard, M., Jefferson, A., Norris, F., Masiarz, F., Cousens, L., Majerus, P., and Williams, L. T. 1996. 'Multiple forms of an inositol polyphosphate 5-phosphatase form signaling complexes with Shc and Grb2', *Curr. Biol.*, 6: 438-45.

Kavran, J. M., Klein, D. E., Lee, A., Falasca, M., Isakoff, S. J., Skolnik, E. Y., and Lemmon, M. A. 1998. 'Specificity and promiscuity in phosphoinositide binding by pleckstrin homology domains', *J. Biol. Chem.*, 273: 30497-508.

Kielkowska, A., Niewczas, I., Anderson, K. E., Durrant, T. N., Clark, J., Stephens, L. R., and Hawkins, P. T. 2014. 'A new approach to measuring phosphoinositides in cells by mass spectrometry', *Adv. Biol. Regul.*, 54: 131-41.

Kim, M.-S., Pinto, S. M., Getnet, D., Nirujogi, R. S., Manda, S. S., Chaerkady, R., Madugundu, A. K., Kelkar, D. S., Isserlin, R., and Jain, S. 2014. 'A draft map of the human proteome', *Nature*, 509: 575-81.

Kim, S., Garcia, A., Jackson, S. P., and Kunapuli, S. P. 2007. 'Insulin-like growth factor-1 regulates platelet activation through PI3-Kα isoform', *Blood*, 110: 4206-13.

Kim, Y. J., Sekiya, F., Poulin, B., Bae, Y. S., and Rhee, S. G. 2004. 'Mechanism of B-cell receptor-induced phosphorylation and activation of phospholipase C-γ2', *Mol. Cell. Biol.*, 24: 9986-99.

Kisseleva, M. V., Wilson, M. P., and Majerus, P. W. 2000. 'The isolation and characterization of a cDNA encoding phospholipid-specific inositol polyphosphate 5-phosphatase', *J. Biol. Chem.*, 275: 20110-16.

Knight, C. G., Morton, L. F., Onley, D. J., Peachey, A. R., Ichinohe, T., Okuma, M., Farndale, R. W., and Barnes, M. J. 1999. 'Collagen–platelet interaction: Gly-Pro-Hyp is uniquely specific for platelet Gp VI and mediates platelet activation by collagen', *Cardiovasc. Res.*, 41: 450-57.

Kolay, S., Basu, U., and Raghu, P. 2016. 'Control of diverse subcellular processes by a single multi-functional lipid phosphatidylinositol 4, 5-bisphosphate [PI (4, 5) P 2]', *Biochem. J.*, 473: 1681-92.

Koupenova, M., Kehrel, B. E., Corkrey, H. A., and Freedman, J. E. 2017. 'Thrombosis and platelets: an update', *Eur. Heart J.*, 38: 785-91.

Kovacsovics, T. J., Bachelot, C., Toke, A., Vlahos, C. J., Duckworth, B., Cantley, L. C., and Hartwig, J. H. 1995. 'Phosphoinositide 3-kinase inhibition spares actin assembly in activating platelets but reverses

platelet aggregation', *J. Biol. Chem.*, 270: 11358-66.

Kramer, R. M., and Sharp, J. D. 1997. 'Structure, function and regulation of Ca2+-sensitive cytosolic phospholipase A2 (cPLA2)', *FEBS Lett.*, 410: 49-53.

Kucera, G. L., and Rittenhouse, S. E. 1990. 'Human platelets form 3-phosphorylated phosphoinositides in response to alpha-thrombin, U46619, or GTP gamma S', *J. Biol. Chem.*, 265: 5345-48.

Kuhne, M. R., Ku, G., and Weiss, A. 2000. 'A guanine nucleotide exchange factor-independent function of Vav1 in transcriptional activation', *J. Biol. Chem.*, 275: 2185-90.

Kurosu, H., Maehama, T., Okada, T., Yamamoto, T., Hoshino, S.-i., Fukui, Y., Ui, M., Hazeki, O., and Katada, T. 1997. 'Heterodimeric phosphoinositide 3-kinase consisting of p85 and p110β is synergistically activated by the βγ subunits of G proteins and phosphotyrosyl peptide', *J. Biol. Chem.*, 272: 24252-56.

Kurtz, A., Härtl, W., Jelkmann, W., Zapf, J., and Bauer, C. 1985. 'Activity in fetal bovine serum that stimulates erythroid colony formation in fetal mouse livers is insulinlike growth factor I', *J. Clin. Investig.*, 76: 1643-48.

Lagarde, M., Guichardant, M., Menashi, S., and Crawford, N. 1982. 'The phospholipid and fatty acid composition of human platelet surface and intracellular membranes isolated by high voltage free flow electrophoresis', *J. Biol. Chem.*, 257: 3100-04.

Lagrue, A.-H., Francischetti, I. M., Guimarães, J. A., and Jandrot-Perrus, M. 1999. 'Phosphatidylinositol 3′-kinase and tyrosine-phosphatase activation positively modulate Convulxin-induced platelet activation. Comparison with collagen', *FEBS Lett.*, 448: 95-100.

Lamerton, R. E., Lightfoot, A., Nieves, D. J., and Owen, D. M. 2021. 'The role of protein and lipid clustering in lymphocyte activation', *Front. Immunol.*, 12: 600961.

Lapetina, E. G., and Michell, R. H. 1973. 'Phosphatidylinositol metabolism in cells receiving extracellular stimulation', *FEBS Lett.*, 31: 1-10.

Laurent, P.-A., Séverin, S., Hechler, B., Vanhaesebroeck, B., Payrastre, B., and Gratacap, M.-P. 2015. 'Platelet PI3Kβ and GSK3 regulate thrombus stability at a high shear rate', *Blood*, 125: 881-88.

Lebozec, K., Jandrot-Perrus, M., Avenard, G., Favre-Bulle, O., and Billiald, P. 2017. "Design, development and characterization of ACT017, a humanized Fab that blocks platelet's glycoprotein VI function without causing bleeding risks." *MAbs*, 9:945-58.

Lecut, C., Feeney, L., Kingsbury, G., Hopkins, J., Lanza, F., Gachet, C., Villeval, J. L., and Jandrot-Perrus, M. 2003. 'Human platelet glycoprotein VI function is antagonized by monoclonal antibody-derived Fab fragments', *J. Thromb. Haemost.*, 1: 2653-62.

Leech, A. P., Baker, G. R., Shute, J. K., Cohen, M. A., and Gani, D. 1993. 'Chemical and kinetic mechanism of the inositol monophosphatase reaction and its inhibition by Li+', *Eur. J. Biochem.*, 212: 693-704.

Lees, J. A., Li, P., Kumar, N., Weisman, L. S., and Reinisch, K. M. 2020. 'Insights into lysosomal PI (3, 5) P2 homeostasis from a structural-biochemical analysis of the PIKfyve lipid kinase complex', *Mol. Cell*, 80: 736-43. e4.

Lemmon, M. A., Ferguson, K. M., O'Brien, R., Sigler, P. B., and Schlessinger, J. 1995. 'Specific and high-affinity binding of inositol phosphates to an isolated pleckstrin homology domain', *Proc. Natl. Acad. Sci.*, 92: 10472-76.

Li, P., and Lämmerhofer, M. 2021. 'Isomer selective comprehensive lipidomics analysis of phosphoinositides in biological samples by liquid chromatography with data independent acquisition tandem mass spectrometry', *Anal. Chem.*, 93: 9583-92.

Liu, Y., Hu, M., Luo, D., Yue, M., Wang, S., Chen, X., Zhou, Y., Wang, Y., Cai, Y., and Hu, X. 2017. 'Class III PI3K positively regulates platelet activation and thrombosis via PI (3) P-directed function of NADPH oxidase', *Arterioscler. Thromb. Vasc. Biol.*, 37: 2075-86.

Lockyer, S., Okuyama, K., Begum, S., Le, S., Sun, B., Watanabe, T., Matsumoto, Y., Yoshitake, M., Kambayashi, J., and Tandon, N. N. 2006. 'GPVI-deficient mice lack collagen responses and are protected against experimentally induced pulmonary thromboembolism', *Thromb. Res.*, 118: 371-80.

Lombardi, F., De Chaumont, C., Shields, D. C., and Moran, N. 2012. 'Platelet signalling networks: pathway perturbation demonstrates differential sensitivity of ADP secretion and fibrinogen binding', *Platelets*, 23: 17-25.

Mahaut-Smith, M. P., Jones, S., and Evans, R. J. 2011. 'The P2X1 receptor and platelet function', *Purinergic Signal.*, 7: 341-56.

Maier, U., Babich, A., and Nürnberg, B. 1999. 'Roles of non-catalytic subunits in Gβγ-induced activation of class I phosphoinositide 3-kinase isoforms β and γ', *J. Biol. Chem.*, 274: 29311-17.

Mangin, P. H., Onselaer, M.-B., Receveur, N., Le Lay, N., Hardy, A. T., Wilson, C., Sanchez, X., Loyau, S., Dupuis, A., and Babar, A. K. 2018. 'Immobilized fibrinogen activates human platelets through glycoprotein VI', *Haematologica*, 103: 898.

Maqsood, Z., Clark, J. C., Martin, E. M., Cheung, Y. F. H., Morán, L. A., Watson, S. E., Pike, J. A., Di, Y., Poulter, N. S., and Slater, A. 2022. 'Experimental validation of computerised models of clustering of platelet glycoprotein receptors that signal via tandem SH2 domain proteins', *PLoS Comp. Biol.*, 18: e1010708.

Marée, A. F., Grieneisen, V. A., and Edelstein-Keshet, L. 2012. 'How cells integrate complex stimuli: the effect of feedback from phosphoinositides and cell shape on cell polarization and motility', *PLoS Comp. Biol.*, 8: e1002402.

Martin, V., Guillermet-Guibert, J., Chicanne, G., Cabou, C., Jandrot-Perrus, M., Plantavid, M., Vanhaesebroeck, B., Payrastre, B., and Gratacap, M.-P. 2010. 'Deletion of the p110β isoform of phosphoinositide 3-kinase in platelets reveals its central role in Akt activation and thrombus formation in vitro and in vivo', *Blood*, 115: 2008-13.

Martínez-Gómez, K., Flores, N., Castañeda, H. M., Martínez-Batallar, G., Hernández-Chávez, G., Ramírez, O. T., Gosset, G., Encarnación, S., and Bolivar, F. 2012. 'New insights into Escherichia coli metabolism: carbon scavenging, acetate metabolism and carbon recycling responses during growth on glycerol', *Microb. Cell Factories*, 11: 1-21.

Matus, V., Valenzuela, G., Sáez, C., Hidalgo, P., Lagos, M., Aranda, E., Panes, O., Pereira, J., Pillois,

X., and Nurden, A. 2013. 'An adenine insertion in exon 6 of human GP 6 generates a truncated protein associated with a bleeding disorder in four C hilean families', *J. Thromb. Haemost.*, 11: 1751-59.

Mauco, G., Dangelmaier, C. A., and Smith, J. B. 1984. 'Inositol lipids, phosphatidate and diacylglycerol share stearoylarachidonoylglycerol as a common backbone in thrombin-stimulated human platelets', *Biochem. J.*, 224: 933-40.

May, F., Hagedorn, I., Pleines, I., Bender, M., Vögtle, T., Eble, J., Elvers, M., and Nieswandt, B. 2009. 'CLEC-2 is an essential platelet-activating receptor in hemostasis and thrombosis', *Blood*, 114: 3464-72.

Mazet, F., Tindall, M. J., Gibbins, J. M., and Fry, M. J. 2020. 'A model of the PI cycle reveals the regulating roles of lipid-binding proteins and pitfalls of using mosaic biological data', *Sci. Rep.*, 10: 1-14.

Mazighi, M., Pletan, Y., Comenducci, A., Lapergue, B., Toni, D., Koehrmann, M., Lemmens, R., Lyrer, P., Molina, C., and Avenard, G. 2019. 'Actimis Trial: Safety and Efficacy Evaluation of ACT017, a Novel Antiplatelet Agent on Top of Acute Ischemic Stroke Standard of Care', *Circulation*, 140: A14738-A38.

McLaughlin, S., and Murray, D. 2005. 'Plasma membrane phosphoinositide organization by protein electrostatics', *Nature*, 438: 605-11.

Metwally, H., McAllister, R. G., and Konermann, L. 2015. 'Exploring the mechanism of salt-induced signal suppression in protein electrospray mass spectrometry using experiments and molecular dynamics simulations', *Anal. Chem.*, 87: 2434-42.

Michaelis, L., and Menten, M. L. 1913. 'Die kinetik der invertinwirkung', *Biochem. z*, 49: 352.

Min, S. H., and Abrams, C. S. 2013. 'Regulation of platelet plug formation by phosphoinositide metabolism', *Blood*, 122: 1358-65.

MJ, A., and Burke, J. 2022. 'Molecular mechanisms of PI4K regulation and their involvement in viral replication', *Traffic,* Advance online publication, DOI: 10.1111/tra.12841

Morioka, S., Nakanishi, H., Yamamoto, T., Hasegawa, J., Tokuda, E., Hikita, T., Sakihara, T., Kugii, Y., Oneyama, C., and Yamazaki, M. 2022. 'A mass spectrometric method for in-depth profiling of phosphoinositide regioisomers and their disease-associated regulation', *Nat. Commun.,* 13: 83.

Morris, J. B., Hinchliffe, K. A., Ciruela, A., Letcher, A. J., and Irvine, R. F. 2000. 'Thrombin stimulation of platelets causes an increase in phosphatidylinositol 5-phosphate revealed by mass assay', *FEBS Lett.*, 475: 57-60.

Morrison, C. 2019. 'Nanobody approval gives domain antibodies a boost', *Nat. Rev. Drug Discov.*, 18: 485-88.

Morton, L., Hargreaves, P., Farndale, R., Young, R., and Barnes, M. 1995. 'Integrin α 2 β 1-independent activation of platelets by simple collagen-like peptides: collagen tertiary (triple-helical) and quaternary (polymeric) structures are sufficient alone for α 2 β 1-independent platelet reactivity', *Biochem. J.*, 306: 337-44.

Moser, M., Bertram, U., Peter, K., Bode, C., and Ruef, J. 2003. 'Abciximab, eptifibatide, and tirofiban exhibit dose-dependent potencies to dissolve platelet aggregates', *J. Cardiovasc. Pharmacol.*, 41: 586-92.

Mountford, J. K., Petitjean, C., Putra, H. W. K., McCafferty, J. A., Setiabakti, N. M., Lee, H., Tønnesen, L. L., McFadyen, J. D., Schoenwaelder, S. M., and Eckly, A. 2015. 'The class II PI 3-kinase, PI3KC2α, links platelet internal membrane structure to shear-dependent adhesive function', *Nat. Commun.*, 6: 1-14.

Mücksch, F., Citir, M., Lüchtenborg, C., Glass, B., Traynor-Kaplan, A., Schultz, C., Brügger, B., and Kräusslich, H.-G. 2019. 'Quantification of phosphoinositides reveals strong enrichment of PIP2 in HIV-1 compared to producer cell membranes', *Sci. Rep.*, 9: 1-13.

Mujalli, A., Chicanne, G., Bertrand-Michel, J., Viars, F., Stephens, L., Hawkins, P., Viaud, J., Gaits-Iacovoni, F., Severin, S., and Gratacap, M.-P. 2018. 'Profiling of phosphoinositide molecular species in human and mouse platelets identifies new species increasing following stimulation', *Biochim. Biophys. Acta*, 1863: 1121-31.

Næss, I. A., Christiansen, S., Romundstad, P., Cannegieter, S., Rosendaal, F. R., and Hammerstrøm, J. 2007. 'Incidence and mortality of venous thrombosis: a population-based study', *J. Thromb. Haemost.*, 5: 692-99.

Nagy, M., Perrella, G., Dalby, A., Becerra, M. F., Garcia Quintanilla, L., Pike, J. A., Morgan, N. V., Gardiner, E. E., Heemskerk, J. W., and Azócar, L. 2020. 'Flow studies on human GPVI-deficient blood under coagulating and noncoagulating conditions', *Blood Adv.*, 4: 2953-61.

Nagy, Z., and Smolenski, A. 2018. 'Cyclic nucleotide-dependent inhibitory signaling interweaves with activating pathways to determine platelet responses', *Res. Pract. Thromb. Haemost.* 2: 558-71.

Nakamura, Y., and Fukami, K. 2017. 'Regulation and physiological functions of mammalian phospholipase C', *J. Biochem*, 161: 315-21.

Narita, H., Park, H. J., Tanaka, K.-i., Matsuura, T., and Kito, M. 1985. 'Insufficient mobilization of calcium by early breakdown of phosphatidylinositol 4, 5-bisphosphate for aggregation of human platelets by collagen', *J. Biochem*, 98: 1063-68.

Nieswandt, B., Bergmeier, W., Schulte, V., Rackebrandt, K., Gessner, J. E., and Zirngibl, H. 2000. 'Expression and function of the mouse collagen receptor glycoprotein VI is strictly dependent on its association with the FcRγ chain', *J. Biol. Chem.*, 275: 23998-4002.

Nieswandt, B., Schulte, V., Bergmeier, W., Mokhtari-Nejad, R., Rackebrandt, K., Cazenave, J.-P., Ohlmann, P., Gachet, C., and Zirngibl, H. 2001. 'Long-term antithrombotic protection by in vivo depletion of platelet glycoprotein VI in mice', *J. Exp. Med.*, 193: 459-70.

Nieswandt, B., Varga-Szabo, D., and Elvers, M. 2009. 'Integrins in platelet activation', *J. Thromb. Haemost.*, 7: 206-09.

Nieswandt, B., and Watson, S. P. 2003. 'Platelet-collagen interaction: is GPVI the central receptor?', *Blood*, 102: 449-61.

Nishizuka, Y. 1984. 'The role of protein kinase C in cell surface signal transduction and tumour promotion', *Nature*, 308: 693-98.

Nishizuka, Y. 1988. 'The molecular heterogeneity of protein kinase C and its implications for cellular regulation', *Nature*, 334: 661-65.

Nolan, R. D., and Lapetina, E. G. 1991. 'The production of phosphatidylinositol trisphosphate is stimulated by thrombin in human platelets', *Biochem. Biophys. Res. Commun.*, 174: 524-28.

Nylander, S., Kull, B., Björkman, J., Ulvinge, J., Oakes, N., Emanuelsson, B., Andersson, M., Skärby, T., Inghardt, T., and Fjellström, O. 2012. 'Human target validation of phosphoinositide 3-kinase (PI3K) β: effects on platelets and insulin sensitivity, using AZD6482 a novel PI3Kβ inhibitor', *J. Thromb. Haemost.*, 10: 2127-36.

Offermanns, S. 2000. 'The role of heterotrimeric G proteins in platelet activation', *J. Biol. Chem.*, 381: 389-96.

Offermanns, S. 2006. 'Activation of platelet function through G protein–coupled receptors', *Circul. Res.*, 99: 1293-304.

Olivença, D. V., Uliyakina, I., Fonseca, L. L., Amaral, M. D., Voit, E. O., and Pinto, F. R. 2018. 'A mathematical model of the phosphoinositide pathway', *Sci. Rep.*, 8: 1-12.

Oostindie, S. C., Lazar, G. A., Schuurman, J., and Parren, P. W. 2022. 'Avidity in antibody effector functions and biotherapeutic drug design', *Nat. Rev. Drug Discov.*, 21: 715-35.

Osaki, M., Oshimura, M. a., and Ito, H. 2004. 'PI3K-Akt pathway: its functions and alterations in human cancer', *Apoptosis*, 9: 667-76.

Özdener, F., Dangelmaier, C., Ashby, B., Kunapuli, S. P., and Daniel, J. L. 2002. 'Activation of phospholipase Cγ2 by tyrosine phosphorylation', *Mol. Pharmacol.*, 62: 672-79.

Park, B. O., Ahrends, R., and Teruel, M. N. 2012. 'Consecutive positive feedback loops create a bistable switch that controls preadipocyte-to-adipocyte conversion', *Cell Rep.*, 2: 976-90.

Pearce, A. C., Senis, Y. A., Billadeau, D. D., Turner, M., Watson, S. P., and Vigorito, E. 2004. 'Vav1 and vav3 have critical but redundant roles in mediating platelet activation by collagen', *J. Biol. Chem.*, 279: 53955-62.

Pearce, A. C., Wilde, J. I., Doody, G. M., Best, D., Inoue, O., Vigorito, E., Tybulewicz, V. L., Turner, M., and Watson, S. P. 2002. 'Vav1, but not Vav2, contributes to platelet aggregation by CRP and thrombin, but neither is required for regulation of phospholipase C', *Blood*, 100: 3561-69.

Peng, B., and Ahrends, R. 2015. 'Adaptation of skyline for targeted lipidomics', *J. Proteome Res.*, 15: 291-301.

Peng, B., Geue, S., Coman, C., Münzer, P., Kopczynski, D., Has, C., Hoffmann, N., Manke, M.-C., Lang, F., and Sickmann, A. 2018. 'Identification of key lipids critical for platelet activation by comprehensive analysis of the platelet lipidome', *Blood*, 132: e1-e12.

Perrella, G., Huang, J., Provenzale, I., Swieringa, F., Heubel-Moenen, F. C., Farndale, R. W., Roest, M., van der Meijden, P. E., Thomas, M., and Ariëns, R. A. 2021. 'Nonredundant roles of platelet glycoprotein VI and integrin αIIbβ3 in fibrin-mediated microthrombus formation', *Arterioscler. Thromb. Vasc. Biol.*, 41: e97-e111.

Perrella, G., Montague, S. J., Brown, H. C., Garcia Quintanilla, L., Slater, A., Stegner, D., Thomas, M., Heemskerk, J. W., and Watson, S. P. 2022. 'Role of Tyrosine Kinase Syk in Thrombus Stabilisation at High Shear', *Int. J. Mol. Sci.*, 23: 493.

Perret, B. P., Plantavid, M., Chap, H., and Douste-Blazy, L. 1983. 'Are polyphosphoinositides involved in platelet activation?', *Biochem. Biophys. Res. Commun.*, 110: 660-67.

Pirruccello, M., Nandez, R., Idevall-Hagren, O., Alcazar-Roman, A., Abriola, L., Berwick, S. A., Lucast, L., Morel, D., and De Camilli, P. 2014. 'Identification of inhibitors of inositol 5-phosphatases through multiple screening strategies', *ACS Chem. Biol.*, 9: 1359-68.

Posor, Y., Jang, W., and Haucke, V. 2022. 'Phosphoinositides as membrane organizers', *Nat. Rev. Mol. Cell Biol*, 23: 797-816.

Prado-Franceschi, J., and Brazil, O. V. 1981. 'Convulxin, a new toxin from the venom of the South American rattlesnake Crotalus durissus terrificus', *Toxicon*, 19: 875-87.

Purvis, J. E., Chatterjee, M. S., Brass, L. F., and Diamond, S. L. 2008. 'A molecular signaling model of platelet phosphoinositide and calcium regulation during homeostasis and P2Y1 activation', *Blood*, 112: 4069-79.

Quek, L., Bolen, J., and Watson, S. 1998. 'A role for Bruton's tyrosine kinase (Btk) in platelet activation by collagen', *Curr. Biol.*, 8: 1137-S1.

Ragab, A., Séverin, S., Gratacap, M.-P., Aguado, E., Malissen, M., Jandrot-Perrus, M., Malissen, B., Ragab-Thomas, J., and Payrastre, B. 2007. 'Roles of the C-terminal tyrosine residues of LAT in GPVI-induced platelet activation: insights into the mechanism of PLCγ2 activation', *Blood*, 110: 2466-74.

Rahbarizadeh, F., Ahmadvand, D., and Sharifzadeh, Z. 2011. 'Nanobody; an old concept and new vehicle for immunotargeting', *Immunol. Invest.*, 40: 299-338.

Rayes, J., Watson, S. P., and Nieswandt, B. 2019. 'Functional significance of the platelet immune receptors GPVI and CLEC-2', *J. Clin. Invest.*, 129: 12-23.

Reddy, E. C., and Rand, M. L. 2020. 'Procoagulant phosphatidylserine-exposing platelets in vitro and in vivo', *Front. Cardiovasc. Med.*: 15.

Reininger, A. J., Bernlochner, I., Penz, S. M., Ravanat, C., Smethurst, P., Farndale, R. W., Gachet, C., Brandl, R., and Siess, W. 2010. 'A 2-step mechanism of arterial thrombus formation induced by human atherosclerotic plaques', *J. Am. Coll. Cardiol.*, 55: 1147-58.

Ribes, A., Oprescu, A., Viaud, J., Hnia, K., Chicanne, G., Xuereb, J.-M., Severin, S., Gratacap, M.-P., and Payrastre, B. 2020. 'Phosphoinositide 3-kinases in platelets, thrombosis and therapeutics', *Biochem. J.*, 477: 4327-42.

Ridderstråle, M., Degerman, E., and Tornqvist, H. 1995. 'Growth hormone stimulates the tyrosine phosphorylation of the insulin receptor substrate-1 and its association with phosphatidylinositol 3-kinase in primary adipocytes', *J. Biol. Chem.*, 270: 3471-74.

Roovers, R. C., Laeremans, T., Huang, L., De Taeye, S., Verkleij, A. J., Revets, H., de Haard, H. J., and van Bergen en Henegouwen, P. M. 2007. 'Efficient inhibition of EGFR signalling and of tumour growth by antagonistic anti-EGFR Nanobodies', *Cancer Immunol., Immunother.*, 56: 303-17.

Sadeghnezhad, G., Romão, E., Bernedo-Navarro, R., Massa, S., Khajeh, K., Muyldermans, S., and Hassania, S. 2019. 'Identification of new DR5 agonistic nanobodies and generation of multivalent nanobody constructs for cancer treatment', *Int. J. Mol. Sci.*, 20: 4818.

Sadler, J. E. 1998. 'Biochemistry and genetics of von Willebrand factor', *Annu. Rev. Biochem.*, 67: 395-424.

Saito, K., Scharenberg, A. M., and Kinet, J.-P. 2001. 'Interaction between the Btk PH domain and phosphatidylinositol-3, 4, 5-trisphosphate directly regulates Btk', *J. Biol. Chem.*, 276: 16201-06.

Sang, Y., Huskens, D., Wichapong, K., de Laat, B., Nicolaes, G. A., and Roest, M. 2019. 'A synthetic triple helical collagen peptide as a new agonist for flow cytometric measurement of GPVI-specific platelet activation', *Thromb. Haemost.*, 119: 2005-13.

Sargentini-Maier, M. L., De Decker, P., Tersteeg, C., Canvin, J., Callewaert, F., and De Winter, H. 2019. 'Clinical pharmacology of caplacizumab for the treatment of patients with acquired thrombotic thrombocytopenic purpura', *Expert Rev. Clin. Pharmacol.*, 12: 537-45.

Sbrissa, D., Ikonomov, O. C., Filios, C., Delvecchio, K., and Shisheva, A. 2012. 'Functional dissociation between PIKfyve-synthesized PtdIns5P and PtdIns (3, 5) P2 by means of the PIKfyve inhibitor YM201636', *Am. J. Physiol. Cell Physiol.*, 303: C436-C46.

Schink, K. O., Raiborg, C., and Stenmark, H. 2013. 'Phosphatidylinositol 3-phosphate, a lipid that regulates membrane dynamics, protein sorting and cell signalling', *Bioessays*, 35: 900-12.

Schönberger, T., Ziegler, M., Borst, O., Konrad, I., Nieswandt, B., Massberg, S., Ochmann, C., Jürgens, T., Seizer, P., and Langer, H. 2012. 'The dimeric platelet collagen receptor GPVI-Fc reduces platelet adhesion to activated endothelium and preserves myocardial function after transient ischemia in mice', *Am. J. Physiol. Cell Physiol.*, 303: C757-C66.

Selvadurai, M. V., Moon, M. J., Mountford, S. J., Ma, X., Zheng, Z., Jennings, I. G., Setiabakti, N. M., Iman, R. P., Brazilek, R. J., and Z. Abidin, N. A. 2020. 'Disrupting the platelet internal membrane via PI3KC2α inhibition impairs thrombosis independently of canonical platelet activation', *Sci. Transl. Med.*, 12: eaar8430.

Senis, Y. A., Atkinson, B. T., Pearce, A. C., Wonerow, P., Auger, J. M., Okkenhaug, K., Pearce, W., Vigorito, E., Vanhaesebroeck, B., and Turner, M. 2005. 'Role of the p110δ PI 3-kinase in integrin and ITAM receptor signalling in platelets', *Platelets*, 16: 191-202.

Senis, Y. A., Mazharian, A., and Mori, J. 2014. 'Src family kinases: at the forefront of platelet activation', *Blood*, 124: 2013-24.

Serunian, L. A., Auger, K. R., and Cantley, L. C. 1991. 'Identification and quantification of polyphosphoinositides produced in response to platelet-derived growth factor stimulation', *Methods Enzymol.*, 198: 78-87.

Séverin, S., Pollitt, A. Y., Navarro-Nuñez, L., Nash, C. A., Mourão-Sá, D., Eble, J. A., Senis, Y. A., and Watson, S. P. 2011. 'Syk-dependent phosphorylation of CLEC-2: a novel mechanism of hem-immunoreceptor tyrosine-based activation motif signaling', *J. Biol. Chem.*, 286: 4107-16.

Shattil, S. J. 1999. 'Signaling through platelet integrin αIIbβ3: inside-out, outside-in, and sideways', *Thromb. Haemost.*, 82: 318-25.

Slater, A., Di, Y., Clark, J. C., Jooss, N. J., Martin, E. M., Alenazy, F., Thomas, M. R., Ariëns, R. A., Herr, A. B., and Poulter, N. S. 2021. 'Structural characterization of a novel GPVI-nanobody complex reveals

a biologically active domain-swapped GPVI dimer', *Blood*, 137: 3443-53.

Smejkal, G. B., and Kakumanu, S. 2019. 'Enzymes and their turnover numbers', *Expert Rev. Proteom.*, 16: 543-44.

Smyth, E. M. 2010. 'Thromboxane and the thromboxane receptor in cardiovascular disease', *Clin. Lipidol.*, 5: 209-19.

Smyth, S. S., Tsakiris, D. A., Scudder, L. E., and Coller, B. S. 2000. 'Structure and function of murine αIIbβ3 (GPIIb/IIIa): studies using monoclonal antibodies and β3-null mice', *Thromb. Haemost.*, 84: 1103-08.

Smyth, S. S., Woulfe, D. S., Weitz, J. I., Gachet, C., Conley, P. B., Goodman, S. G., Roe, M. T., Kuliopulos, A., Moliterno, D. J., and French, P. A. 2009. 'G-protein–coupled receptors as signaling targets for antiplatelet therapy', *Arterioscler. Thromb. Vasc. Biol.*, 29: 449-57.

Snell, D. C., Schulte, V., Jarvis, G. E., Arase, K., Sakurai, D., Saito, T., Watson, S. P., and Nieswandt, B. 2002. 'Differential effects of reduced glycoprotein VI levels on activation of murine platelets by glycoprotein VI ligands', *Biochem. J.*, 368: 293-300.

Sorisky, A., Pardasani, D., and Lin, Y. 1996. 'The 3-phosphorylated phosphoinositide response of 3T3-L1 preadipose cells exposed to insulin, insulin-like growth factor-1, or platelet-derived growth factor', *Obesity Res.*, 4: 9-19.

Spalton, J. C., Mori, J., Pollitt, A. Y., Hughes, C. E., Eble, J. A., and Watson, S. P. 2009. 'The novel Syk inhibitor R406 reveals mechanistic differences in the initiation of GPVI and CLEC-2 signaling in platelets', *J. Thromb. Haemost.*, 7: 1192-99.

Speich, H., Earhart, A., Hill, S., Cholera, S., Kueter, T., Smith, J., White, M., and Jennings, L. 2009. 'Variability of platelet aggregate dispersal with glycoprotein IIb–IIIa antagonists eptifibatide and abciximab', *J. Thromb. Haemost.*, 7: 983-91.

Speich, H. E., Furman, R. R., Lands, L. T., Moodie, G. D., and Jennings, L. K. 2013. 'Elevating local concentrations of GPIIb–IIIa antagonists counteracts platelet thrombus stability', *J. Thromb. Thrombolysis*, 36: 31-41.

Stefanini, L., and Bergmeier, W. 2010. 'CalDAG-GEFI and platelet activation', *Platelets*, 21: 239-43.

Steiner, D., Merz, F. W., Sonderegger, I., Gulotti-Georgieva, M., Villemagne, D., Phillips, D. J., Forrer, P., Stumpp, M. T., Zitt, C., and Binz, H. K. 2017. 'Half-life extension using serum albumin-binding DARPin® domains', *Protein Eng. Des. Sel.*, 30: 583-91.

Stephens, L., Hawkins, P. T., and Downes, C. P. 1989. 'Metabolic and structural evidence for the existence of a third species of polyphosphoinositide in cells: D-phosphatidyl-myo-inositol 3-phosphate', *Biochem. J.*, 259: 267-76.

Streb, H., Irvine, R. F., Berridge, M., and Schulz, I. 1983. 'Release of Ca2+ from a nonmitochondrial intracellular store in pancreatic acinar cells by inositol-1, 4, 5-trisphosphate', *Nature*, 306: 67-69.

Suzuki-Inoue, K., Inoue, O., Frampton, J., and Watson, S. P. 2003. 'Murine GPVI stimulates weak integrin activation in PLC γ 2–/–platelets: involvement of PLCγ1 and PI3-kinase', *Blood*, 102: 1367-73.

Suzuki-Inoue, K., Kato, Y., Inoue, O., Kaneko, M. K., Mishima, K., Yatomi, Y., Yamazaki, Y., Narimatsu,

H., and Ozaki, Y. 2007. 'Involvement of the Snake Toxin Receptor CLEC-2, in Podoplanin-mediated Platelet Activation, by Cancer Cells', *J. Biol. Chem.*, 282: 25993-6001.

Suzuki-Inoue, K., Tulasne, D., Shen, Y., Bori-Sanz, T., Inoue, O., Jung, S. M., Moroi, M., Andrews, R. K., Berndt, M. C., and Watson, S. P. 2002. 'Association of Fyn and Lyn with the proline-rich domain of glycoprotein VI regulates intracellular signaling', *J. Biol. Chem.*, 277: 21561-66.

Thiele, J. C., Kurth, W., and Grimm, V. 2014. 'Facilitating parameter estimation and sensitivity analysis of agent-based models: A cookbook using NetLogo and R', *Jasss*, 17: 11.

Timmis, A., Townsend, N., Gale, C. P., Torbica, A., Lettino, M., Petersen, S. E., Mossialos, E. A., Maggioni, A. P., Kazakiewicz, D., and May, H. T. 2020. ' European Society of Cardiology: cardiovascular disease statistics 2019.', *Eur. Heart J.*, 41: 12-85.

Tiosano, D., Baris, H. N., Chen, A., Hitzert, M. M., Schueler, M., Gulluni, F., Wiesener, A., Bergua, A., Mory, A., and Copeland, B. 2019. 'Mutations in PIK3C2A cause syndromic short stature, skeletal abnormalities, and cataracts associated with ciliary dysfunction', *PLoS Genet.*, 15: e1008088.

Tomlinson, R., and Ballou, C. E. 1961. 'Complete characterization of the myo-inositol polyphosphates from beef brain phosphoinositide', *J. Biol. Chem.*, 236: 1902-06.

Traynor-Kaplan, A., Kruse, M., Dickson, E. J., Dai, G., Vivas, O., Yu, H., Whittington, D., and Hille, B. 2017. 'Fatty-acyl chain profiles of cellular phosphoinositides', *Biochim. Biophys. Acta*, 1862: 513-22.

Trinh, R., Gurbaxani, B., Morrison, S. L., and Seyfzadeh, M. 2004. 'Optimization of codon pair use within the (GGGGS) 3 linker sequence results in enhanced protein expression', *Mol. Immunol.*, 40: 717-22.

Tysnes, O.-B. 1992. 'Inositol phosopholipid metabolism in resting and stimulated huamn platelets', *Cell. Signal.*, 4: 611-17.

Valet, C., Chicanne, G., Severac, C., Chaussade, C., Whitehead, M. A., Cabou, C., Gratacap, M.-P., Gaits-Iacovoni, F., Vanhaesebroeck, B., and Payrastre, B. 2015. 'Essential role of class II PI3K-C2α in platelet membrane morphology', *Blood*, 126: 1128-37.

Valet, C., Levade, M., Chicanne, G., Bilanges, B., Cabou, C., Viaud, J., Gratacap, M.-P., Gaits-Iacovoni, F., Vanhaesebroeck, B., and Payrastre, B. 2017. 'A dual role for the class III PI3K, Vps34, in platelet production and thrombus growth', *Blood*, 130: 2032-42.

van der Meijden, P. E., Feijge, M. A., Giesen, P. L., Huijberts, M., van Raak, L. P., and Heemskerk, J. W. 2005. 'Platelet P2Y12 receptors enhance signalling towards procoagulant activity and thrombin generation', *Thromb. Haemost.*, 93: 1128-36.

Van Roy, M., Ververken, C., Beirnaert, E., Hoefman, S., Kolkman, J., Vierboom, M., Breedveld, E., t Hart, B., Poelmans, S., and Bontinck, L. 2015. 'The preclinical pharmacology of the high affinity anti-IL-6R Nanobody® ALX-0061 supports its clinical development in rheumatoid arthritis', *Arthrit. Res. Ther.*, 17: 1-16.

Varga-Szabo, D., Authi, K. S., Braun, A., Bender, M., Ambily, A., Hassock, S. R., Gudermann, T., Dietrich, A., and Nieswandt, B. 2008. 'Store-operated Ca 2+ entry in platelets occurs independently of transient receptor potential (TRP) C1', *Pflug. Arch. Eur.*, 457: 377-87.

Varga-Szabo, D., Braun, A., and Nieswandt, B. 2011. 'STIM and Orai in platelet function', *Cell Calcium*,

50: 270-78.

Varga-Szabo, D., Braun, A., and Nieswandt, B. 2009. 'Calcium signaling in platelets', *J. Thromb. Haemost.*, 7: 1057-66.

Versteeg, H. H., Heemskerk, J. W., Levi, M., and Reitsma, P. H. 2013. 'New fundamentals in hemostasis', *Physiol. Rev.*, 93: 327-58.

Vivanco, I., and Sawyers, C. L. 2002. 'The phosphatidylinositol 3-kinase–AKT pathway in human cancer', *Nat. Rev. Cancer*, 2: 489-501.

Voors-Pette, C., Lebozec, K., Dogterom, P., Jullien, L., Billiald, P., Ferlan, P., Renaud, L., Favre-Bulle, O., Avenard, G., and Machacek, M. 2019. 'Safety and tolerability, pharmacokinetics, and pharmacodynamics of ACT017, an antiplatelet GPVI (glycoprotein VI) Fab: first-in-human healthy volunteer trial', *Arterioscler. Thromb. Vasc. Biol.*, 39: 956-64.

Waage, P., and Guldberg, C. 1864. 'Studier over affiniteten', *Forhandlinger i Videnskabs-selskabet i Christiania*, 1: 35-45.

Wang, C., Palavicini, J. P., Wang, M., Chen, L., Yang, K., Crawford, P. A., and Han, X. 2016. 'Comprehensive and quantitative analysis of polyphosphoinositide species by shotgun lipidomics revealed their alterations in db/db mouse brain', *Anal. Chem.*, 88: 12137-44.

Wang, J., Christison, T. T., Misuno, K., Lopez, L., Huhmer, A. F., Huang, Y., and Hu, S. 2014. 'Metabolomic profiling of anionic metabolites in head and neck cancer cells by capillary ion chromatography with Orbitrap mass spectrometry', *Anal. Chem.*, 86: 5116-24.

Watson, A. A., Eble, J. A., and O'Callaghan, C. A. 2008. 'Crystal structure of rhodocytin, a ligand for the platelet-activating receptor CLEC-2', *Protein Sci.*, 17: 1611-16.

Watson, S., Auger, J., McCarty, O., and Pearce, A. 2005. 'GPVI and integrin αIIbβ3 signaling in platelets', *J. Thromb. Haemost.*, 3: 1752-62.

Watson, S., Herbert, J., and Pollitt, A. Y. 2010. 'GPVI and CLEC-2 in hemostasis and vascular integrity', *J. Thromb. Haemost.*, 8: 1456-67.

Watson, S. P. 2009. 'Platelet activation by extracellular matrix proteins in haemostasis and thrombosis', *Curr. Pharm. Des.*, 15: 1358-72.

Watson, S. P., and Lapetina, E. G. 1985. '1, 2-Diacylglycerol and phorbol ester inhibit agonist-induced formation of inositol phosphates in human platelets: possible implications for negative feedback regulation of inositol phospholipid hydrolysis', *Proc. Natl. Acad. Sci.*, 82: 2623-26.

Watson, S. P., Reep, B., McConnell, R. T., and Lapetina, E. G. 1985. 'Collagen stimulates [3H] inositol trisphosphate formation in indomethacin-treated human platelets', *Biochem. J.*, 226: 831-37.

White, C., and Bridge, L. J. 2019. 'Ligand binding dynamics for pre-dimerised G protein-coupled receptor homodimers: linear models and analytical solutions', *Bull. Math. Biol.*, 81: 3542-74.

Whitman, M., Downes, C. P., Keeler, M., Keller, T., and Cantley, L. 1988. 'Type I phosphatidylinositol kinase makes a novel inositol phospholipid, phosphatidylinositol-3-phosphate', *Nature*, 332: 644.

Wilson, D. B., Neufeld, E., and Majerus, P. 1985. 'Phosphoinositide interconversion in thrombin-stimulated human platelets', *J. Biol. Chem.*, 260: 1046-51.

Wolins, N. E., Quaynor, B. K., Skinner, J. R., Tzekov, A., Park, C., Choi, K., and Bickel, P. E. 2006. 'OP9 mouse stromal cells rapidly differentiate into adipocytes: characterization of a useful new model of adipogenesis', *J. Lipid Res.*, 47: 450-60.

Workman, P., Clarke, P. A., Raynaud, F. I., and van Montfort, R. L. 2010. 'Drugging the PI3 kinome: from chemical tools to drugs in the clinic', *Cancer Res.*, 70: 2146-57.

Woulfe, D. S. 2010. 'Akt signaling in platelets and thrombosis', *Expert Rev. Hematol.*, 3: 81-91.

Yamamoto, K., Graziani, A., Carpenter, C., Cantley, L., and Lapetina, E. 1990. 'A novel pathway for the formation of phosphatidylinositol 3, 4-bisphosphate. Phosphorylation of phosphatidylinositol 3-monophosphate by phosphatidylinositol-3-monophosphate 4-kinase', *J. Biol. Chem.*, 265: 22086-89.

Yau, J. W., Teoh, H., and Verma, S. 2015. 'Endothelial cell control of thrombosis', *BMC Cardiovasc. Disord.*, 15: 1-11.

Yi, W., Li, Q., Shen, J., Ren, L., Liu, X., Wang, Q., He, S., Wu, Q., Hu, H., and Mao, X. 2014. 'Modulation of platelet activation and thrombus formation using a pan-PI3K inhibitor S14161', *PLoS One*, 9: e102394.

Zhang, W., Sloan-Lancaster, J., Kitchen, J., Trible, R. P., and Samelson, L. E. 1998. 'LAT: the ZAP-70 tyrosine kinase substrate that links T cell receptor to cellular activation', *Cell*, 92: 83-92.

Zhang, W., Trible, R. P., Zhu, M., Liu, S. K., McGlade, C. J., and Samelson, L. E. 2000. 'Association of Grb2, Gads, and phospholipase C-γ1 with phosphorylated LAT tyrosine residues: effect of LAT tyrosine mutations on T cell antigen receptor-mediated signaling', *J. Biol. Chem.*, 275: 23355-61.

Zhao, L., Thorsheim, C. L., Suzuki, A., Stalker, T. J., Min, S. H., Lian, L., Fairn, G. D., Cockcroft, S., Durham, A., and Krishnaswamy, S. 2017. 'Phosphatidylinositol transfer protein-α in platelets is inconsequential for thrombosis yet is utilized for tumor metastasis', *Nat. Commun.*, 8: 1-12.

Zou, J., Wu, J., Roest, M., and Heemskerk, J. W. 2021. 'Long-term platelet priming after glycoprotein VI stimulation in comparison to Protease-Activating Receptor (PAR) stimulation', *PLoS One*, 16: e0247425.